Inaugural dissertation

for

obtaining the doctoral degree

of the

Combined Faculty of Mathematics, Engineering and Natural Sciences

of the

Ruprecht - Karls - University

Heidelberg

Presented by

Dr. med. Christoph Hofmann

born in: Heppenheim (Bergstraße)

Oral examination: October 29, 2024

**Translational Control of an Inflammatory Network in the Heart**

Referees: Prof. Dr. rer. nat. Markus Hecker

Prof. Dr. med. Mirko Völkers

*To my family*

**Summary**

In this thesis I investigated a previously unrecognized translational burst of the infarct and border zone after cardiac reperfusion in a mouse model of ischemia/reperfusion injury. This translational response is mediated partly by border zone cardiomyocytes, which increasingly translate mRNAs related to inflammation and cell migration in response to reperfusion. Among those increasingly translated transcripts is the mRNA that encodes C-C Motif Chemokine Ligand 2 *(*CCL2), a chemokine that is involved in the attraction of monocytes to the injured heart. A transient pharmacological inhibition of the mechanistic target of rapamycin complex 1 (mTORC1) - eukaryotic translation initiation factor 4E binding protein 1 (4EBP1) - eukaryotic translation initiation factor 4E (eIF4E) axis, which I found to be involved in the translational activation of border zone cardiomyocytes, inhibited myocardial inflammatory, monocyte infiltration, improved cardiac contractility, reduced infarct size, and strongly suppressed cardiac *Ccl2* expression and release from the infarcted heart in a preclinical model of ischemia/reperfusion in mice. Reduced *Ccl2* gene expression after inhibition of the mTORC1-4EBP1-eIF4E axis was at least partly derived from attenuated translation of the *Ccl2* transcript. In addition, a direct inhibitory effect of rapamycin and 4EGI-1, pharmacological inhibitors of mTORC1-dependent translation, on circulating monocytes was observed, which may contribute to the attenuation of inflammatory monocyte infiltration into the infarcted heart after mTORC1-4EBP1-eIF4E axis inhibition. Improved cardiac function after pharmacological mTORC1-4EBP1-eIF4E axis inhibition may thus result from the attenuation of a pro-inflammatory translational network, involving the inhibition of translation of the mRNA encoding for the chemokine CCL2 by border zone cardiomyocytes, as well as a direct inhibitory effect on circulating monocytes, thus attenuating maladaptive aspects of cardiac inflammation and remodeling after myocardial infarction and reperfusion.

**Zusammenfassung**

In dieser Doktorarbeit untersuche ich eine bisher unbekannte Aktivierung der Proteinsynthese im Infarktkern und der Infarkt-Randzone nach kardialer Reperfusion in einem Mausmodell des Ischämie-/Reperfusionsschadens. Diese Translationsreaktion wird zum Teil durch Kardiomyozyten der Infarkt-Randzone vermittelt, welche als Reaktion auf die Reperfusion vermehrt mRNAs translatieren, die mit einer Entzündungsreaktion und Zellmigration in Zusammenhang stehen. Zu diesen vermehrt translatierten Transkripten gehört auch die mRNA, die für C-C Motif Chemokine Ligand 2 (CCL2) kodiert, ein Chemokin, das an der Chemotaxis von Monozyten zum Herzen nach einem Myokardinfarkt beteiligt ist. Eine vorübergehende und potenziell klinisch umsetzbare pharmakologische Hemmung des mechanistic target of rapamycin complex 1 (mTORC1) - eukaryotic translation initiation factor 4E binding protein 1 (4EBP1) - eukaryotic translation initiation factor 4E (eIF4E) Signalweges, welcher an der Aktivierung der Proteinsynthese von Kardiomyozyten der Infarkt-Randzone beteiligt ist, hemmte die myokardiale Infiltration von pro-inflammatorischen Monozyten, verbesserte die kardiale Kontraktilität, verringerte die Infarktgröße und unterdrückte die kardiale Expression des *Ccl2*-Gens und die Freisetzung des CCL2 Proteins aus dem Herzen nach einem Myokardinfarkt in einem präklinischen Ischämie/Reperfusion-Modell in Mäusen. Die verringerte Expression des *Ccl2*-Gens nach Hemmung der mTORC1-4EBP1-eIF4E-Achse war in Teilen auf eine verminderte Translation des *Ccl2* Transkripts in Kardiomyozyten der Randzone zurückzuführen. Darüber hinaus wurde eine direkte hemmende Wirkung von Rapamycin und 4EGI-1, pharmakologischen Inhibitoren der mTORC1-abhängigen Translation, auf zirkulierende Monozyten beobachtet, was zur Abschwächung der Infiltration pro-inflammatorisch determinierter Monozyten in das infarzierte Herz nach Hemmung der mTORC1-4EBP1-eIF4E-Achse beitragen könnte. Die verbesserte

kardiale Funktion nach pharmakologischer Hemmung der mTORC1-4EBP1-eIF4E-Achse ist daher in Teilen auf die Abschwächung eines entzündungsfördernden Translationsnetzwerks zurückzuführen. An diesem Mechanismus ist die Inhibition der Translation der für das Chemokin CCL2 kodierenden mRNA beteiligt, welches unter anderem von Kardiomyozyten der Infarkt-Randzone vermehrt translatiert wird, sowie eine direkte hemmende Wirkung von zirkulierenden pro-inflammatorischen Monozyten.

## Table of Contents

# 1 List of Figures

## 2 List of Abbreviations and Acronyms

| | |
|---|---|
| **4EBP1** | eIF4E-binding protein 1 |
| **αMHC** | alpha myosin heavy chain |
| **AAV9** | adeno-associated virus 9 |
| **ARCM** | adult rat ventricular cardiomyocytes |
| **Bord** | border zone |
| **Ccl2** | C-C Motif Chemokine Ligand 2 |
| **Ctr** | control |
| **EF** | ejection fraction |
| **eIF** | eukaryotic initiation factor |
| **FACS** | fluorescence-activated cell sorting |
| **HA** | human influenza hemagglutinin |
| **hTNT** | human Troponin T |
| **HW** | heart weight |
| **Inf** | infarct |
| **iPSC-CM** | induced pluripotent stem cell-derived human cardiomyocytes |
| **I/R** | ischemia/reperfusion |
| **Isch** | ischemia |
| **LAD** | left anterior descending coronary artery |
| **LVDevP** | left ventricular developed pressure |
| **m7GTP** | 7-methylguanosin |
| **MI** | myocardial infarction |
| **MNK1/2** | mitogen-activated protein kinase-interacting kinases 1 and 2 |
| **mTOR** | mechanistic target of rapamycin |
| **mTORC1** | mechanistic target of rapamycin complex 1 |

| | |
|---|---|
| **NRCM** | neonatal rat ventricular cardiomyocytes |
| **OPP** | O-propargyl-puromycin |
| **Puro** | puromycin |
| **Rep** | reperfusion |
| **Ribo-Seq** | ribosome profiling |
| **Ribo-tag** | ribosome-tagged |
| **RNA-Seq** | RNA-sequencing |
| **Rpl22** | ribosomal protein L22 |
| **sI** | simulated ischemia |
| **sI/R** | simulated ischemia/reperfusion |
| **TL** | tibia length |
| **TnT** | troponin T |
| **TOP** | terminal oligopyrimidine |
| **TUNEL** | terminal deoxynucleotidyl transferase dUTP nick end labeling |
| **WT** | wildtype |

# 3 Introduction

## 3.1 Ischemic heart disease

Ischemic heart disease is the leading cause of cardiovascular death worldwide that is caused by a combination of lifestyle factors, genetics and medical complications.[1–4] Sometimes also referred to as coronary heart disease or coronary artery disease, ischemic heart disease is caused by inadequate blood flow to the cardiac muscle that results in acute or chronic ischemia of the heart. In most cases ischemic heart disease is caused by atherosclerosis-mediated stenosis of the coronary arteries. Ischemic heart disease may be symptomatic and often presents as angina pectoris, dyspnea, fatigue, or arrhythmias but can also remain asymptomatic for many years until it eventually manifests as acute coronary syndrome. Especially women or patients with other comorbidities such as diabetes may show atypical or no symptoms at all, which can complicate diagnosis. The global burden of cardiovascular disease (Figure 1) and from ischemic heart disease (Figure 2) varies between regions, ethnicities and subpopulations, but remains a leading cause of death worldwide.[1,2,5] While overall numbers of ischemic heart disease increase globally, age-standardized prevalence remains relatively stable with a small continues decline of ischemic heart disease prevalence in western regions over time.[6]

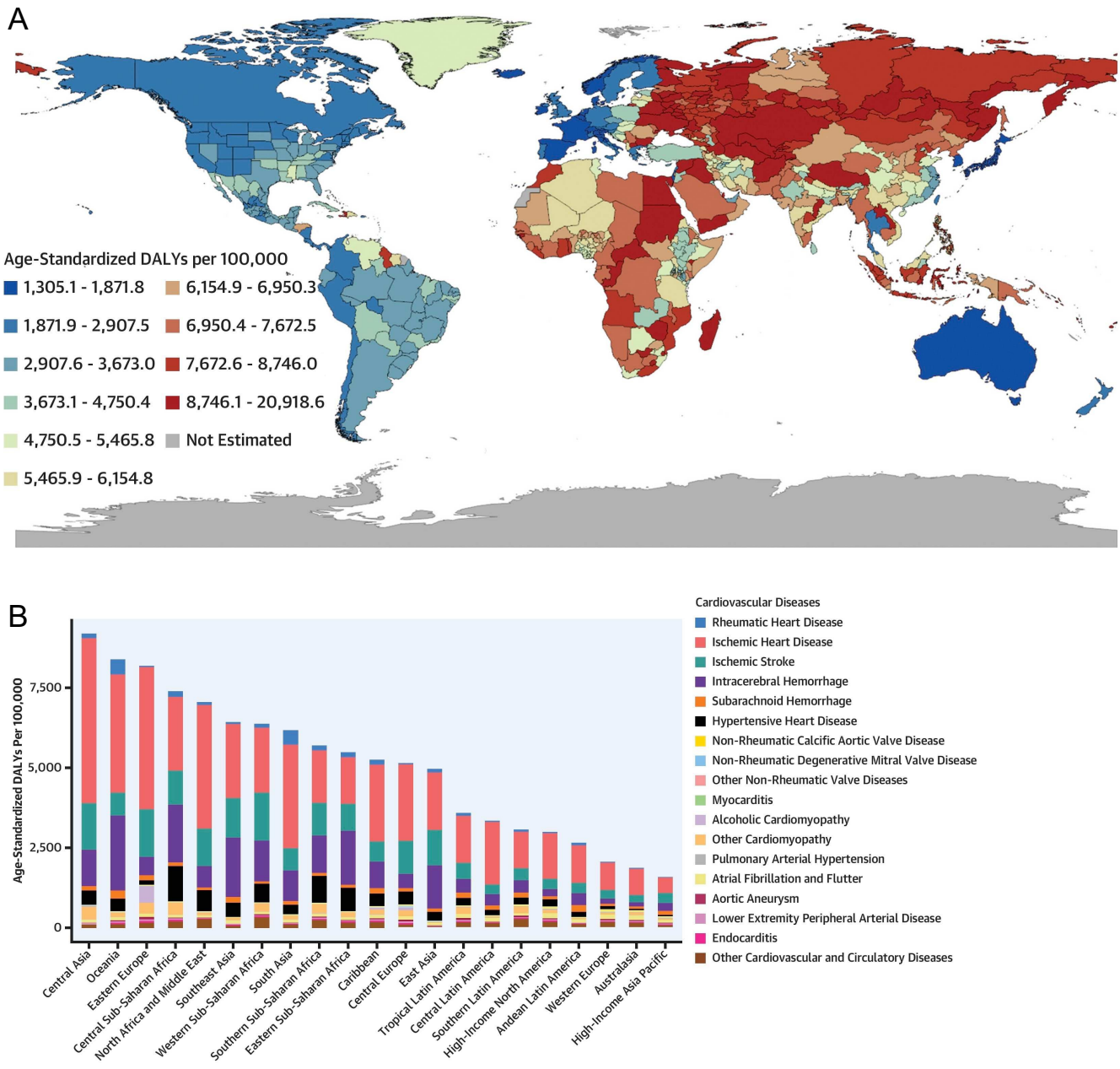


**Figure 1 | Global Burden of Cardiovascular Diseases**

**A**, Age-standardized disability-adjusted life years (DALYs) per 100,000 for cardiovascular diseases globally. **B**, Age-standardized DALYs specific for individual cardiovascular diseases by region. Reproduced with permission from 'The Global Burden of Cardiovascular Diseases and Risk: A Compass for Future Health'[1]. This article was published in Journal of the American College of Cardiology, Vol. 80 No. 25, Muthiah Vaduganathan, George A. Mensah, Justine Varieur Turco, Valentin Fuster, and Gregory A. Roth, The Global Burden of Cardiovascular Diseases and Risk: A Compass for Future Health, 2361–2371, Copyright American College of Cardiology Foundation. Published by Elsevier (2022).

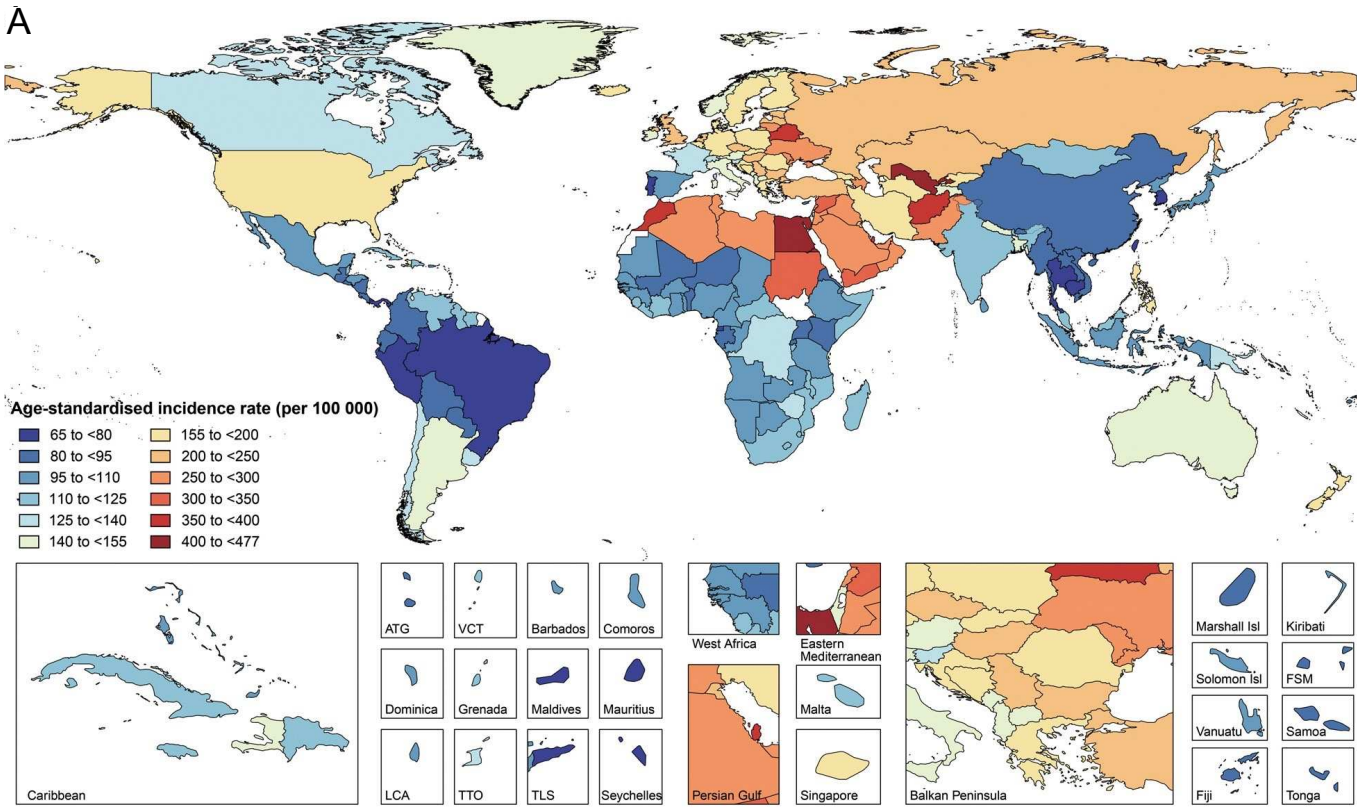
A
Age-standardised incidence rate (per 100 000)
65 to <80
80 to <95
95 to <110
110 to <125
125 to <140
140 to <155
155 to <200
200 to <250
250 to <300
300 to <350
350 to <400
400 to <477
Caribbean
ATG
VCT
Barbados
Comoros
Dominica
Grenada
Maldives
Mauritius
LCA
TTO
TLS
Seychelles
West Africa
Eastern Mediterranean
Persian Gulf
Malta
Singapore
Balkan Peninsula
Marshall Isl
Kiribati
Solomon Isl
FSM
Vanuatu
Samoa
Fiji
Tonga

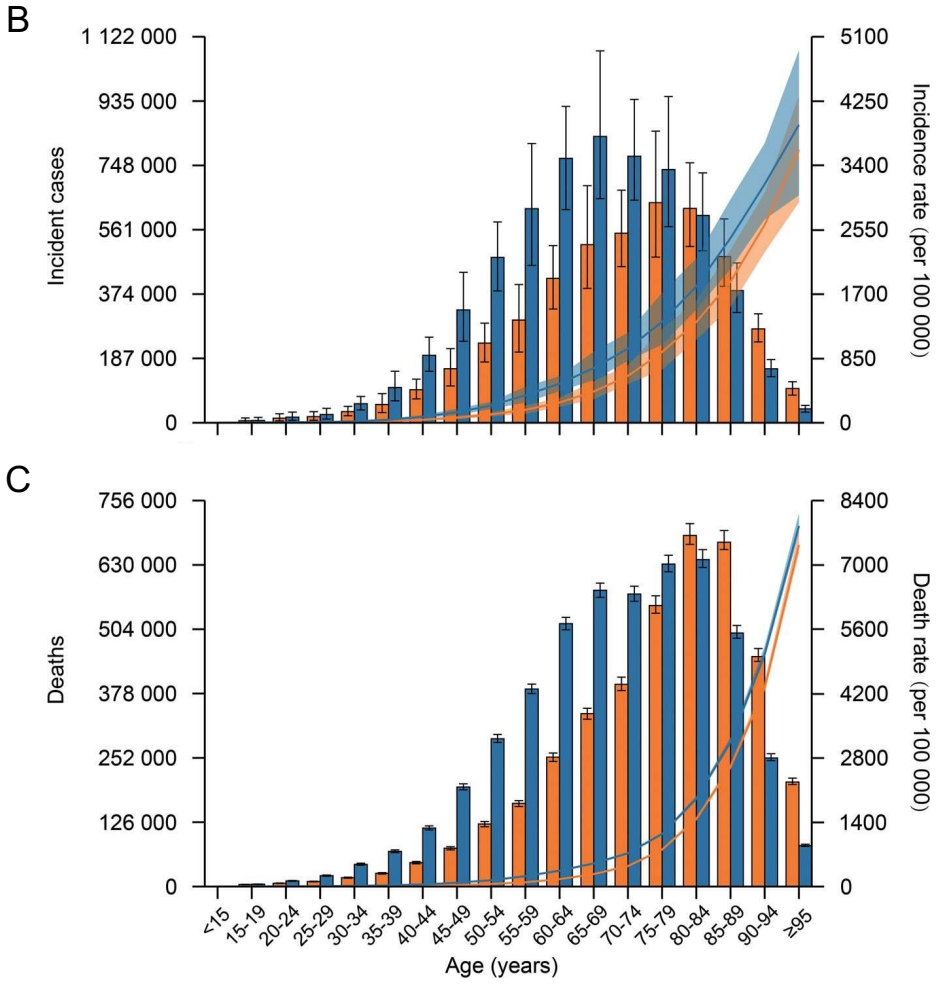
B
Incident cases
1 122 000
935 000
748 000
561 000
374 000
187 000
0
Incidence rate (per 100 000)
5100
4250
3400
2550
1700
850
0
C
Deaths
756 000
630 000
504 000
378 000
252 000
126 000
0
Death rate (per 100 000)
8400
7000
5600
4200
2800
1400
0
<15
15-19
20-24
25-29
30-34
35-39
40-44
45-49
50-54
55-59
60-64
65-69
70-74
75-79
80-84
85-89
90-94
≥95
Age (years)

**Figure 2 | Global Burden of Ischemic Heart Disease**
**A** Age-standardized incidence rate of ischemic heart disease per 100,000 across 195 countries and territories for both sexes, 2017. **B, C** Age-specific numbers, and rates of incident cases (**B**) and deaths (**C**) of ischemic heart disease by sex, 2017. Error bars indicate the 95% uncertainty interval (UI) for numbers. Shading indicates the 95% UI for rates. Adapted with permission from 'Global, regional, and national burden of ischaemic heart disease and its attributable risk factors, 1990–2017: results from the Global Burden of Disease Study 2017'[5].

## 3.2 Acute myocardial infarction

### 3.2.1 Pathophysiology of cardiac ischemia

Myocardial infarction represents an acute and severe manifestation of ischemic heart disease that is a major contributor to mortality worldwide.[7,8] It is caused by inadequate blood supply to the myocardium, resulting in acute ischemia and subsequent cardiac injury.[9] Prolonged duration of ischemia during myocardial infarction causes progressive and irreversible loss of viable cardiac tissue, which is associated with a large number of adverse events, such as arrhythmia, ventricular aneurysm and rupture, valve dysfunctions, pericarditis and severe inflammatory reactions, cardiogenic shock and heart failure, that can ultimately result in death.[9–12]

Ischemia is defined as insufficient blood supply that does not meet a tissues oxygen demand, most of the time going along with insufficient cellular nutrient supply.[13] Exceeding cell type- and tissue-specific intensity and duration thresholds, ischemia will cause cell injury that may progress to cell death and organ dysfunction. Ischemia does not need to go along with reduced tissue blood flow and is in general caused by insufficient blood supply. For example, ischemia can be caused by constant blood flow during conditions of increased tissue oxygen demand, when the blood and oxygen supply cannot be sufficiently increased to meet higher oxygen need. In the heart, determinants of oxygen consumption are 1) myocardial mass, 2) myocardial work

(determined by heart rate and blood pressure), 3) pre-contraction tension (defined by ventricular dimensions) and 4) inotropic status.[13] Some of these remain relatively constant, such as myocardial mass, while others can change rapidly, resulting in drastic changes in myocardial oxygen demand.

Compared to other organs, the heart extracts high levels of coronary blood oxygen. Even at rest, the myocardium extracts more than 70% of coronary oxygen levels and as such, increased myocardial oxygen demand has to be met with increased coronary blood flow, resulting in an almost linear relation between myocardial oxygen consumption and coronary artery blood flow.[13] While under basal conditions, the human heart receives approximately 1/20$^{th}$ of the cardiac output, this may rise fourfold to meet increased oxygen demand during phases of increased workload. As such, myocardial ischemia is in most cases caused by insufficient coronary blood flow, however other causes, such as anemia can significantly contribute to ischemia. For a more in depth description of the complex determining factors of coronary blood flow, such as perfusion pressure, resistance, elasticity, stenosis, relative length of systole and diastole, metabolic autoregulation and other factors, readers are referred to related literature[13,14].

This study modelled acute severe ischemia that results in cell and tissue injury caused by immediate and almost complete loss of oxygen and nutrient supply. Clinically, this scenario is encountered in acute myocardial infarction in which acute ischemia causes subsequent cardiac injury.

### 3.3 Myocardial reperfusion and reperfusion injury

In acute myocardial infarction, a so called ‘border zone’, which is defined as the region surrounding the area of irreversible tissue injury, is characterized by cellular injury that not yet resulted in cell death and therefore has the potential to recover or

instead progress to irreversible cell damage. The border zone separates the poorly perfused ‘infarct zone’ from the ‘remote area’ and was recently demonstrated to occur in human myocardial infarction and further characterized in this setting.[15,16] This area at risk may be rescued by timely reperfusion and is central to the strategy of preventing progressive injury by percutaneous coronary interventions. As cardiac function after myocardial infarction is directly correlated to the remaining viable tissue, current gold-standard for the treatment of myocardial infarction is rapid restoration of coronary blood flow by reperfusion, which restores cellular oxygen and nutrients and thereby prevents further cell death resulting from ischemia.[17]

While this, if performed early enough, significantly improves survival and long-term cardiac function, reperfusion itself is thought to cause cardiac injury by mechanisms proposed to involve arrhythmias, myocardial stunning, oxidative stress, calcium overload, metabolic dysregulation, vascular damage, inflammation and other mechanisms.[18,19] Despite of substantial investigation of ‘reperfusion injury’, its underlying molecular mechanisms remain incompletely understood. Some investigator even question the existence of ‘lethal reperfusion injury’, the ‘reperfusion-induced death of cardiomyocytes which were viable or reversibly injured at the end of ischemia’.[20] It is even questioned by some authors whether lethal reperfusion injury exists in humans.[21] As it remains challenging to directly demonstrate reperfusion-induced cell death, reperfusion injury has been primarily defined by preclinical studies, performed in rodents and other animals, that revealed that interventions undertaken shortly before or after reperfusion further improve outcome and decrease final infarct size, indicative of some form of targetable injury that occurs during or after reperfusion.[18,20,21]

Current therapies for myocardial infarction target only the ischemic aspect, whereas no intervention to reduce reperfusion injury has been successfully translated

into the clinic.[18] Thus, there is great need to define mechanisms that mediate cell injury after reperfusion that may be targeted to further improve outcomes after acute myocardial infarction.

### 3.4 Inflammation after myocardial infarction and cardiac reperfusion

The injured myocardium initiates an inflammatory response after myocardial infarction.[22] Myocardial necrosis and injury induces complement activation, free radical generation and triggers a cytokine response that attracts immune cells.[22,23] This inflammatory reaction is further accelerated and augmented if the ischemic area is reperfused.[22,24] While cardiac inflammation is a prerequisite for healing and scar formation, such processes, if allowed to proceed and continue in an excessive degree, may result in secondary damage, causing adverse remodeling and impaired contractility.[23] Experimental insights of preclinical studies and promising results of clinical studies provided evidence that anti-inflammatory actions can reduce myocardial injury after myocardial infarction, further supporting the concept that some maladaptive elements of the inflammatory response after myocardial infarction extends cardiac injury and mediate adverse myocardial remodeling.[23,25] Indeed, many patients with myocardial infarction present with signs of inflammation and blood levels of the inflammatory protein 'C-reactive protein' is a strong predictor of future cardiovascular events.[23,26] However, the evolutionary conserved inflammatory response also serves important adaptive functions that mediate aspects of healing, regeneration and scar formation and a large number of anti-inflammatory clinical trials did not improve or even impaired outcomes, partly related to impaired host defense.[23,25] Translating findings from preclinical animal models of cardiac inflammation to humans has been challenging, which is likely in part dependent on significant differences between murine and human inflammatory responses despite of

many similarities. For example, systemic administration of corticosteroids as broad anti-inflammatory strategy decreased infarct size in a canine model of myocardial infarction.[27] While a similar approach inhibited leukocyte infiltration in humans, it resulted in deleterious outcomes due to delayed healing and collagen deposition.[22,28,29] As such, it remains a central challenge to identify the molecular mechanisms that drive maladaptive and adaptive aspects of inflammation that may be of relevance to humans. Mechanistic studies over the last decades have revealed a complex and dynamic interplay between basically all major cardiac and circulating immune cell types that mediate the myocardial inflammatory response, which is functionally divided into different phases.[23] The first immune phase that last up to approximately 4 days in humans and up to 3 days in mice is sometimes referred to as inflammatory phase.[30,31] Immediately after myocardial infarction and reperfusion, damage-associated molecular patterns released from injured cardiac cells result in inflammasome activation and induction of a sterile inflammatory response mediated by a cascade of cytokines that results in successive waves of inflammatory cell infiltration.[23,30] This initial inflammatory response clears injured and necrotic cells from the damaged myocardium which is necessary for scar formation and maturation.[30] Thus, this controlled inflammatory response is an vital process indispensable for repair and healing.[23] However, some authors describe evidence for an acute 'overshooting inflammatory burst' that increases cardiac injury during this phase, which may be targeted to improve cardiac outcome.[23]

The inflammatory phase is followed by a proliferative phase which is characterized by the development of granulation tissue.[30] This phase approximately occurs from day 5 to day 14 after myocardial infarction in humans and from days 4 to 7 in mice.[30,31] During this time many populations of inflammatory leukocytes are released from the injured myocardium, transform into more reparative states and

several and additional anti-inflammatory, pro-reparative immune cell populations infiltrate the myocardium.[30] During the proliferative phase granulation tissue is formed which is mediated by the induction of angiogenesis and the secretion and modification of collagen and other extracellular matrix components by various cardiac cell types.[30,31] In the final maturation phase, which continuous for weeks or months after myocardial infarction, the extracellular matrix is further modified, angiogenesis is downregulated and immune cells, fibroblasts and other cell types are released from the site of injury, leaving a mostly acellular fibrous scar tissue.[30,31] The maturation phase may be associated with a basal inflammatory activity that can contribute to adverse cardiac remodeling.[30]

All three phases of the post-myocardial infarction response are mediated by various immune cell populations, which infiltrate the myocardium in characteristic waves that are orchestrated by cardiac and extracardiac gene expression and cytokine programs (Figure 3). In a first wave, that occurs within hours to approximately three days after myocardial infarction, polymorphonuclear neutrophils enter the myocardium.[23,30,32,33] This is followed by a second wave, in which monocytes/macrophages enter the site of injury. Numerically monocytes/macrophages are the largest fraction of immune cells that infiltrate the myocardium after myocardial infarction. This second wave can be further divided into two-phases. The first phase that occurs approximately 1 to 4 days after myocardial infarction, is dominated by the infiltration and proliferation of pro-inflammatory monocytes/macrophages, that are sometimes referred to as Ly6C$^{high}$ Ccr2$^{+}$ or M1 monocytes/macrophages, dependent on the markers used for identification, which represent partly overlapping pro inflammatory cell populations. The second phase, which occurs approximately 2 to 10 days after myocardial infarction, is dominated by pro-reparative

monocytes/macrophages, referred to as Ly6C$^{low}$ Ccr2$^{-}$ or M2 monocytes/macrophages. The third wave represents the infiltration of lymphocytes to the site of injury, in part due to the formation of autoantigens generated by the release of intracellular proteins upon myocardial damage activating lymphocytes of heart-draining mediastinal lymph nodes, which occurs approximately from day 1 to 10 and peaking dependent on the cell type at day 5 to 7 after myocardial infarction. Currently, the functions and molecular mechanisms mediated by other less frequent immune cell types remains largely unexplored in the context of myocardial infarction and reperfusion and is not further described in this thesis.

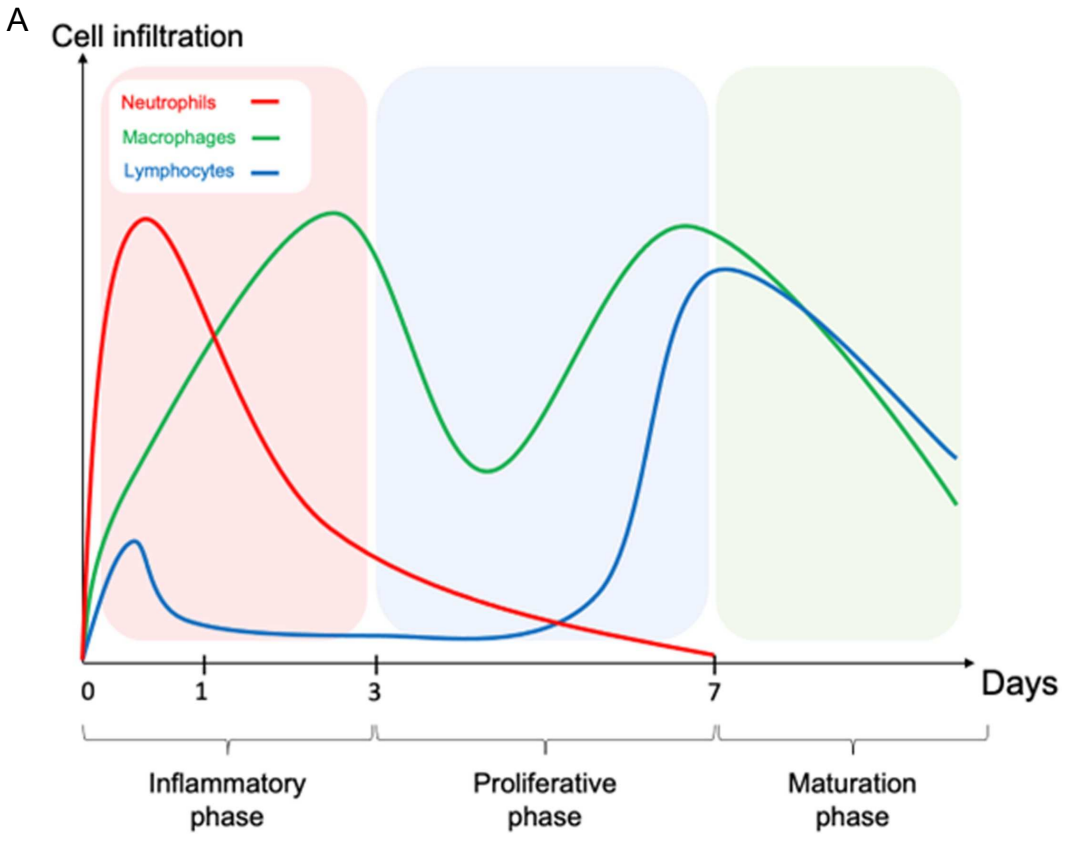


**Figure 3 | Neutrophil, macrophage, and lymphocyte cellular infiltration kinetics after myocardial infarction in mice**

**A**, In the immediate inflammatory response to MI, neutrophils accumulate in the microvasculature. These leukocyte infiltration kinetics govern the length and function of each of the 3 phases of cardiac repair. Compiled from Yan et al[33] and Rusinkevich et al[32]. Reproduced with permission from 'Impact of Reperfusion on Temporal Immune Cell Dynamics After Myocardial Infarction'[30].

### 3.4.1 Neutrophils

Neutrophils are maximally activated approximately 4 hours after myocardial infarction in humans.[30] After infiltrating the injured myocardium they release reactive oxygen species, various enzymes such as metalloproteinases, myeloperoxidase and neutrophil elastase, proinflammatory cytokines and alarmins.[30,34] For example, neutrophils are a primary source of the inflammatory alarmins S100A8 and S100A9, which further stimulates cytokine release and leukocyte recruitment and is a predictor of poor outcome.[30,35–37] Clinical studies consistently showed that high numbers of circulating neutrophils and high neutrophil-to-lymphocyte ratios around reperfusion are associated with increased mortality, poor left ventricular contractility, and an increased risk of developing heart failure.[30,38] Preclinical studies indicate that attenuating early neutrophile accumulation, which peaks at approximal 1 day in mice, is cardioprotective and shifts the infiltrating monocyte/macrophage population towards a more reparative state.[23,30,39] Proposed mechanisms by which neutrophils may further increase myocardial injury include the amplification of the following inflammatory response, release of damaging reactive oxygen species, enzymes and neutrophil extracellular traps, microvascular obstruction and the induction of cardiomyocyte apoptosis.[30] While neutrophil infiltration peaks at approximately 1 day post myocardial infarction, they continue to contribute to the proliferative and maturation phase (Figure 4).[30,39,40]

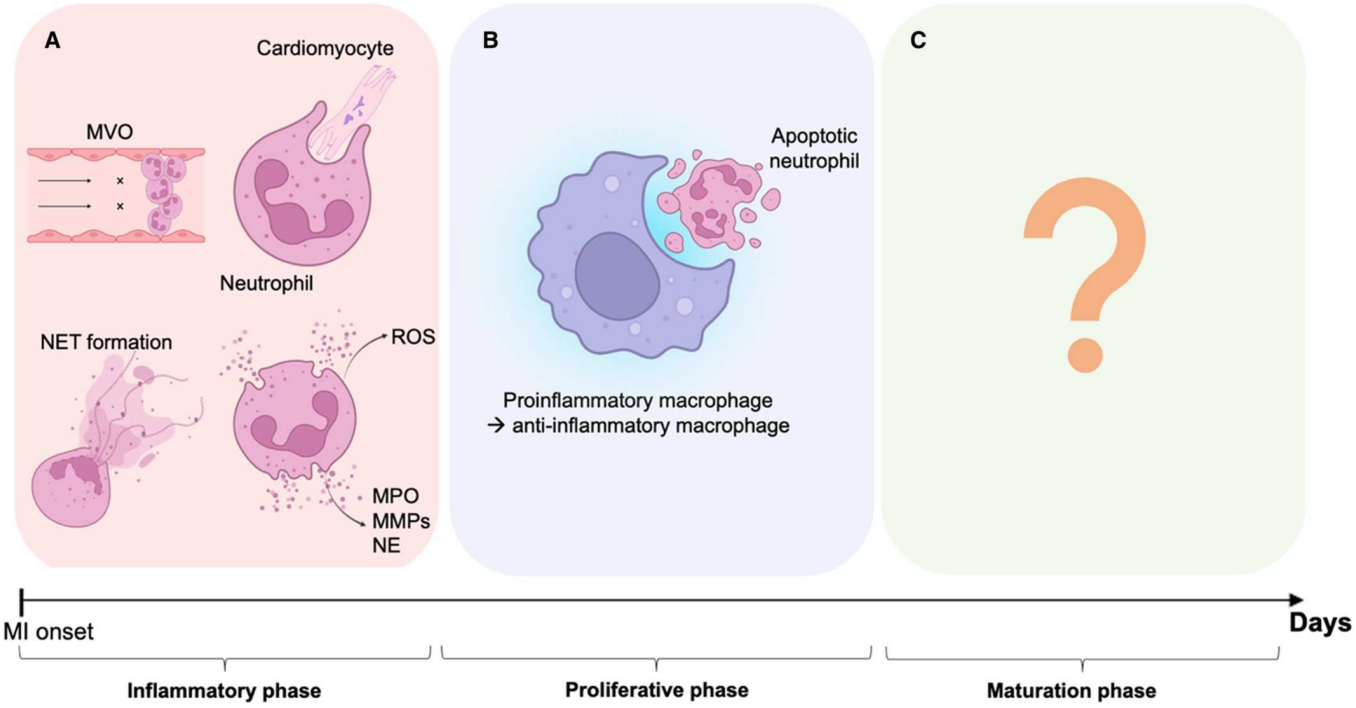


**Figure 4 | Temporal dynamics of neutrophil infiltration and function after myocardial infarction and reperfusion**

**A**, In the immediate inflammatory response to MI, neutrophils accumulate in the microvasculature and impair reperfusion by blocking further blood flow, causing microvascular obstruction (MVO). The formation of neutrophil extracellular traps (NETs) can also exacerbate ischemia/reperfusion injury. Once in the myocardial tissue, neutrophils can phagocytose dying cardiomyocytes, produce reactive oxygen species (ROS), and release inflammatory enzymes, including myeloperoxidase, matrix metalloproteinases, and neutrophil elastase, all of which exacerbate inflammation and cause additional myocardial injury. **B**, In the proliferative phase, neutrophils reach the end of their natural lifespan, undergo apoptosis, and are taken up by macrophages through efferocytosis. This polarizes the macrophages to an anti-inflammatory phenotype, leading to the resolution of inflammation and the initiation of the proliferative phase. **C**, The long-term actions of neutrophils in the maturation phase remain poorly understood. MI indicates myocardial infarction; MMPs, matrix metalloproteinases; MPO, myeloperoxidase; MVO, microvascular obstruction; NE, neutrophil elastase; NET, neutrophil extracellular trap; and ROS, reactive oxygen species. Reproduced with permission from 'Impact of Reperfusion on Temporal Immune Cell Dynamics After Myocardial Infarction'[30].

### 3.4.2 Monocytes/macrophages

The cardiac monocyte/macrophage compartment and its regulation in response to myocardial infarction and reperfusion is complex and controversial. At baseline, different sub-populations of tissue resident macrophages populate the myocardium

and different monocytes populations enter and leave the heart.[41–44] Those sub-populations are represented by different cellular gene expression and various presentation of cell surface receptors. While recent single cell RNA sequencing experiments revealed the complexity of different monocyte/macrophage cell states, those states are classically divided into pro-inflammatory Ly6C$^{high}$ Ccr2$^{+}$ monocytes or M1 macrophages and pro-reparative Ly6C$^{low}$ Ccr2$^{-}$ monocytes or M2 macrophages in mice.[45,46] However, it needs to be noted that this classification, which is also used in parts of this study, likely represents an oversimplification of a complex system that may be capable to quantify and categorize certain biological mechanisms. In humans and mice, monocytes from the spleen are released to the circulation in response to myocardial infarction and infiltrate the injured myocardium within few days, which is sustained by extramedullary monocytopoiesis.[47–49] Reperfusion further promotes monocyte recruitment to the heart.[30] Monocyte and macrophage numbers peak at approximately three days after myocardial infarction.[32,33] After infiltration to the myocardium, some monocytes differentiate to macrophages that clear necrotic cells and break down extracellular matrix.[30] In addition, they release cytokines that drives further leukocyte infiltration and shape the cardiac inflammatory response.

Proinflammatory monocytes/macrophages were reported to directly contribute to cardiac injury after myocardial injury and reperfusion through the release of reactive oxygen species, proteolytic enzymes and cytokines that directly induce apoptosis of cardiac cells.[30] While recent investigations revealed that certain elements of the proinflammatory monocyte/macrophage system mediates maladaptive functions that contribute to cardiac injury,[50,51] monocytes/macrophages are also necessary for proper healing of the injured myocardium.[52,53] For example, monocyte/macrophage inhibition may impair tissue clearance of necrotic and apoptotic cells, which prolongs the

inflammatory phase, results in impaired scar formation and increased risk of ventricular rupture.[30,52,53] Several studies reported that shifting the cardiac monocyte/macrophage phenotype from an inflammatory state towards a reparative state, which is sometimes examined by comparing the relative proportion of Ly6C$^{high}$ Ccr2$^{+}$ monocytes or M1 macrophages to Ly6C$^{low}$ Ccr2$^{-}$ monocytes or M2 macrophages, decreases infarct size and improves cardiac function after myocardial infarction in preclinical rodent models.[30] During the proliferative phase most monocytes/macrophages of the heart have acquired an anti-inflammatory state and coordinate the formation of granulation tissue.[30] Monocytes and macrophages continue to proliferate and become recruited to the scar tissue during the maturation phase in humans and rodents, during which inflammatory populations contribute to adverse cardiac remodeling (Figure 5).[30,54–56]

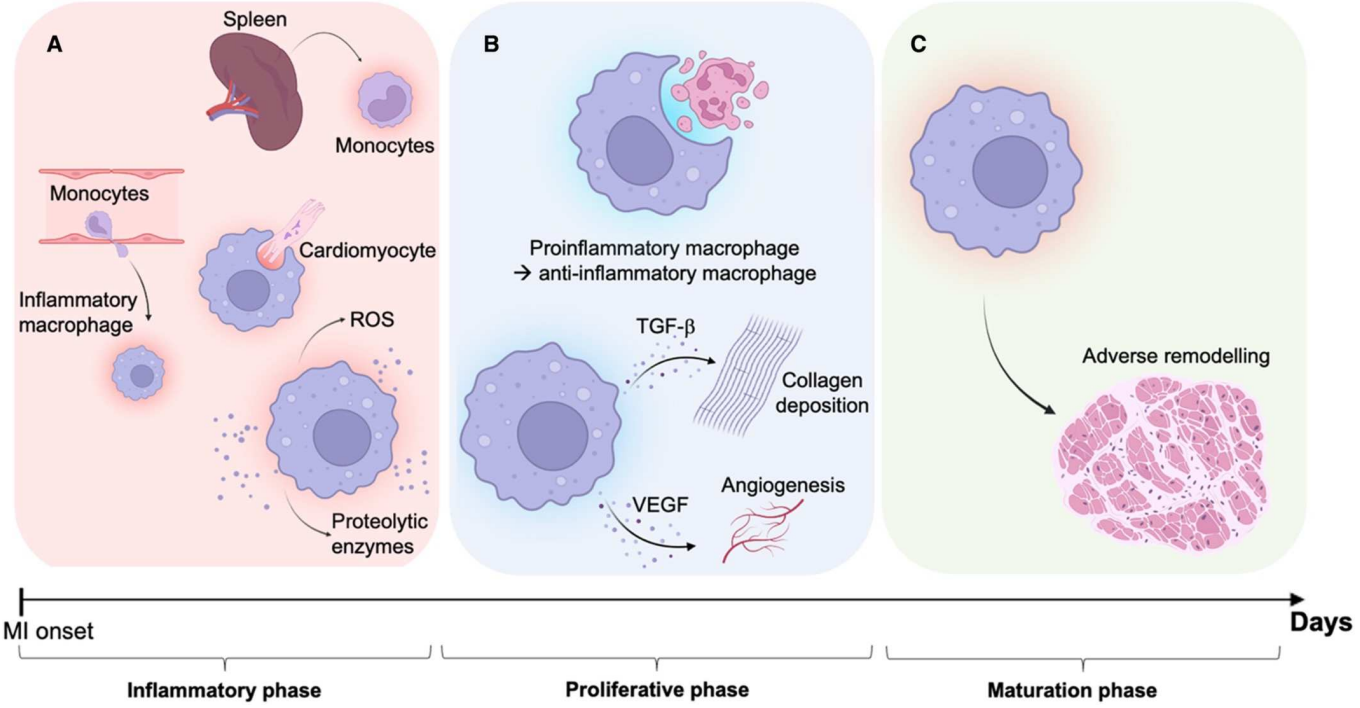


**Figure 5 | Temporal dynamics of monocyte/macrophage infiltration and function after myocardial infarction and reperfusion**

**A**, During the initial period of ischemia/reperfusion injury, macrophages in the myocardium are derived largely from circulating proinflammatory monocytes. Splenic monocyte release sustains the large influx of monocytes into the infarct zone. After entering the myocardial tissue, proinflammatory monocytes differentiate into macrophages that phagocytose dying

cardiomyocytes and release ROS and proteolytic enzymes. **B**, At the onset of the proliferative phase, macrophages polarize from the proinflammatory to the anti-inflammatory phenotype. Throughout this phase, macrophages coordinate the formation of early granulation tissue by inducing deposition of collagen and angiogenesis through the release of TGF-β and VEGF, respectively. **C**, Months after MI, proinflammatory macrophages may persist in the myocardium and contribute to adverse remodeling of the left ventricle. MI indicates myocardial infarction; ROS, reactive oxygen species; TGF-β, transforming growth factor-β; and VEGF, vascular endothelial growth factor. Reproduced with permission from 'Impact of Reperfusion on Temporal Immune Cell Dynamics After Myocardial Infarction'[30].

### 3.4.3 Lymphocytes

The involvement of lymphocytes in cardiac inflammation, scar formation and remodeling after myocardial infarction depends strongly on the lymphocyte subtype. All major lymphocyte subtypes, including B lymphocytes, CD4+ T lymphocytes, CD8+ T lymphocytes and regulatory T lymphocytes (Tregs) were described in the inflammatory and healing response after myocardial infarction.[30] In general, myocardial infiltration of lymphocytes early after myocardial infarction is associated with worse clinical outcome and infarct size in humans.[30,38,57–59] One such maladaptive mechanism appears to involve microvascular obstruction by lymphocytes[58] In general, the specific effects mediated by lymphocyte subpopulations is complex and heavily dependent on intercellular crosstalk that may shift cellular responses towards inflammatory or reparative states. Readers are referred to current reviews that discuss current aspects of lymphocytes in myocardial infarction (Figure 6).[60]

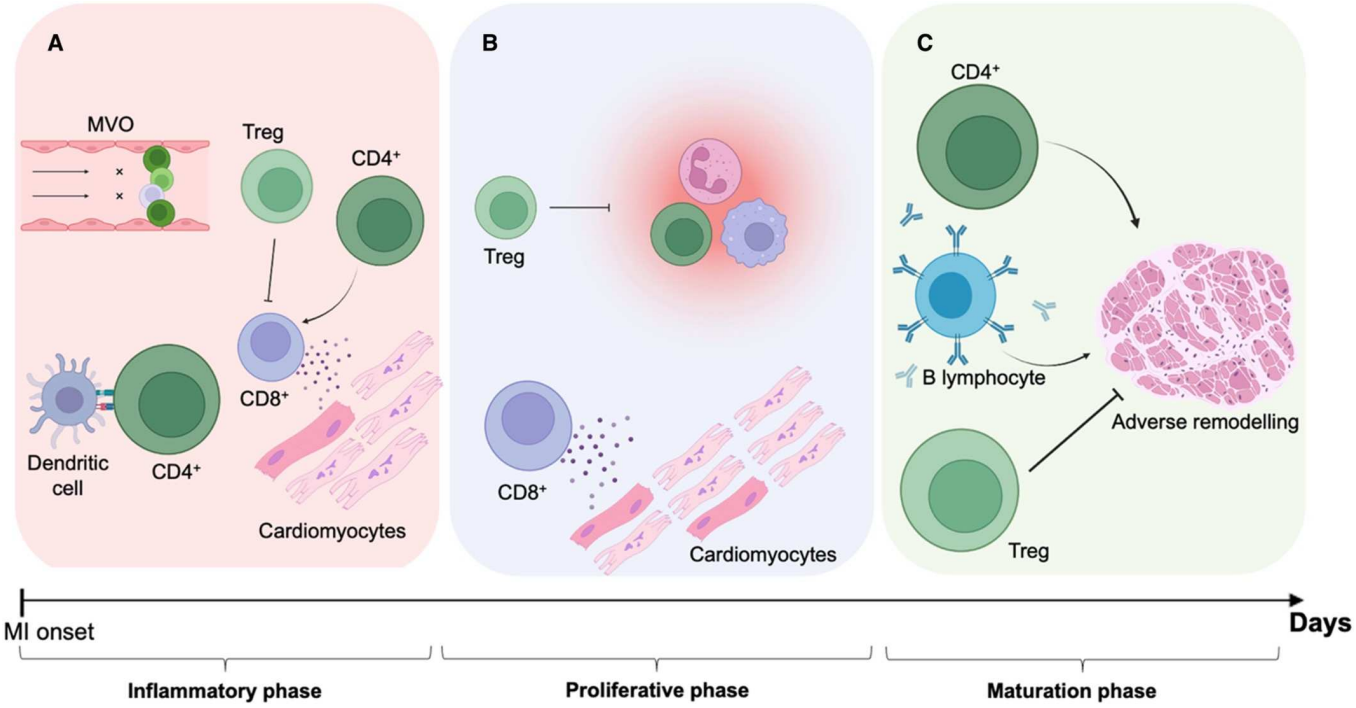


**Figure 6 | Temporal dynamics of lymphocyte infiltration and function after myocardial infarction and reperfusion**

**A**, Immediately following reperfusion, lymphocytes aggregate in the microvasculature and cause MVO, aggravating ischemia/reperfusion injury. Concurrently, dendritic cells also prime the adaptive, antigen-specific immune response by presenting cardiac autoantigens to CD4+ T lymphocytes. In the later stages of the inflammatory phase, CD8+ T lymphocytes impair healing by releasing cytotoxic enzymes, an effect that may be amplified by CD4+ T lymphocytes. However, Tregs can inhibit these detrimental actions and limit cardiac damage. **B**, Throughout the proliferative phase, CD8+ T lymphocytes secrete cytotoxic enzymes while Tregs promote the resolution of inflammation. **C**, In the late maturation phase, the adaptive immune response mounts an autoantigen-specific response involving T and B lymphocytes causing inflammation that contributes to adverse left ventricular remodeling. This detrimental action is opposed by Tregs. CD indicates cluster of differentiation; MI, myocardial infarction; MVO, microvascular obstruction; and Treg, regulatory T lymphocyte. Reproduced with permission from 'Impact of Reperfusion on Temporal Immune Cell Dynamics After Myocardial Infarction'[30].

### 3.5 Cardiac protection and healing mediated by inflammation

Inflammation is a general response to injury and serves important functions in homeostasis, functional and structural integrity of tissues and healing.[61] In the context of myocardial infarction, inflammation is critical for the maintenance of cardiac function by supporting the development of a robust myocardial scar at the site of injury that

resists wall pressure and prevents cardiac rupture. Initial reparative mechanisms are induced by the release of mediators from injured and injury-responsive cells after myocardial necrosis.[23] Those mechanisms involve the release of IL-2 and IL-10, which regulate T-cell and macrophage interaction to promote pro-reparative mechanisms of macrophages.[23] In addition, IL-4 and IL-13, derived from type 2 helper T-cells (Th2), is involved in protective monocyte/macrophage differentiation and polarization.[23,62] T-cell activated monocytes/macrophages produce and secrete a variety of mediators such as growth factors, fibronectin, TGF- β or various other cytokines.[23] Interestingly, those protective effects mediated by certain classes of T-cells may also involve autoreactivity, a hallmark of many autoimmune disease which can also foster tissue repair, is mediated predominantly by myosin heavy chain-derived antigen presentation to $CD4^+$ T cells of mediastinal lymph nodes, which upon antigen stimulation require a pro-reparative Treg phenotype.[63] As described above, $Ly6C^{low}$ $Ccr2^-$ monocytes or M2 macrophages mediate reparative functions, for example by releasing growth factors or adaptive cytokines such as IL-10.[46] However, it should be noted that a large amount of data, such as scRNA-Seq experiments, indicate a spectrum of monocyte/macrophage states, rather than the frequently used M1/M2 or $Ly6C^{high/low}$ $Ccr2^{+/-}$ classification.[46] Caution needs to be taken to attribute adaptive effects to a specific immune cell population. Many inflammatory elements regulate both adaptive and maladaptive functions. As an example, while inhibition of $CD8^+$ cells is associated with improved cardiac function and overall survival in mice, it also results in poor scar formation and higher incidence of cardiac rupture.[64] As described above for corticosteroids, broad anti-inflammatory strategies, such as the strategy used in this thesis, may not be associated with an overall beneficial effect due to the 'off-target inhibition' of protective mechanisms of inflammation involved in scar formation, revascularization and healing and ultimately increase the risk of cardiac rupture in

humans. Similar complications occurred in the context of myocardial infarction after non-steroidal anti-inflammatory drug applications, which pose additional risks such as increased atherothrombotic and cardiorenal risk in patients with known coronary artery disease.[23,65,66] Thus, strategies that preferentially target maladaptive aspects of cardiac inflammation, rather than broad untargeted anti-inflammatory therapies, are likely to have more success in clinical application. The strategy used in this manuscript, transient inhibition of an mTORC1-dependent translationally regulated inflammatory network that controls monocyte infiltration to the myocardium, which is described in more detail below, will likely also mediate unwanted untargeted anti-inflammatory functions. mTORC1 inhibitors are used clinically as immunosuppressants that are proposed to function at least in part by inhibiting T-cell activation and proliferation.[67] While there is evidence for an acute 'overshooting inflammatory burst' that increases cardiac injury early after reperfusion, which might be limited by the transient pharmacological approach used by this study, future more targeted strategies against the translational regulation of inflammation may improve cardiac function yet further and provide a better safety profile.

### 3.6 Acute inflammatory response after myocardial infarction and reperfusion

Inflammation begins immediately in the culprit lesion by the release of damage-associated molecular patterns and cytokines from injured cardiac cells, as well as polymorphonuclear neutrophil, monocyte and lymphocyte activation and infiltration, further increasing local release of pro-inflammatory mediators, such as IL-6.[23,68] This pro-inflammatory cytokine release is further enhanced by reperfusion.[69] As described in more detail above, activated neutrophils release granule enzymes and extracellular traps, inflammasomes become activated, pro-inflammatory monocytes infiltrate the heart and differentiate to macrophages with inflammatory properties, which is in part

regulated by T-cells. All of those inflammatory responses mediate some immediate maladaptive aspects by causing further cell death in viable tissue, especially the border zone, but also impair long-term cardiac function by inducing adverse myocardial remodeling.[23] Some clinical trials that examined the inhibition of mediators of early inflammation have shown promising initial results, however with limited effect size of the overall amount of cardioprotection and significant differences in outcome based on the treatment regime, study population and anti-inflammatory compound.[23,70–78] Yet, no breakthrough clinical success targeting the early inflammatory response has been achieved so far and the task remains to identify an effective and safe agent, its optimal dose, timing, and duration of administration for clinical usage.[23]

### 3.7 Continuous residual inflammatory risk after myocardial infarction

After myocardial infarction, continuing inflammatory activity may impair patient outcome by local inflammatory processes that damage cardiac tissue, as well as by increased atherosclerotic plaque progression and elevated risk for future events such as recurrent myocardial infarction.[23] This concept is often referred to as 'residual inflammatory risk' and it has been proposed that targeting chronic inflammation after myocardial infarction may improve patient outcome. It has been consistently shown that myocardial infarction increases atherosclerosis and future cardiovascular events, which is mechanistically linked to a systemic inflammatory response that liberates progenitor cells from bone marrow niches that results in a sustained boost of monocyte production and increased monocyte recruitment to atherosclerotic lesions.[79] Two large clinical trials confirmed the beneficial effects of chronic anti-inflammatory therapy using the human monoclonal antibody targeting interleukin-1β – Canakinumab[80], or low-dose colchicine[81]. While those trials validated the involvement of chronic inflammation in future cardiovascular events that may be targeted by pharmacological approach, both

trials also reported increased incidences of severe infection with chronic anti-inflammatory treatment.[80,81] Both studies could not demonstrate reduced cardiovascular or all-cause mortality.[80,81]

In summary, a large number of studies point towards the potential of anti-inflammatory therapy for the attenuation of cardiac injury after myocardial infarction. However, many aspects of the regulation of cardiac inflammation in response to myocardial infarction, such as the precise dynamics of inflammation, its mediators and their individual contribution to adaptive and maladaptive responses, the optimal treatment target, initiation timepoint or duration of treatment, remain incompletely defined, which currently hinders routine anti-inflammatory treatment in clinical practice. Some recent insights indicate that those treatment strategies should be initiated early to target the early inflammatory burst, followed by continued anti-inflammatory treatment to inhibit residual inflammatory risk and specifically target inflammatory pathways that are primarily involved in adverse aspects of inflammation.[23] Especially patients with large infarcts might profit from anti-inflammatory therapies, due to their higher inflammatory burden.[23]

The present study highlights some of these aspects and describes a novel layer of translational regulation of inflammatory gene expression in response to myocardial infarction and reperfusion. It provides insights into the functional significance and molecular mechanisms of this pathway and demonstrates how it can be transiently targeted to improve cardiac function in mice. However, further aspects need to be addressed before this concept can be translated into clinical application, which will be elaborated further in the discussion.

### 3.8 Translational regulation of gene expression

Cells and tissues react to changes of their environment with altered gene expression to adapt to the new condition to maintain homeostasis.[82] Gene expression is regulated by a complex layer of pathways that can react rapidly to induce transient or long-lasting effects that influence cell behavior.[82] Those pathways involve epigenetic and transcriptional changes, but also involve many post-transcriptional regulatory networks, such as translation, RNA or protein modifications, transport, or degradation.[82] In general, many different cell types act in collaboration to produce effects that can either affect small cellular compartments, howl tissues or even the overall organism. Traditionally, gene expression has been studied extensively at the level of transcription. In comparison, other pathways that regulate gene expression have been studied in less detail, partly due to the technical difficulties in studying these mechanisms. However, those pathways may be of equal importance for the control of gene expression and adaption to changing environments.[82] Some studies indicate that those posttranscriptional regulatory networks become especially important during phases of cellular stress to determine cellular protein levels.[83] For example, translational mRNA regulation has been consistently shown to be better correlated to cellular protein levels compared to transcription in the heart.[83–85]

To study gene expression, sequencing approaches are often used to examine genes, RNA or proteins. Ribosome profiling (Ribo-Seq), which is based on deep-sequencing of ribosome-protected fragments has been applied to a variety of disease states to identify novel or alternatively translated genome regions, to quantify translational efficiency or to reveal new insights into the translational process itself.[83] The Völkers lab previously combined a ribosome-tagging approach with ribosome profiling, to enable cell-type quantification of translation changes of gene expression *in vivo*.[83] Specifically, Rpl22, a core protein of the large ribosomal subunit, is genetically

tagged with hemagglutinin in mice (Ribo-tag). Crossing Ribo-tag mice with mice that express Cre recombinase under the control of a cell-type specific promotor allows to selectively tag ribosomes of a specific cell-type in mice.[83] Those ribosomes can be purified from whole tissue lysates by a hemagglutinin antibody-mediated pulldown. Using those specific ribosomes and their bound mRNAs as input for ribosome profiling allows to define a snapshot of translational activity of a cell-type of interest in a complex tissue. This study used this technique to investigate translational changes that occur in response to ischemia/reperfusion in mice, as described in further detail in the results section.

### 3.8.1 Canonical eukaryotic translation initiation

Translation of mRNA into protein can be divided into three phases – initiation, elongation and termination, which is followed by ribosome recycling.[86] During initiation a ribosome is positioned at the selected initiation codon. To accomplish this, the small (40S) ribosomal subunit becomes activated to form the 43S pre-initiation complex, which is directed towards the 5´ cap of an mRNA during canonical cap-dependent translation initiation and scans it in 5´ to 3´ direction until the initiation codon AUG is identified.[86] Once the small ribosomal subunit is positioned at the selected initiation codon, subsequent joining of the large (60S) ribosomal subunit to the position results in the formation of the translation competent 80S initiation complex.[86] This process is assisted by a large number of initiation factors, which is described in further detail below. During elongation, repetitive cycles of codon recognition by charged tRNAs, peptide bound formation to elongate the translated polypeptide and translocation of the ribosome to the next codon are repeated.[86,87] Those steps are controlled and facilitated by elongation factors. Termination is the process of releasing the polypeptide from the ribosome upon reaching a stop codon.[86,88] This process is mediated by

release factors. Like initiation, elongation and termination are regulated processes that influences translation and gene expression. While all three steps are critically regulated to determine the quantity of translation of a selected subset of mRNAs, dependent on the current cellular need, the strongest regulation appears to occur at the initiation step.[86,89] As this thesis specifically investigated the regulation of canonical translation initiation via the eukaryotic initiation faction (eIF) complex eIF4F in response to ischemia and reperfusion in cardiomyocytes, it will proceed to further introduce mechanisms of canonical translation initiation. For further information on non-canonical initiation, elongation, termination and other regulatory elements of translation, readers are referred to current reviews of those topics.[89] Translation initiation describes the process of positioning an elongation-competent 80S ribosome at the initiation site (Figure 7). It consists of two major steps, the formation of the 48S initiation complex positioned at the initiation codon, which forms on most mRNAs via a 5´ to 3´ scanning mechanism, and the joining of the 60S subunit.[90] Before participating in a new round of translation, 40S and 60S ribosomal subunits are separated and made available either by ribosome biogenesis or the recycling of 80S ribosomes that are released from an mRNA after termination.[90] Recycling of the 80S ribosome and its dissociation into its subunits is supported by release factors, the initiation factors eIF3, eIF1 and eIF1A, that remain bound to the free 40S subunit to prevent re-association with 60S subunits, as well as the recycling factor ABCE1.[90] Those initiation factors that are recruited to the 40S ribosome during recycling later form the 43S complex, which consists the 40S ribosomal subunit, eIF3, eIF1, eIF1A, eIF5, and the ternary complex consisting of the trimeric eIF2, the initiator methionyl tRNA and GTP.[86,90] Despite of participating in ribosome recycling, each of those initiation factors conducts essential functions during the first steps of translation initiation.

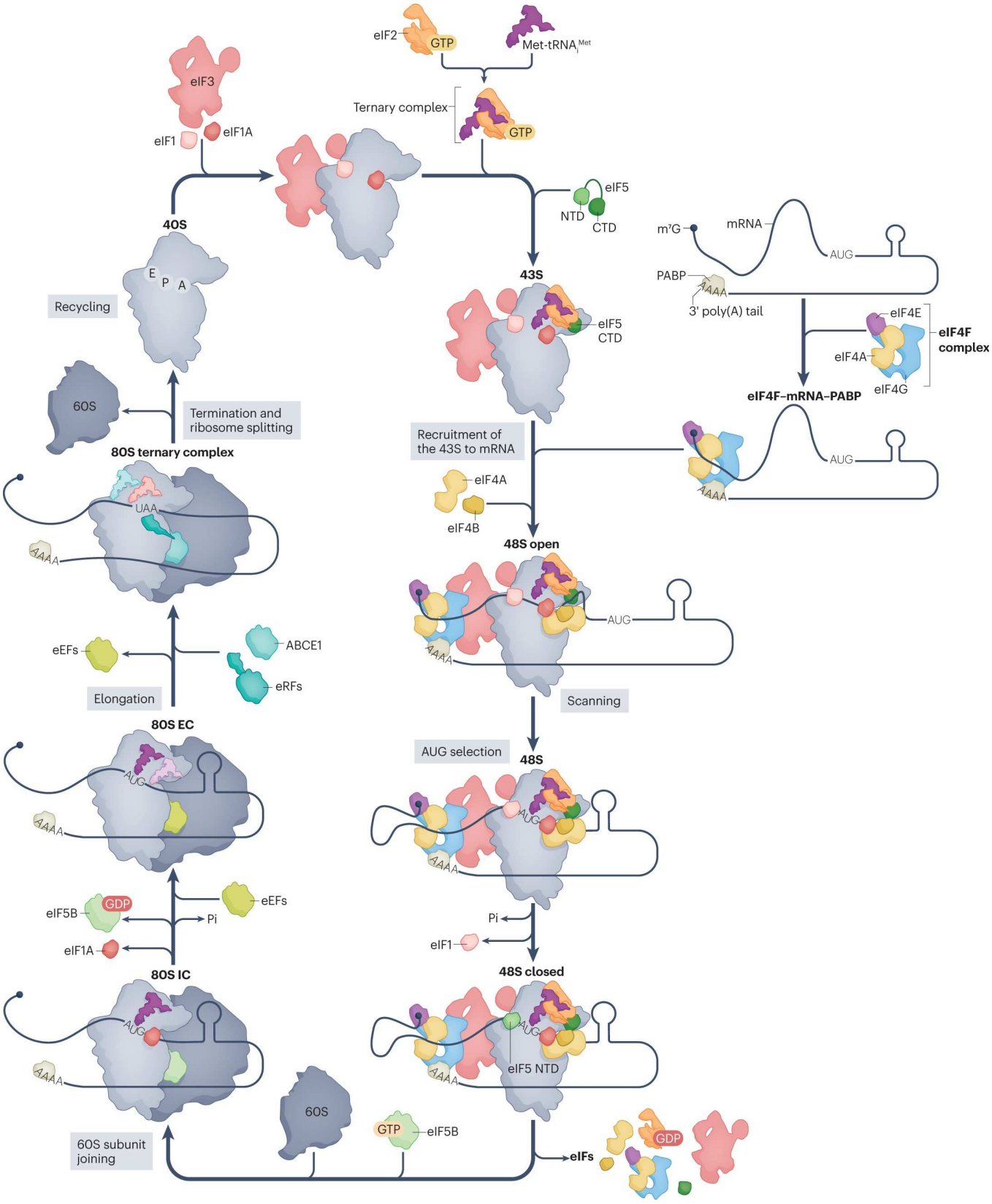


**Figure 7 | Eukaryotic translation initiation**

Translation initiation starts with the binding of eukaryotic translation initiation factor 1 (eIF1), eIF1A and eIF3 to the 40S small ribosomal subunit (top left and clockwise). eIF5 and a ternary complex of eIF2, guanosine 5′-triphosphate (GTP) and the methionine initiatior tRNA (Met-tRNAiMet) binds to this complex to form a 43S translation pre-initiation complex (43S). Once

assembled, the 43S is recruited to the mRNA to form the scanning-competent 48S complex (48S open). The activation of mRNA by the cap-binding complex eIF4F is crucial for recruitment. eIF4F and polyadenylate-binding protein (PABP) bind to the mRNA's 5′ end and poly(A) tail, respectively, selecting the appropriate mRNA for the recruitment. During the scanning of the 5′ untranslated region (UTR) of mRNA, eIF5 interacts with eIF2 and accelerates the hydrolysis of eIF2-bound GTP (not shown). Start-codon selection triggers the release of eIF1 and inorganic phosphate (Pi) from the complex. The amino-terminal domain (NTD) of eIF5 occupies the position vacated by eIF1 near the P site of the ribosome. eIF2–GDP has a lower affinity for Met-tRNAiMet; therefore, the release of Pi triggers the release of eIF2–GDP and eIF5, as well as eIF3 and eIF4 factors. The release of eIF2–GDP allows the binding of eIF5B, which promotes joining of the 60S large ribosome subunit and formation of the 80S initiation complex (80S IC). Formation of the 80S IC triggers the hydrolysis of eIF5B-bound GTP and the release of eIF1A. Following the release of eIF1A, eIF5B undergoes a conformational change that places the aminoacylated end of the Met-tRNAiMet in the peptidyl transfer centre of the ribosome (not shown). The release of eIF5B marks the end of translation initiation and the beginning of elongation (80S EC). During elongation (not shown), eukaryotic elongation factor 1A (eEF1A)–GTP delivers the aminoacylated tRNA into the A site of the ribosome. Following the release of eEF1A–GDP and formation of the peptide bond, eEF2–GTP promotes the translocation of the tRNA from the A site to the P and E sites of the ribosome. The release of eEF2–GDP and the deacylated tRNA from the E site allows a new cycle of elongation. Translation termination by eukaryotic release factors (eRFs) occurs when a stop codon (for example, UAA) is reached and recognized by eRFs. ATP-binding cassette sub-family E member 1 (ABCE1) binds to the 80S termination complex and stimulates peptidyl-tRNA hydrolysis by eRF1. In addition, ABCE1 is crucial for recycling by splitting the 80S into the 40S and 60S ribosomal subunits. Following the 80S splitting, the mRNA and tRNA are removed from the 40S by recycling factors (not shown), which allows the 40S to become available for a new round of translation. CTD, carboxy-terminal domain; m7G, 7-methylguanosine. Reproduced with permission from Querido et al.[89]

The trimeric eIF2 complex forms the ternary complex together with Met-tRNA$_i$ (initiator methionyl-tRNA) and GTP. It facilitates the binding to the ribosomal 40S subunit to form the 43S complex.[90]

eIF2B ist the guanosine nucleotide exchange factor that promotes GDP–GTP exchange on eIF2.[90]

eIF3, a large multi-subunit complex consisting of at least 12 subunits and one transiently associated element eIF3j, which is not considered a bona fide subunit of the complex by some authors, is involved in many steps of translation.[90,91] Among the several functions of the eIF3 complex are serving as a scaffold and binding the 40S

subunit, eIF1, eIF5; promoting the binding of eIF2–GTP–Met-tRNA$_i$ to 40S subunits; establishing the interaction with the eIF4F complex by binding to eIF4G and thus promoting the interaction of the 43S complexes with mRNA and subsequent scanning; as well as assisting in ribosome dissociation and the prevention of re-joining of the 40S and the 60S subunits.[90,91]

eIF1 stimulates the interaction of the 40S subunit to the ternary complex and later ensures the fidelity of initiation codon selection and promotes ribosomal scanning, a process that is promoted by eIF1A.[90]

eIF5 is a GTPase-activating protein that specifically hydrolyses the eIF2-bound GTP on recognition of the initiation codon, which results in dissociation of most initiation factors from the complex to allow joining of the 60S ribosomal subunit.[90]

In parallel to 43S preinitiation complex formation, other initiation factors that center around the trimeric eIF4F complex activate to-be-translated mRNAs. During canonical cap-dependent translation initiation, the trimeric eIF4F complex, which consists of eIF4E, eIF4G and eIF4A, binds mRNAs together with eIF4B to unwind the mRNA´s cap-proximal region in an ATP-dependent manner.[90] This results in the formation of an mRNA loop in which both the 5´ cap and the 3´ poly-A tail of the mRNA are bound to the eIF4F complex with assistance of the poly-A-binding protein PABP (Figure 8).[90]

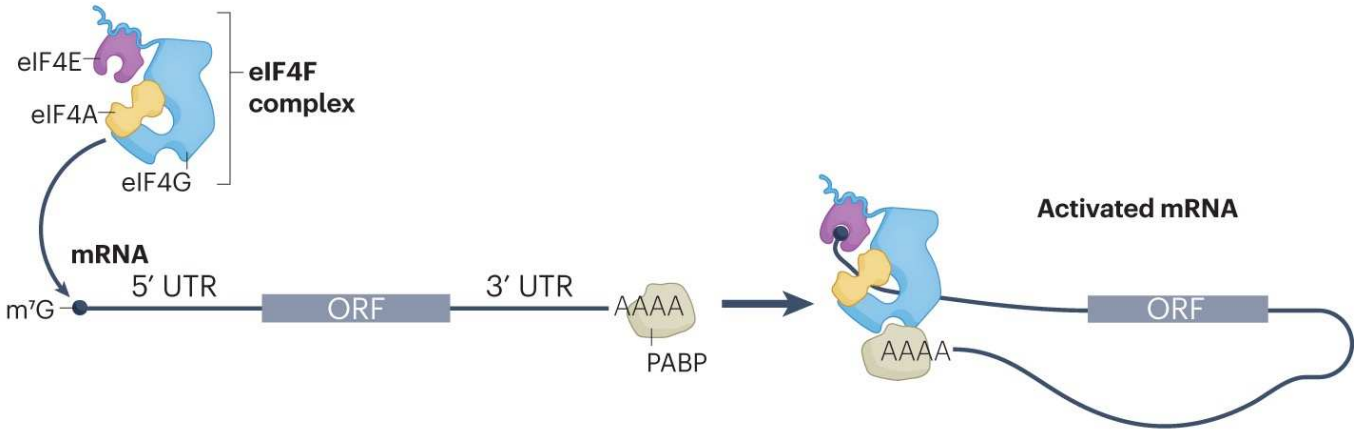


**Figure 8 | The eukaryotic eIF4F complex**
The eukaryotic translation initiation factor 4F (eIF4F) complex consist of the cap-binding protein eIF4E, the RNA helicase eIF4A and the scaffold protein eIF4G. The illustration shows the recruitment of eIF4F to mRNA through eIF4E–7-methylguanosine (m7G) cap and eIF4G–polyadenylate-binding protein (PABP)–poly(A) interactions. Adapted with permission from Querido et al.[89]

Specifically, eIF4E binds the $m^7$GpppG 5′ terminal cap' structure of mRNA.

eIF4G, a large scaffolding protein binds eIF4E, eIF4A, eIF3, PABP, mRNA and other regulating elements and thus serves as a central interaction mediator between the 43S preinitiation complex with the 40S subunit, eIF4F and the mRNA. In addition eIF4G regulates the helicase activity of eIF4A.[90]

eIF4A is an ATP-dependent RNA helicase that unwinds the secondary structure of the mRNA 5' UTR to render it more accessible to ribosomal binding and subsequent translation.[90] For the scanning of mRNAs with long and highly structured 5′ UTRs, other helicases, such as mammalian DHX29 and DDX3 may be required.[89] eIF4A is present in much larger quantities over other initiation factors in the cell and recent studies indicate that eIF4A has additional functions in translation initiation other than eIF4F-dependent mRNA 5´ unwinding.[89,92–94]

eIF4B is an RNA-binding protein which regulates and enhances the helicase activity of eIF4A. eIF4B bind to the eIF3 complex through the eIF3A subunit and thus serves in recruitment of the 43S preinitiation complex to the mRNA.[90]

eIF4H is homologous to a fragment of eIF4B and enhances the helicase activity of eIF4A.[90] By itself, eIF4A displays weak ATP-dependent helicase activity that is strongly enhanced through a functional interaction with eIF4H or eIF4B. Thus, eIF4H or eIF4B are necessary for efficient unwind of the mRNAs 5´ UTR secondary structures to promote the efficient scanning of the ribosome for the start codon.[95]

eIF5B is a ribosome-dependent GTPase that mediates ribosomal subunit joining and displacement of several initiation factors. Upon hydrolysis of eIF5B it is released together with eIF1A to leave a elongation competent 80S ribosome at the start codon.[90]

In summary, translation regulation of gene expression is primarily regulated at the initiation step. Initiation describes the process of forming an elongation-competent 80S ribosome at the initiation site, which is mediated by 43S formation, eIF4F-dependent activation of a to-be-translated mRNA, loading of the 43S complex to the mRNA to form the 48S complex, scanning in 5´ to 3´ direction to identify the start codon, and joining of the 60S ribosomal subunit to form the final 80S ribosome, positioned at the start site.[89,90] This study specifically made use of different genetic and pharmacological strategies to inhibit the eIF4F complex to suppress translation initiation during cardiac reperfusion.

### 3.9 The mechanistic target of rapamycin complex 1 (mTORC1)

Regulation of mRNA translation occurs through different signaling pathways that couple information about the cellular environment with subsequent responses to maintain cell homeostasis.[96] A key signaling pathway that controls both the overall amount of translation as well as the selective translation of specific transcripts is

controlled by the kinase mechanistic target of rapamycin (mTOR).[97] mTOR functions as a serine/threonine protein kinase that belongs to the family of phosphatidylinositol 3-kinase-related kinases.[97] mTOR serves as the core catalytic component of two protein complex, known as mTOR complex 1 and 2 (mTORC1/2). Among the canonical functions of mTORC1 is the regulation of mRNA translation and cell size as well as autophagy, and metabolism. In contrast, mTORC2 is involved in a variety of cellular functions, the most cited being survival, metabolism, proliferation, cytoskeletal rearrangements and migration.[97–99] Mechanistically, mTORC1 serves as a cellular hub that integrates information about the availability of nutrients, growth factors, energy, oxygen and stress to promote anabolism and protein synthesis during favorable conditions by phosphorylating specific downstream targets, including the eukaryotic translation initiation factor 4E-binding proteins (4EBP), ribosomal protein S6 kinase beta-1, also known as p70 S6 kinase, LARP1 and others.[97]

Eukaryotes express at least three different isoforms of 4EBPs, namely 4EBP1, 4EBP2 and 4EBP3. All three 4EBP isoforms bind eIF4E to prevent its interaction with the mRNA cap and thus eIF4F formation (Figure 9).[100] mTORC1 activity results in hyperphosphorylation of 4EBPs, which disrupts their interaction with eIF4E, liberating eIF4E to interact with eIF4G and form the functional eIF4F complex.[97] The regulation of the 4EBP-eIF4E interaction is considered a central element of mTORC1-dependent regulation of translation.[100] As all three 4EBP isoforms are highly homologous and the differences between the three isoforms are largely unknown. An antibody targeting 4EBP1, which is likely to also interact with 4EBP2 and possibly 4EBP3, was used in this study. Thus, conclusions drawn for 4EBP1 by this thesis may also apply to the other 4EBP isoforms.

The serine/threonine kinase p70 S6 kinase serves as a second node of mTORC1-dependent control of translation.[97] p70 S6 kinase is bound to eIF3 in its

inactive state and in response to mTORC1-dependent phosphorylation becomes released to phosphorylate a number of its own downstream targets.[101]

Some of the many phospho-targets of p70 S6 kinase include ribosomal protein S6, which is involved in translation, proliferation and cell growth, eIF4B and PDCD4, which regulate eIF4A activity, eIF4G (potentially indirectly) or eEF2 kinase, involved in elongation.[97,102,103] While in this study the phosphorylation state of ribosomal protein S6 was used in some instances as an indicator of mTORC1 activity, it should be noted that ribosomal protein S6 can also be phosphorylated by other kinases at this site, thus it is possible that the phosphorylation of ribosomal protein S6 under these conditions was not necessarily mediated by p70 S6 kinase.[104]

Inhibition of mTORC1 strongly suppresses translation, which depends on the combined suppression of mTORC1-mediated effects on the cellular translation apparatus. However, mTORC1 appears to preferentially control the translation of a selected subset of mRNAs. Those mRNAs that are preferentially translated during mTORC1 activation contain elements in their 5´ UTR that are known as TOP- or TOP-like motifs, a process that is controlled by mTORC1-mediated phosphorylation of 4EBP1 and LARP1.[97,100,105,106] In general, mTORC1 activity thus leads to activation of the translational apparatus and increased translation of TOP motif-containing mRNAs. Since many mRNAs containing TOP motifs encode ribosomal proteins, it is assumed that sustained mTORC1 activity leads to a general increase in ribosomes and thus further increases cellular translational activity.[97]

### 3.9.1 mTORC1 as a regulator of cardiac function

mTORC1 activity is essential for cardiac function and several of the effector proteins regulated by mTORC1 have been associated with both adaptive and maladaptive functions in the cardiac context.[107–109] In general, mTORC1 activity was

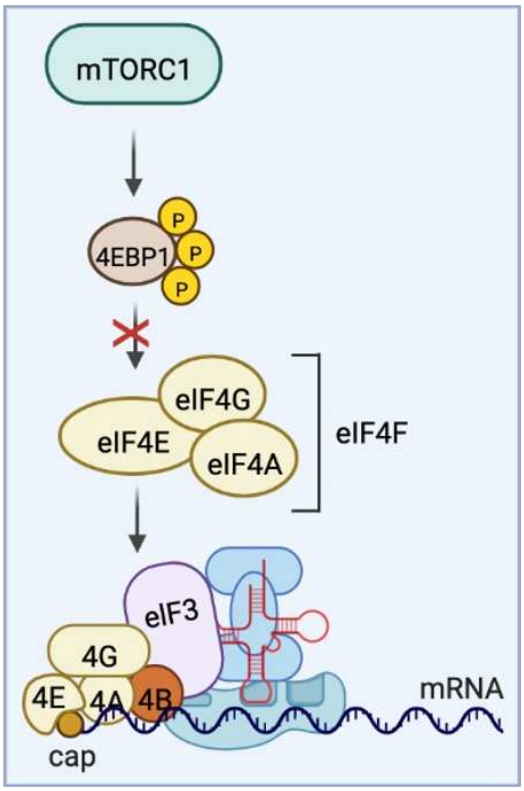


**Figure 9 | Regulation of cap-dependent translation initiation by mTORC1**
mTORC1 controls cap-dependent translation via its regulatory phosphorylation of 4E-binding proteins (4EBP). In its hypophosphorylated state, 4EBPs bind eIF4E and prevent its interaction with eIF4G and the formation of the eIF4F complex. Upon phosphorylation by mTORC1, 4EBPs are released from eIF4E, thus promoting formation of eIF4F and translation initiation. Illustration made in ©BioRender - biorender.com.

shown to become activated in response to a variety of pathological cardiac conditions in animal models as well as in diseased human hearts.[83,85,107] In addition, the activity of mTORC1 correlates with adverse cardiac outcome in cardiac pathology such as nonischemic dilated cardiomyopathy.[110] Currently it remains controversial how and when the mTORC1 pathway should be targeted for the treatment of heart disease.[107,111,112] While complete gene inactivations of essential mTORC1 components are lethal, numerous studies have demonstrated that partial inhibition of the mTORC1 pathway is protective in different animal models of heart disease.[107,109,112–117] These preclinical studies prompted exploratory off-label testing in

humans, which showed promising initial results.[74,118,119] However, systemic inhibition of the mTORC1 pathway is associated with adverse side effects, partly limiting its clinical application.[120] Nevertheless, mTORC1 is considered a highly attractive target for many different disease, including cardiac disase.[98,121] Previous studies have shown that inhibition of mTORC1 protects against ischemic damage and I/R injury.[114,115,122,123] However, the mechanistic basis of the cardioprotective effect of pharmacological mTORC1 inhibition and whether it is mediated by translational regulation of gene expression remain to be fully elucidated. In addition other studies indicated that long-term mTORC1 inhibition may be maladaptive in the context of ischemia/reperfusion, highlighting the importance of treatment duration for targeting the mTORC1 pathway.[111]

### 3.9.2 mTORC1-dependent regulation of immune responses

Pharmacological mTORC1 inhibitors such as rapamycin (sirolimus) or everolimus are widely used drugs with immunosuppressive properties due to their broad spectrum of inhibitory effects on immune cells. As such, they are used clinically as immunosuppressants after solid organ transplantation.[124] While initially, mTORC1 inhibitors were thought to mediate their immunosuppressive actions by inhibiting T cell proliferation, more recent studies identified the complex nature of anti-inflammatory properties of mTORC1 inhibitors that appear to be related to the inhibition of drastic metabolic, translational and proliferative responses of immune cells that are required for their activation.[125–128] In general, the activation of many immune cells goes along with a stimulation of protein synthesis and strong adaptions of gene expression, regulated at least in part by translational mechanisms that involve the mTOR pathways.[126,129] In response to myocardial infarction, mTORC1 appears to shift the landscape of cardiac macrophages towards a pro-inflammatory phenotype.[130–132]

However, the underlying mechanisms of mTORC1-dependent regulation of the cardiac inflammatory response remain largely unknown.

### 3.10 Objectives

As outlined in the previous chapters, numerous studies suggest that an inflammatory response of the heart that occurs after myocardial infarction and reperfusion regulates cardiac function. Maladaptive aspects of cardiac inflammation may serve as a target for interventions to improve outcomes. However, the complex network of immune responses remains incompletely understood, knowledge of which is essential for translating efficient therapies into the clinic that sparse adaptive elements of inflammation while targeting maladaptive pathways. The mTORC1 pathway regulates key functions of cardiac inflammation. This study examines how mTORC1-dependent translational control is involved the cardiac inflammatory response after myocardial infarction. Specifically, the following points are addressed in this study:

1. How is mTORC1 activity and translation regulated after ischemia and reperfusion in the heart?
2. Are changes of translational activity in response to reperfusion controlled by the mTORC1 pathway?
3. Is the cardiac inflammatory response regulated by mTORC1-dependent control of translation?
4. What are mechanisms of translational regulation of cardiac inflammation mediated by the mTORC1 pathway?
5. What are the consequences of inhibiting mTORC1-dependent translation after reperfusion on cardiac inflammation and function?

# 4 Methods

The methods section is based on and replicated from the research article 'Transient inhibition of translation improves cardiac function after ischemia/reperfusion by attenuating the inflammatory response'[133], written by me:

"

## 4.1 Cultured cardiomyocytes

Neonatal rat ventricular cardiomyocytes (NRCMs) were isolated from one to two-day old animals via enzymatic digestion and purified by Percoll density gradient centrifugation. Cardiac myocytes were then plated at a density of 0.5 X $10^6$ cells per well on 34.8 mm plastic plates that had been pre-treated with 0.1% gelatine for 1 h at 37 °C (cat# F1141, Sigma-Aldrich) and then cultured in DMEM/F12 1:1 (cat# 11330032, Thermo Fisher Scientific), containing 10% fetal bovine serum, 100 units/mL of penicillin, 100µg/mL streptomycin and 292 µg/ml glutamine (cat# 10378016, Thermo Fisher Scientific). Adult rat ventricular myocytes (ARCM) were isolated from adult male rats via enzymatic digestion. Cells were plated in Medium 199 (cat# M7528, Sigma-Aldrich) supplemented with 100 units/mL of penicillin, 100µg/mL streptomycin and 10µg/mL laminin (cat# L2020, Sigma-Aldrich). After one hour, media was changed to ischemia medium (see below) and subjected to the respective treatments. hiPSC-CM differentiation was performed according to Siede et al.[134]

## 4.2 Simulated ischemia/reperfusion *in vitro*

Cells were cultured as described above. Cells were washed twice with PBS and medium was changed to ischemia medium: low-nutrient DMEM without D-glucose, sodium pyruvate, HEPES, L-glutamine and phenol red (cat# A1443001, Thermo Fisher

Scientific), supplemented with 0.5% dialyzed fetal bovine serum (cat# A3382001, Thermo Fisher Scientific), 100 units/ml penicillin, 100µg/ml streptomycin, and 292 µg/ml glutamine. Cells were then incubated in a hypoxia incubator at 37°C, 5.0% $CO_2$ and 0.2% $O_2$ for one to 24 hours. For subsequent simulated reperfusion, medium was changed to DMEM/F-12 supplemented with 10% fetal bovine serum and 100 units/mL of penicillin, 100µg/mL streptomycin and 292 µg/ml glutamine, followed by incubation in an incubator at 37°C, 5.0% $CO_2$ and 21% $O_2$. Control cells were cultured in DMEM/F-12 supplemented with 10% fetal bovine serum and 100 units/mL of penicillin, 100µg/mL streptomycin and 292 µg/ml glutamine at 37°C, 5.0% $CO_2$ and 21% $O_2$ for as long as the longest ischemia/reperfusion timepoint.

### 4.3 Laboratory animals

All animal experiments were approved by the institutional animal care and use committee of Heidelberg University. All experiments were performed in 10- to 12-week-old male or female C57BL/6N mice. All animals were fed ad libitum and were housed at Heidelberg University in a temperature- and humidity-controlled facility with a 12-h light-dark cycle. Cardiomyocyte-specific Ribo-tag mice were previously described.[83] Briefly, Ribo-tag mice (JAX ID 011029) were bred to αMHC-Cre mice to obtain Rpl22-HA-expressing homozygous mice in cardiomyocytes. Dosing studies were performed with 6 mg/kg rapamycin or 10 to 100 mg/kg 4EGI-1. In I/R-operated mice receiving drug treatment, mice received a first dose of 6 mg/kg rapamycin or 50 mg/kg 4EGI-1 30 minutes before reperfusion and a second dose of 2 mg/kg rapamycin or 50 mg/kg 4EGI-1 24 hours after surgery. Control mice in these experiments received equal amounts of vehicle at the same time points.

### 4.4 Ischemia/reperfusion and myocardial infarction surgery *in vivo*

Animals were randomly assigned to each experimental group. Ischemia was induced by knotting a suture over a PE-10 tube which was placed over the left anterior descending (LAD) coronary artery, thereby compressing the lumen of the artery. Ischemia was maintained for 60 minutes. The first dose of pharmacological inhibitors or vehicle were injected i.p. 30 minutes before reperfusion. For reperfusion, the PE-10 tube was pulled out. Permanent myocardial infarction surgery was performed by permanently ligating the left anterior descending artery according to the procedure described above. Sham surgeries were performed following the same procedures except that the LAD was not ligated.

### 4.5 Puromycin incorporation assay

Changes in the amount of protein synthesis of differentially treated cells were followed by puromycin incorporation. *In vitro* 0.5 µg/ml was added to the culture medium 30 minutes before harvesting the cells. Cells were washed once with ice-cold PBS and then harvested as described above. To assess translation rates *in vivo*, mice were i.p. injected with 50mg/kg puromycin or O-propargyl-puromycin 30 minutes before the animals were sacrificed. O-propargyl-puromycin was detected with the Click-iT Plus OPP Alexa Fluor™ 594 Protein Synthesis Assay Kit according to manufacturer's instructions.

### 4.6 *Ex vivo* ischemia/reperfusion injury

Langendorff heart perfusions were performed according to Byrne et al.[135] Briefly, hearts were isolated from 11-13 week-old male C57Bl/6J mice and perfused in the Langendorff retrograde mode at constant pressure of 60 mmH with Krebs buffer containing (in mmol/L) 128 NaCl, 5.0 KCl, 15 $NaHCO_3$, 1.3 $MgSO_4$, 1.0 $KH_2PO_4$, 2.5

$CaCl_2$, 5.0 glucose, gassed with 95% $O_2$ and 5% $CO_2$. Left ventricular pressure was monitored from a water-filled balloon placed through the left atrial appendage and connected to a Millar transducer (Millar Instruments). The balloon was inflated to achieve an end-diastolic pressure of 7 to 10 mmHg. Hearts were perfused for 20 min of baseline (stabilization) and then subjected to 20 min of global no flow ischemia followed by 40 min of reperfusion. Vehicle (0.011% DMSO) or 4EGI-1 (10 or 25 μM) were introduced to the perfusion buffer 10 minutes prior to the onset of ischemia. After 40 min of reperfusion, hearts were immediately frozen and stored at −80°C.

### 4.7 Serum Troponin T and CK measurement

Twenty-four hours after surgery, the mouse was brought to brief anesthesia with moderate respiratory slowing with isoflurane to allow retrobulbar blood sampling. Heparin-coated capillaries were used for retrobulbar blood sampling. Blood samples were kept on ice and centrifuged for 10 minutes at 1000rcf. 10μl of plasma was taken from the supernatant and diluted 1:30 in PBS. Troponin T and CK analysis was performed at the central laboratory of Heidelberg University Hospital.

### 4.8 Echocardiography

Echocardiography was carried out on anesthetized mice using a Visualsonics Vevo 2100 high-resolution echocardiograph. Anesthesia was administered via a facial mask and maintained by a minimum dose of isoflurane (1.0–2.0%). Echocardiography was performed at a heart rate of 450-550 bpm.

### 4.9 Preparation of tissue lysates

Mice were sacrificed and left ventricles were rapidly excised, washed in PBS and snap frozen in liquid nitrogen. Tissue used for Ribo-Seq and RNA-Seq analysis was washed

in PBS containing 100 µg/ml cycloheximide. Left ventricles were homogenized using a tissue homogenizer in 5 volumes of ice-cold polysome buffer containing 20mM Tris pH 7.4, 10mM MgCl, 200mM KCl and 1% Trition X-100. Tissue used for Ribo-Seq and RNA-Seq analysis was homogenized in polysome buffer containing 20 mM Tris pH 7.4, 10 mM MgCl, 200 mM KCl, 2 mM DTT, 1% Triton X-100, 1U DNAse/µl and 100 µg/ml CHX. For library construction lysates were processed as previously described.[83] For protein analysis via immunoblotting, initial lysates were further diluted with 9 volumes of RIPA buffer containing 20mM Tris-HCl (pH 7.4), 150mM NaCl, 1% Triton X-100, 0.1% SDS, 0,5% Sodium deoxycholate, protease inhibitor cOmplete ULTRA (cat# 05892791001, Roche) and phosphatase inhibitor PhosSTOP (cat# 04906837001, Sigma-Aldrich). RNA was isolated from tissue lysates using TRIzol (cat# 15596026, Invitrogen). To separate the infarct, border zone and remote area a protocol of Zhang et al.[136] was followed. Protein and RNA of the respective regions were isolated similar to whole heart lysates as described above.

### 4.10 Adenoviral and AAV9 generation and usage in NRCMs and mice

pDONR223_EIF4EBP1_WT was a gift from Jesse Boehm & William Hahn & David Root (Addgene plasmid #82206; http://n2t.net/addgene:82206; RRID:Addgene_82206). Human 4EBP1 was cloned into a recipient pAd_CMV_nV5_Dest backbone using the gateway system to generate an adenovirus expressing human WT 4EBP1 (Ad4EBP1). To determine the optimal MOI, a preliminary dose-escalation experiment was conducted with different doses of Ad4EBP1. Ad4EBP1 was added to the culture media for 24h before follow-up treatment was initiated. To obtain AAV9 expressing 4EBP1, human WT 4EBP1 was cloned into a recipient pSSV9 vector under a cardiomyocyte specific TnT promotor (AAV9-4EBP1). To determine the optimal dosage, a preliminary dose-escalation

experiment was conducted with different doses of AAV9-4EBP1. AAV9-4EBP1 was injected into the tail vein of WT mice and follow-up experiments were conducted 2 weeks after i.v. injection to ensure sufficient cardiac expression.

### 4.11 m7GTP pulldown

To enrich mRNA cap associated proteins from cell lysates, agarose beads coupled to 7-Methylguanosine-5'-triphosphate (m7GTP) were used, which mimics the mRNA 5´ cap structure. Cells were washed once with ice-cold PBS and harvested in 600µl NP-40 lysis buffer supplemented with 1x PhosSTOP and 1x protease inhibitor cOmplete ULTRA. Maximum lysate volume of the sample with the lowest protein concentration was taken as input for the following pull-down, to which all other samples were normalized (around 2000 - 3500µg, ~ 500µl lysate). The corresponding input volumes were filled up to 700µl with NP-40 lysis buffer to ensure sufficient rotation of the beads during incubation. 40µl of the lysates were kept as an input control for western blotting to estimate pull-down efficiency. For the following steps, low retention tubes were used. For each sample 50µl of m7GTP agarose beads were used. To equilibrate the beads, they were washed three times with 1 ml cold NP-40 lysis buffer and centrifuged at 500G and 4°C for 3 minutes. After the last washing step, the beads were resuspended 1:2 in cold NP-40 lysis buffer and 150µl of the diluted beads were added to the prepared samples, then they were rotated (10 rpm) over night at 4°C. The next day, the samples were centrifuged at 500 G and 4°C for 3 minutes, the supernatant was discarded, and the beads were washed three times with 1ml cold NP-40 lysis buffer. To separate bound proteins from the beads, 40µl 1x Laemmli Sample Buffer with 10% β-Mercaptoethanol was added to each sample and the samples were cooked at 95°C for 5 minutes. After centrifugation at 500G for 3 minutes, the supernatant was

collected, and a western blot was performed. For each sample, maximal volume of the respective supernatant as well as 30µg of the input control were loaded.

### 4.12 Immunoblotting

Cultured cells were lysed in RIPA Buffer consisting of 50mM Tris pH 7.5, 150mM NaCl, 1% Triton X-100 and 1% SDS, which was supplemented with protease inhibitor cOmplete ULTRA (cat# 05892791001, Roche) and phosphatase inhibitor PhosSTOP (cat# 04906837001, Roche). Tissue lysates were prepared as described above. Lysates were cleared by centrifugation at 4 °C for 10 minutes at 20.000 rcf. Lysate protein concentration was determined using the DC Protein Assay Kit II (cat# 5000112, Bio-Rad) according to the manufacturer's instructions. Equivalent amounts of protein, usually 20-30 µg, were brought up to similar volume, mixed with Laemmli Sample Buffer (Bio-Rad; 161-0747) and 2-Mercapoethanol (cat# M6250, Sigma-Aldrich) and boiled at 95°C for 5 minutes. Samples were separated on SDS-PAGE gels and transferred to Immobilon-P transfer membranes (cat# IPVH00010, Merck Millipore). The following antibodies were used to probe the membranes: eIF4G (cat# 2498, Cell Signaling Technology, 1:5000), eIF4A (cat# C32B4, 2013, Cell Signaling Technology, 1:1000), Phospho-eIF4E Ser209 (cat# 9741, Cell Signaling Technology, 1:1000), eIF4E (cat# 9742, Cell Signaling Technology, 1:5000), Phospho-p70 S6 Kinase Thr389 (cat#9205, Cell Signaling Technology, 1:1000), p70 S6 Kinase (cat# 49D7, 2708, Cell Signaling Technology, 1:1000), Phospho-Akt Ser473 (cat# 9271, Cell Signaling Technology, 1:1000), Phospho-Ribosomal S6 Ser235/236 (cat# D57.2.2E, 4858, Cell Signaling Technology, 1:5000), Ribosomal S6 Ser235/236 (cat# 54D2, 2317, Cell Signaling Technology, 1:1000), Phospho-4EBP1 Thr37/46 (cat# 236B4, 2855, Cell Signaling Technology, 1:5000), 4EBP1 (cat# 9452, Cell Signaling Technology, 1:5000), P-AMPK (cat# 2535, Cell Signaling Technology, 1:1000), AMPK

(cat# 2532, Cell Signaling Technology, 1:1000), Phospho-ERK1/2 Thr202/Tyr204 (cat# 9101, Cell Signaling Technology, 1:5000), Phospho-p38 MAPK Thr180/Tyr182 (cat# D3F9, 4511, Cell Signaling Technology, 1:1000), Phospho-Hsp27 Ser82 (cat# D1H2F6, 9709, Cell Signaling Technology, 1:1000), Ccl2 (cat# 66272-1-Ig, 1B9F7, proteintech, 1:1000), Puromycin (cat# MABE343, Merck Millipore; 1:10,000-50,000), GAPDH (cat# G-9, sc-365062, Santa Cruz Biotechnology; 1:20,000), β-Actin (cat# C4, sc-47778, Santa Cruz Biotechnology; 1:20,000), Ponceau solution was prepared with Ponceau BS (cat# B6008, Sigma Aldrich). All immunoblots were normalized to a loading control. All phosphorylated protein quantifications were first normalized to a loading control and then normalized to the detected levels of the unphosphorylated protein.

### 4.13 Quantitative Real Time PCR

Total RNA was isolated from cultured cardiomyocytes using the Quick-RNA MiniPrep Kit (cat# R1055, Zymo Research) and from tissue using the RNeasy Mini Kit (cat# 74104, Qiagen) according to the manufacturer's instructions. cDNA was generated by reverse transcription using Superscript III First-Strand Synthesis System (Invitrogen; 18080-051). Quantitative Real Time PCR was performed with Maxima SYBR Green/ROX qPCR Master Mix (Thermo Fisher cat# K0222) in a StepOnePlus RT-PCR System (Thermo Fisher). The following primers were used:

Mouse-*Ccl2*-F: CACTCACCTGCTGCTACTCA

Mouse-*Ccl2*-R: TTGAGCTTGGTGACAAAAACTACA

Mouse-*Ccr2*-F: AGGAGCCATACCTGTAAATGCC

Mouse-*Ccr2*-R: ATGCCGTGGATGAACTGAGG

Mouse-*Icam-1*-F: CCCACGCTACCTCTGCTC

Mouse-*Icam-1*-R: GATGGATACCTGAGCATCACC

Mouse-*Il-1β*-F: AGCTGGATGCTCTCATCAGG

Mouse-*Il-1β*-R: AGTTGACGGACCCCAAAAG

Mouse-*Il6*-F: GATGCTACCAAACTGGATATAATC

Mouse-*Il6*-R: GGTCCTAGCCACTGGATCTGTG

Mouse-*mSelectin*-F: TGGTCATCTCCAGAGCCAAT

Mouse-*mSelectin*-R: GCAGTCCATGGTACCCAACT

Mouse-*Pecam-1*-F: CGGTGTTCAGCGAGGTCC

Mouse-*Pecam-1*-R: ACTCGACAGGATGGAAATCAC

Mouse-*Tnf-α*-F: CCATTCCTGAGTTCTGCAAAG

Mouse-*Tnf-α*-R: GCAAATATAAATAGAGGGGGGC

Mouse-*Vcam1*-F: TCTTACCTGTGCGCTAATGAGT

Mouse-*Vcam1*-R: ACTGGATCTTCAGGGAATGAG

Human-*CCL2*-F: CCCCAGTCACCTGCTGTTAT

Human-*CCL2*-R: AGATCTCCTTGGCCACAATG

Human-*HPRT*-F: CCTGGCGTCGTGATTAGTGA

Human-*HPRT*-R: CGAGCAAGACGTTCAGTCCT

### 4.14 Immunofluorescence of mouse heart sections

Immunocytofluorescence of cardiac sections was performed as previously described.[83] Briefly, hearts were retroperfused with PBS at 70 mmHg, arrested in diastole with 60mM KCl, fixed by perfusion for 15 minutes with 10% formalin (Sigma; HT501128), excised and fixed in formalin for 24 hours at room temperature. Fixed hearts were then dehydrated and paraffinized using a HistoCore Pearl and Arcadia H, sectioned and placed on glass slides. For immunofluorescence staining, the sections were deparaffinized and boiled in 10mM citrate buffer (pH 6.0) for 12 min. After cooling, the sections were washed 2x for 5 min with PBS and then treated with TNB blocking

solution (0.5% TSA blocking reagent dissolved in TN buffer (0.1 M Tris-HCl (pH 7.5), 0.15 M NaCl)) for 60 minutes. Sections were stained with antibodies against Troponin T (cat#ab209813, Abcam, 1:300), Phospho-S6 Ribosomal Protein (Ser235/236) (D57.2.2E) XP® Rabbit mAb (Alexa Fluor® 488 Conjugate) (cat#4803, Cell Signaling Technology, 1:200) or Ccl2 (MCP-1 Monoclonal Antibody (2D8), cat#MA5-1704, Invitrogen, 1:200) and co-stained with DAPI. OP-Puromycin (Click-iT™ Plus OPP Alexa Fluor™ 594 Protein Synthesis Assay Kit, cat#C10457, Invitrogen) was used according to the manufacturer's protocol, TUNEL staining (In Situ Cell Death Detection Kit, Fluorescein, cat#11684795910, Roche) was used according to the manufacturer's protocol. The secondary antibody used was Cy3 AffiniPure Donkey Anti-Rabbit IgG (H+L) (cat# 711-165-152, Jackson ImmunoResearch, 1:100).

### 4.15 TUNEL cell death assay

Cardiac sections were prepared as described above. The TUNEL staining was performed according to the manufacturer's protocol (In Situ Cell Death Detection Kit, Fluorescein, cat#11684795910, Roche). For each heart, 10 randomly selected images with an edge length of 488µm were acquired near the infarct area and TUNEL-positive cells were quantified using ImageJ.

### 4.16 Infarct size quantification

Isolated hearts were cut into five transversal sections and further processed as described above. Cardiac sections were then stained with Masson's trichrome stain. An Axio Vert. A1 microscope was used to take pictures of each heart. The percentage of the blue fibrous area to the total area of the cardiac section was defined as infarct area. ImageJ was used to determine the infarct area using the threshold area. The investigator was blinded to treatment during quantification.

### 4.17 Flow cytometry – Apoptosis assay *in vitro*

Apoptosis of isolated cardiomyocytes was induced using $H_2O_2$ (50 µM) for 4 hours. Cells were treated with the appropriate inhibitors during $H_2O_2$ treatment. Apoptosis was quantified using the Dead Cell Apoptosis Kits with Annexin V for Flow Cytometry (cat# V13242, Invitrogen) according to the manufacturer's protocol. Flow cytometry was performed using a FACS verse. Data were analyzed using FlowJo v10.

### 4.18 Flow cytometry – Immune response *in vivo*

Hearts were harvested 48 hours after I/R surgery, cleared of blood and placed in 1ml PBS on ice. To obtain a single cell solution, hearts were cut into small pieces and digested in 1ml digestion solution consisting of 1% collagenase XI, 0.5% hyaluronidase, 4.5% collagenase I, 0.3% DNase, 2% 1M HEPES and PBS at 37°C for 60 minutes. The digestion solution was filtered through a 40µm cell strainer with 40ml FACS buffer consisting of 2% FCS, 2mM EDTA and PBS and centrifuged at 4°C and 800 rcf for 5 minutes. Cells were washed twice with FACS buffer and then stained with Ly6C, F4/80, CD45, CD11b, and lineage (Ter119, CD90, B220, CD49b, NK1.1, Ly6G) for 30 minutes, each diluted 1:200 at 4°C. Afterwards, the staining was stopped using 900µl FACS buffer and the cell solution was transferred to a counting tube after re-centrifugation and resuspension in 1ml FACS buffer. For CCL2 quantification, cells were fixed with the BD Cytofix/Cytoperm Fixation/Permeabilization Kit according to manufacturer's instructions and afterwards stained with CD45, CD11b, Ly6G, Ly6C, F4/80 and CCL2. Flow cytometry was performed using a FACS verse. Data were analyzed using FlowJo v10. Gating strategy was performed as previously described.[137]

### 4.19 Adoptive transfer of CD11b+ immune cells

Adoptive transfer of CD11b+ cells was performed with modifications based on Sicklinger et al[137]. Specifically, single-cell suspensions of spleens and peripheral blood of donor CD45.1 mice were prepared, and the monocyte-enriched CD11b+ fraction was isolated using IMag™ Anti-CD11b Magnetic Particles (BD Biosciences, Clone M1/70) according to manufacturer´s instructions. Isolated cells of all donor mice were pooled and equally divided across each treatment group. One donor mouse was used per two recipient mice. Cells were resuspended in 200µL RPMI-1640 medium and treated *ex vivo* with 100nM rapamycin, 100µM 4EGI-1 or DMSO as a vehicle for 3h at room temperature. CD45.2 recipient mice were randomly assigned to respective groups and operated 24h before cell transfer by I/R surgery. Approximately 300.000 isolated living cells were i.v. injected to each recipient mouse. 24h after cell transfer (2d reperfusion), hearts of operated recipient mice were isolated. FACS analysis was performed of left anterior wall lysates of CD45.2 recipient mice to enrich for infiltrated immune cells. Stainings were performed as described above but with an additional CD45.1 antibody.

### 4.20 Measurement of *ex vivo* cell survival

Cells were isolated using IMag™ Anti-CD11b Magnetic Particles (BD Biosciences, Clone M1/70) as described above. Cells were cultured *ex vivo* in RPMI-1640 medium and treated *ex vivo* with 100nM rapamycin, 100µM 4EGI-1 or DMSO for 3h or 6h at 4°C or 37°C in two independent experimental sets. After respective treatment, cells were stained with a 1:10 dilution of Trypan Blue Solution, 0.4%. Unstained spherical cells were counted as viable, stained cells were counted as dead. 200-300 cells were counted in total per condition.

### 4.21 Quantification of secreted CCL2 levels

CCL2 proteins levels were quantified in the supernatant media of isolated primary adult rat ventricular cardiomyocytes after simulated reperfusion using the Ebioscience Rat MCP 1 Instant ELISA Kit (cat# BMS631INST, Invitrogen). In mice, CCL2 protein levels were determined in blood serum 2d after reperfusion using the MCP-1 Mouse ELISA Kit (cat# BMS6005, Invitrogen). Both kits were used according to manufacturer's instructions, except of using sample dilutions (1:2 to 1:4) to increase signal intensity.

### 4.22 Polysome fractionation

Polysome fractionation was performed as previously described.[108] Briefly, cells were lysed in 500 µl polysome buffer (20 mM Tris pH 7.4, 10 mM MgCl, 200 mM KCl, 2 mM DTT, 100 µg/ml CHX, 1% Triton X-100, 1 U DNAse/µl) containing 100 µg/ml CHX. For complete lysis, the samples were kept on ice for 10 min, homogenized further by passing the lysate through a 23-gauge syringe needle ten times and subsequently centrifuged at 20,000 G to precipitate cell debris and the supernatant was immediately used in the further steps. Sucrose solutions were prepared in polysome gradient buffer. Sucrose density gradients (10–50% wt/vol) were freshly made in SW40 ultracentrifuge tubes using a BioComp Gradient Master (BioComp). Cell lysates were loaded onto sucrose gradients, followed by centrifugation for 250 min at 220,000 G, 4°C, in an SW40 rotor. Separated samples were fractionated at 0.375 ml/min by using a fractionation system BioComp Gradient Station (BioComp) that continually monitors OD254 values.

### 4.23 Parallel generation of Ribo-seq and RNA-seq libraries

Libraries were generated as previously described.[83] For each animal, the heart was lysed in 700µl polysome buffer (20 mM Tris pH 7.4, 10 mM MgCl, 200 mM KCl, 2 mM

DTT, 1% Triton X-100, 1U DNAse/µl and 100 µg/ml CHX) using a tissue homogenizer (Bullet Blender, NextAdvance). The tissue was homogenized further by passing the lysate through a 23-gauge syringe needle ten times. Homogenates were centrifuged at 4°C and 18,000xg for 10 min, and the supernatant was immediately used in the further steps. For complete lysis, the samples were kept on ice for 10 min and subsequently centrifuged at 20,000 G to precipitate cell debris. To accurately dissect translation and transcription, both Ribo-seq and RNA-seq libraries were prepared for each biological replicate from the identical lysate. Ribosome footprints were generated after immunoprecipitation of cardiomyocyte-specific polysomes with Anti-HA magnetic beads after treating the lysate with RNAse I (Ambion). Libraries were generated according to the mammalian Ribo-seq kit (Illumina). Barcodes were used to perform multiplex sequencing and create sequencing pools containing at least eight different samples and always an equal amount of both RNA and ribosome protected fragments (RPF) libraries. Sample pools were sequenced on the HiSeq 2000 platform using 50-bp sequencing chemistry.

### 4.24 Sequencing data processing and quality control

Sequencing data processing and quality control was performed as previously described.[83] Adapters removal was done with Flexbar v3.0.36 using standard filtering parameters (no prior trimming). Reads with more than 1 uncalled base were not included in the output: flexbar --may-uncalled 1 --pre-trim-left 0. Reads aligning to a custom bowtie2 v2.3.07 index including mouse rRNA, mtRNA, tRNA, snRNA and other ncRNA (Ensembl mus muculus release 97 – ncrna) were discarded. Remaining reads were then aligned in genomic coordinates to the mouse genome (GRCm38.p6) with STAR, v.2.5.3a8, inserting annotations on the fly: STAR --quantMode TranscriptomeSAM --alignIntronMin 20 --alignIntronMax 100000 --

outFilterMismatchNmax 1 --outFilterIntronMotifs RemoveNoncanonicalUnannotated --outFilterMismatchNoverLmax 0.04 --sjdbOverhang 50. Only uniquely mapping reads were kept for analysis. For Ribo-seq data, only periodic fragment lengths were kept that showed a distinctive triplet periodicity. An automatic Bayesian selection of read lengths and ribosome P-site offsets (BPPS) method[138] was used to select and shift aligned reads to properly account for P-site of the ribosome. For the RNA-seq data, reads were trimmed from the 3' end after adapter removal, such that the read length before alignment did match the maximum periodic fragment length of the corresponding Ribo-seq sample, as determined with the BPPS method. Finally, abundance estimates and read count to coding sequences were obtained using HTSeq-count[139], taking into account the strand-specific protocols. edgeR with standard parameters was used for differential gene expression analysis. An cutoff of FDR<0.01 was used.

### 4.25 Gene ontology analysis

For GO term analysis, genes with FDR <0.05 were considered for further analysis. GOTERM_BP_DIRECT in DAVID 2021[140,141] was used with the subset of expressed protein-coding genes as background set. Only enriched GO terms with at least five significantly changed genes were kept for further analysis and ranked by p-value. Top enriched terms were retained and visualized with a custom plotting routine showing p-value of enrichment.

### 4.26 Mass spectrometry sample preparation SP3 and TMT labeling, OASIS

Reduction of disulfide bridges in cysteine containing proteins was performed with dithiothreitol (56°C, 30 min, 10 mM in 50 mM HEPES, pH 8.5). Reduced cysteines were alkylated with 2-chloroacetamide (room temperature, in the dark, 30 min, 20 mM

in 50 mM HEPES, pH 8.5). Samples were prepared using the SP3 protocol[142] and trypsin (sequencing grade, Promega) was added in an enzyme to protein ratio 1:50 for overnight digestion at 37°C. Next day, peptide recovery in HEPES buffer by collecting supernatant on magnet and combining with second elution wash of beads with HEPES buffer.

Peptides were labelled with TMT10plex[143] Isobaric Label Reagent (ThermoFisher) according to the manufacturer's instructions. Samples were combined for the TMT10plex and for further sample clean up an OASIS® HLB µElution Plate (Waters) was used. Offline high pH reverse phase fractionation was carried out on an Agilent 1200 Infinity high-performance liquid chromatography system, equipped with a Gemini C18 column (3 µm, 110 Å, 100 x 1.0 mm, Phenomenex).[144]

### 4.27 LC-MS/MS

An UltiMate 3000 RSLC nano LC system (Dionex) fitted with a trapping cartridge (µ-Precolumn C18 PepMap 100, 5 µm, 300 µm i.d. x 5 mm, 100 Å) and an analytical column (nanoEase™ M/Z HSS T3 column 75 µm x 250 mm C18, 1.8 µm, 100 Å, Waters). Trapping was carried out with a constant flow of 0.05% trifluoroacetic acid at 30 µL/min onto the trapping column for 6 minutes. Subsequently, peptides were eluted via the analytical column with a constant flow of 0.3 µL/min with increasing percentage of solvent B (0.1% formic acid in acetonitrile). The outlet of the analytical column was coupled directly to a QExactive plus (Thermo) mass spectrometer using the Nanospray Flex™ ion source in positive ion mode. The peptides were introduced into the QExactive plus via a Pico-Tip Emitter 360 µm OD x 20 µm ID; 10 µm tip (New Objective) and an applied spray voltage of 2.3 kV. The capillary temperature was set at 320°C. Full mass scan was acquired with mass range 375-1200 m/z in profile mode with resolution of 70000. The filling time was set at maximum of 10 ms with a limitation

of $3x10^6$ ions. Data dependent acquisition (DDA) was performed with the resolution of the Orbitrap set to 35000, with a fill time of 120 ms and a limitation of $2x10^5$ ions. A normalized collision energy of 32 was applied. Dynamic exclusion time of 30 s was used. The peptide match algorithm was set to 'preferred' and charge exclusion 'unassigned', charge states 1, 5 - 8 were excluded. MS data was acquired in profile mode.

### 4.28 Mass spectrometry data analysis

IsobarQuant[145] and Mascot (v2.2.07) were used to process the acquired data, which was searched against a Mus musculus GRCm38 pep database containing common contaminants and reversed sequences. The following modifications were included into the search parameters: Carbamidomethyl (C) and TMT10 (K) (fixed modification), Acetyl (Protein N-term), Oxidation (M) and TMT10 (N-term) (variable modifications). For the full scan (MS1) a mass error tolerance of 10 ppm and for MS/MS (MS2) spectra of 0.02 Da was set. Further parameters were set: Trypsin as protease with an allowance of maximum two missed cleavages: a minimum peptide length of seven amino acids; at least two unique peptides were required for a protein identification. The false discovery rate on peptide and protein level was set to 0.01. The raw output files of IsobarQuant (protein.txt – files) were processed using the R programming language (ISBN 3-900051-07-0). Only proteins that were quantified with at least two unique peptides were considered for the analysis. Raw TMT intensities (signal_sum columns) were first cleaned for batch effects using limma[146] and further normalized using vsn (variance stabilization normalization)[147]. Proteins were tested for differential expression using the limma package. The replicate information was added as a factor in the design matrix given as an argument to the 'lmFit' function of limma. A protein was annotated as a hit with a false discovery rate (fdr) smaller 5 % and a fold-change

of at least 50 % and as a candidate with a fdr below 25 % and a fold-change of at least 50 %.

### 4.29 scRNA-seq analysis

Processed gene count data from previously published cardiac single cell RNA-seq data[148] was downloaded from the GEO database (IDs: GSM4376680 – GSM4376710). Gene raw counts were post processed to correct gene names as well as duplicate gene entries. Seurat v4.1 was employed for single cell data processing[149] following the integration approach[150]. Subsequently, data was converted for usage with the shinycell web application as described by Ouyang et al[151]. All processed data is available at: https://shiny.jakobilab.org/Hofmann_et_al_2022/.

### 4.30 Spatial tanscriptomics analysis

For the spatial analyses, Illumina data from Boileau et al.[152] was analyzed. Cell types were inferred using spatial spot deconvolution, as explained in Boileau et al. A unique cell type was assigned at each spot using the highest probability among all cell types. Remote zones were merged into a single remote zone.

### 4.31 ATAC-Seq analysis

ATAC-seq analysis was performed according to Beisaw et al[153]. Briefly, raw data from accession GSE110209 (samples SRR6676832, SRR6676833, SRR6676834, SRR6676835) were downloaded from the European Nucleotide Archive (https://www.ebi.ac.uk/ena). Trimmomatic version 0.36 was employed to trim reads after a quality drop below a mean of Q15 in a window of 5 nucleotides.[154] Only reads longer than 15 nucleotides were cleared for further analyses. Trimmed and filtered reads were aligned versus the Ensembl mouse genome version mm10 using STAR

2.6.1d with the parameters “--outFilterMismatchNoverLmax 0.1 --outFilterMatchNmin 20 --alignIntronMax 1 --outFilterMultimapNmax 1”8 retaining only unique alignments. Reads were deduplicated using Picard 2.18.16 (Picard: A set of tools (in Java) for working with next generation sequencing data in the BAM format) to mitigate PCR artefacts leading to multiple copies of the same original fragment. The Macs2 peak caller version 2.1.1 was employed for each sample with parameters “-q 0.0001”.[155] The region of interest was defined as the ATAC peak called by the Macs2 peak calling software for the *Ccl2* promoter. Peaks overlapping ENCODE blacklisted regions (known misassemblies, satellite repeats) were excluded. In order to be able to compare peaks in different samples to assess reproducibility, the resulting lists of significant peaks were overlapped and unified to represent identical regions. Reads were recounted after normalization for sequencing depth with bamCoverage 2.5.7 using bigWigAverageOverBed (UCSC Toolkit)[156].

### 4.32 Transcription factor binding prediction

Transcription factor binding motifs in the *Ccl2* promoter region (-500 bps to +100 bps from the TSS, mm9) and in two ATAC-seq peaks near the *Ccl2* promoter (chr11: 81848935 -81849122: 188bps, chr11: 81846518-81846775: 258bps, mm9) were retrieved by an automated matching of the sequences to all available motifs of the JASPAR database in R (version 4.3.1). The JASPAR2018 (version 1.38.0) and TFBSTools (version 1.1.1) packages were used for in-house scripting. The relative profile score threshold was set to 80%. A motif with an FDR ≤ 0.05 was considered as significantly enriched.

### 4.33 Randomization

All anesthesia, analgesia, treatments, surgeries and echocardiographies were performed by surgeons, who were blinded to whether the animals received vehicle or pharmacological inhibitors. A serum TnT level >1500 pg/ml at 24h after reperfusion was defined as threshold for study inclusion of I/R operated mice. Mice that deceased prior to blood sampling at 24h after reperfusion were only included in the survival analysis. One mouse of the vehicle (rapamycin set) and one mouse of the rapamycin treated group did not meet the required threshold and were excluded. All other mice with available serum TnT levels reached the predefined threshold after IR operation and were included for subsequent analysis. All Sham mice were included in the analysis.

### 4.34 Statistical analysis

Statistical analysis was performed using GraphPad Prism 7.0 (Graphpad Software Inc; www.graphpad.com) or R (R Foundation; https://www.r-project.org). Data values are presented as mean ± standard error of the mean (SEM). For statistical analysis one-way ANOVA with Tukey post-hoc analysis was used. When only two conditions where compared, unpaired two tailed t-test was used. $P < 0.05$ was defined as significant difference. Details of the statistical analyses of the sequencing data can be found in the respective methods section. Biological replicate numbers for each figure can be found in the accompanying figure legend.

”133

# 5 Results

Cells rapidly adapt their translational activity in response to stress.[82,83] They shape their translational network so that gene expression alters cell function to adjust to the new cell environment, and they can react with a general suppression overall protein synthesis to maintain sufficient energy levels or proteostasis under conditions where nutrients or oxygen are limited, or in response to proteotoxic stress to prevent the accumulation of toxic misfolded proteins.[83,157] While the heart was previously shown to reduce its translational activity during ischemia, it remained unknown how the heart responds to reperfusion, when nutrient and oxygen levels of the heart are restored within seconds, while other maladaptive conditions such as the abrupt rise of reactive oxygen species occur at the same time.[158,159] Such immediate changes of the cardiac environment could result in conditions where translation becomes activated through the induction of anabolic signaling pathways due to a rapid influx of growth factors or nutrients, while the cellular environment remains imperfect for protein synthesis - e.g. insufficient levels of chaperones or other proteostasis elements - resulting in the accumulation of misfolded proteins, energy depletion or the translation of maladaptive gene programs that mediate cell death or cardiac dysfunction. To confirm the downregulation of cellular translation in response to ischemia, I subjected different cell types, including human embryonic kidney 293 cells (HEK-293), neonatal rat ventricular cardiomyocytes (NRCMs), human induced pluripotent stem cell-derived cardiomyocytes (iPSC-CMs), and adult rat ventricular cardiomyocytes (ARCMs) to increasing timepoints of simulated ischemia (nutrient and oxygen deprivation *in vitro*) of different oxygen tensions, followed by labeling of newly synthesized polypeptides by puromycin incorporation and its quantification by western blotting (Figure 10). As expected, simulated ischemia resulted in the suppression of cellular translation rates,

which correlated with increasing ischemia times or decreasing oxygen tensions (Figure 10). Interestingly, different cell types showed varying degrees of translational suppression during simulated ischemia (Figure 10). While HEK-293 cells or ARCMs reacted with a rapid and immediate downregulation of protein synthesis, NRCMs and iPSC-CMs remained more resistant to ischemia, which might be related to their immaturity and the lower levels of oxygen saturation that are experienced by cells during fetal development.[160]

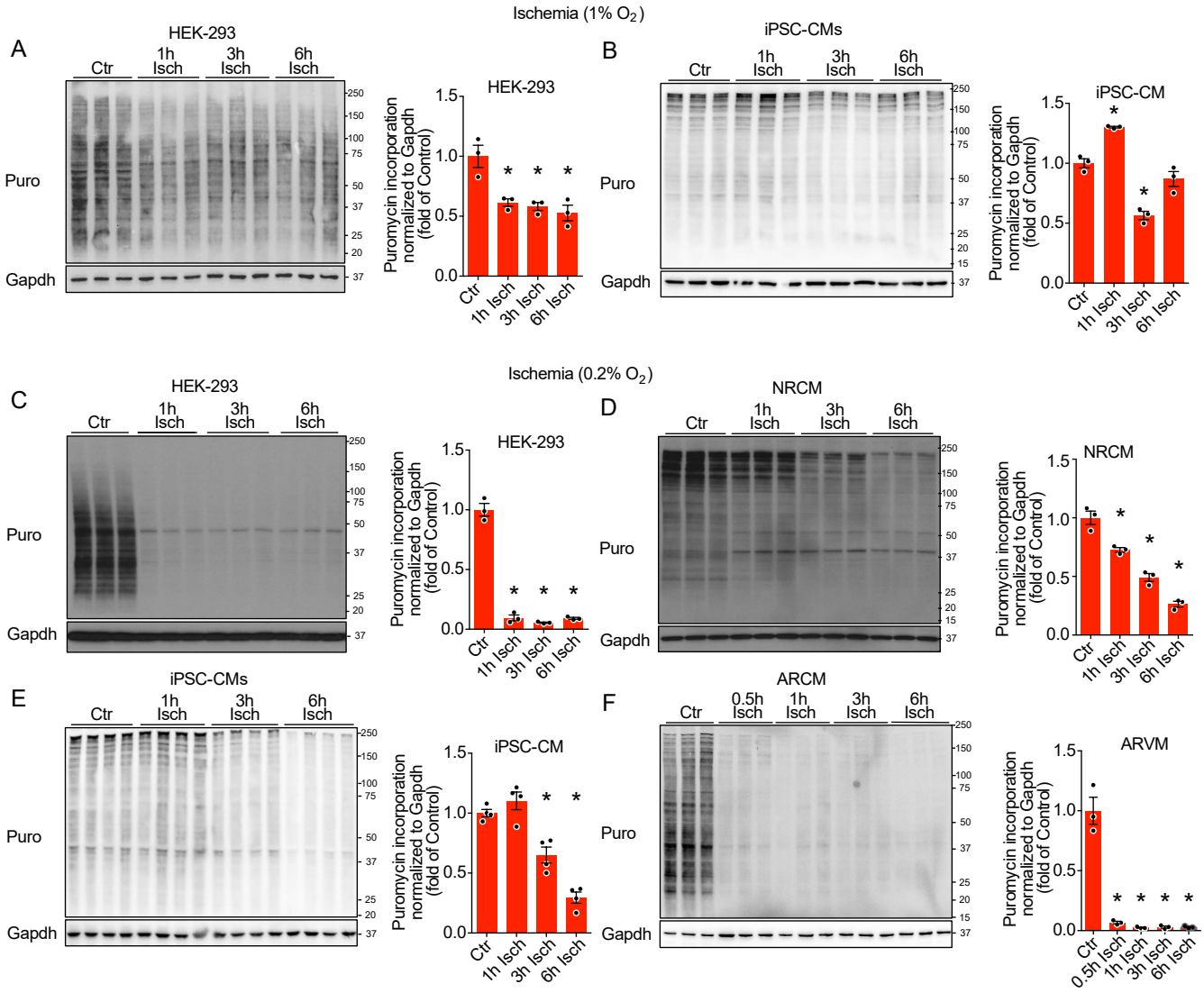


**Figure 10 | Suppression of translation in response to simulated ischemia**
**A** and **B**, Puromycin immunoblots and quantification of HEK-293 cells (**A**) or iPSC-CMs (**B**) at increasing timepoints of simulated ischemia with 1% $O_2$, n = 3. **C** to **F**, Puromycin immunoblots and quantification of HEK-293 cells (**C**), NRCMs (**D**), iPSC-CMs (**E**) or ARCMs (**F**) at increasing timepoints of simulated ischemia with 0.2% $O_2$, n = 3-4. * indicates p<0.05 from control. For statistical analysis one-way ANOVA with Tukey post-hoc analysis was used. p < 0.05 was defined as significant difference. Error bars show standard error of the mean. Figure legends from Hofmann et al. 2024[133].

After confirming that cardiomyocyte translation rates are suppressed in response to simulated ischemia *in vitro*, and that such changes can be quantified by puromycin incorporation, I quantified translation rates in HEK-293 cells, NRCMs, iPSC-CMs and ARCMs that were subjected to increasing timepoints of simulated reperfusion *in vitro* (restoration of cellular oxygen and nutrient levels) (Figure 11). While all tested cell types reacted with a restoration of translation rates in response to simulated reperfusion, dynamics and total levels of translation after reperfusion varied by cell type. HEK-293 cells, NRCMs and iPSC-CMs reacted with a continued suppression or even further drop of translation rates shortly after reperfusion, whereas ARCMs already completely restored proteins synthesis levels within 1 hour after simulated reperfusion (Figure 11). At 24 hours NRCMs and iPSC-CMs returned translation rates to baseline levels which were observed before ischemia (Figure 11B and 11C). In contrast, HEK-293 cells and ARCMs reacted with an overshooting protein synthesis response that exceeded baseline levels (Figure 11A and 11D). In general, translational dynamics during simulated ischemia and after reperfusion appeared to differ between immature cardiomyocytes and adult cardiomyocytes, potentially related to differentiation and maturity.

To assess translational dynamics in response to ischemia *in vivo*, adult mice were subjected to surgical ligation of the left anterior descending coronary artery (LAD) for 3 hours. Successful induction of a myocardial infarction was confirmed by plasma creatine kinase at 3 hours post-surgery (Figure 12A). Translation rates were quantified *in vivo* by i.p. injection of puromycin 30 minutes before isolation of the left ventricle. Assessment of puromycin incorporation into left ventricular lysates by western blotting showed reduced a puromycin signal at 3 hours of myocardial infarction (Figure 12B).

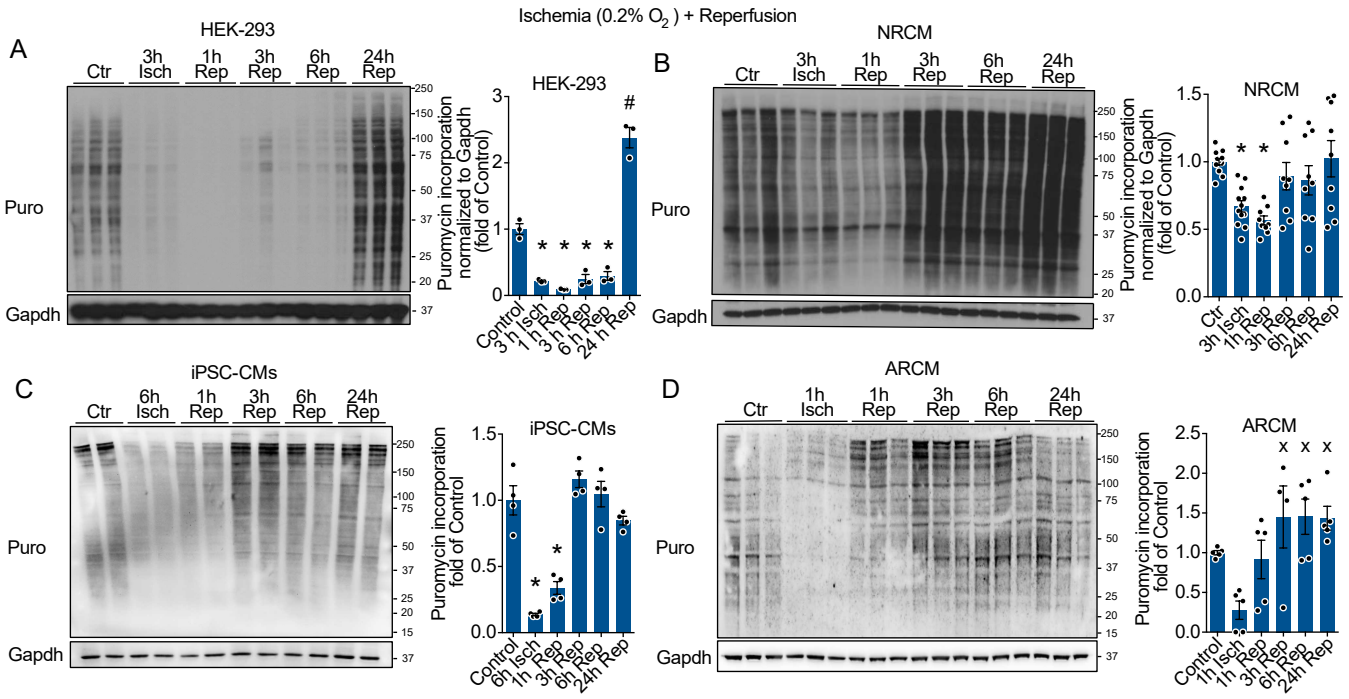


**Figure 11 | Dynamics of cellular translation rates in response to simulated ischemia and reperfusion**

**A** to **D**, Puromycin immunoblots and quantification of HEK-293 cells (**A**), NRCMs (**B**), iPSC-CMs (**C**) or ARCMs (**D**) at increasing timepoints of reperfusion, n = 3-9. * indicates p<0.05 from control. For statistical analysis one-way ANOVA with Tukey post-hoc analysis was used. p < 0.05 was defined as significant difference. Error bars show standard error of the mean. Data of Figure 11B was produced jointly with Fereshteh S. Younesi. Figure legends from Hofmann et al. 2024[133].

Puromycin signal by western blot negatively correlated with plasma CK levels, indicating that larger myocardial injury results in stronger suppression of cardiac translation rates (Figure 12C). However, it must be noted that permanent ligation of a coronary artery may limit puromycin delivery to the cardiac tissue, therefore biasing the result towards reduced puromycin incorporation. As such, those results need to be interpreted with caution. Next, cardiac translation rates were assessed in adult mice *in vivo* after 60 minutes of surgical ligation of the LAD, followed by reestablishing coronary blood flow, resulting in rapid reperfusion of the ischemic tissue. Cardiac injury was confirmed by blood sampling at 24 hours post-reperfusion and measurement of plasma Troponin T levels (Figure 13A).

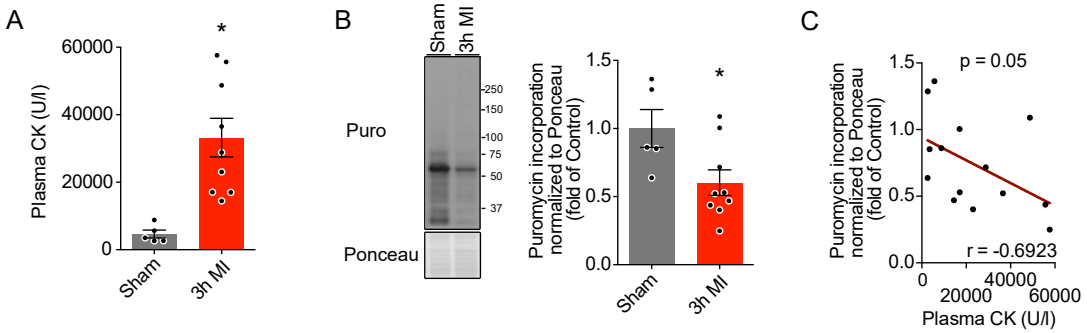


## Figure 12 | Cardiac translation rates in response to myocardial infarction

Plasma CK levels, n = 5-9 (**A**), puromycin incorporation, measured by immunoblot, n = 5-9 (**B**) and Pearson´s correlation coefficient of Plasma CK and cardiac puromycin incorporation (**C**) of left ventricular lysates of mice 3 hours after sham surgery or LAD ligation (MI). * indicates p<0.05 from sham. For statistical analysis an unpaired two tailed t-test was used for **A** and **B**. Pearson correlation with two-tailed p value was computed with GraphPad Prism 7.0 for **C**. p < 0.05 was defined as significant difference. Error bars show standard error of the mean. Data of Figure 12 was produced jointly with Ole M. Schwerdt. Figure legends from Hofmann et al. 2024[133].

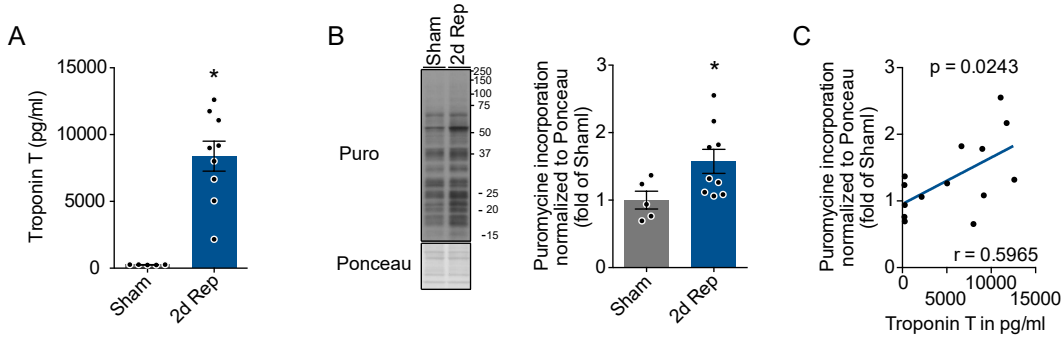


## Figure 13 | Translational activation after cardiac reperfusion

Serum Troponin T (TnT) levels, n = 5-9 (**A**), puromycin incorporation, measured by immunoblot, n = 5-9 (**B**) and Pearson´s correlation coefficient of serum TnT and cardiac puromycin incorporation (**C**) of left ventricular lysates from mice 2 days after sham or I/R surgery. * indicates p<0.05 from sham. For statistical analysis an unpaired two tailed t-test was used for **A** and **B**. Pearson correlation with two-tailed p value was computed with GraphPad Prism 7.0 for **C**. p < 0.05 was defined as significant difference. Error bars show standard error of the mean. Data of Figure 13 was produced jointly with Ole M. Schwerdt. Figure legends from Hofmann et al. 2024[133].

Similar to isolated adult cardiomyocytes, the adult heart reacted with an overshooting translational response that exceeded baseline levels at 2 days post-reperfusion by approximately 50% (Figure 13B). Interestingly, puromycin incorporation was positively correlated to plasma Troponin T levels, indicating that larger myocardial injury is associated with an increased translational response after reperfusion (Figure 13C). To identify the relative location and cell types responsible for the induction of cardiac translation *in vivo*, I performed immunofluorescent imaging of heart sections from mice 2 days after reperfusion. Mice were treated with O-propargyl(OP)-puromycin, an alkyne analog of puromycin that has improved pharmacological properties over puromycin for visualizing translation *in vivo*. OP-puromycin incorporates into the translating polypeptide chain and can be visualized via Cu(I)-catalyzed click chemistry which leads to a chemoselective ligation between OP-puromycin and a fluorescent dye, allowing for highly selective detection of newly synthesized proteins *in vivo*.[161] This revealed an upregulation of cardiac translation which especially affected cells of the border zone but also within the infarct of mouse hearts after reperfusion (Figure 14A). Among those translational active cells were Troponin T-positive cardiomyocytes of the border zone, indicating that those cells contribute to the upregulation of translation observed in left ventricular lysates. To confirm that the border zone and infarct area contributed to translation activation after reperfusion, I separated the infarct area, border zone and remote area of puromycin injected mice either 30 minutes or 2 days after reperfusion and quantified puromycin incorporation by western blot (Figure 14B). I selected the 30 minutes timepoint because a recent manuscript, which was published by Zhang et al[136] during the preparation of this thesis, showed suppressed cardiac translation at 30 minutes after reperfusion. While I could confirm the decreased translational activity of the infarct and border zone early after reperfusion described by Zhang et al. (Figure 14C), those same areas showed increased translational activity at

2 days after reperfusion (Figure 14D). Together with data of an additional timepoint at 1 hour after reperfusion by Zhang et al[136] the data suggests a dynamic translational response of the injured heart with initial suppression of translation rates immediately after reperfusion, which is followed by a restoration of protein synthesis that later exceeds baseline levels in the infarct and border zone (Figure 14E).

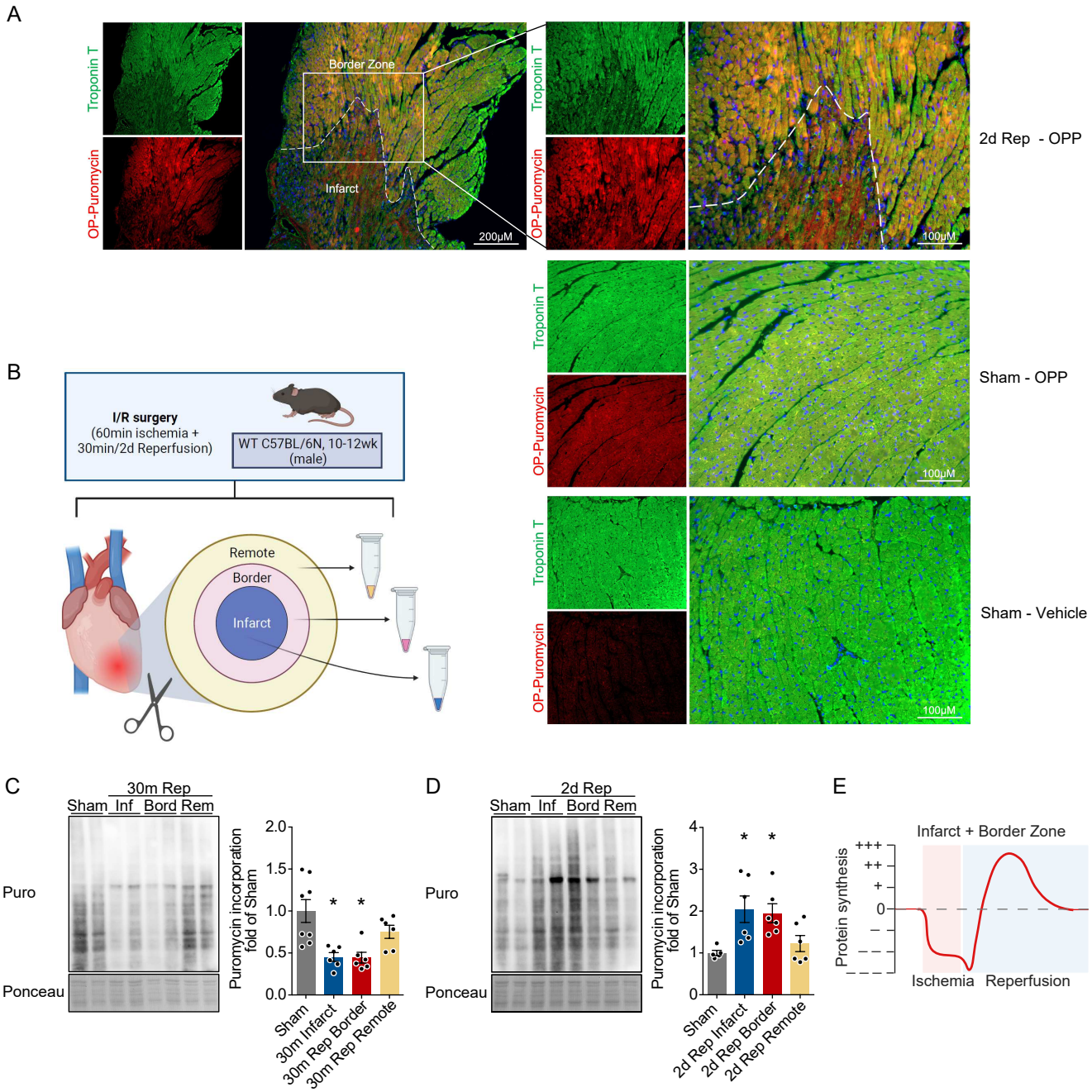


**Figure 14 | Translational activation of the infarct and border zone after ischemia/reperfusion**

**Figure 14 | Translational activation of the infarct and border zone after ischemia/reperfusion**

**A**, OP-Puromycin immunostaining of the infarct region and border zone of mice 2 days after I/R surgery and of the remote area of sham mice. **B** to **D** Diagram of the experimental setup (**B**) and puromycin incorporation into the sham, infarct, border zone and remote area of mouse hearts 30 minutes (**C**) or 2 days (**D**) after they were subjected to I/R or sham surgery. **E**, Diagram of the proposed temporal dynamics of translational activation of the infarct and border zone after ischemia and reperfusion. Rep (reperfusion), Puro (puromycin), Inf (infarct area), Bord (border zone), Rem (remote area). * indicates p<0.05 from sham. For statistical analysis a one-way ANOVA with Tukey post-hoc analysis was used for **C** and **D**. $p < 0.05$ was defined as significant difference. Error bars show standard error of the mean. B and E made in ©BioRender - biorender.com. Figure legends from Hofmann et al. 2024[133].

To identify the molecular events that mediate the regulation of cardiac translation during ischemia and reperfusion, I subjected NRCMs to simulated ischemia (Figure 15) and reperfusion (Figure 16) to assess intracellular signaling pathways known to be involved into the regulation of cellular translational activity. Isolated cardiomyocytes were used since the OP-puromycin imaging data revealed that border zone cardiomyocytes are involved into the regulation of cardiac translation rates after reperfusion (Figure 14A). Assessment of the activity of intracellular signaling pathways that are thought to control cellular translation rates revealed that simulated ischemia results in a substantial downregulation of pathways involved in cap-dependent translation initiation in NRCMs (Figure 15).

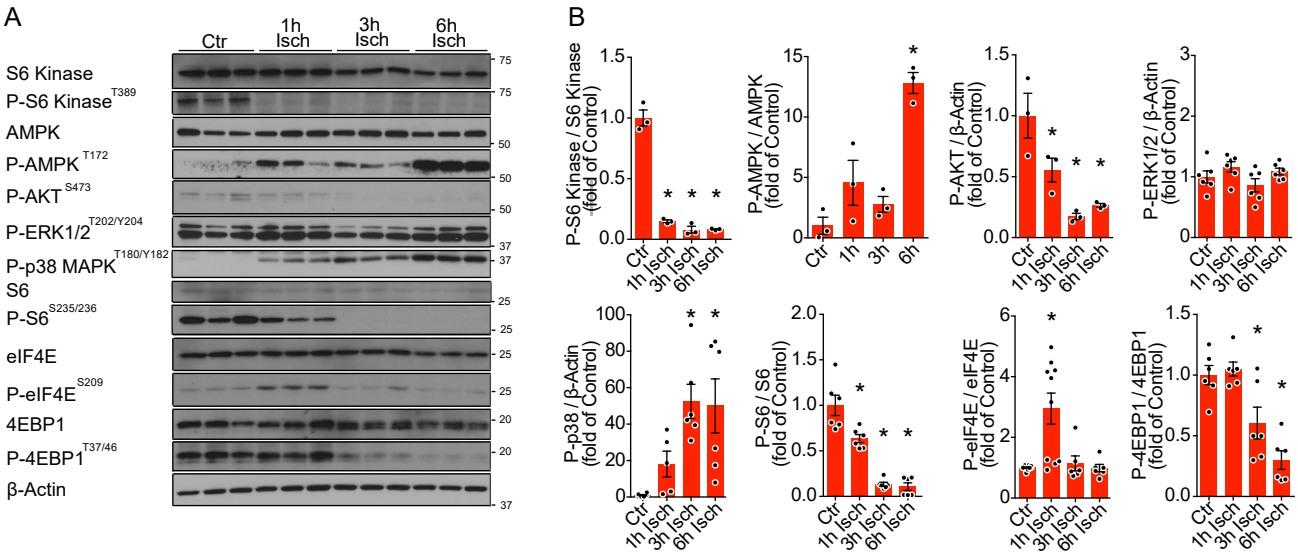


**Figure 15 | Regulation of signaling pathways controlling eIF4F-dependent translation initiation in response to simulated ischemia in cardiomyocytes**

**Figure 15 | Regulation of signaling pathways controlling eIF4F-dependent translation initiation in response to simulated ischemia in cardiomyocytes**
**A** and **B,** Immunoblots (**A**) and quantifications (**B**) of proposed eIF4F-regulatory pathways of NRCMs in response to increasing timepoints of ischemia, n = 3-10. * indicates p<0.05 from control. For statistical analysis one-way ANOVA with Tukey post-hoc analysis was used. p < 0.05 was defined as significant difference. Error bars show standard error of the mean. Data of Figure 15 was produced jointly with Fereshteh S. Younesi. Figure legends from Hofmann et al. 2024[133].

Cap-dependent translation initiation is a rate limiting step of cellular translational activity. Specifically, the activity of translation initiation is regulated by the formation of the ternary complex, formation of 43S, as well as formation of the eIF4F complex. In this thesis I specifically investigated the involvement of the eIF4F complex in translational regulation in response to cardiac ischemia and reperfusion (Figure 16A). Pull-down of m7GTP associated proteins, which mimics the 5´ mRNA cap, confirmed the disruption of the eIF4F complex during simulated ischemia, and re-association after simulated reperfusion in NRCMs (Figure 16B). I found upstream pathways known to regulate eIF4F formation, specifically the mTORC1-4EBP1-eIF4E axis, as well as the MAPK-MNK1/2-eIF4E axis to be highly regulated both during simulated ischemia (Figure 15) and after simulated reperfusion in NRCMs (Figure 16C) and were therefore considered as candidate pathways that may be responsible for the dynamic changes of cardiac translational activity observed after ischemia/reperfusion.

The phosphorylation of ribosomal protein S6 at S235/236, often used as a surrogate of mTORC1 activity, was confirmed to occur in the myocardium in response to reperfusion (Figure 17). However, it must be considered that this phosphorylation side was also shown to be phosphorylated by other kinases, and as such S6 phosphorylation at this site *in vivo* may also be mediated by other signaling pathways.

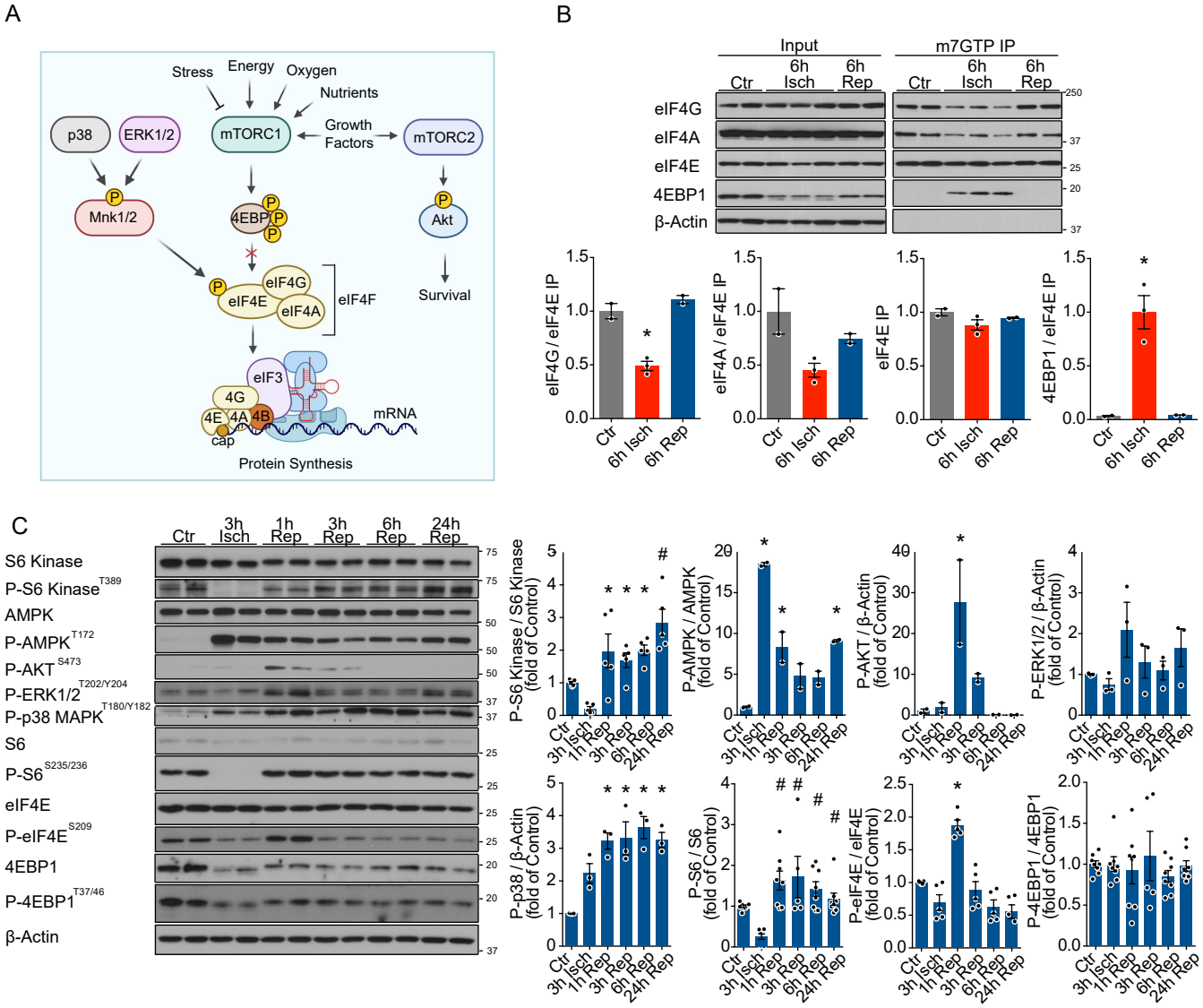


**Figure 16 | Activation of signaling pathways controlling eIF4F-dependent translation initiation after simulated reperfusion**

**A**, Diagram of major signaling pathways proposed to regulate eIF4F-dependent translation initiation. **B**, Quantification of eIF4F complex assembly by pull-down of mRNA cap-binding proteins via $m^7$GTP-coupled agarose beads after simulated ischemia or ischemia (6 hours) followed by reperfusion in NRCMs, n = 2-3. **C** Immunoblots and quantifications of proposed eIF4F-regulatory pathways of NRCMs after ischemia (3 hours) followed by increasing times of reperfusion, n = 2-8 * indicates p<0.05 from control. For statistical analysis one-way ANOVA with Tukey post-hoc analysis was used for **B** and **C**. p < 0.05 was defined as significant difference. Error bars show standard error of the mean. A made in ©BioRender - biorender.com. Data of Figure 16B-C was produced jointly with Fereshteh S. Younesi. Figure legends from Hofmann et al. 2024[133].

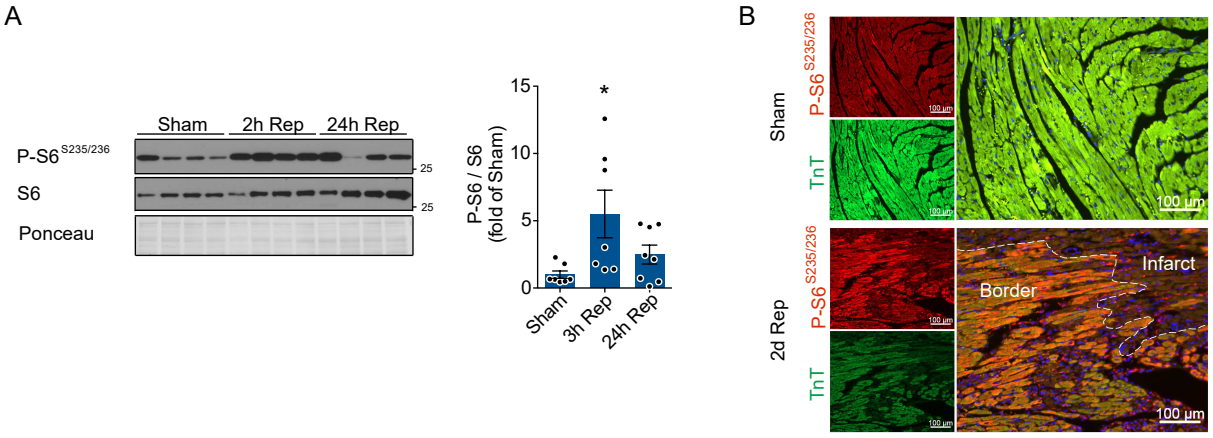


**Figure 17 | Increased S6$^{S235/236}$ phosphorylation after cardiac reperfusion**
**A**, Representative immunoblot and quantification of S6$^{S235/236}$ phosphorylation of left ventricular lysates 2 or 24 hours after I/R surgery in mice, n = 7-8. **B**, Representative phospho-S6$^{S235/236}$ immunostaining of the infarct region and border zone 2 days after sham or I/R surgery in mice. Rep (reperfusion), * indicates $p<0.05$ from sham. # indicates $p<0.05$ from 3h ischemia. For statistical analysis one-way ANOVA with Tukey post-hoc analysis was used for **A**. $p < 0.05$ was defined as significant difference. Error bars show standard error of the mean. Data of Figure 17B was produced jointly with Ole M. Schwerdt. Figure legends from Hofmann et al. 2024[133].

To further assess the involvement of different upstream pathways proposed to control eIF4F formation, I used different pharmacological inhibitors that target specific upstream pathways of the eIF4F complex in NRCMs (Figure 18A). Rapamycin, a partly selective mTORC1 inhibitor, Torin1, a selective ATP-competitive mTORC1 and mTORC2 inhibitor, eFT508, a MNK1/2 inhibitor, and 4EGI-1, a competitive eIF4E/eIF4G interaction inhibitor, were studied. I determined minimal required effective dosages at baseline in NRCMs (Figure 18B and Figure 19). I selected higher dosages (100nM) for rapamycin for follow-up experiments to avoid potential insufficient mTORC1 inhibition upon mTORC1 pathway activation after reperfusion.

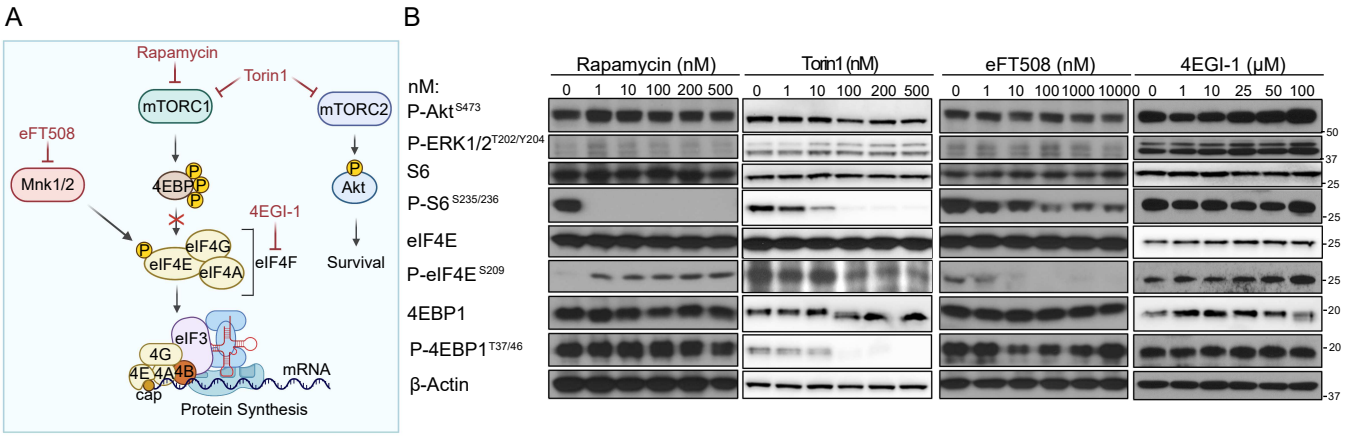


**Figure 18 | Dosage testing of pharmacological inhibitors targeting upstream signaling pathways of eIF4F**

**A**, Diagram of signaling pathways affected by the pharmacological compounds used to modulate translation initiation in this study. **B**, Representative immunoblots of the activity of eIF4F-regulatory pathways in response to increasing doses of the indicated pharmacological compounds in NRCMs. Cells were lysed 6 hours after exposure to the pharmacological inhibitor. A made in ©BioRender - biorender.com. Figure legends from Hofmann et al. 2024[133].

As 4EGI-1 is a competitive eIF4E/eIF4G interaction inhibitor that has no effects on upstream signaling pathway activity (Figure 18B), I determined its minimal required dosage to inhibit the eIF4F complex in NRCMs at baseline by puromycin incorporation and m7GTP pull-down assays (Figure 19B and 19D). In addition, I quantified cellular apoptosis in response to increasing concentrations of 4EGI-1 to avoid toxic dosages (Figure 19A and 19C). A 4EGI-1 concentration of 100μM was effective to inhibit translation, disrupt the eIF4F complex, and did not cause significant amounts of apoptosis for up to 24h after drug exposure in NRCMs, and was therefore selected for follow-up experiments (Figure 19).

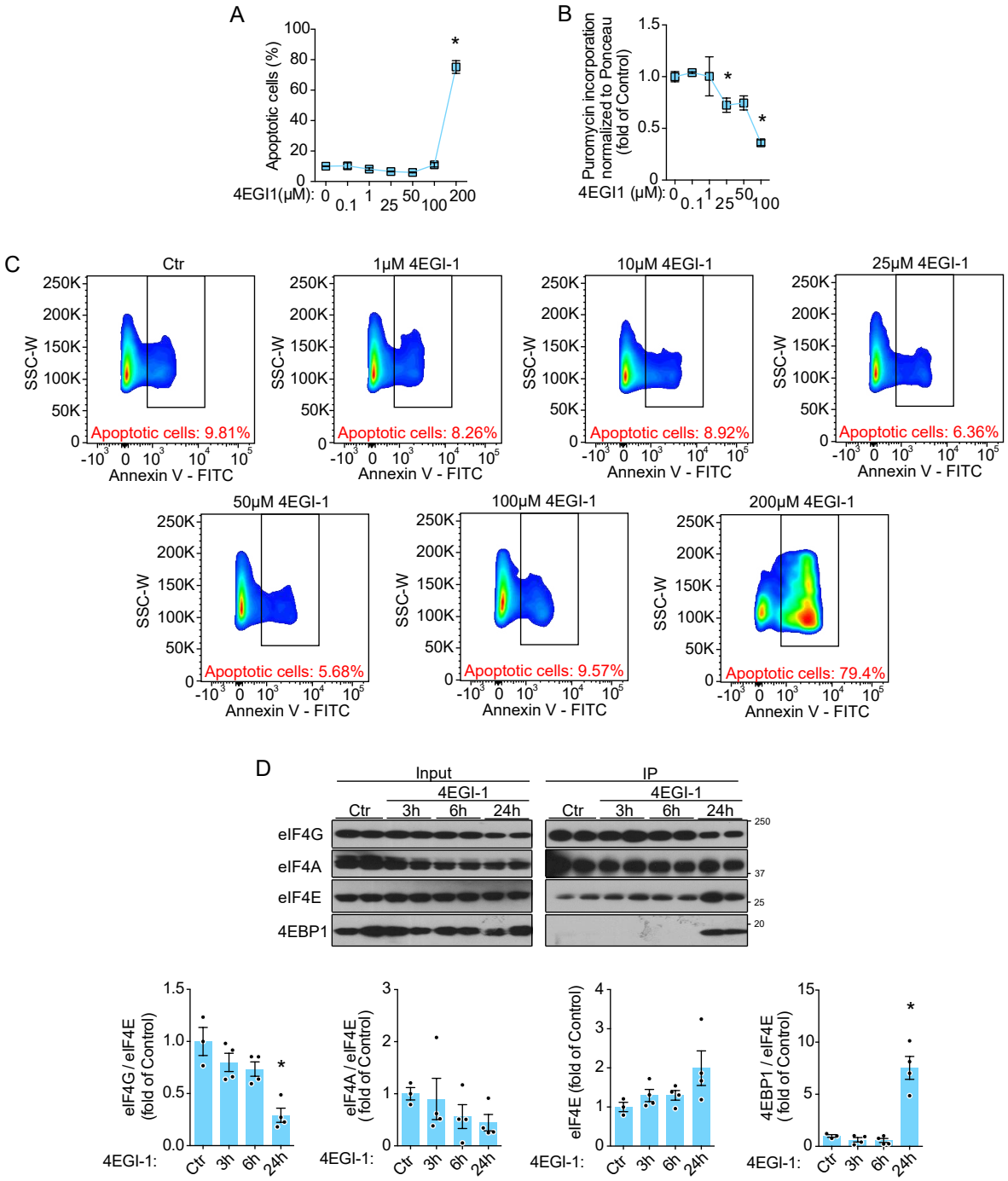


**Figure 19 | 4EGI-1 effectively suppresses eIF4F complex formation and protein synthesis in cardiomyocytes without causing cell death**

**A** and **C**, Quantification of NRCM apoptosis by FACS analysis 24 hours after treatment with increasing doses of 4EGI-1 (**A**), n = 2. Representative FACS plots of each condition are shown below (**C**). **B**, Quantification of puromycin incorporation 6 hours after treatment with increasing doses of 4EGI-1 in NRCMs. **D**, Representative immunoblot and quantification of eIF4F complex assembly in NRCMs by pulldown of mRNA cap-binding proteins via m7GTP-coupled agarose beads at increasing timepoints after 4EGI-1 (100μM) treatment, n = 3-4. Ctr (control), * indicates p<0.05 from 0μM 4EGI-1 or control. For statistical analysis one-way ANOVA with Tukey post-hoc analysis was used for **A**, **B** and **D**. p < 0.05 was defined as significant difference. Error bars show standard error of the mean (SEM). Data of Figure 19D was produced jointly with Fereshteh S. Younesi. Figure legends from Hofmann et al. 2024[133].

To assess the effect of the different pharmacological compounds on eIF4F complex formation and translation rates in response to reperfusion, I subjected NRCMs to simulated ischemia, followed by simulated reperfusion and immediate exposure to the different inhibitors (Figure 20). Only those inhibitors that targeted the mTORC1-4EBP1-eIF4E axis disrupted the eIF4F complex and inhibited translation rates. In contrast eFT508, which inhibits eIF4E S209 phosphorylation, had no effect on eIF4F complex formation or cardiomyocyte translation rates after reperfusion (Figure 20). Of note, cardiomyocytes treated with rapamycin showed first evidence of reduced translation rates at 24 hours of drug exposure, even though eIF4F complex was already disrupted after 6 hours. This might be explainable by additional effects mediated by rapamycin, as well as the technical properties of the puromycin assay, which quantifies amino-acid incorporation into elongating polypeptides rather than directly quantifying translation initiation.

Next, I assessed the impact of the different pharmacological inhibitors regulating eIF4F assembly or eIF4E S209 phosphorylation in NRCMs in response to $H_2O_2$ treatment. Only 4EGI-1 treatment was associated with a significant inhibition of apoptosis, assessed by Propidiumiodid and Annexin V staining and quantification by FACS (Figure 21). As expected, Torin1 treatment trended towards increased cell death, likely due to its inhibitory action on mTORC2, which regulates cell survival (Figure 21).

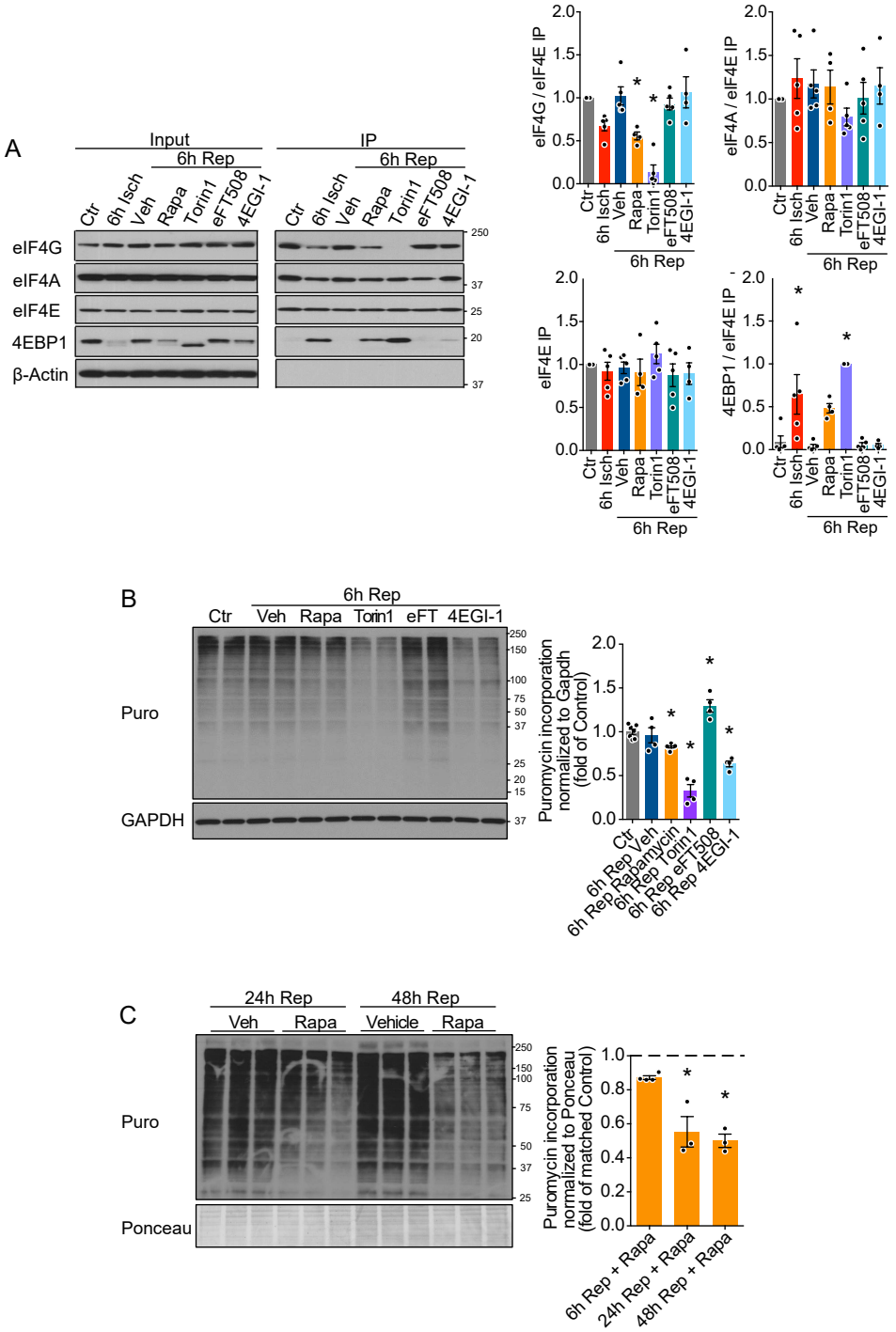


**Figure 20 | Control of translation rates in response to reperfusion by the mTORC1-4EBP1-eIF4F signaling axis**

**A** and **B**, Pull-down of eIF4F proteins via m$^7$GTP-coupled agarose beads, n = 4-5 (**A**) and puromycin immunoblot, n = 4 (**B**) of NRCMs in response to sI/R and pharmacological inhibitor treatment. A representative immunoblot is shown on the left, and quantification of all replicates is shown on the right **C**, Representative immunoblot and quantification of puromycin incorporation 24h and 48h after rapamycin and sI/R in NRCMs. The 6-hour quantification was derived from D. Rep (reperfusion), Veh (vehicle). Inhibitors were added with reperfusion. The following concentrations were used for **A**, **B** and

**C**: Rapamycin 100nM, Torin1 100nM, eFT508 100nM, 4EGI-1 100µM. Ctr (control), Isch (ischemia), Rep (reperfusion), * indicates p<0.05 from control. For statistical analysis one-way ANOVA with Tukey post-hoc analysis was used for **A**, **B** and **C**. p < 0.05 was defined as significant difference. Error bars show standard error of the mean. Data of Figure 20A-B was produced jointly with Fereshteh S. Younesi. Figure legends from Hofmann et al. 2024[133].

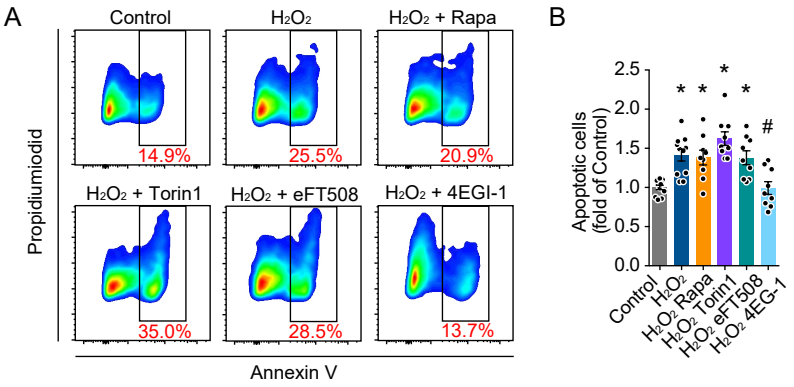


**Figure 21 | 4EGI-1 inhibits apoptosis in response to $H_2O_2$ in cardiomyocytes**
**A** and **B**, Quantification of NRCM apoptosis by FACS analysis 4 hours after simultaneous $H_2O_2$ (50 µM) and pharmacological inhibitor treatment, n = 9-12. Representative FACS graphs of each condition are shown on the left. The following concentrations were used: Rapamycin 100nM, Torin1 100nM, eFT508 100nM, 4EGI-1 100µM. Ctr (control), Isch (ischemia), Rep (reperfusion), * indicates p<0.05 from control. # indicates p<0.05 from $H_2O_2$. For statistical analysis one-way ANOVA with Tukey post-hoc analysis was used. p < 0.05 was defined as significant difference. Error bars show standard error of the mean. Data of Figure 21 was produced jointly with Fereshteh S. Younesi. Figure legends from Hofmann et al. 2024[133].

To further investigate eIF4E phosphorylation after simulated reperfusion, the upstream signaling mediators proposed to control eIF4F S209 phosphorylation, ERK1/2 and p38 MAP kinase, were evaluated in NRCMs. For this the MEK1/2 inhibitor U0126 (to suppress ERK1/2 activity) and the p38 inhibitor SB202190 were used. Their activity and specificity were confirmed in NRCMs by blotting for ERK1/2 T202/Y204 phosphorylation as well as HSP27 S82 phosphorylation, a downstream target of p38 MAP kinase (Figure 22A and 22B). In cardiomyocytes (at baseline, during simulated ischemia and after simulated reperfusion) eIF4E S209 phosphorylation was exclusively regulated by the MEK1/2-ERK1/2 axis and not by p38 MAP kinase (Figure 22C).

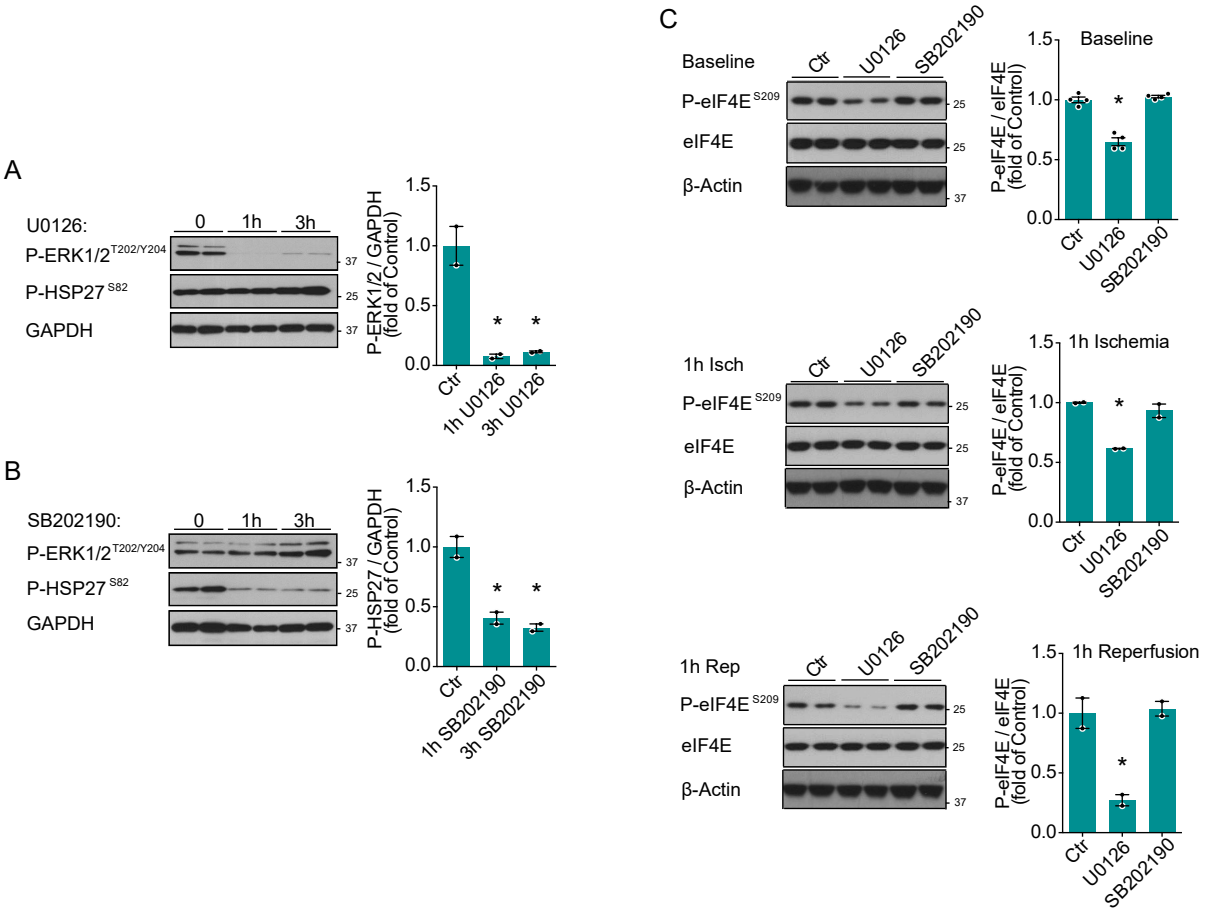


**Figure 22 | eIF4E$^{S209}$ phosphorylation is controlled by ERK1/2 and not by p38 in cardiomyocytes at baseline and during ischemia or reperfusion**

**A**, Immunoblots and quantifications of ERK1/2$^{T202/Y204}$ and HSP27$^{S82}$ phosphorylation (downstream target of p38) in response to U0126 treatment of NRCMs, n = 2. **B**, Immunoblots and quantifications of ERK1/2$^{T202/Y204}$ and HSP27$^{S82}$ phosphorylation (downstream target of p38) in response to SB202190 treatment of NRCMs, n = 2. **C**, Immunoblots and quantifications of eIF4E$^{S209}$ phosphorylation in response to U0126 or SB202190 treatment of NRCMs at baseline, after simulated ischemia (1 hour) or ischemia (3 hours) followed by reperfusion (1 hour). Ctr (control), Isch (ischemia), Rep (reperfusion), n = 2. * indicates $p<0.05$ from control. For statistical analysis one-way ANOVA with Tukey post-hoc analysis was used for **A** to **C**. $p < 0.05$ was defined as significant difference. Error bars show standard error of the mean. Data of Figure 22 was produced jointly with Fereshteh S. Younesi. Figure legends from Hofmann et al. 2024[133].

To further test whether eIF4E S209 phosphorylation is regulating overall translation rates *in vitro*, wild type (WT)-eIF4E and phospho-dead eIF4E S209 were overexpressed in HEK293-T cells (Figure 23A). Neither overexpression of WT-eIF4E or eIF4E S209 phospho-dead resulted in a significant change of translation rates of HEK293-T cells (Figure 23B), indicating that eIF4E S209 phosphorylation is not regulation overall cellular translational activity.

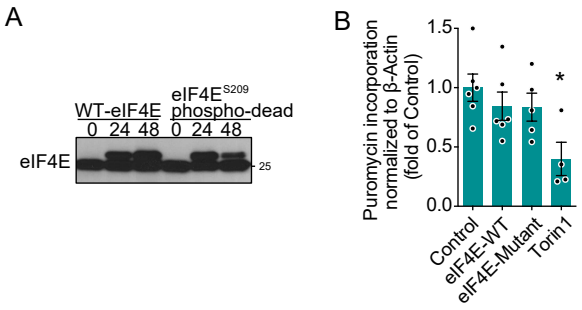


**Figure 23 | eIF4E$^{S209}$ phosphorylation does not regulate overall translation rates**
**A**, Representative immunoblot of eIF4E after WT-eIF4E or eIF4E$^{S209}$ phospho-dead expression in HEK293-T cells. **B**, Quantification of puromycin incorporation in HEK293-T cells 48 hours after transfection, n = 4-6. A 6-hour treatment of 100nM Torin1 was used as a positive control. * indicates $p<0.05$ from control. For statistical analysis one-way ANOVA with Tukey post-hoc analysis was used for **B**. $p < 0.05$ was defined as significant difference. Error bars show standard error of the mean. Data of Figure 23 was produced jointly with Fereshteh S. Younesi. Figure legends from Hofmann et al. 2024[133].

While the ERK1/2-MNK1/2-eIF4E S209 does not seem to control overall translational activity, eIF4E S209 phosphorylation may regulate the translation of specific transcripts, which could have an impact on overall cardiac function after reperfusion. To examine the involvement of eIF4E S209 phosphorylation on cardiac function, I conducted a trial experiment of eFT508 treatment of male adult mice treated with eFT508 shortly before cardiac reperfusion (Figure 24). A single i.p. injection of 10mg/kg eFT508 resulted in rapid and persistent inhibition of eIF4E S209 phosphorylation in whole left ventricular lysates (Figure 24A). However, eFT508 did not affect plasma Troponin T levels or ejection fraction 2 weeks after cardiac ischemia/reperfusion (Figure 24B and 24C), which is why eFT508 and eIF4E S209 phosphorylation were not further investigated. I concluded that the mTORC1-4EBP1-eIF4E axis is the primary regulator of eIF4F complex formation in cardiomyocytes after reperfusion. I therefore focused my next experiments on this pathway.

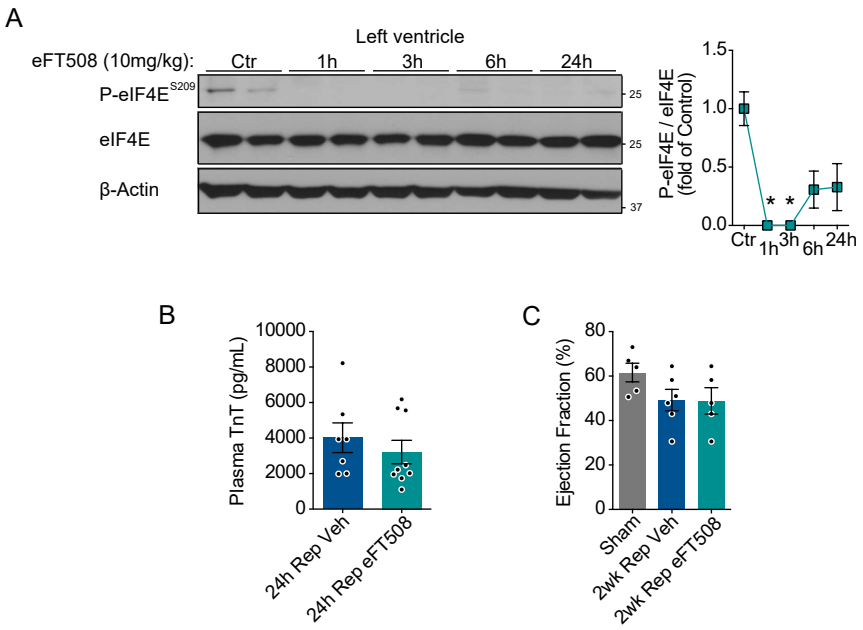


**Figure 24 | Pharmacological inhibition of eIF4E$^{S209}$ phosphorylation does not affect cardiac function after ischemia/reperfusion *in vivo***

**A**, Immunoblot and quantification of eIF4E$^{S209}$ phosphorylation in mouse left ventricular lysates at increasing timepoints after i.p. injection of 10 mg/kg eFT508. **B**, Plasma Troponin T levels in male mice treated with vehicle or eFT508 (10 mg/kg) 24 hours after I/R surgery, n = 7-9. **C**. Left ventricular ejection fraction of male mice 2 weeks after sham or I/R surgery operated mice treated with vehicle or 10 mg/kg eFT508, n = 5-6. Ctr (control), Rep (reperfusion), Veh (vehicle). * indicates p<0.05 from control. For statistical analysis one-way ANOVA with Tukey post-hoc analysis was used for **A** and **C**. An unpaired two tailed t-test was used for **B**. p < 0.05 was defined as significant difference. Error bars show standard error of the mean. Figure legends from Hofmann et al. 2024[133].

As the competitive eIF4E/eIF4G interaction inhibitor 4EGI-1 had not been used in differentiated adult cardiomyocytes prior to this study, I confirmed its pharmacological activity in these cell types. As in immature neonatal cardiomyocytes, 4EGI-1 resulted in the suppression of translational activity both at baseline and after reperfusion in adult cardiomyocytes (Figure 25A). *In vivo*, 4EGI-1 did not inhibit upstream mTORC1 activity, as observed in NRCMs (Figure 25B).

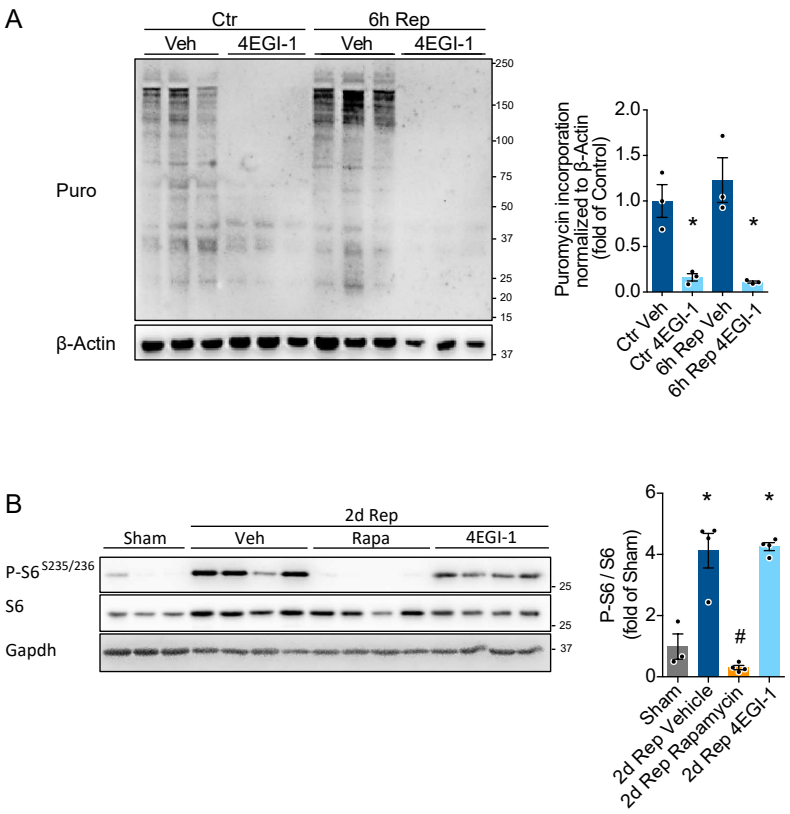


**Figure 25 | 4EGI-1 inhibits translation rates in adult cardiomyocytes**

**A,** Immunoblots and quantifications of puromycin incorporation in adult cardiomyocytes after 4EGI-1 treatment at baseline and after sI/R. B, Immunoblots and quantifications of mTORC1 activity of left ventricular lysates in response to rapamycin or 4EGI-treatment 2d after I/R surgery, n = 3-4. * indicates $p<0.05$ from control. # indicates $p<0.05$ from all other conditions. For statistical analysis a two-way ANOVA was used for **A** and a one-way ANOVA with Tukey post-hoc analysis was used for **B**. $p < 0.05$ was defined as significant difference. Error bars show standard error of the mean. Data of Figure 25B was produced jointly with Adrian Serafin. Figure legends from Hofmann et al. 2024[133].

My previous experiments used pharmacological compounds to investigate the involvement of the mTORC1-4EBP1-eIF4E axis on translational regulation after reperfusion. However, small molecular inhibitors may show unspecific targeting of other signaling pathways. To confirm the involvement of the mTORC1-4EBP1-eIF4E axis on cardiac translational regulation, I overexpressed 4EBP1 for 24 hours in NRCMs by adenovirus-mediated gene delivery (Ad4EBP1) and compared this condition to a control adenovirus (AdCtr) or no viral transfection, and quantified cellular translation rates. I determined optimal dosages by virus titration (Figure 26). I confirmed

overexpression of 4EBP1 by western blot (Figure 26). As described previously, overexpression of 4EBP1 caused a dimer formation, reported to increase the binding affinity towards eIF4E and eIF4F disruption, as shown below (Figure 27).[162] As expected, 4EBP1 overexpression in NRCMs resulted in suppression of translational activity (Figure 26A and 26B).

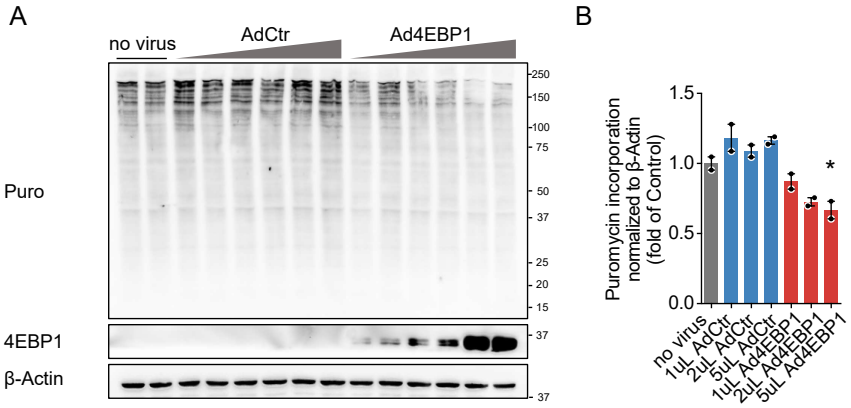


**Figure 26 | 4EBP1 inhibits translation in cardiomyocytes *in vitro***
**A** and **B**, Immunoblot and quantification of puromycin incorporation in response to increasing amounts of 4EBP1 overexpression with Ad4EBP1 in NRCMs, n = 2. * indicates p<0.05 from no virus. For statistical analysis one-way ANOVA with Tukey post-hoc analysis was used. p < 0.05 was defined as significant difference. Error bars show standard error of the mean. Figure legends from Hofmann et al. 2024[133].

Similar to the results observed by pharmacological eIF4F inhibition with 4EGI-1, 4EBP-1 overexpression in NRCMs resulted in strong suppression of the eIF4F complex (Figure 27A and 27B), as well as significant inhibition of cardiomyocyte translation rates after reperfusion *in vitro* (Figure 27C).

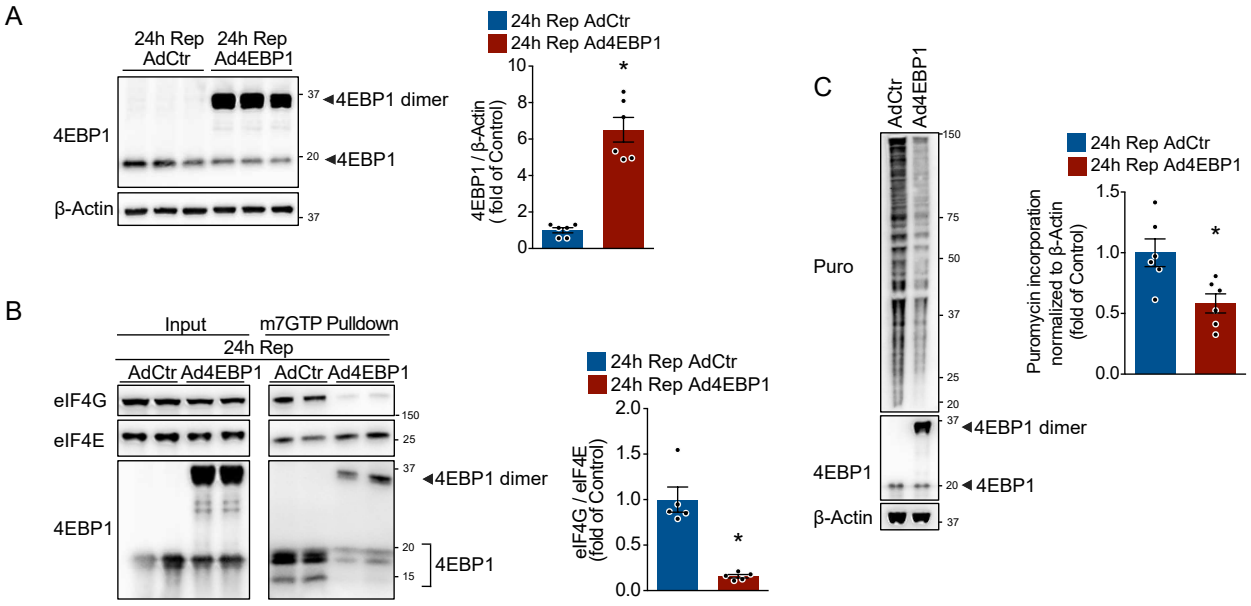


**Figure 27 | 4EBP1 overexpression inhibits eIF4F complex formation and translational rates after reperfusion in cardiomyocytes *in vitro***

**A** to **C**, Representative immunoblot and quantification of 4EBP1, n = 6 (**A**), eIF4F complex assembly, n = 5 (**B**) and puromycin incorporation, n = 6 (**C**) after AdCtr or Ad4EBP1 treatment and sI/R (24h Rep) in NRCMs. Adenovirus treatment was initiated 24h before induction of ischemia. WT 4EBP1 and dimer formation after overexpression as previously described[162] indicated by arrows. Rep (reperfusion), Puro (puromycin), Ctr (control), * indicates p<0.05 from AdCtr. For statistical analysis an unpaired two tailed t-test was used. p < 0.05 was defined as significant difference. Error bars show standard error of the mean. Figure legends from Hofmann et al. 2024[133].

To further confirm the impact of the mTORC1-4EBP1-eIF4E axis on cardiac translational activity after reperfusion *in vivo*, I used AAV9 encoding 4EBP-1 under control of a cardiomyocyte-specific Troponin T promotor to specifically overexpress 4EBP1 in cardiomyocytes of adult male mice (Figure 28A). I confirmed 4EBP1 overexpression two weeks after i.p. virus injection by western blot (Figure 28B). In comparison to 4EBP1 overexpression in NRCMs, AAV9-4EBP1 did not cause dimer formation *in vivo*, which is likely based on differences of baseline 4EBP1 phosphorylation *in vitro* and *in vivo*, which determines the tendency to form dimers.[162] 2 weeks after cardiomyocyte-specific overexpression of 4EBP1, mice were subjected

to I/R surgery (60 minutes ischemia). 24 hours after reperfusion, blood was collected, and serum Troponin T levels were quantified. 2 days after reperfusion I i.p. injected mice with puromycin and after 30 minutes isolated the hearts which I divided into infarct, border zone and remote areas (Figure 28A). While cardiomyocyte-specific overexpression did not affect serum Troponin T levels 24 hours after reperfusion (Figure 28C), it significantly attenuated translation rates of the border zone (Figure 28D to 28F), which is in line with the puromycin imaging data that showed increased translation rates of border zone cardiomyocytes after reperfusion (Figure 14A).

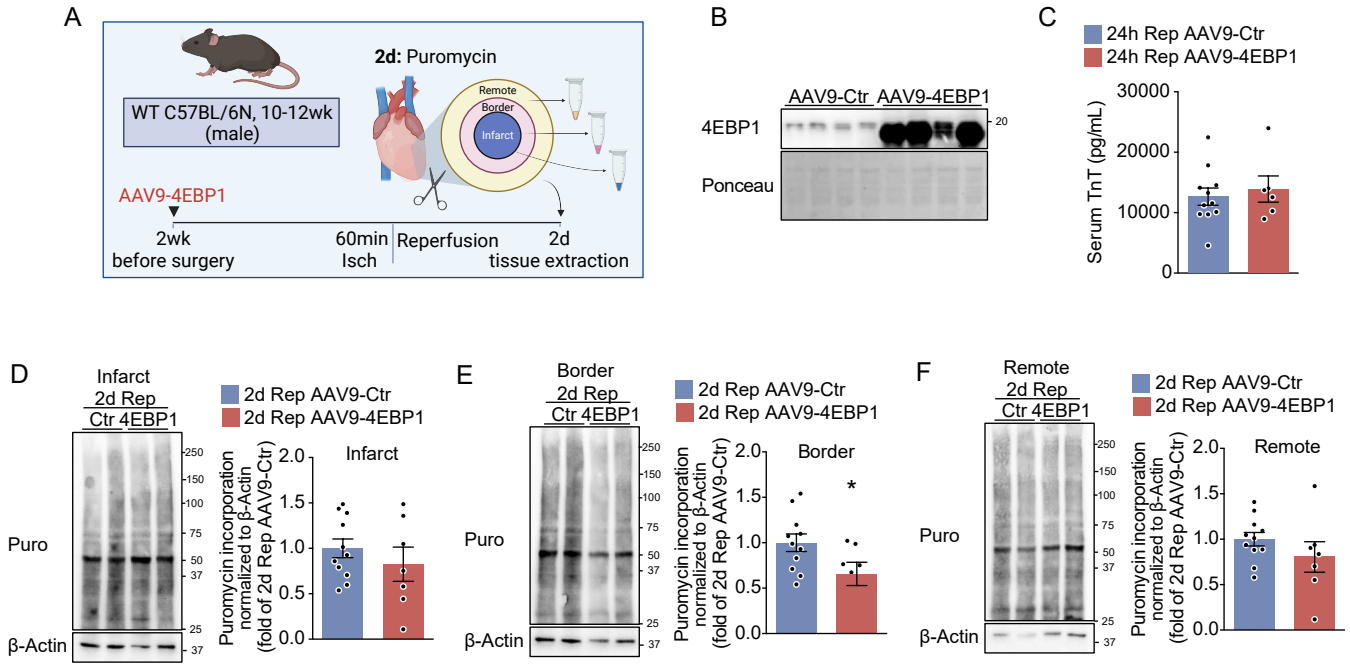


**Figure 28 | Cardiomyocyte-specific 4EBP1 overexpression inhibits translational activation of the border zone after reperfusion *in vivo***

**A**, Diagram of the experimental strategy used for B-F. **B**, Representative 4EBP1 immunoblot of left ventricular lysates 2 weeks after AAV9-Ctr or AAV9-4EBP1 i.v. injection. **C**, Serum Troponin T (TnT) levels 24h after I/R surgery in AAV9-Ctr and AAV9-4EBP1 treated mice, n = 7-11. **D** to **F**, Representative immunoblot and quantification of puromycin incorporation into the infarct (**D**), border zone (**E**) or remote area (**F**) 2d after reperfusion in AAV9-Ctr and AAV9-4EBP1 treated mice, n = 7-11. Rep (reperfusion), Puro (puromycin), Ctr (control), * indicates p<0.05 from AAV9-Ctr. For statistical analysis an unpaired two tailed t-test was used. p < 0.05 was defined as significant difference. Error bars show standard error of the mean. A made in ©BioRender - biorender.com. Figure legends from Hofmann et al. 2024[133].

To investigate the function of the translational burst observed after cardiac reperfusion, which was at least partly regulated by the mTORC1-4EBP1-eIF4F axis in the heart, rapamycin and 4EGI-1 were used in an *in vivo* model of ischemia/reperfusion to study the consequences of transient pharmacological inhibition of translation during cardiac reperfusion (Figure 29 to Figure 34). A singly i.p. injection of 6 mg/kg rapamycin was sufficient to suppress cardiac mTORC1 activity, assessed by ribosomal S6 S235/236 phosphorylation levels of left ventricular lysates, for up to 24 hours (Figure 29A and 29B). I selected a two-phased injection strategy, injecting 6 mg/kg rapamycin 30 minutes before reperfusion, followed by a 2 mg/kg maintenance dose after 24 hours. I reasoned that this could resemble a clinical translatable scenario during which rapamycin is immediately injected to patients with a confirmed ST-elevation myocardial infarction, followed by reperfusion in the catheterization laboratory and an additional drug administration at the next day. This treatment regime resulted in strong suppression of mTORC1 activity and inhibited cardiac translational activation at 2 days after reperfusion in mice (Figure 29C and 29D).

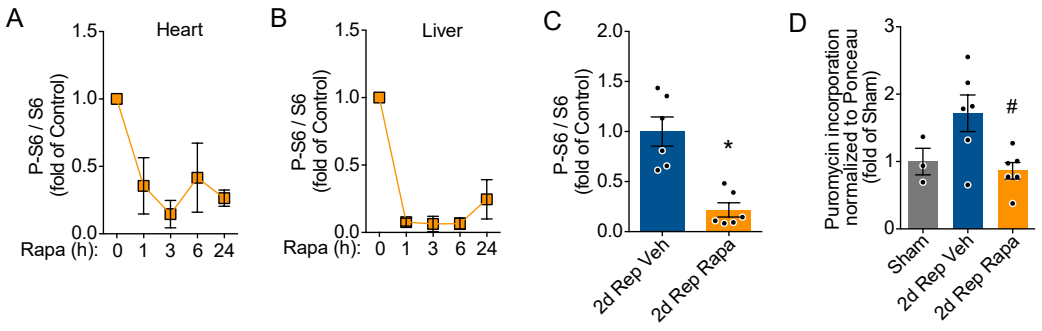


**Figure 29 | Rapamycin attenuates translational activation of the heart after reperfusion**

**A** and **B**, Quantification of cardiac (left ventricular lysates) (**A**) and hepatic (**B**) $S6^{S235/236}$ phosphorylation in male mice at different timepoints after 6 mg/kg rapamycin treatment, n = 5 (control), n = 4 (6 hours), n = 3 (24 hours) as assessed by immunoblot. **C**, $S6^{S235/236}$ phosphorylation of left ventricular lysates of vehicle or 2 and 6 mg/kg rapamycin treated mice 2 days after I/R surgery assessed by immunoblot, n = 6. **D**, Quantification of myocardial puromycin incorporation of left ventricular lysates *in vivo* 2 days after I/R surgery in response to 6 and 2 mg/kg rapamycin treatment, n = 3-6. Rep (reperfusion), Veh (vehicle),

Rapa (rapamycin). * indicates p<0.05 from control or sham. # indicates p<0.05 from 2wk Rep Veh. For statistical analysis an unpaired two tailed t-test was used for **C** and one-way ANOVA with Tukey post-hoc analysis for **D**. p < 0.05 was defined as significant difference. Error bars show standard error of the mean. Data of Figure 29 was produced jointly with Ole M. Schwerdt. Figure legends from Hofmann et al. 2024[133].

To further assess how this treatment regime affects cardiac injury and function, female and male 10-12 weeks old C57BL/6N mice were subjected to ischemia/reperfusion surgery and the rapamycin treatment regime described above, followed by functional assessment (Figure 30A). I compared Rapamycin treated mice to vehicle treated mice after I/R surgery and with sham operated mice. Rapamycin treatment did not affect myocardial cell death 24 hours after reperfusion, as assessed by a terminal deoxynucleotidyl transferase dUTP nick end labeling (TUNEL) assay (Figure 30B and 30C) or serum Troponin T levels (Figure 30D). However, rapamycin treatment showed a trend towards improved survival 2 weeks after reperfusion (Figure 30E). While heart weight to tibia length ratio (HW/TL) was not different between all groups (Figure 30F), left ventricular ejection fraction was significantly improved in rapamycin treated mice compared to vehicle treated mice 2 weeks after I/R surgery (Figure 30G). Further, infarct size at 2 weeks after reperfusion was reduced in rapamycin treated mice (Figure 30H). However, I observed no differences between expression levels of the heart failure markers Nppa, Nppb, Myh7 and Col1a1 between sham or rapamycin treated animals (Figure 30I).

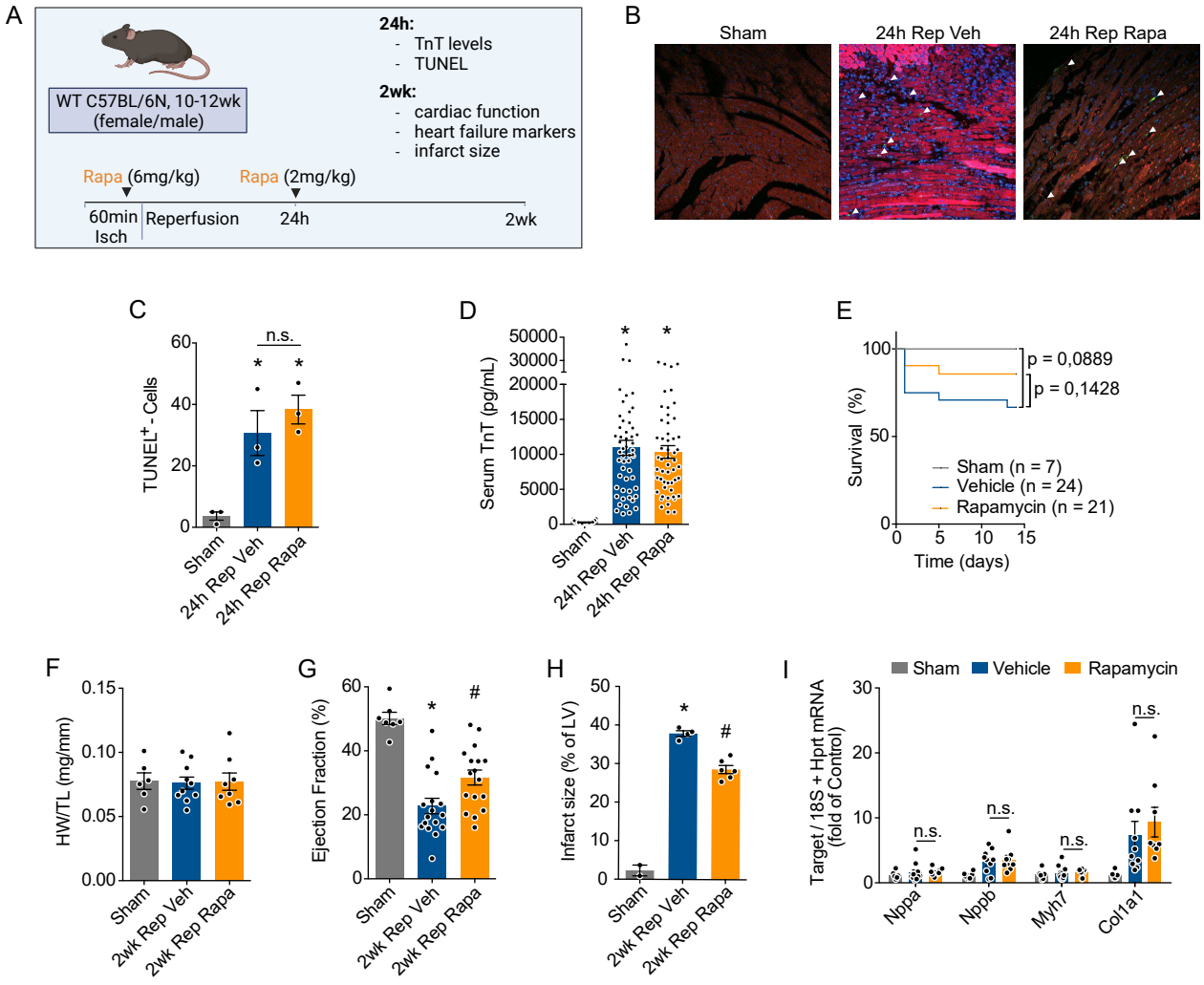


**Figure 30 | Pharmacological mTORC1 inhibition during reperfusion protects against I/R injury and improves cardiac function**

**A** Diagram of the experimental strategy used for B-I. **B** and **C**, Representative immunostaining and quantification of TUNEL⁺-cells per view by immunofluorescence in sham or I/R surgery operated mice treated with vehicle or 2 and 6 mg/kg rapamycin, n = 3-4. **D**, Serum Troponin T levels at 24 hours after I/R surgery in female and male mice (n = 24-53). **E**, 2-week survival of sham or I/R surgery operated mice treated with vehicle or 2 and 6 mg/kg rapamycin corresponding to mice used for J to M, n = 7-24. **F** to **I**, Heart weight (HW) to body weight (BW) ratio (**F**), left ventricular ejection fraction of female (n = 3-10) and male mice (n = 4-7) (**G**), infarct size (n = 2-6, male mice) (**H**), and left ventricular expression of Nppa, Nppb, Myh7 and Col1a1 (n = 6 for sham, n = 10 for vehicle and n = 8 for rapamycin, female mice) (**I**) 2 weeks after sham or I/R surgery operated mice treated with vehicle or 2 and 6 mg/kg rapamycin. Rep (reperfusion), Veh (vehicle), Rapa (rapamycin). * indicates $p<0.05$ from control or sham. # indicates $p<0.05$ from 2wk Rep Veh. For statistical analysis one-way ANOVA with Tukey post-hoc analysis was used for **C**, **D**, **F**, **G**, **H** and **I**. The logrank test was used to test for differences between survival curves using GraphPad Prism 7.0 for **E**. $p < 0.05$ was defined as significant difference. Error bars show standard error of the mean. A made in ©BioRender - biorender.com. Data of Figure 30 was produced jointly with Ole M. Schwerdt. Figure legends from Hofmann et al. 2024[133].

I observed no obvious sex differences for serum Troponin T levels or left ventricular ejection fraction between male and female mice after I/R surgery and rapamycin treatment (Figure 31). However, in the separate analysis between female and male mice, left ventricular ejection fraction of rapamycin treated mice did not reach statistically significant difference compared to vehicle treated mice after I/R surgery (cutoff of $p < 0.05$).

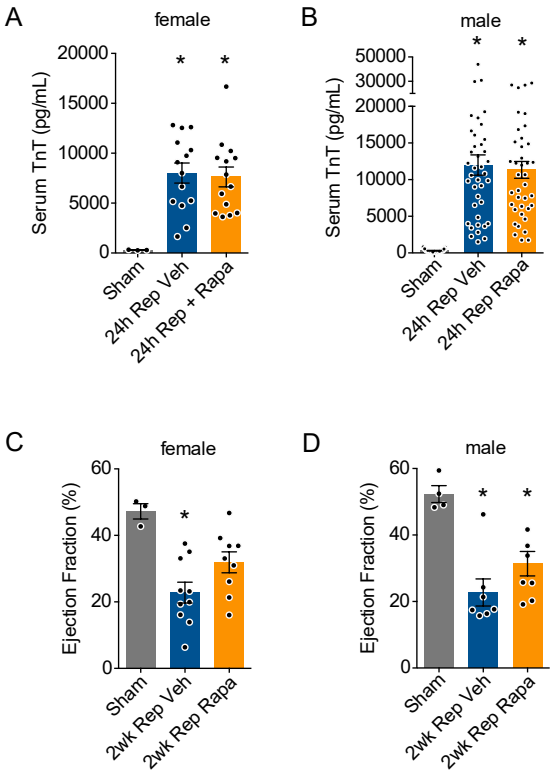


**Figure 31 | Sex-based sub-analysis of rapamycin treated mice after I/R surgery**
**A** and **B**, Serum Troponin T levels of female (**A**) and male (**B**) mice that were treated with vehicle or rapamycin. Serum TnT levels of blood taken 24 hours after I/R surgery. **C** and **D**, Left ventricular ejection fraction of female (**C**) and male (**D**) mice 2 weeks after sham or I/R surgery operated mice treated with vehicle or rapamycin. Rep (reperfusion), Veh (vehicle). * indicates $p<0.05$ from control or sham. # indicates $p<0.05$ from 2wk Rep Veh. For statistical analysis one-way ANOVA with Tukey post-hoc analysis was used. $p < 0.05$ was defined as significant difference. Error bars show standard error of the mean. Data of Figure 31 was produced jointly with Ole M. Schwerdt. Figure legends from Hofmann et al. 2024[133].

Rapamycin is a partly selective pharmacological mTORC1 inhibitor. Therefore, the observed cardioprotective effects may have also resulted from effects independent of translational regulation by the mTORC1-4EBP1-eIF4F axis. To more specifically study the functional relevance of mTORC1-dependent translational activity after reperfusion, the competitive eIF4E/eIF4G interaction inhibitor 4EGI-1 was used *in vivo*. First, increasing dosages of 4EGI-1 were i.p. injected to male mice and translational activity of left ventricular lysates were assessed by a puromycin assay (Figure 32A). Both 50mg/kg and 100mg/kg 4EGI-1 resulted in a significant attenuation of cardiac translation rates 6 hours after i.p. injection (Figure 32A). However, as the 100mg/kg dosage was associated with signs of systemic toxicity (3 of 5 injected mice deceased), I selected 50mg/kg 4EGI-1 i.p. for further investigation. A single i.p. injection of 50 mg/kg 4EGI-1 resulted in persistent attenuation of left ventricular translation rates for at least 24 hours, without disrupting upstream mTORC1 activity (Figure 32B and 32C).

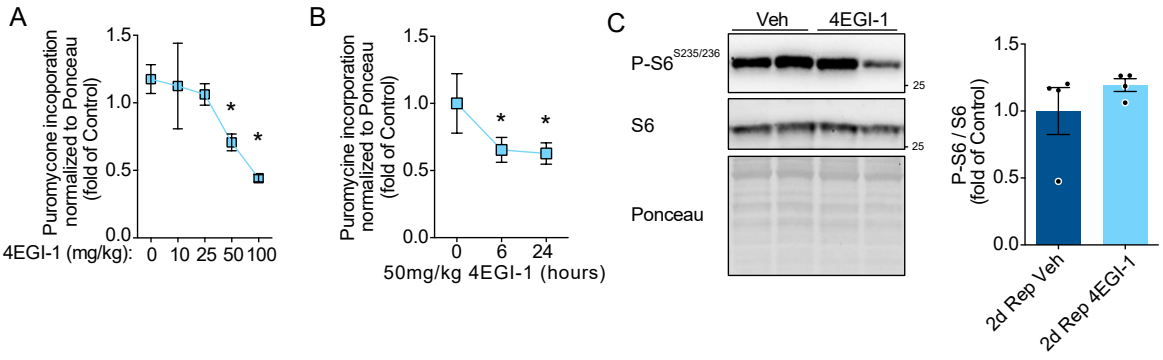


**Figure 32 | 4EGI-1 inhibits cardiac translation *in vivo***

**A** and **B**, Quantification of myocardial puromycin incorporation *in vivo* after 6 hours of 4EGI-1 treatment with different concentrations, n = 6 (0, 25 and 50 mg/kg); n = 2 (10 mg/kg and 100 mg/kg), (**A**) or at different timepoints after 4EGI-1 treatment, n = 5 (control), n = 4 (6 hours), n = 3 (24 hours) (**B**) as assessed by immunoblot. Puromycin was i.p. injected 30 minutes before animals were sacrificed. **C**, $S6^{S235/236}$ phosphorylation of left ventricular lysates of vehicle or 50 mg/kg 4EGI-1 treated mice 2 days after I/R surgery assessed by immunoblot, n = 4. Rep (reperfusion), Veh (vehicle). * indicates $p<0.05$ from control. For statistical analysis one-way ANOVA with Tukey post-hoc analysis was used for **A** and **B**. An unpaired two tailed t-test was used for **C**. $p < 0.05$ was defined as significant difference. Error bars show standard error of the mean. Data of Figure 32 was produced jointly with Ole M. Schwerdt. Figure legends from Hofmann et al. 2024[133].

Next, female and male mice were subjected to I/R surgery and treated with 4EGI-1. A similar approach comparable to the selected rapamycin treatment was chosen (50mg/kg 4EGI-1 i.p. 30 minutes before reperfusion, followed by a second 50mg/kg 4EGI-1 i.p. injection after 24 hours) (Figure 33A). The success of I/R surgery was determined by serum Troponin T, which was positively correlated to myocardial cell death, assessed by TUNEL staining (Figure 33B). No difference of myocardial cell death between vehicle and 4EGI-1 treated mice was observed by the quantification of TUNEL positive cells 24 hours after reperfusion (Figure 33C and 33D). Further, 4EGI-1 treatment did not affect serum Troponin T levels 24 hours after reperfusion, or survival up to 2 weeks or heart weight to tibia length ratios (Figure 33E to 33G). However, similar to the observations made with rapamycin treatment, transient 4EGI-1 treatment during and shortly after reperfusion resulted in improved left ventricular ejection fraction (Figure 33H) and reduced infarct size (Figure 33I). There was a trend towards reduced expression of heart failure markers in 4EGI-1-treated mice after I/R surgery compared to vehicle, but this only reached significance for Myh7 (Figure 33J).

As with rapamycin, I observed no obvious sex differences between female and male mice for serum Troponin T levels or left ventricular ejection fraction after I/R surgery compared to vehicle treated animals (Figure 34).

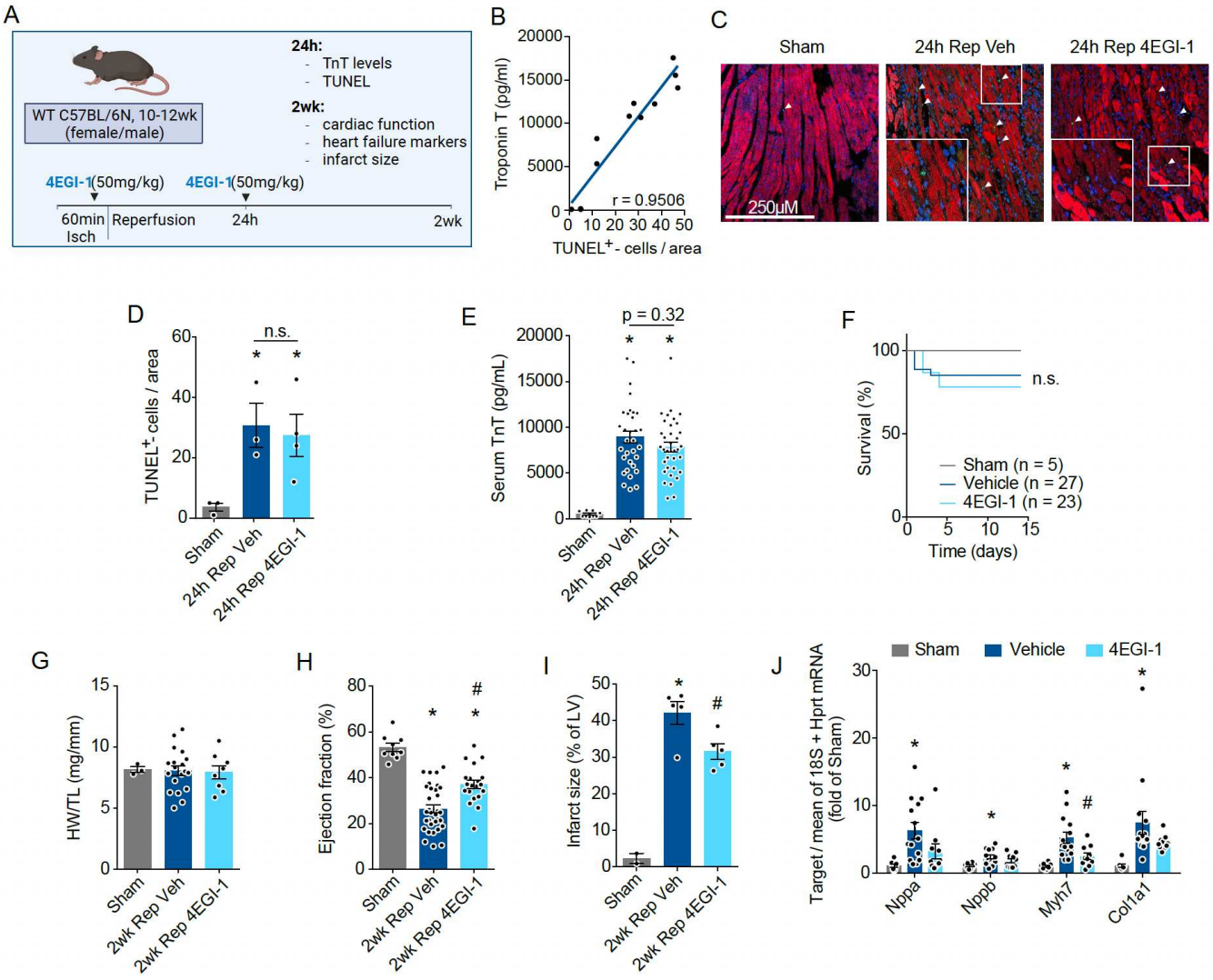


**Figure 33 | Short-term inhibition of eIF4F-dependent translation during reperfusion improves cardiac function**

**A**, Diagram of the experimental strategy used for B-J. **B**, Correlation of TUNEL+-cells to serum Troponin T levels. **C**, Representative immunostaining and **D**, quantification of TUNEL$^+$-cells per view by immunofluorescence in sham or I/R surgery operated mice treated with vehicle or 50 mg/kg 4EGI-1, n = 3-4. **E**, Serum Troponin T levels at 24 hours after I/R surgery in female (n = 2-13) and male mice (n = 7-25). **F**, 2-week survival of sham or I/R surgery operated mice treated with vehicle or 50 mg/kg 4EGI-1 corresponding to mice used for G to J, n = 5-27. **G, H, I** and **J**, Heart weight (HW) to body weight (BW) ratio (**G**), left ventricular ejection fraction of female (n = 2-13) and male mice (n = 7-19) (**H**), infarct size (n = 2-5 male mice) (**I**), and left ventricular expression of Nppa, Nppb, Myh7 and Col1a1 (n = 4-6 female mice and 8-14 male mice) (**J**) 2 weeks after sham or I/R surgery operated mice treated with vehicle or 50 mg/kg 4EGI-1. Rep (reperfusion), Veh (vehicle). * indicates p<0.05 from control or sham. # indicates p<0.05 from 2wk Rep Veh. For statistical analysis one-way ANOVA with Tukey post-hoc analysis was used for **D**, **E**, **G**, **H**, **I** and **J**. The logrank test was used to test for differences between survival curves using GraphPad Prism 7.0 for **F**. p < 0.05 was defined as significant difference. Error bars show standard error of the mean. A made in ©BioRender - biorender.com. Data of Figure 33B-D was produced jointly with Adrian Serafin. Data of Figure 33E-J was produced jointly with Ole M. Schwerdt. Figure legends from Hofmann et al. 2024[133].

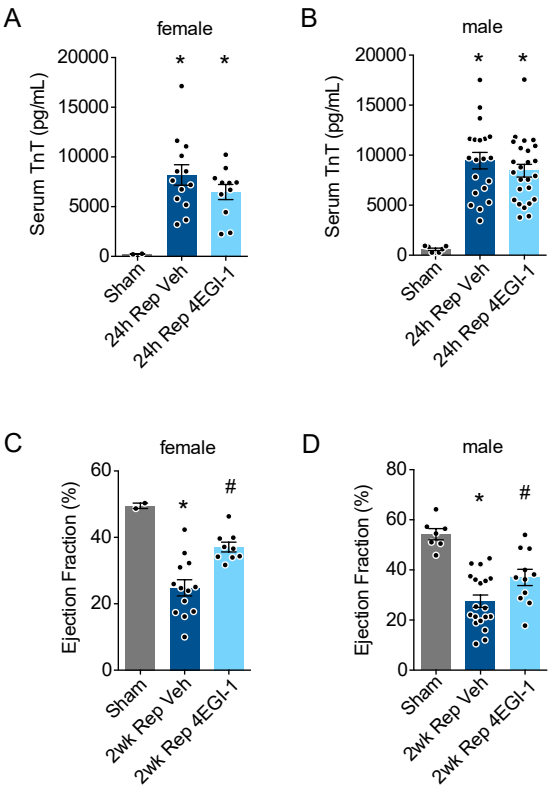


**Figure 34 | Sex-based sub-analysis of 4EGI-1 treated mice after I/R surgery**
**A** and **B**, Serum Troponin T levels of female (**A**) and male (**B**) mice that were treated with vehicle or 4EGI-1. Serum TnT levels of blood taken 24 hours after I/R surgery. **C** and **D**, Left ventricular ejection fraction of female (**C**) and male (**D**) mice 2 weeks after sham or I/R surgery operated mice treated with vehicle or 4EGI-1. Rep (reperfusion), Veh (vehicle). * indicates $p<0.05$ from control or sham. # indicates $p<0.05$ from 2wk Rep Veh. For statistical analysis one-way ANOVA with Tukey post-hoc analysis was used. $p < 0.05$ was defined as significant difference. Error bars show standard error of the mean. Data of Figure 34 was produced jointly with Ole M. Schwerdt. Figure legends from Hofmann et al. 2024[133].

After confirming a cardioprotective effect of transient inhibition of translation after reperfusion, I determined the mRNA network translated after reperfusion by ribosomal profiling (Ribo-Seq). This translational network expressed after reperfusion may facilitate maladaptive functions that are inhibited by transient inhibition of protein synthesis after reperfusion. I selected a cardiomyocyte-specific Ribo-Seq approach as this thesis focused on cardiomyocytes and their response to ischemia and reperfusion. I prepared cardiomyocyte-specific Ribo-Seq libraries from left ventricular lysates 2 days after reperfusion and generated them in parallel with RNA-Seq libraries for each

biological replicate from the identical lysate. Library quality control revealed high data quality (Figure 35). I removed reads from rRNAs, mtRNAs, tRNAs, snRNAs and of other ncRNAs from all libraries prior to further data analysis (Figure 35A and 35B). Ribo-Seq libraries retained sufficient periodic and uniquely mapping reads of correct ribosomal footprint length, that primarily mapped to mRNA coding sequence and showed in-frame periodicity (Figure 35C to 35E). Read p-site offset and read length were chosen by unbiased Bayesian model selection for each library and I selected reads mapping to genes with an average count of 10 per million reads for further analysis (Figure 35G to 35J). Principal component analysis strongly separated sham from I/R operated mice both for Ribo-Seq and RNA-Seq libraries (Figure 35K and 35L).

Reads of translated mRNAs (Ribo-Seq) covered most detected transcripts (RNA-Seq) and detected almost all proteins detected by mass spectrometry across all libraries (Figure 36A). There was a positive correlation between relative changes of gene expression after reperfusion by mass spectrometry compared to RNA-Seq and Ribo-Seq (Figure 36B and 36C). As expected, Ribo-Seq correlated slightly better with gene expression changes by mass spectrometry compared to RNA-Seq ($r = 0.5636$ vs $r = 0.5169$). At a false discovery rate (FDR) cutoff of $< 0.01$ 569 genes were significantly different expressed by both RNA-Seq and Ribo-Seq, 425 genes exclusively by RNA-Seq and 325 genes exclusively by Ribo-Seq (Figure 36D).

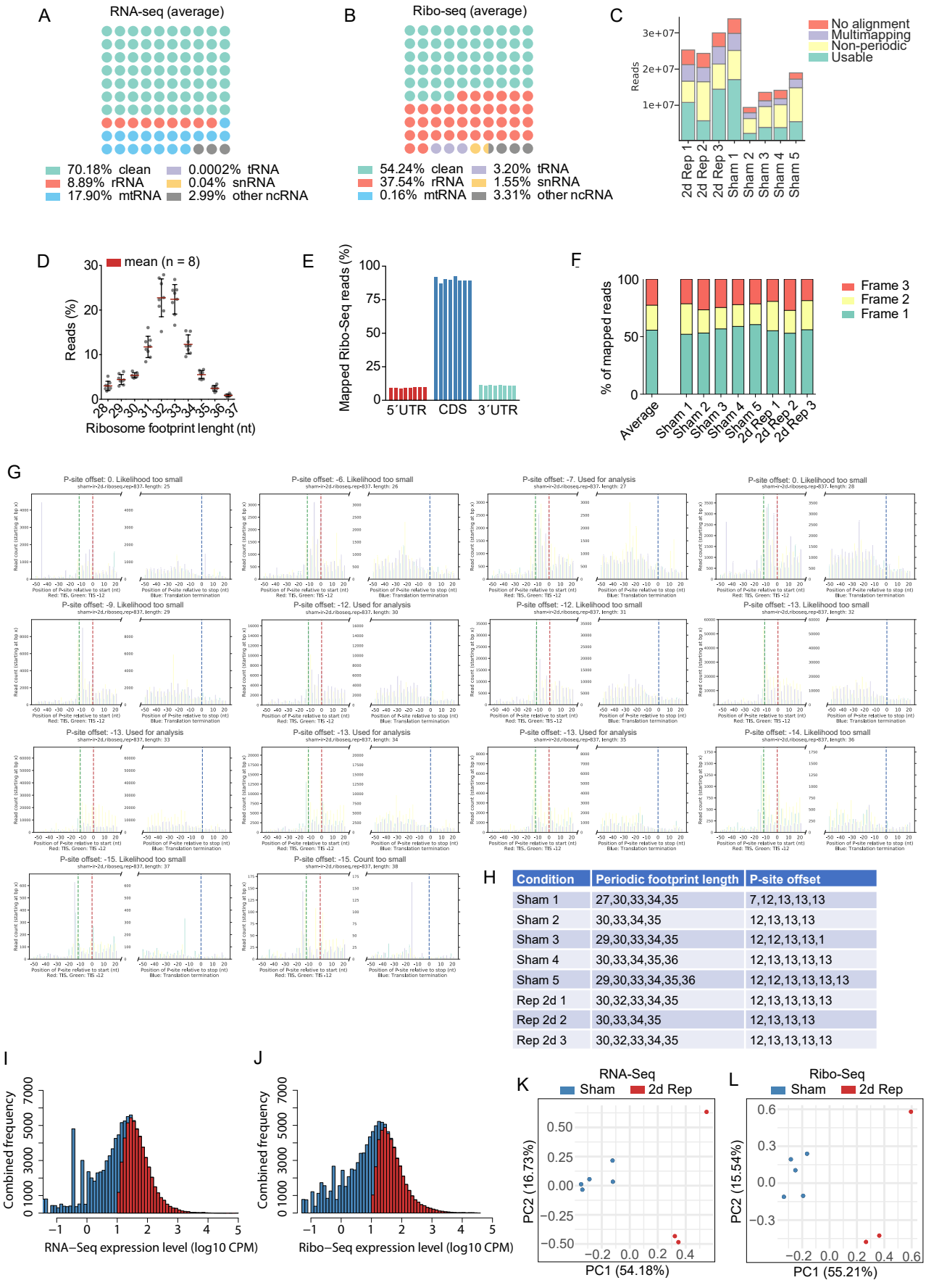


| Condition | Periodic footprint length | P-site offset |
|---|---|---|
| Sham 1 | 27,30,33,34,35 | 7,12,13,13,13 |
| Sham 2 | 30,33,34,35 | 12,13,13,13 |
| Sham 3 | 29,30,33,34,35 | 12,12,13,13,1 |
| Sham 4 | 30,33,34,35,36 | 12,13,13,13,13 |
| Sham 5 | 29,30,33,34,35,36 | 12,12,13,13,13,13 |
| Rep 2d 1 | 30,32,33,34,35 | 12,13,13,13,13 |
| Rep 2d 2 | 30,33,34,35 | 12,13,13,13 |
| Rep 2d 3 | 30,32,33,34,35 | 12,13,13,13,13 |

**Figure 35 | Quality control of RNA-Seq and Ribo-Seq data of sham or I/R surgery operated mice**

## Figure 35 | Quality control of RNA-Seq and Ribo-Seq data of sham or I/R surgery operated mice

**A** and **B**, Dot plot displaying the average fraction of raw sequence reads derived from rRNA, mtRNA, tRNA, snRNA and other ncRNA for RNA-Seq (**A**) and Ribo-Seq (**B**) data of left ventricular lysates derived from sham or I/R surgery operated mice. Only the 'cleaned' reads are used for subsequent data analysis. **C**, Ribo-seq read counts of all libraries showing periodic (usable), non-periodic, multi-mapped and non-aligning reads, when mapped to the mouse transcriptome. **D**, Beeswarm plot visualizing the sequenced ribosome footprint lengths across all samples. **E**, Bar plot showing the percentage of reads mapping to the coding sequence (CDS) and 5′ and 3′ untranslated regions (UTR) of annotated protein-coding genes. Each line represents a separate sample. **F**, Bar plot summarizing the ribosome protected footprint periodicity for all samples as the percentage of footprints that match the three reading frames of the annotated coding sequence genome wide. **G**, Graphical representation of the periodic profile Bayesian model selection showing results for different read lengths and p-site offsets for one typical library. **H**, Periodic footprint lengths and P-offset for all used libraries. **I** and **J**, Histograms showing the expression level of genes as measured by RNA-seq (**I**) and Ribo-Seq (**J**). Expression levels of all genes across all samples are included. Genes that met our expression cutoff of 10 counts per million (CPM) are colored red. **K** and **L**, Principal component analysis of RNA-seq (**K**) and Ribo-seq (**L**) libraries after sham or I/R surgery. Rep (reperfusion). Detailed information on statistical analysis can be found in the method section. Figure legends from Hofmann et al. 2024[133].

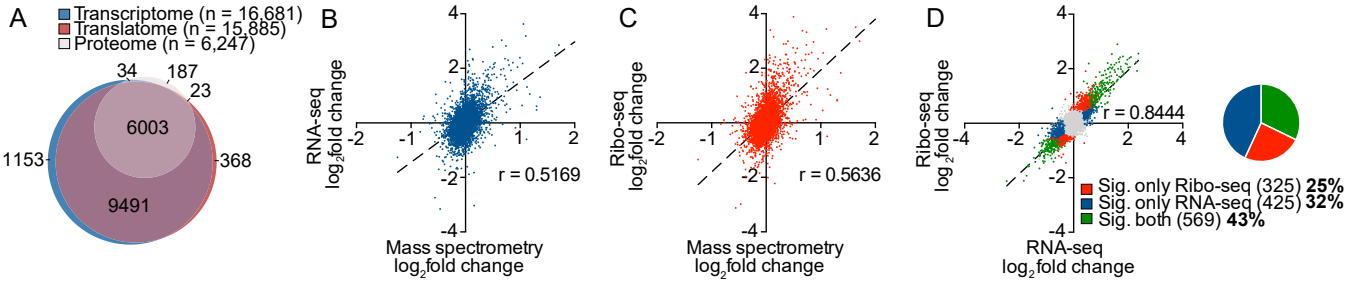


## Figure 36 | Parallel generation of RNA-seq, Ribo-seq and Mass spectrometry libraries of mouse hearts after reperfusion

**A**, Venn diagram of gene products detected in the transcriptome, translatome, and proteome of left ventricular lysates 2 days after I/R surgery in this study. **B** and **C**, Gene-based scatterplot showing the correlation between RNA-seq (blue, **B**) and Ribo-seq (red, **C**) expression levels and protein abundance by mass spectrometry. Correlation coefficients are Pearson r values. **D**, Scatter plot of Ribo-seq vs. RNA-seq in sham- and I/R-operated mice 2 days after surgery. Transcripts were considered significant when false discovery rate <0.01. Gray dots indicate no significant change. Significant change at translational level is shown in red, at transcriptional level in blue, and regulation at both translational and transcriptional levels in green. N ≥ 3 for each time point. RNA-seq Sham n = 5, RNA-seq Rep n = 3, Ribo-seq Sham n = 5, Ribo-seq Rep n = 3, mass spectrometry Sham = 2, mass spectrometry Rep n = 3. Rep (reperfusion). Detailed information on statistical analysis can be found in the method section. Figure legends from Hofmann et al. 2024[133].

A gene ontology analysis of biological processes enriched in genes expressed significantly different by Ribo-Seq revealed that transcripts related to processes of cell migration, cell adhesion, inflammation and cytoskeleton organization were significantly more translated, whereas transcripts related to mitochondrial translation, mitochondrial respiration and cardiac muscle contraction were significantly less translated in cardiomyocytes 2 days after reperfusion (Figure 37A and 37B). Transcripts previously shown to be encoded in an mTOR-dependent manner were significantly more translated after reperfusion, while their transcription was not different to other genes (Figure 37C). This further indicates that activation of the mTORC1 pathway results in translational activation of specific classes of transcripts in response to cardiac ischemia/reperfusion.

Due to the strong upregulation of genes related to inflammation and cell inflammation, the effects of transient inhibition of translation after reperfusion on immune cell infiltration to the injured myocardium was assessed. The gating strategy selected leukocytes by CD45, followed by gating of neutrophils and macrophages/monocytes by CD11b and the relative signal intensity of a lineage panel consisting of Ter119, CD90, B220, CD49b, NK1.1 and Ly6G (Figure 38). Monocytes and macrophages were further differentiated by the relative signal intensity for Ly6C and F40/80 (Figure 38).

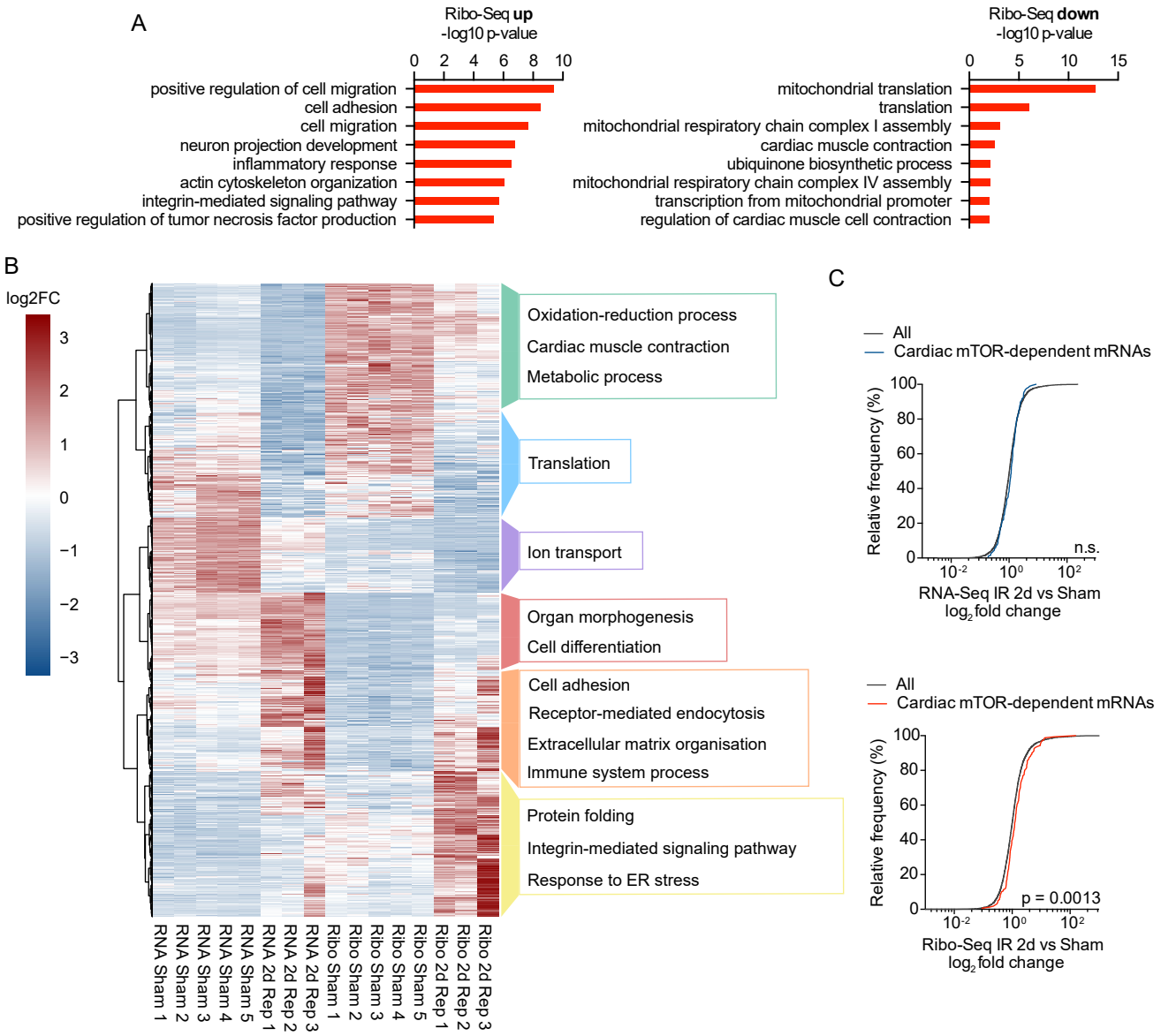


**Figure 37 | Cell-type-specific Ribo-seq identifies the translational response of cardiomyocytes to reperfusion**

**A**, Enrichment of GO terms for translationally up- and downregulated transcripts in cardiomyocytes 2d after reperfusion. The eight most significant GO terms per group were displayed. **B**, Unbiased clustering analysis of RNA-seq and Ribo-Seq of differently expressed genes 2d after I/R surgery. Different colors indicate different clusters. Enriched GO terms containing more than 5 significantly regulated genes/transcripts are shown on the right for each cluster. **C**, Cumulative fraction of all detected transcripts and detected cardiac mTOR-dependent mRNAs relative to their fold change of RNA-seq (top) or Ribo-seq (below). Cardiac mTOR-dependent mRNAs were defined as genes with a heart-specific TOP score ≥ 2 from Philippe et al[105] that were expressed in our RNA-seq and Ribo-seq datasets. RNA-seq Sham n = 5, RNA-seq Rep n = 3, Ribo-seq Sham n = 5, Ribo-seq Rep n = 3, mass spectrometry Sham = 2, mass spectrometry Rep n = 3. Rep (reperfusion). Detailed information on statistical analysis can be found in the method section. Figure legends from Hofmann et al. 2024[133].

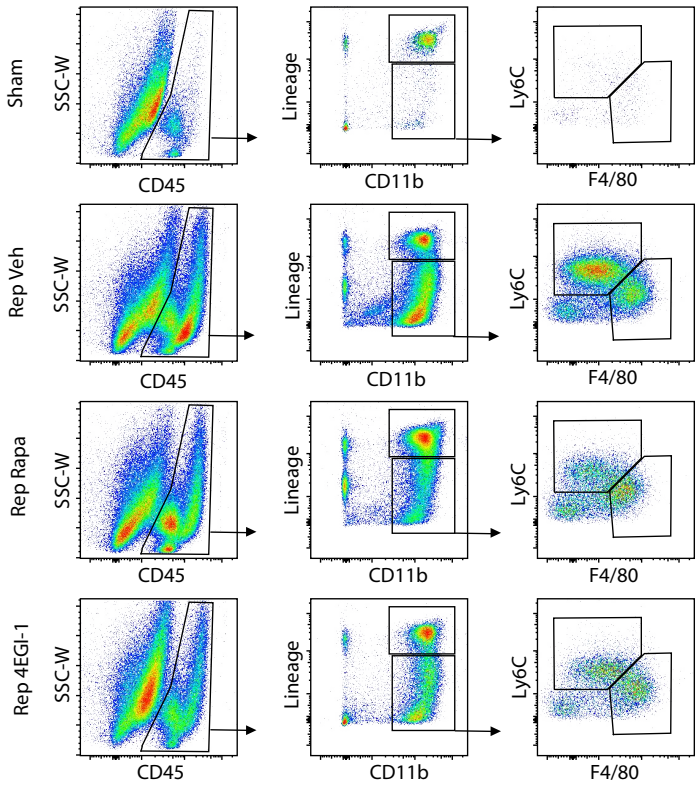


**Figure 38 | FACS gating strategy used for Figure 39**

**A**, Gating strategy and representative flow cytometric plots of mouse hearts 2 days after sham or I/R surgery treated with vehicle, 2 and 6 mg/kg rapamycin or 50 mg/kg 4EGI-1. Left ventricular anterior walls that contained the infarct and border zone were lysed and used as input to enrich for infiltrated immune cells. Lineage represents the combined signal intensity for Ter119, CD90, B220, CD49b, NK1.1 and Ly6G. Data of Figure 38 was produced jointly with Adrian Serafin. Figure legends from Hofmann et al. 2024[133].

FACS based immune cell enumeration revealed that both a transient treatment with rapamycin or 4EGI-1 resulted in a marked reduction of myocardial monocytes/macrophage numbers (Figure 39). There was a stronger suppression of proinflammatory Ly6C$^{high}$ monocytes compared to Ly6C$^{low}$ macrophages (Figure 39C and 39D), indicative of an inhibition of the infiltration of monocytes during the early inflammatory phase after cardiac injury by pharmacological inhibition of the mTORC1-4EBP1-eIF4E axis. There was no effect on myocardial neutrophil numbers (Figure 42B), suggesting that rapamycin or 4EGI-1 affect a signaling axis early after reperfusion that specifically regulates monocyte infiltration rather than acting anti-inflammatory in general.

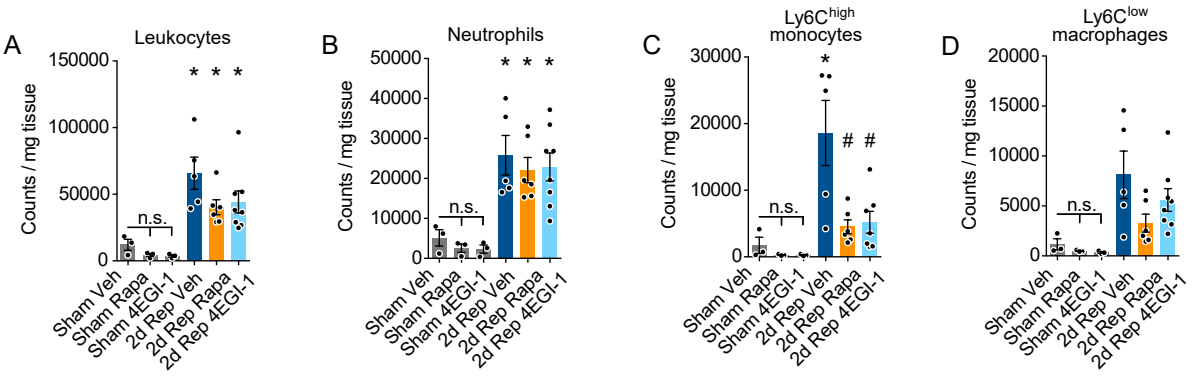


**Figure 39 | Pharmacological inhibition of the mTORC1-4EBP1-eIF4F axis attenuates proinflammatory Ly6C$^{high}$ monocyte infiltration to the myocardium**
**A** to **D**, Flow-cytometry based enumeration of leukocytes (**A**), neutrophiles (**B**). Ly6C$^{high}$ monocytes (**C**) and Ly6C$^{lo}$/F40$^{+}$ macrophages (**D**) per mg heart tissue 2 days after sham or I/R surgery in animals treated with vehicle, 2 and 6 mg/kg rapamycin, or 50 mg/kg 4EGI-1, n = 3-8. Rep (reperfusion), Veh (vehicle). * indicates $p<0.05$ from sham. # indicates $p<0.05$ from 2d Rep Veh. For statistical analysis one-way ANOVA with Tukey post-hoc analysis was used for **A, B, C** and **D**. $p < 0.05$ was defined as significant difference. Error bars show standard error of the mean. Data of Figure 39 was produced jointly with Adrian Serafin. Figure legends from Hofmann et al. 2024[133].

mTORC1 inhibitors are clinically used as immunosuppressants or anti-proliferative agents. To evaluate immunosuppressive off-target effects, circulating immune cells and proliferative bone marrow cells were quantified (Figure 40 and Figure 41). Neither rapamycin or 4EGI-1 reduced circulating monocyte numbers (Figure 40) or proliferative bone marrow cells (Figure 41), suggesting that the reduced myocardial monocyte numbers after transient inhibition of the mTORC1-4EBP1-eIF4E axis results from an impairment of cell infiltration rather than cell proliferation, which would be in line with the Ribo-Seq data that showed that transcripts that are significantly more translated 2 days after reperfusion are enriched for functions related to cell migration (Figure 37A).

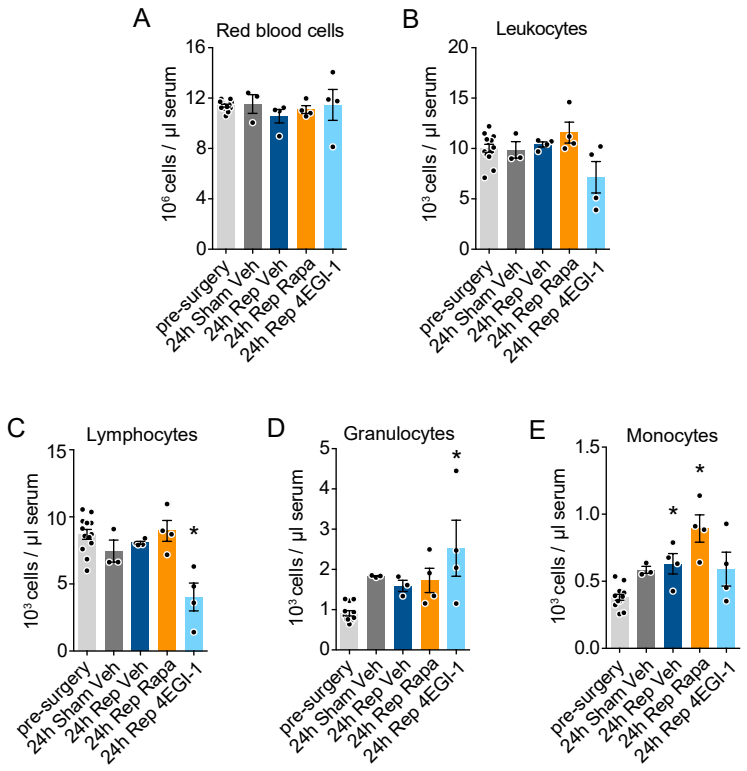


**Figure 40 | Blood cell count of mice after I/R surgery and treatment with rapamycin or 4EGI-1**

**A** to **E**, Blood cell count of red blood cells (**A**), leucocytes (**B**), lymphocytes (**C**), granulocytes (**D**) and monocytes (**E**) 24 hours after I/R surgery in male mice in treated with vehicle, 2 and 6 mg/kg rapamycin or 50 mg/kg 4EGI-1, n = 3-13. Rep (reperfusion), Veh (vehicle), Rapa (rapamycin). * indicates p<0.05 from pre-surgery. For statistical analysis one-way ANOVA with Tukey post-hoc analysis was used for **A** to **E**. p < 0.05 was defined as significant difference. Error bars show standard error of the mean. Data of Figure 40 was produced jointly with Adrian Serafin. Figure legends from Hofmann et al. 2024[133].

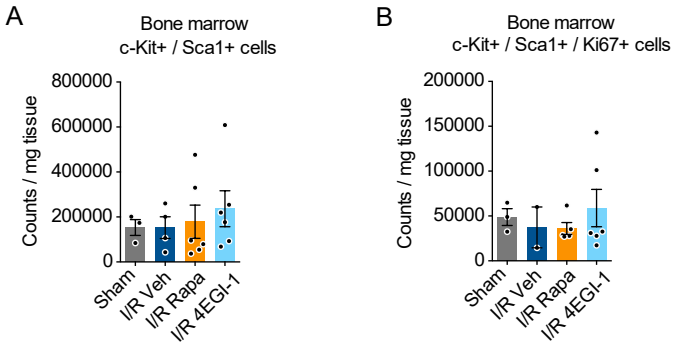


**Figure 41 | Bone marrow proliferative cells of mice after I/R surgery and treatment with rapamycin or 4EGI-1**

**A** and **B.** Flow-cytometry based enumeration of bone marrow c-Kit$^+$/Sca1$^+$ cells (**A**) and bone marrow c-Kit$^+$/Sca1$^+$/Ki67$^+$ cells (**B**) 2 days after sham or I/R surgery in animals treated with vehicle, 2 and 6 mg/kg rapamycin, or 50 mg/kg 4EGI-1, n = 2-6. Rep (reperfusion), Veh (vehicle). For statistical analysis one-way ANOVA with Tukey post-hoc analysis was used. p < 0.05 was defined as significant difference. Error bars show standard error of the mean. Data of Figure 41 was produced jointly with Adrian Serafin. Figure legends from Hofmann et al. 2024[133].

As transient pharmacological inhibition of the mTORC1-4EBP1-eIF4E axis appeared to inhibit certain inflammatory signals that may be involved in the cardioprotective effects of rapamycin and 4EGI-1 after I/R surgery, the expression of classical inflammatory markers of sham or I/R operated mice, treated with vehicle, rapamycin or 4EGI-1 was quantified in left ventricular lysates (Figure 42). While there was a trend towards attenuated tumor necrosis factor (Tnf) expression after rapamycin or 4EGI-1 treatment, which did not reach statistical significance defined as $p < 0.05$ by one-way ANOVA, and a decrease of interleukin 1b (Il1b) expression after 4EGI-1 treatment, the examined gene expression profile did not indicate a downregulation of cardiac inflammation in general as the driving factor of inhibition of monocyte infiltration to the injured heart (Figure 42), further supporting the hypothesis of a specific mTORC1-4EBP1-eIF4E axis-regulated pathway that mediates monocyte infiltration.

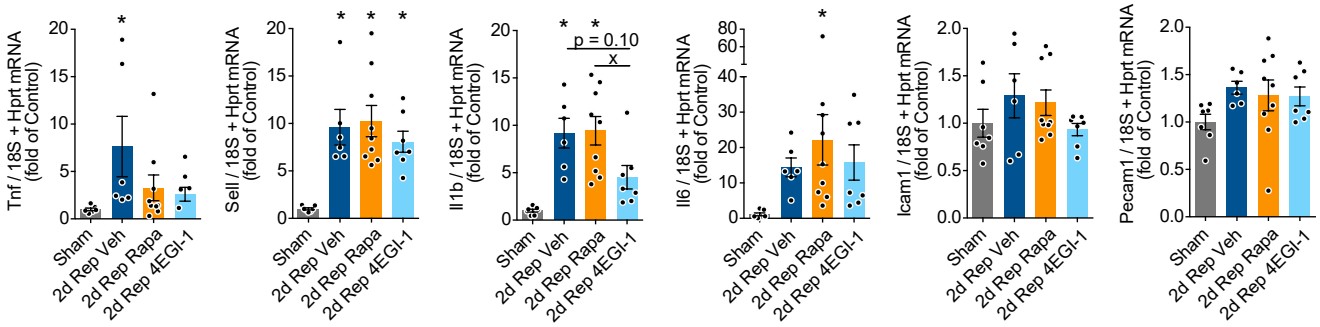


**Figure 42 | Inhibition of the mTORC1-4EBP1-eIF4F axis has minor effects on selected inflammatory markers that do not explain impaired monocyte infiltration**

mRNA levels of selected inflammatory genes of left ventricular lysates 2 days after sham or I/R surgery in animals treated with vehicle, 2 and 6 mg/kg rapamycin, or 50 mg/kg 4EGI-1 measured by RT-qPCR, n = 6-9. Rep (reperfusion), Veh (vehicle). * indicates $p<0.05$ from sham. x indicates $p<0.05$ from 2d Rep Rapa. For statistical analysis one-way ANOVA with Tukey post-hoc analysis was used. $p < 0.05$ was defined as significant difference. Error bars show standard error of the mean. Data of Figure 42 was produced jointly with Adrian Serafin. Figure legends from Hofmann et al. 2024[133].

The RNA-Seq and Ribo-Seq data revealed that C-C Motif Chemokine Ligand 2 (*Ccl2*) gene and transcript, also known as Monocyte Chemoattractant Protein-1 (MCP-1), was one of the strongest regulated genes 2 days after reperfusion (Figure 43A to 43C). The CCL2 protein is a secreted chemokine that displays strong chemotactic activity for monocytes.[163] It has been implicated as an essential element for the attraction of monocytes to the injured heart after myocardial infarction.[22,163] The *Ccl2* gene was previously primarily shown to be expressed by immune cells and fibroblasts,[164] however recent reports also indicated *Ccl2* gene expression and release of the CCL2 protein by cardiomyocytes in response to ischemia and reperfusion.[165–167] Indeed, *Ccl2* transcript expression was almost undetectable at baseline in the cardiomyocyte-specific Ribo-Seq dataset but was strongly expressed after I/R (Figure 43C). Whole left ventricular lysates of vehicle, rapamycin or 4EGI-1 treated mice revealed that *Ccl2* mRNA and CCL2 protein is strongly induced 2 days after reperfusion compared to sham-operated mice and that this upregulation was significantly blunted after rapamycin or 4EGI-1 treatment both on the transcript and protein level (Figure 43D and Figure 43E). This indicates translational dependence of CCL2 upregulation after cardiac reperfusion. However, as monocytes themself strongly express *Ccl2* mRNA and CCL2 protein, reduced *Ccl2* transcript levels and CCL2 protein levels may also stem from impaired monocyte infiltration to the myocardium. CCL2 staining of the border zone of vehicle or 4EGI-1 treated animals revealed a perinuclear vesicle like staining pattern typical of a secreted chemokine and confirmed that a variety of different cell types, including cardiomyocytes, induce CCL2 protein after reperfusion (Figure 43F). This upregulation of CCL2 in border zone cells was attenuated after pharmacological inhibition of mTORC1-dependent translation (Figure 43F). A FACS analysis of the reperfused left ventricular anterior wall showed that 4EGI-1 treatment did not affect the relative frequency and intensity of CCL2 of

cardiac monocytes but reduced overall numbers of detected monocytes by FACS (Figure 43G to 43I). The gating strategy I used to quantify CCL2 levels of cardiac monocytes is shown in Figure 44. This data indicates that the inhibition of cardiac CCL2 protein levels after pharmacological inhibition of the mTORC1-4EBP1-eIF4E axis is the result of both attenuated *Ccl2* gene activation and synthesis of border zone cells, as well as of impaired infiltration of CCL2-expressing monocytes.

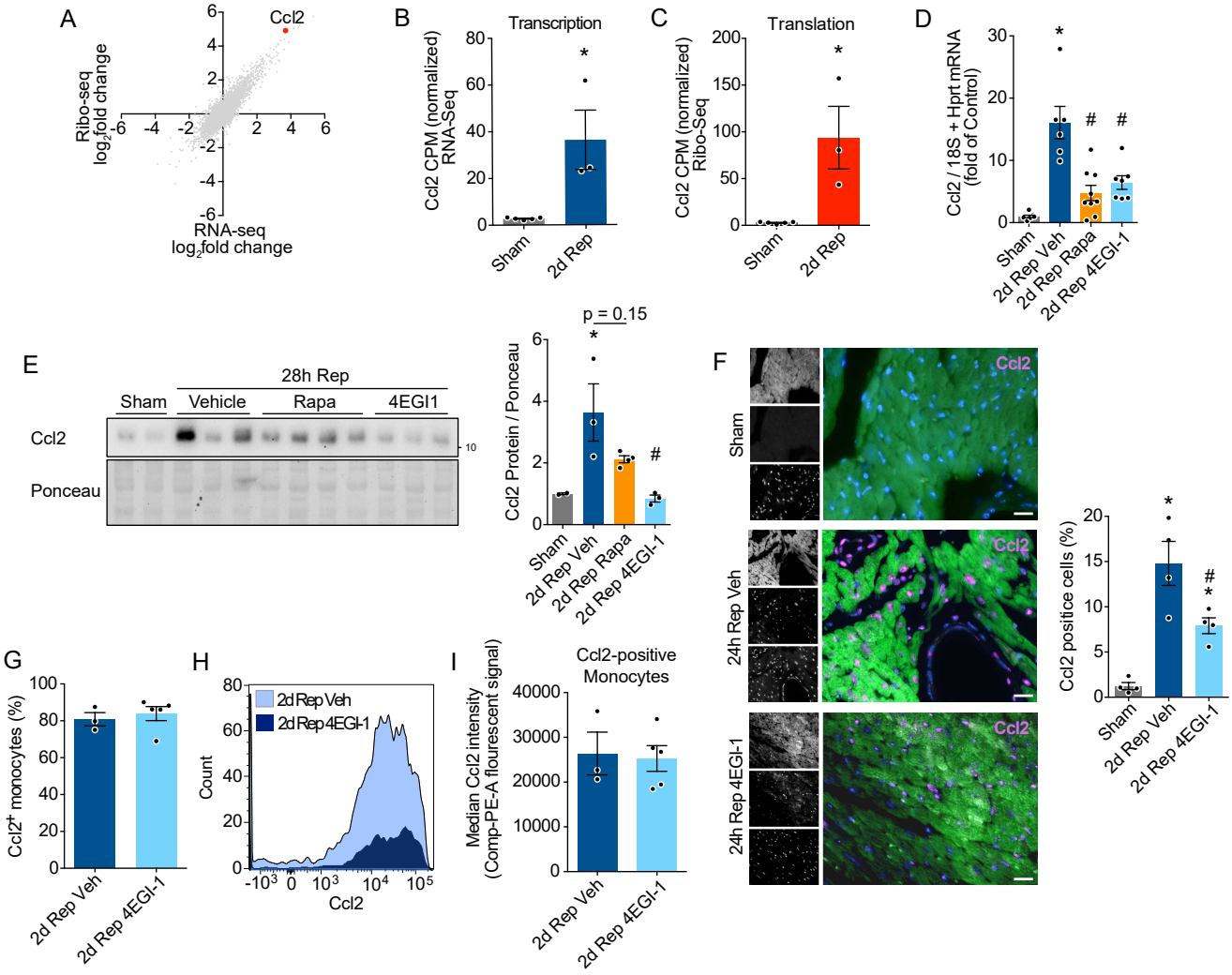


**Figure 43 | Inhibition of mTORC1-4EBP1-eIF4F dependent translation during reperfusion attenuates cardiac *Ccl2* expression**

**A**, Scatter plot of Ribo-seq vs. RNA-seq in sham- and I/R-operated mice 2 days after surgery highlighting Ccl2 expression (red). **B** and **C**, RNA-seq and Ribo-seq expression data of *Ccl2* in sham and I/R operated mice (CPM - count per million), n = 3-5. **D** and **E**, *Ccl2* mRNA levels, measured by RT-qPCR n = 6-9 (**D**) and CCL2 immunoblot, n = 2-4 (**E**) of left ventricular lysates 2d after sham or I/R surgery in animals treated with vehicle, 2 and 6 mg/kg rapamycin, or 50 mg/kg 4EGI-1. **F** Representative CCL2

(pink) and Troponin T (green) immunostaining and respective quantifications of the border zone of mice 24h after sham or I/R surgery which were treated with vehicle or 50mg/kg 4EGI-1, n = 4, approximately 600 cells were counted per animal. **G** to **I**, FACS quantification of CCL2 positive Ly6C$^{hi}$ monocytes (**G**), representative CCL2 monocyte histogram (**H**) and quantification of median CCL2 intensity of CCL2-positive Ly6C$^{hi}$ monocytes (**I**) of vehicle or 4EGI-1 treated mice 48h after I/R surgery. Rep (reperfusion), Veh (vehicle). * indicates p<0.05 from sham. # indicates p<0.05 from 2d Rep Veh. x indicates p<0.05 from 2d Rep Rapa. For statistical analysis one-way ANOVA with Tukey post-hoc analysis was used for **D, E** and **F**. An unpaired two tailed t-test was used for **B, C, G** and **I**. p < 0.05 was defined as significant difference. Error bars show standard error of the mean. Data of Figure 43D was produced jointly with Adrian Serafin. Figure legends from Hofmann et al. 2024[133].

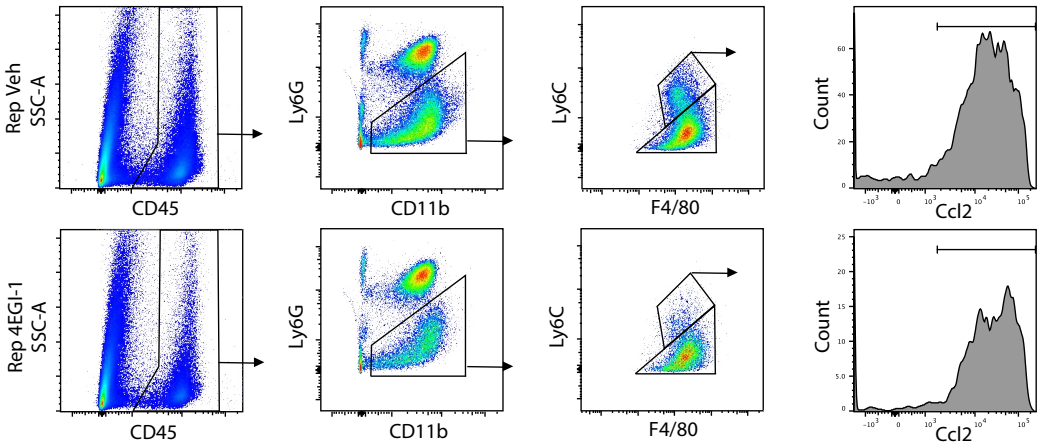


**Figure 44 | FACS gating strategy used to quantify monocyte CCL2 levels**
**A**, Gating strategy and representative flow cytometric plots of mouse hearts 2 days after sham or I/R surgery treated with vehicle or 50 mg/kg 4EGI-1. Left ventricular anterior walls that contained the infarct and border zone were lysed and used as input to enrich for infiltrated immune cells. The marked area of the histogram was defined as CCL2$^{+}$ monocytes. Figure legends from Hofmann et al. 2024[133].

As rapamycin and 4EGI-1 treatment resulted in an inhibition of cardiac *Ccl2* transcript levels, their mode of action may also involve the inhibition of an upstream transcriptional activator required for transcriptional induction of *Ccl2* in the injured myocardium. To test this hypothesis the *Ccl2* promotor was screened for transcription factor binding motifs, revealing predicted binding sites of 256 transcription factors (Figure 45A). I screened those transcription factors for translational upregulation in response to cardiac reperfusion at 2 days. This revealed the 3 transcription factors JUNB, FOSL2 and STAT3 that are translationally regulated and are predicted to bind

regulation of *Ccl2* transcript levels (Figure 45A). Of those, JUNB and STAT3 were previously shown to regulate *Ccl2* expression during conditions of cellular stress.[168,169] Interestingly, Junb and Fosl2 form the AP-1 transcription factor that is involved in the regulation of inflammatory responses in the heart.[170] Through analysis of previously published Assay for Transposase-Accessible Chromatin coupled to high-throughput sequencing (ATAC-Seq) data of mouse hearts after myocardial infarction[171] I revealed an AP-1 consensus motif and several JASPAR-predicted AP-1 and STAT3 binding sites in two *Ccl2* promotor regions that have increased chromatin accessibility after myocardial infarction (Figure 45B and 45C). However, neither rapamycin or 4EGI-1 reduced JUNB or FOSL2 levels after reperfusion (Figure 45D). In addition, both drugs did not affect AP-1 promotor activity of a luciferase reporter expressed in Hela cells (Figure 45E). While this data makes the AP-1 transcription factor less likely to be a responsible driver of reduced cardiac CCL2 levels after pharmacological inhibition of the mTORC1-4EBP1-eIF4E axis, it cannot be fully excluded that AP-1 or other transcription factors such as STAT3 are at least partly involved in the translational-dependent regulation of CCL2 in the injured heart after reperfusion.

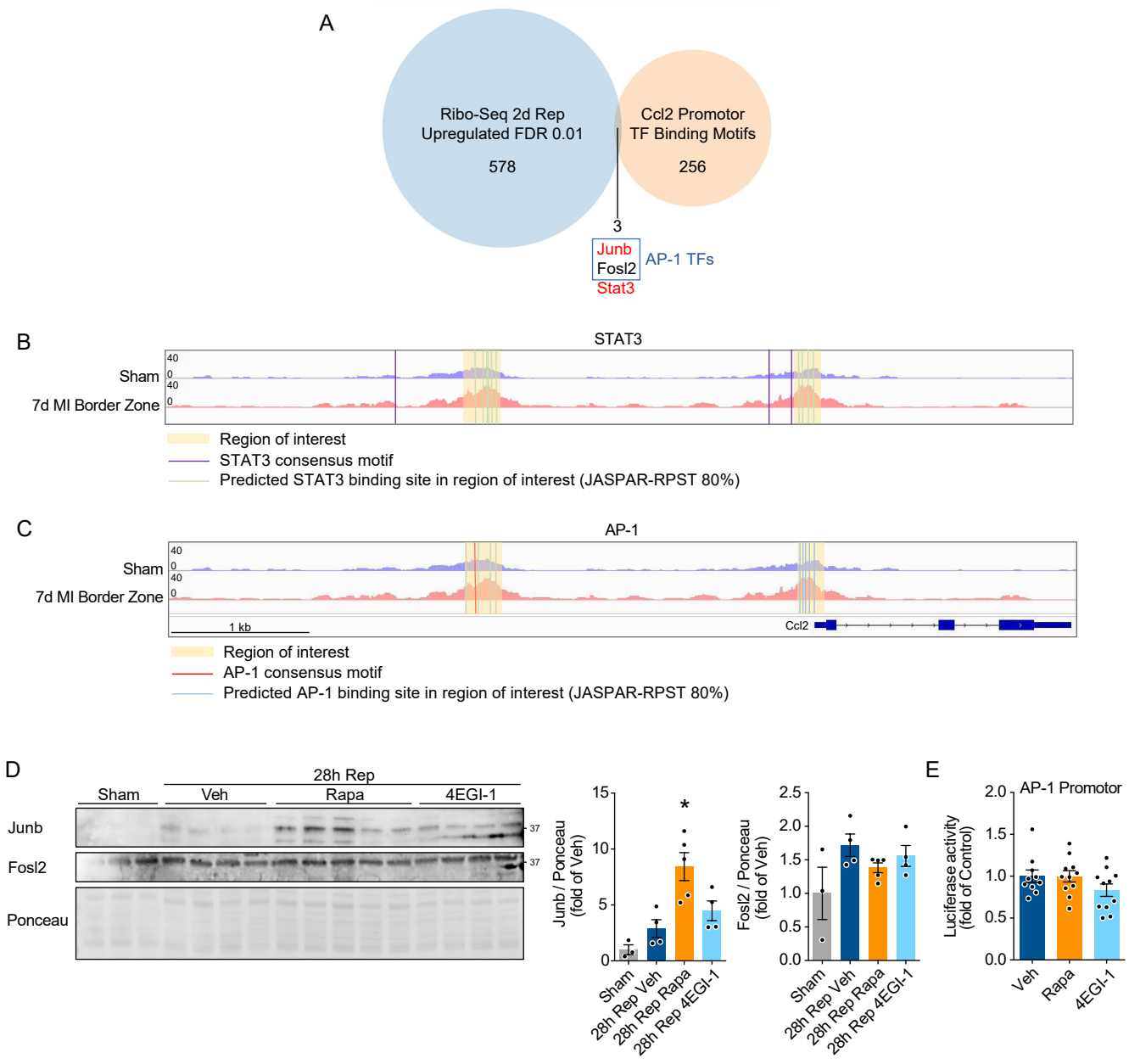


**Figure 45 | Candidate transcription factors regulated by translation that control *Ccl2* expression after myocardial infarction and reperfusion**

**A**, Venn diagram showing the intersection of transcripts significantly upregulated 2d after reperfusion and of transcriptions factors predicted to bind the *Ccl2* promotor sequence. The blue square labels gene products that form the AP-1 transcription factor. Gene names labeled in red were previously shown to control *Ccl2* expression. Binding sites were analyzed -500bps to +100bps of the *Ccl2* transcription start site. **B** and **C**, Integrated Genome Viewer (IGV) tracks of normalized Assay for Transposase-Accessible Chromatin coupled to high-throughput sequencing (ATAC-Seq) data of sham or 7d MI operated mice at the *Ccl2* locus showing chromatin accessibility and its relative localization to STAT3 (**B**) or AP-1 (**C**) binding sites. The region of interest was defined as the ATAC peak called by the Macs2 peak calling software for the *Ccl2* promoter. **D**, Immunoblot and quantification of JUNB and FOSL2 protein levels of left ventricular lysates after rapamycin or 4EGI-1 treatment 2d after reperfusion, n = 3-5. **E**, Effect of rapamycin or 4EGI-1 on the activity of AP-1 binding sites upstream of a luciferase reporter expressed in Hela cells. * indicates p<0.05 from sham. For statistical analysis one-way ANOVA with Tukey post-hoc analysis was used. p < 0.05 was defined as significant difference. Error bars show standard error of the mean. Data was generated from publicly available ATAG-Seq data published by van Duijvenboden et al[171]. Figure legends from Hofmann et al. 2024[133].

To further explore the involvement of cardiomyocytes in the regulation of cardiac CCL2 levels, I confirmed the secretion of CCL2 protein from isolated adult rat cardiomyocytes *in vitro*. Simulated ischemia and reperfusion resulted in secretion of CCL2 from cardiomyocytes to the culture medium, confirming that cardiomyocytes do express and release the CCL2 protein in response to reperfusion (Figure 46A). The amount of CCL2 protein detected in the culture medium was strongly inhibited after 4EGI-1 treatment, further confirming the involvement of the mTORC1-4EBP1-eIF4E axis in the release of CCL2 from cardiomyocytes (Figure 46B). To study whether the inhibition of the mTORC1-4EBP1-eIF4E axis directly affects the translation of cardiac *Ccl2* mRNA in cardiomyocytes of mice subjected to I/R surgery, I isolated ribosomes of cardiomyocytes from Ribo-tag mice infected with a cardiotropic control-AAV9 or 4EBP1-AAV9 2 days after reperfusion (Figure 46C). Input lysates confirmed the overexpression of 4EBP1 and blotting of human influenza hemagglutinin (HA) after HA-RPL22 immonuprecipitation showed successful isolation of ribosomes (Figure 46C). Quantification of ribosome-associated *Ccl2* mRNA, indicative of active translation of the transcript, revealed increased ribosome association of *Ccl2* mRNA 2 days after reperfusion in cardiomyocytes, which was completely inhbited after 4EBP1 overexpression (Figure 46D). I observed similar findings when I isolated *Ccl2* mRNA from actively translating polysomes after pharmacological eIF4F inhibition with 4EGI-1 (Figure 46E). Serum CCL2 protein of mice 2 days after reperfusion was significantly inhibited after AAV9-mediated overexpression of 4EBP1 in cardiomyocytes, indicating that the translational-dependent upregulation of CCL2 protein in cardiomyocytes contributes to total CCL2 levels and may contribute to the release of CCL2 protein from the injured myocardium (Figure 46F).

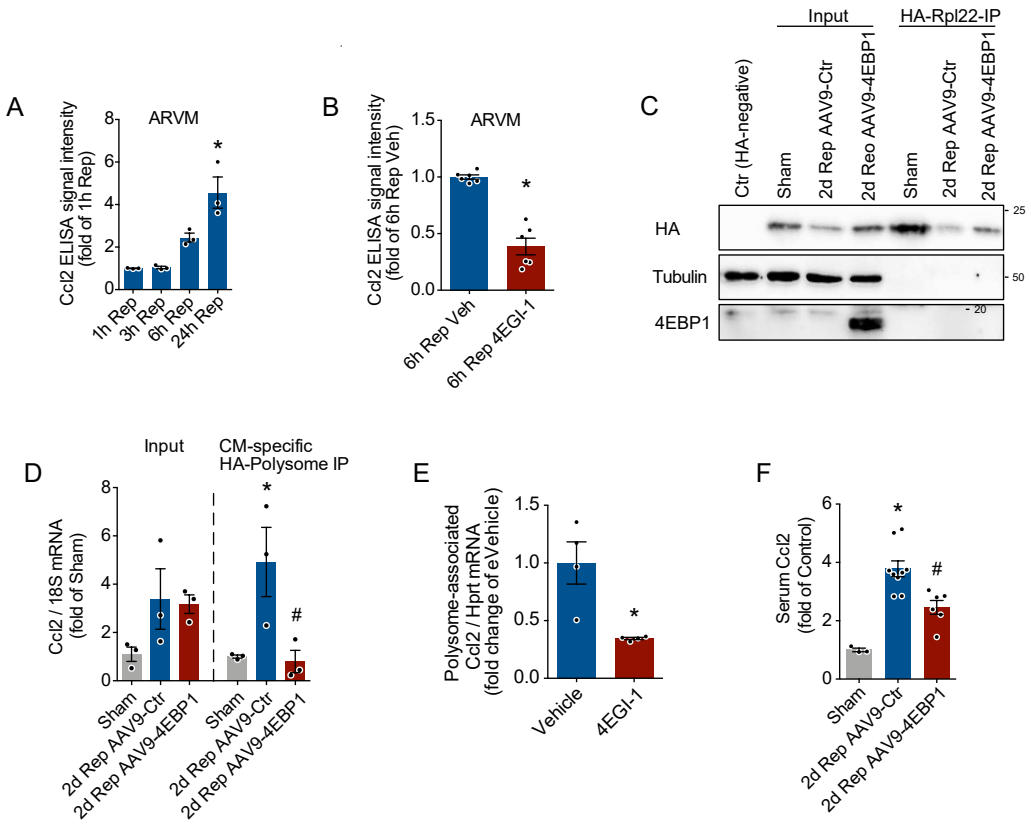


## Figure 46 | eIF4F-dependent translation of the chemokine CCL2 in border zone cardiomyocytes

**A**, CCL2 media levels of ARCMs after sI/R (1h ischemia and increasing times of reperfusion). **B**, CCL2 media levels of ARCMs treated with vehicle or 100µM 4EGI-1 after sI/R (1h ischemia and 6h reperfusion). Treatment was initiated with reperfusion. **C**, Representative immunoblot of input and HA-RPL22 immunoprecipitation of border zone lysates 2 days after sham or I/R surgery in animals treated with AAV9-Ctr or AAV9-4EBP1, confirming successful precipitation and 4EBP1 overexpression in cardiomyocytes. **D**, *Ccl2* mRNA levels of cardiac border zone lysates 2 days after sham or I/R surgery in animals treated with AAV9-Ctr or AAV9-4EBP1 (left) and quantification of RPL22-associated *Ccl2* mRNA levels - indicative of active translation of *Ccl2* transcripts - of border zone lysates 2 days after sham or I/R surgery in animals treated with AAV9-Ctr or AAV9-4EBP1 (right). **E**, Quantification of polysome-associated *Ccl2* mRNA transcript levels normalized to polysome-associated *Hprt* transcript levels. All polysome-associated mRNA levels were normalized to their respective input (cell lysate) mRNA levels. n = 4. **F**, Serum CCL2 protein levels 2 days after reperfusion following cardiomyocyte-specific 4EBP1 overexpression in AAV9-Ctr or AAV9-4EBP1 treated mice. * indicates p<0.05 from sham. # indicates p<0.05 from 2d Rep AAV9-Ctr. For statistical analysis one-way ANOVA with Tukey post-hoc analysis was used for **A**, **D** and **F**. An unpaired two tailed t-test was used for **B** and **E.** p < 0.05 was defined as significant difference. Error bars show standard error of the mean. Figure legends from Hofmann et al. 2024[133].

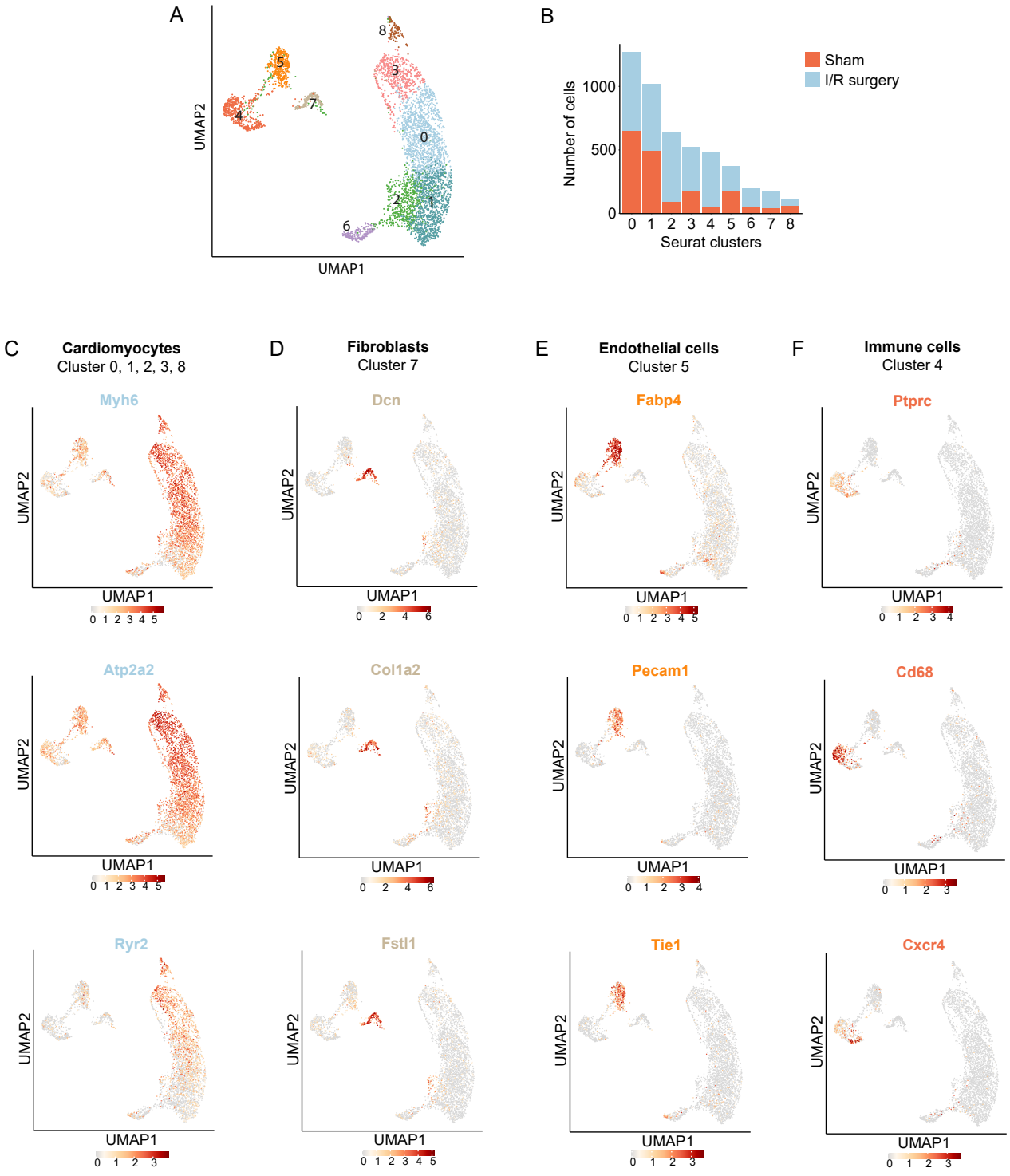


**Figure 47 | Clustering of cardiac cells based on gene expression from sham or I/R surgery operated mice**

**A**, Uniform manifold approximation and projection (UMAP) clustering of cardiac cells from sham (1d and 14d) and I/R operated mice (1d, 3d, 14d). **B**, Number of cells per cluster originating from sham or I/R surgery operated mice. **C** to **F**, Violin plots showing the mRNA expression of marker genes of main cardiac cell types to identify cardiomyocytes (**C**), fibroblasts (**D**), endothelial cells (**E**) and immune cells (**F**). Data are shown as normalized transcript counts on a color-coded linear scale. Data was generated from publicly available mouse single-cell transcriptomics data published by Molenaar et al[148]. Figure legends from Hofmann et al. 2024[133].

As the significant contribution of cardiomyocytes to cardiac CCL2 protein levels and CCL2 protein release after injury was a rather unexpected finding, the relative expression of *Ccl2* mRNA across different cardiac cell types was assessed in a previously published single cell RNA-Seq dataset of hearts after I/R surgery.[148] The raw sequencing data was re-analyzed and uniform manifold approximation and projection (UMAP) clustering of cardiac cells from sham (1d and 14d) and I/R operated mice (1d, 3d, 14d) revealed separate clustering of eight populations in four major clusters, which I defined as cardiomyocytes, fibroblasts, endothelial cells and immune cells (Figure 47).

The single cell RNA-Seq dataset revealed the upregulation of *Ccl2* transcript levels early after reperfusion across all detected cell types, including cardiomyocytes (Figure 48). The transient increase of *Ccl2* mRNA expression with a peak at day 1, followed by attenuation of its transcription at 3 days and return to baseline levels at 14 days after reperfusion is in line with the dynamics of monocyte infiltration to the injured myocardium after reperfusion.[30]

To further quantify the localization of cardiac *Ccl2* mRNA expression after myocardial infarction, a previously published full-length spatial transcriptomics dataset of infarcted mouse hearts[152] revealed that *Ccl2* becomes specifically expressed in cells of the infarct and border zone (Figure 49A and Figure 49C). The quantification of *Ccl2* mRNA levels across different cell types confirmed that almost every cell type increased *Ccl2* mRNA expression after myocardial infarction and that in cardiomyocytes this response was limited to border zone cells (Figure 49B and 49D).

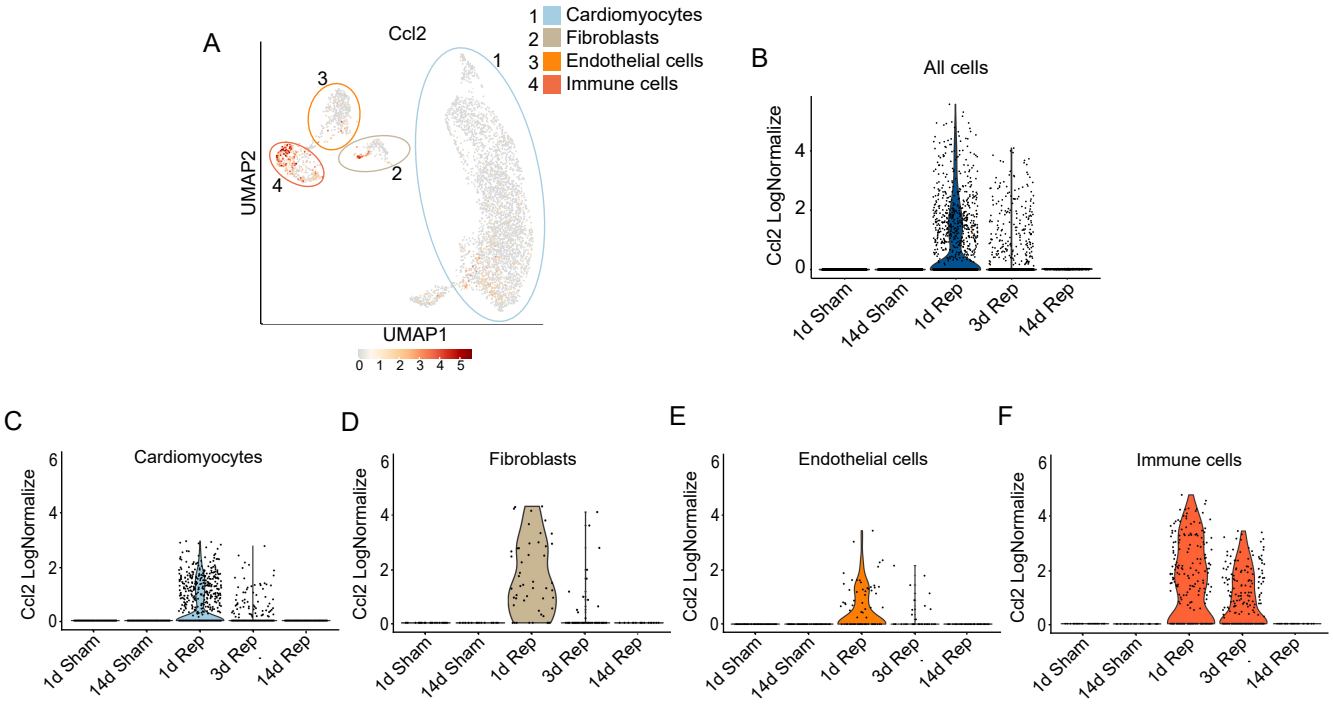


**Figure 48 | *Ccl2* mRNA expression across different cardiac cell types after reperfusion**

**A**, Uniform manifold approximation and projection (UMAP) map indicating the expression of *Ccl2* mRNA in different identified cardiac cell populations. Data are shown as normalized transcript counts on a color-coded linear scale. Different cell populations are highlighted by colored circles. **B** to **F**, Violin plots showing the mRNA expression of *Ccl2* in all cells (**B**), cardiomyocytes (**C**), fibroblasts (**D**), endothelial cells (**E**) and immune cells (**F**) in sham mice or after increasing timepoints after reperfusion. According to Seurat LogNormalize, gene expression measurements for each cell are normalized to total expression, multiplied by a scaling factor of 10000, and log-transformed. A to F were generated from publicly available mouse single-cell transcriptomics data published by Molenaar et al.[148] Detailed information on the statistical analysis of scRNA-seq can be found in the method section. Figure legends from Hofmann et al. 2024[133].

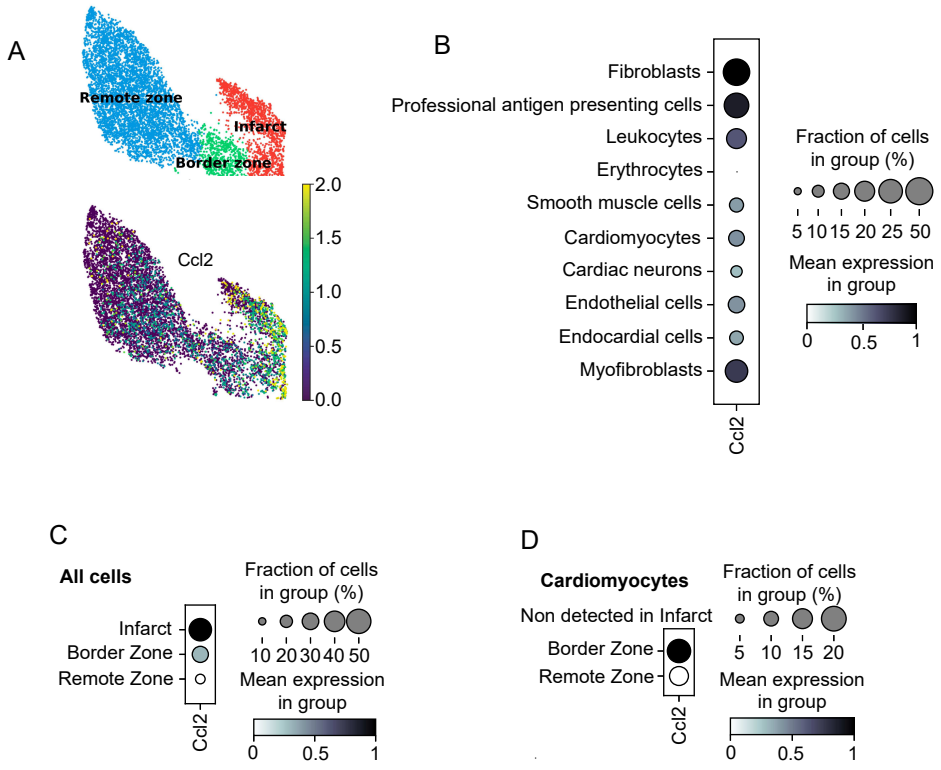


**Figure 49 | Cell-type-specific *Ccl2* expression across the infarct, border, and remote zone of infarcted mouse hearts**

**A**, Annotation of mouse heart regions after myocardial infarction via short-read clustering. UMAP representation of regions (top) and expression of *Ccl2* mRNA in the respective regions (bottom). **B** to **D**, Dot plot showing the expression of *Ccl2* mRNA across all inferred cells (**B**), across the infarct, border zone and remote area for all calls (**C**), and across the infarct, border zone and remote area only for cardiomyocytes (**D**). Detailed information on the statistical analysis of full-length spatial transcriptomics data can be found in the method section. Data was generated from publicly available mouse transcriptomics data published by Boileau et al[152]. Figure legends from Hofmann et al. 2024[133].

The full-length spatial transcriptomics dataset of infarcted mouse hearts was also used to assess the mRNA expression of the potential upstream *Ccl2* regulators *Junb*, *Fosl2* and *Stat3*. All three candidate transcription factors were increasingly expressed by a variety of cell types, including cardiomyocytes, at similar regions of *Ccl2* mRNA expression, again not excluding their involvement in cardiac *Ccl2* transcript regulation (Figure 50).

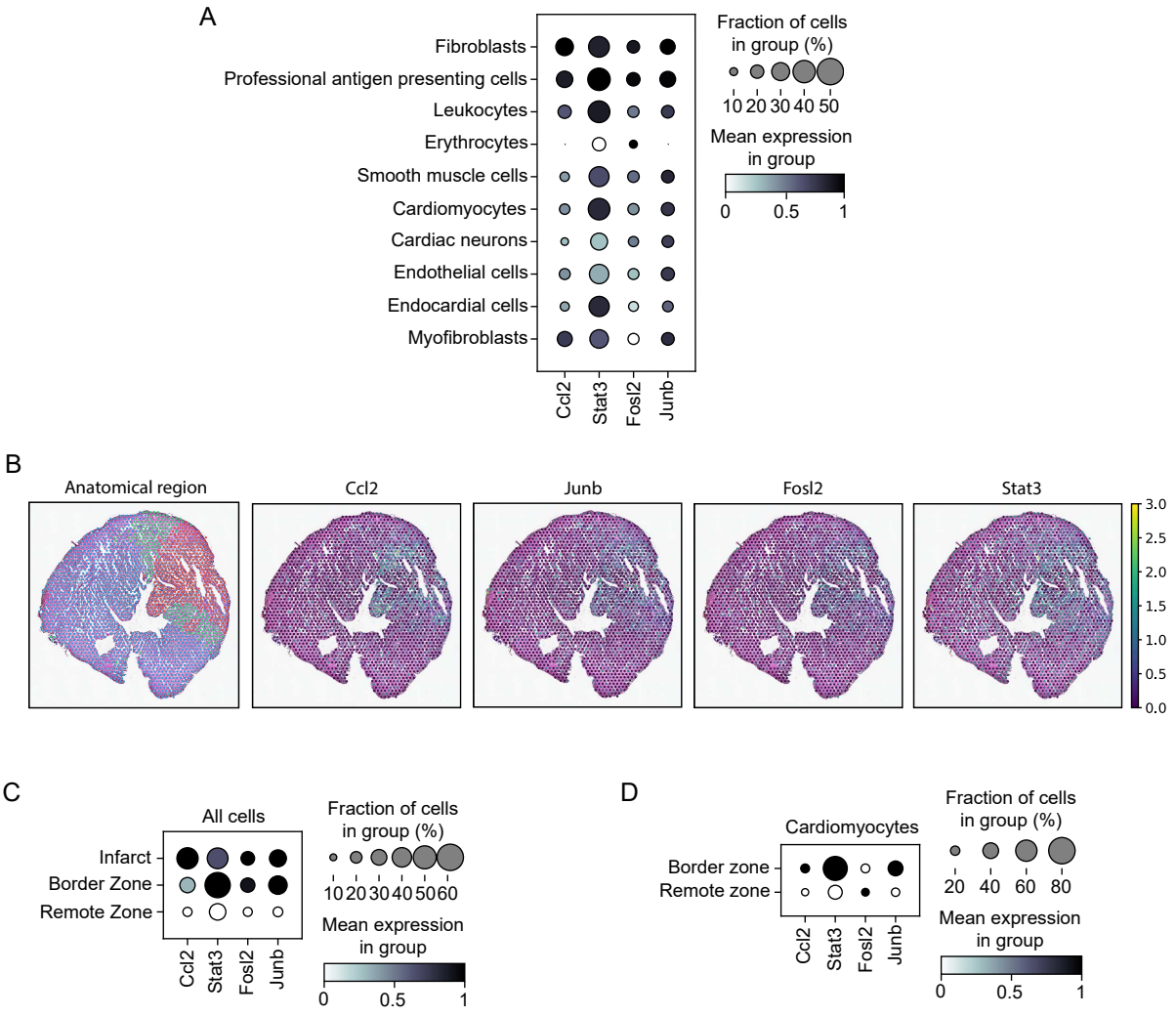


**Figure 50 | Spatial and cell-type-specific expression of *Ccl2* and potential upstream transcriptional regulators after myocardial infarction**

**A,** Dot plot showing the expression of *Ccl2*, *Stat3*, *Fosl2* and *Junb* mRNA across all inferred cells in the heart after MI. **B**, Expression of selected markers in one representative heart axis section. **C** and **D**, Dot plot showing the expression of *Ccl2*, *Stat3*, *Fosl2* and *Junb* mRNA across all inferred cells across the infarct, border zone and remote area for all calls (**C**), and across the border zone and remote area only for cardiomyocytes (**D**). Figure legends from Hofmann et al. 2024[133].

If transient pharmacological inhibition of the mTORC1-4EBP1-eIF4E axis improves cardiac function after reperfusion by attenuating proinflammatory monocyte infiltration to the injured heart, the cardioprotective effect should be at least partly reduced in an *ex vivo* I/R model where circulating immune cells are absent. To test this hypothesis, isolated mouse hearts were subjected to *ex vivo* I/R surgery and treated with 4EGI-1 in the reperfusion medium (Figure 51A). While 4EGI-1 treatment resulted

in attenuated release of CCL2 protein to the perfusion media (Figure 51B), *ex vivo* 4EGI-1 treatment was not associated with improved cardiac function and contractility at concentrations up to 25µM (Figure 51C to 51E). Higher dosages (50µM) resulted in strong cardiac toxicity with near complete loss of contractility and left ventricular developed pressure, further highlighting the risk of fully inhibiting translation in the heart. This data indicates the absence of an immediate protective effect that is mediated by cardiac-intrinsic cells after pharmacological mTORC1-4EBP1-eIF4E axis inhibition, suggesting a non-immediate effect, potentially mediated by immune cells.

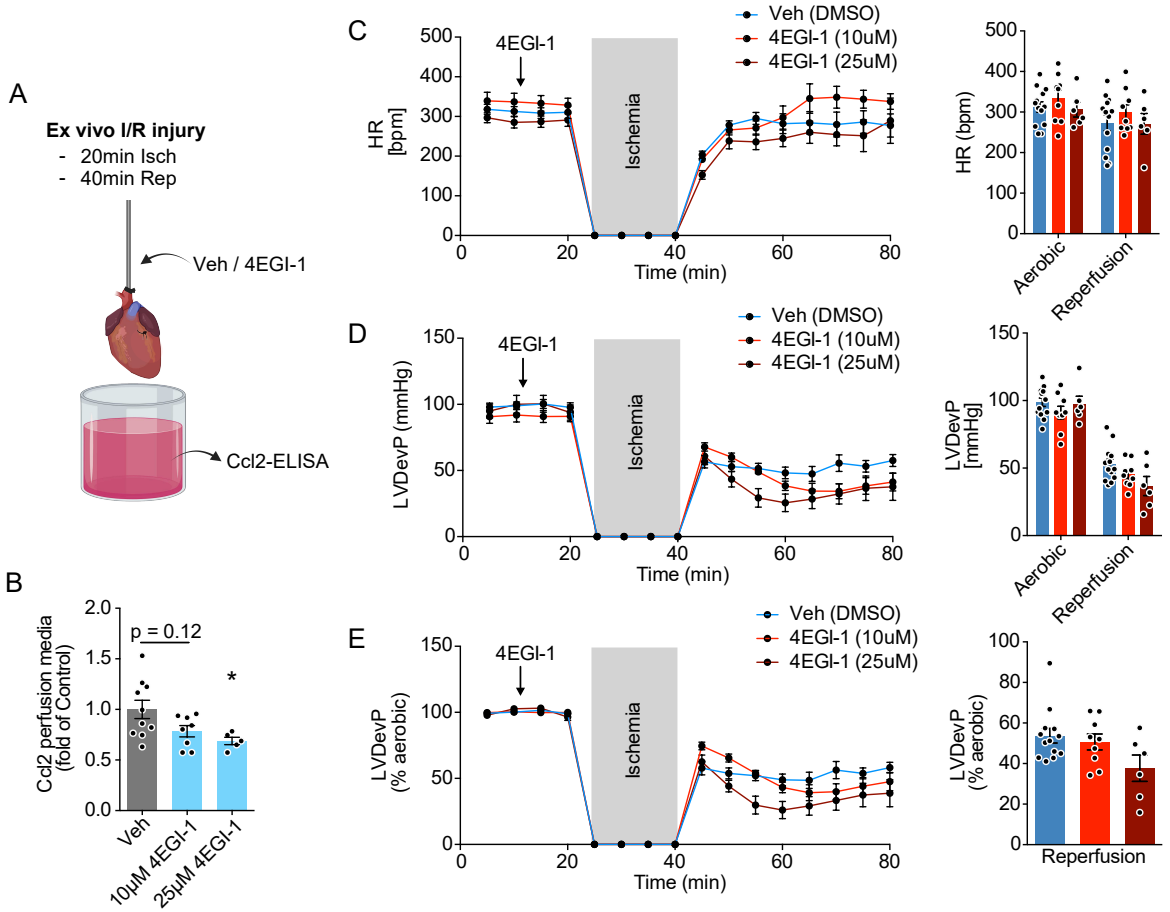


**Figure 51 | Absence of an immediate protective effect of 4EGI-1 on cardiac function in an *ex vivo* reperfusion model**

**A** and **B**, Diagram and quantification of CCL2 protein from perfusion media after *ex vivo* cardiac I/R surgery. **C** to **E**, Line graphs and respective visualization of end-point measurements as bar/dot plot of heart rate (HR) (**C**), and total (**D**) and relative (**E**) evolution of left ventricular developed pressure

4EGI-1 or 25µM 4EGI-1. Isch (ischemia), Rep (reperfusion), Veh (vehicle). * indicates p<0.05 from Veh. For statistical analysis one-way ANOVA with Tukey post-hoc analysis was used for B, C, D and E. A made in ©BioRender - biorender.com. *Ex vivo* surgeries, heart rate and LVDevP measurements for Figure legends from Hofmann et al. 2024[133].

Pharmacological mTORC1 inhibitors are clinically used as immunosuppressants that directly suppress inflammatory functions and proliferation of immune cells, likely involving circulating immune cells. As this study injected rapamycin and 4EGI-1 i.p. and thus results in systemic drug distribution, they may also directly inhibit the activation of circulating monocytes, thereby reducing their capacity to infiltrate the infarcted heart after reperfusion. To examine whether rapamycin or 4EGI-1 may directly act on circulating monocytes and thereby limit their infiltration to the heart, I isolated CD11b$^+$ immune cells, including monocytes and neutrophils, from the blood and spleens of genetically tagged CD45.1 donor mice and treated *ex vivo* with vehicle, rapamycin or 4EGI-1. Leukocytes of CD45.1 mice are genetically different of CD45.2 cells and can be distinguished from CD45.2 leukocytes by a CD45.1 selective antibody. I quantified the viability of isolated and treated CD45.1 leukocytes 3 hours and 6 hours after isolation and treatment both at 4°C and 37°C, confirming good viability 3 hours after *ex vivo* treatment (Figure 52). Both inhibitors are expected to fully inhibit their respective target at 3 hours at a temperature of 37°C.

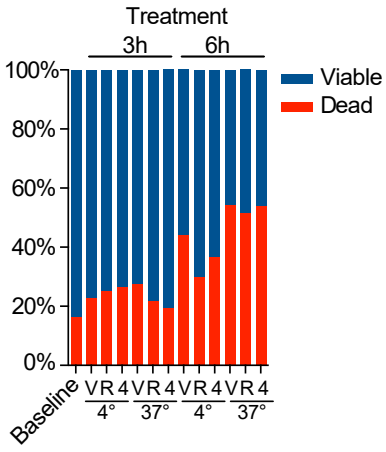


**Figure 52 | Viability of *ex vivo* treated CD11b+ immune cells**

**Figure 52 | Viability of *ex vivo* treated CD11b+ immune cells**

**A,** Bar graph showing the relative amount of viable cells of isolated CD11b+ immune cells from the blood and spleen of CD45.1 donor mice 3h to 6h of *ex vivo* vehicle, rapamycin or 4EGI-1 treatment at 4°C or 37°C. Baseline represents the relative amount of viable cells immediately after cell isolation. Isolated cells of 4 donor mice were equally divided between each condition. Figure legends from Hofmann et al. 2024[133].

CD45.2 recipient mice were subjected to I/R surgery. On the next day, I isolated $CD11b^+$ immune cells from the blood and spleen of CD45.1 donor mice, treated them *ex vivo* with vehicle, rapamycin or 4EGI-1 for 3 hours at 37°C, after which they were i.v. injected to operated CD45.2 mice 24 hours after reperfusion (Figure 53A). 48 hours after reperfusion and 24 hours after i.v. injection of *ex vivo* treated CD45.1 cells, I analyzed cardiac cells of the left anterior ventricular wall of CD45.2 donor mice by FACS (Figure 53A). If rapamycin and 4EGI-1 have the capacity to inhibit monocyte infiltration to the injured heart by acting on circulation cells, lower numbers of *ex vivo* rapamycin or 4EGI-1 treated and transplanted CD45.1 monocytes should be detected in comparison to vehicle treated and transplanted cells. Indeed, the infiltration of *ex vivo* treated CD45.1 monocytes was strongly suppressed by *ex vivo* treatment with rapamycin or 4EGI-1, whereas the cardiac infiltration of *ex vivo* treated and transplanted CD45.1 neutrophils was not affected by pharmacological inhibition of the mTORC1-4EBP1-eIF4E axis (Figure 53B to 53D). The gating strategy used to quantify CD45.1 monocytes and neutrophils is shown in Figure 54. The data suggests that systemically administered rapamycin and 4EGI-1 also acts on circulating monocytes to inhibit their infiltration to the injured heart after reperfusion.

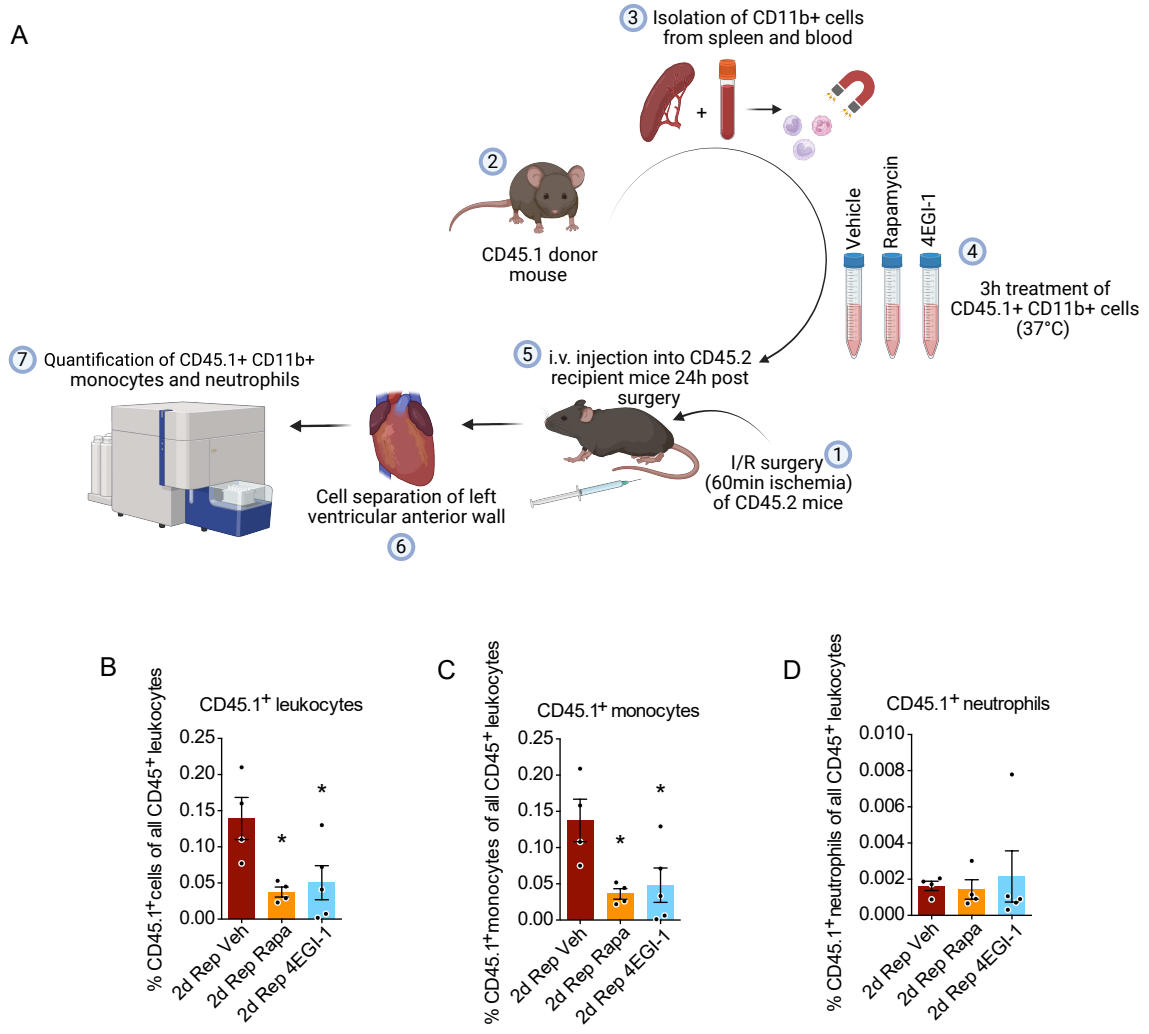


## Figure 53 | A direct immunosuppressive effect of eIF4F inhibition on circulating monocytes

**A** Diagram of experimental strategy to investigate the direct effect of rapamycin or 4EGI-1 on circulating CD11b$^+$ cells and its impact on immune cell infiltration to the heart. **B** to **D**, Quantification of transplanted CD45.1 donor leukocyte (**B**), monocyte (**C**) and neutrophil (**D**) infiltration to the reperfused heart of CD45.2 recipient mice 2d after I/R surgery by flow-cytometry based enumeration. FACS analysis was performed of left anterior wall lysates of CD45.2 recipient mice to enrich for infiltrated immune cells. Isolated cells of all donor mice were pooled and equally divided across each treatment group. One donor mouse was used per two recipient mice. Approximately 300.000 isolated living cells were injected to each recipient mouse. Isolated cells were *ex vivo* pre-treated with 100nM rapamycin, 100µM 4EGI-1 or DMSO as a vehicle for 3h at room temperature. Rep (reperfusion), Veh (vehicle). * indicates $p<0.05$ from 2d Rep Veh. For statistical analysis one-way ANOVA with Tukey post-hoc analysis was used for B, C and D. A made in ©BioRender - biorender.com. Figure legends from Hofmann et al. 2024[133].

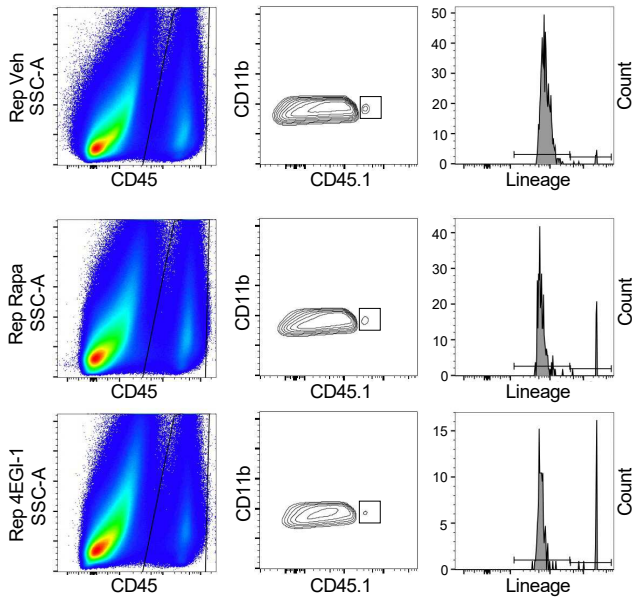


**Figure 54 | FACS gating strategy used for Figure 53**
**A**, Gating strategy and representative flow cytometric plots of recipient mouse hearts 2 days after I/R surgery and 24h after injection of vehicle, rapamycin or 4EGI-1 pre-treated CD45.1+ CD11b+ immune cells. FACS analysis was performed of left anterior wall lysates of CD45.2 recipient mice to enrich for infiltrated immune cells. Isolated cells of all donor mice were pooled and equally divided across each treatment group. One donor mouse was used per two recipient mice. Approximately 300.000 isolated living cells were injected to each recipient mouse. Isolated cells were *ex vivo* pre-treated with 100nM rapamycin, 100µM 4EGI-1 or DMSO as a vehicle for 3h at room temperature. Figure legends from Hofmann et al. 2024[133].

# 6 Discussion

## 6.1 Dynamic regulation of translation in cardiac ischemia and reperfusion

This study indicates that cardiac translation rates are changed dynamically after ischemia and reperfusion, with rapid suppression of protein synthesis during ischemia, followed by a continuous or even further inhibition of translation immediately after reperfusion, which is then followed by activation of cardiac translation rates at 2 days after reperfusion. For this conclusion, this thesis and two other recent studies used pharmacological compounds (puromycin[133,136] or azidonorleucine[172]) that are

incorporated into nascent polypeptides and later quantified to determine translation rates after myocardial infarction. Those methods are limited by the delivery of the quantifying substance to the area of interest, which is compromised in hearts that underwent myocardial infarction surgery without reperfusion and also in part after reperfusion due to microvascular injury.[18] As such, those methods will likely suffer from a bias towards decreased translation rates of injured tissues. Older studies using methods not necessarily limited by impaired substrate delivery in *ex vivo* hearts, papillary muscles or myocardial slices revealed inconclusive results, with the downregulation of translation rates depending on the intensity and duration of the hypoxic or ischemic stimulus.[173]

Similar results of a dependency of translation rates on intensity and duration of hypoxia were found in this thesis in isolated cells subjected *in vitro* to simulated ischemia. While it is plausible to assume that ischemia of the infarct core will inhibit translation rates, its exact dynamics in the *in vivo* context remain uncertain. Some data of this thesis also suggested a further drop of cardiac translation rates immediately after reperfusion. However, this hypothesis is primarily based on this finding in some, but not all studied cell types *in vitro*, as well as on the observation by Zhang et al. showing that eIF2α is increasingly phosphorylated 30 minutes after reperfusion compared to the ischemic state prior to reperfusion.[136] Therefore, while the overall trend of decreased translation rates during ischemia and immediately after reperfusion, and increased translation rates 2 days after reperfusion appear valid, exact dynamics of translation rates in response to ischemia and reperfusion, especially in humans, remain unknown.

With the above-mentioned limitations, I concluded that translation rates of the left ventricle are reduced at 3 hours of ischemia by LAD ligation *in vivo*. While I continued to investigate how reperfusion alters left ventricular translation rates 2 days after reperfusion *in vivo*, the data of this thesis does not allow to robustly conclude that reperfusion increases translation rates compared to non-reperfused conditions in vivo, as different timepoints for MI and ischemia/reperfusion were investigated. 2 days after the ischemic injury, the heart may have already started to undergo remodeling, including hypertrophic cardiomyocyte growth, a process that is known to be driven by increased translation rates.[83] While the data of this thesis clearly indicates that reperfusion results in increased translation rates compared to ongoing ischemia *in vitro*, increased translation rates 2 days after reperfusion *in vivo* may not necessarily be driven by reperfusion itself.

While there have been some inconsistent observation, some previous studies have found that mTORC1 is activated after myocardial infarction *in vivo*[115,131,174,175]. As the mTORC1 pathway is a major driver of protein synthesis it is possible that chronic LAD ligation also results in increased translation rates 2 days after surgery *in vivo*. One study directly compared mTORC1 activity at identical timepoints after chronic LAD ligation or after ischemia/reperfusion surgery, which showed that both conditions increased mTORC1 activity, with a stronger activation observed in reperfused hearts.[174] From a theoretical standpoint, the infarct core should have limited availability of ATP and nutrients, thus limited capacity to perform translation rates. My *in vitro* data that used a simulated ischemia/reperfusion model more closely resembles the conditions of the infarct area and only to a lesser extend those conditions of the border zone. I would argue that observations that were made in this thesis, especially increased translation rates of the injured myocardium and translation-dependent

infiltration of monocytes to the site of injury, may represent general responses of the injured heart and thus do also occur, potentially to a lesser extent, after chronic coronary artery occlusion without reperfusion. However, this is purely hypothetical and would need to be studied in the future.

A recent study showed, with some technical limitations as described above, that myocardial infarction without reperfusion causes a decrease of translation rates at the infarct and the border zone at 24h post-infarction, which remained true when newly synthesized proteins were labeled before the induction of myocardial infarction, thereby circumventing some of the technical issues described above.[172] While sarcomeric proteins and components of the tricarboxylic acid cycle and respiratory electron transport, as well as some ion channels, were among the mostly synthesized proteins of cardiomyocytes at baseline, with additional enrichments of protein functions related to cell-cell interactions, ubiquitin protein ligase binding and mRNA binding, the landscape of synthesized proteins of cardiomyocytes after myocardial infarction shifted towards increased synthesis of proteins related to MAP-kinase activity, GTPase activity and lipid/cholesterol/sterol transporter activity, and decreased translation of proteins related to mitochondrial function and cytoskeletal components.[172]

Thus, all three recent publications that investigated which proteins are newly synthesized in response to myocardial infarction or ischemia/reperfusion came to the conclusion that the translation of mitochondrial proteins is strongly suppressed in response to myocardial infarction or ischemia/reperfusion, while the functions of proteins that are increasingly translated differed substantially between all three studies, which can be likely explained by technical differences, different disease models, and different investigated timepoints after injury.[133,136,172]

In this thesis I used an HA-based immunoprecipitation model of HA-tagged ribosomes of cardiomyocytes from whole left ventricular lysates 2 days after ischemia/reperfusion surgery in mice.[133] This model is highly enriching for cardiomyocyte-specific ribosomes, however, ribosomes from other cell types may contaminate the immunoprecipitation and thus few read counts from the final Ribo-seq library may come from non-myocyte cells. While a previous publication confirmed the strong enrichment of cell-type specific transcripts by this method in the heart,[83] it cannot be excluded that some inflammatory transcripts that showed increased translation in the Ribo-seq library, had higher transcript counts after reperfusion due to higher number of immune cells in the whole left ventricular lysate and thus higher levels of non-myocyte contamination. Despite those limitations, the expression of *Ccl2* in cardiomyocytes and its responsiveness to ischemia/reperfusion was confirmed by several other methods and should therefore represent a true biological event. However, the observations of this thesis should be replicated in other studies and by additional methods, before translational applications are considered.

## 6.2 Cardiomyocyte translation rates are dependent on the mTORC1-4EBP1-eIF4E axis

Translation rates are regulated at the step of translation initiation, which is the positioning of an initiator tRNA-loaded ribosome over the start codon of a selected mRNA.[89] Translation is a highly regulated process that is controlled by several conserved signaling pathways that serve as ‘gatekeepers’ by sensing the cellular environment and either promote or inhibit protein synthesis depending on cellular stress, energy, oxygen, nutrient and growth factor availability.[89] Among those signaling pathways is the mTORC1 pathway, which controls the formation of the eIF4F complex, as well as those pathways that control eIF2α phosphorylation, thereby controlling 43S

translation pre-initiation complex formation.[89] While those two steps of translation initiation are often considered 'master regulators' of cellular translation rates, many other factor that are involved in initiation, elongation, termination and ribosome recycling, as well as those involved in processing, posttranscriptional modification and localization of RNAs, including RNA-binding proteins, regulate mRNA translation.[89]

This thesis focused on the mTORC1 and MNK1/2 pathways and their involvement in the formation of the eIF4F complex during ischemia and reperfusion, but many other factors will be essential for the control of cardiac translation rates after reperfusion.[136] Using pharmacological inhibitors and genetic manipulation, this thesis revealed the involvement of the mTORC1-4EBP1-eIF4E axis in translation rates of cardiomyocytes 2 days after reperfusion *in vitro* and *in vivo*. Among those different pharmacological inhibitors targeting the mTORC1-4EBP1-eIF4E axis was rapamycin, a partially selective first-generation mTORC1 inhibitor, that is often considered to have limited inhibitory activity towards the 4EBP1 sub-branch of the mTORC1 pathway and thus does only weakly inhibit translation rates.[176,177] However, 6 hours of rapamycin treatment resulted in a significant disruption of the eIF4F complex and chronic rapamycin treatment for 24 hours or 48 hours strongly inhibited translation in NRCMs. Further rapamycin was sufficient to completely inhibit the cardiac translational burst after reperfusion *in vivo*. Thus, while showing weaker mTORC1-4EBP1-eIF4E axis inhibition compared to second generation non-selective mTOR inhibitors, such as Torin1, rapamycin was clearly sufficient to inhibit translation in cardiomyocytes and the heart after reperfusion at the tested concentrations without showing any obvious off-target inhibition. However, the relative dynamics of this process remains incompletely resolved.

Rapamycin attenuated the formation of the eIF4F complex in NRCMs within 6 hours of reperfusion, whereas reduced translation rates became apparent at 24 hours after simulated reperfusion using a puromycin incorporation assay. Technically, the puromycin incorporation assay quantifies elongation rates, which could be dynamically uncoupled from initiation rates, however those findings further support the involvement of other signaling pathways and subbranches of the mTORC1 pathway in the regulation of translation rates after reperfusion. Similar discrepancies between the timely dynamics of puromycin assay and eIF4F disruption were found for 4EGI-1 *in vitro*. In addition, genetic inhibition of the eIF4F complex in cardiomyocytes via cell type-specific overexpression of 4EBP1 suppressed translation rates in the border zone, but did not reach significance ($p < 0.05$, unpaired two tailed t-test) in the infarct and remote areas, indicating that other cell types or signaling pathways are involved in translation rates there.

In summary, the mTORC1-4EBP1-eIF4E axis of cardiomyocytes is involved in the activation of border zone translation 2 days after reperfusion, but other signaling pathways and cell types will be involved in the regulation of cardiac translation, which was not further investigated in this thesis.

One such pathway is the integrated stress response, regulated by the eIF2 pathway and Zhang et al. recently showed that this pathway is involved in the downregulation of translation during the first minutes after reperfusion in mice.[136] Specifically, Zhang et al. showed that ischemia/reperfusion results in activation of the PERK-branch of the unfolded protein response during ischemia and after reperfusion and that this may be functionally related to eIF2α phosphorylation and inhibition of translation rates early after reperfusion.[136] However, one discrepancy of their study

was that PERK phosphorylation, sometimes used as a readout of PERK activation, was equally activated after simulated ischemia and simulated ischemia/reperfusion, while eIF2α became increasingly phosphorylated early after reperfusion compared to ischemia alone, further indicating that multiple pathways are involved in the regulation of cardiac translation rates during ischemia and reperfusion.[136]

### 6.3 Transient pharmacological inhibition of eIF4F-dependent translation improves cardiac function after myocardial infarction

To investigate the impact of translational activation on infarct size and cardiac function after reperfusion, this thesis used the pharmacological mTORC1-4EBP1-eIF4E inhibitors rapamycin and 4EGI-1. Both compounds attenuated translation *in vivo*, reduced infarct size and improved cardiac function at least up to 2 weeks after reperfusion in mice. Classical heart failure and remodeling markers including *Nppa*, *Nppb*, *Myh7* and *Col1a1* transcripts were not consistently downregulated in rapamycin or 4EGI-1 treated animals, while 4EGI-1 treated animals showed a clear trend for overall decreased expression of those marker, which did not meet significance by the predefined threshold of $p < 0.05$. Troponin T and TUNEL quantifications revealed no difference of myocardial cell death between rapamycin/4EGI-1 or vehicle treated animals 24 hours after I/R surgery.

Those discrepancies between the absence of early protection from injury but a reduced infarct size at 2 weeks indicate a protective mechanism that is mediated by the prevention of late reperfusion injury, which may be mediated by excess inflammation and maladaptive cardiac remodeling. In line with this hypothesis was the finding that both pharmacological inhibitors strongly prevented monocyte infiltration to the injured heart, suggestive of an anti-inflammatory effect. Surprising was the finding

that neither rapamycin nor 4EGI-1 affected neutrophil infiltration to the heart, indicative of a specific pathway that is affected by pharmacological mTORC1-4EBP1-eIF4E axis inhibition, that is essential for monocyte activation or infiltration. This study did not specifically examine immune cell populations other than monocytes/macrophages or neutrophils. As the clinically observed anti-inflammatory effects of the mTORC1 inhibitors everolimus or silolimus (rapamycin) in the context of immunosuppression in solid organ transplantation are thought to be mediated by the inhibition of the progression through the G1/S transition of T-cells, attenuation of the infiltration of T-cell may also be involved in the cardioprotective effects of rapamycin or 4EGI-1 after reperfusion in mice.

In this thesis I used a pharmacological treatment protocol that may have translational application for patient care. The pharmacological inhibitors were i.p. injected 30 minutes before reperfusion, followed by a second i.p. injection at the second day. This may represent a clinical scenario where a patient receives an i.v. injection during first aid or when arriving in the hospital, and later additional treatments in the following days.

I specifically decided to use a protocol that is based on i.p. injections to facilitate rapid systemic accumulation of effective drug concentrations, as reperfusion injury and the inflammatory response occurs early after reperfusion. In addition, a transient treatment protocol was selected to circumvent side effects that may result from chronic suppression of translation. Rapamycin, a partly selective mTORC1 inhibitor, was previously shown to also inhibit mTORC2 assembly when administered chronically, and mTORC2 is known to mediate adaptive effects in response to myocardial infarction.[115,178,179] A previous study that pre-treated pigs for 7 days with rapamycin

showed that mTORC1-inhibitor treated pigs had a worse outcome after myocardial infarction.[111] In addition, several eIF4E-binding compounds induce cell death after chronic treatment, thus indicating that full translational inhibition may only be tolerated short-term, if at all.[180,181]

4EGI-1, one of the compounds used by me in this thesis, had a low tolerance both *in vitro* and *in vivo* and only a very limited concentration range could be identified that inhibited translation without being severely toxic. Despite showing protective effects at the selected concentration in the ischemia/reperfusion model used in this thesis, clinical application of 4EGI-1 in its current form is unlikely and the results should be seen as proof of mechanism, that requires further investigating before it can be considered as a therapeutic option in humans.

Surprisingly, rapamycin, which is often described as a rather weak translational inhibitor due to its limited inhibition of the 4EBP1 sub-branch of the mTORC1 pathway compared to other mTOR inhibitors, fully inhibited translational activation *in vivo* and resulted in translational suppression *in vitro* after treatment for 12 hours. In addition, rapamycin improved cardiac function to a similar degree as 4EGI-1 and even showed a clear trend for improved survival, compared to the trend for impaired survival observed after 4EGI-1 treatment.

Rapamycin is an approved drug, clinically known as sirolimus, which is used for the treatment of several disease, including coronary artery disease (drug-eluting stents are covered with sirolimus or related compounds).[182] Despite of certain side effects that can occur after long-term treatment with sirolimus or similar compounds, their short-term use is considered to be safe, making sirolimus or related drugs optimal

candidate drugs for the treatment of myocardial infarction. In addition, the OSIRIS trial revealed that an adjunctive sirolimus treatment with an intensified loading regimen before coronary intervention resulted in a significant improvement in angiographic parameters of restenosis.[183]

During the preparation of this thesis, the results of the Controlled-Level EVERolimus in Acute Coronary Syndrome (CLEVER-ACS, clinicaltrials.gov NCT01529554) trial got published, which did not show any improvement of infarct size or cardiac function after everolimus treatment in patients with a myocardial infarction that underwent percutaneous coronary intervention-based reperfusion.[184] CLEVER-ACS was a phase II randomized, double-blind, multi-center, placebo-controlled trial on the effects of a 5-day course of oral everolimus on infarct size, LV remodeling, and inflammation in patients with acute ST-elevation myocardial infarction.[74]

Within 5 days of successful primary percutaneous coronary intervention, patients were randomly assigned to everolimus (first 3 days: 7.5 mg every day; days 4 and 5: 5.0 mg every day) or placebo, respectively.[74] The primary efficacy outcome was the change from baseline (defined as 12 hours to 5 days after pPCI) to 30-day follow-up in myocardial infarct size as measured by cardiac magnetic resonance imaging.[74] Secondary endpoints comprised corresponding changes in cardiac and inflammatory biomarkers as well as microvascular obstruction and LV volumes assessed by cardiac magnetic resonance imaging.[74] Everolimus is pharmacologically very similar to sirolimus, with shorter half-lifes and improved bioavaiability.[185,186] However, conclusions made from clinical trials using everolimus are very likely also applicable to sirolimus.

Therefore, results from the CLEVER-ACS trial are in strong contrast to the beneficial effects observed by me in this thesis and by other that used rodent models of myocardial infarction and ischemia/reperfusion.[114] While other treatment protocols that showed beneficial effects of rapamycin in mice are comparable to the one used by the CLEVER-ACS trial (oral treatment initiation days after ischemic event),[114] the treatment protocol used by me in this thesis (i.p. application, treatment initiation during ischemic event and once again after 24 hours). In this thesis I concluded that at least some of the protective effects of rapamycin treatment in mice was mediated by inhibition of pro-inflammatory monocyte infiltration to the injured myocardium. As further described in the introduction, those pro-inflammatory monocytes infiltrate the heart very early after myocardial infarction and later are replaced by reparative monocytes.[30] Thus, delayed oral drug treatment is potentially missing the critical time window to target pro-inflammatory monocytes, which could explain the discrepancies between the results of this thesis and the CLEVER-ACS trial, as also noted by the authors of the CLEVER-ACS trial 'however, we cannot rule out that regimens including periprocedural drug application with intravenous formulations of mTOR inhibitors or longer treatment durations could have favorably affected the results.'[184]

However, it must be noted that a post hoc analysis of 8 patients in which everolimus therapy was initiated within 12 hours after percutaneous intervention vs. 13 patients that received placebo within 12 hours (10 patients at follow-up) did not show differences in the relative change in infarct size from baseline (12 hours to 5 days after percutaneous intervention) to follow up (30 days).[184] Based on this small sample size it appears less likely that an earlier treatment initiation after percutaneous intervention of oral everolimus would have resulted in a different outcome, even though this sample size is severely underpowered to draw such a conclusion. Other relevant differences

may be i.p/i.v. vs. oral drug administration, rapamycin (sirolomus) vs. everolimus and treatment initiation before percutaneous intervention vs. treatment initiation after percutaneous intervention.

Others have hypothesized that only rapamycin treatment prior to reperfusion is protective,[121] but this conclusion is in my opinion currently not adequately supported by the available literature. I suggest that future studies should compare oral and i.v., as well as early (before reperfusion) and late (after reperfusion) treatment initiation protocols using rapamycin (sirolimus), everolimus or newer generation mTORC1-selective inhibitors in randomized, double-blind, placebo-controlled large animal models of ischemia/reperfusion to guide future clinical trial design.

### 6.4 Inhibition of eIF4F-dependent translation attenuates cardiac expression and secretion of the monocyte attracting chemokine CCL2

Transcripts increasingly translated 2 days after reperfusion were enriched for functions associated with cell migration, cell adhesion and inflammation. Among those transcripts was the mRNA encoding the monocyte attracting chemokine CCL2, which was one of the genes/transcripts with the strongest relative increase of transcription and translation. As increased *Ccl2* expression showed a near identical relative increase between RNA-Seq (transcription) and Ribo-Seq (translation), its upregulation may be primarily upregulated at the transcriptional level, or by an increased presence of *Ccl2* expressing cells. However, as this study used transcriptional expression data of bulk RNA-Seq and compared it to cardiomyocyte-specific Ribo-Seq data, relative expression levels may not necessarily be derived from the same cell populations. As *Ccl2* transcript and CCL2 protein expression was highly sensitive to the inhibition of eIF4F-dependent translation and as such seems to require a functional translational

apparatus for its upregulation and secretion, its regulation is at least partly dependent on translation.

As many other transcripts related to inflammation and immune cell attraction were upregulated by translation, rapamycin and 4EGI-1 will mediate their anti-inflammatory actions not necessarily exclusively due to their regulation of CCL2. For example, other candidate transcripts are those that are involved in tumor necrosis factor secretion, as they were highly enriched among increasingly translated mRNAs 2 days after reperfusion and cardiac Tnf levels showed a clear trend towards decreased expression, which did not reach the predefined significance threshold, likely due to high variance across individual samples. In addition, rapamycin is well known to regulate proteostasis and protein processing in part through its regulation of mTORC1-dependent autophagy, and other proteostasis-regulating pathways, or simply be inhibiting the synthesis of proteins that could misfold.[98,187] Further, attenuating translation may improve cardiac function through the regulation of many other pathways that are compromised during ischemia/reperfusion, e.g. increasing energy availability due to inhibiting protein synthesis, a highly energy demanding process.

The attenuation of of *Cc2* mRNA levels after rapamycin or 4EGI-1 treatment indicate that either upstream transcriptional regulators of *Ccl2* are regulated by the mTORC1-4EBP1-eIF4F axis, or that changes in transcript levels are dependent on different numbers of infiltrating immune cells that themselves express *Ccl2* mRNA and thereby increase overall cardiac *Ccl2* mRNA levels. In this thesis I tried to identify an upstream transcription factor that is controlled by translation and responsible for the transcriptional regulation of *Ccl2.* Promising candidates included Junb, Fosl2 and Stat3 and I could identify motifs of their transcription factor binding sites in the promotor

region of *Ccl2* which become increasingly accessibly after myocardial infarction. Neither Junb nor Fosl2 appeared to mediate the effects of pharmacological mTORC1-4EBP1-eIF4F axis inhibition. Stat3 was not further investigated and remains a high priority candidate that should be investigated in future experiments.

Previous studies suggest that immune cells and fibroblasts are the primary source of CCL2 secretion. However, cardiomyocyte-specific Ribo-Seq suggested an involvement of cardiomyocytes to cardiac CCL2 protein expression. In addition, endothelial cells, which will play critical roles during the control of immune cell infiltration in response to ischemia/reperfusion were previously shown to express *Ccl2* mRNA and CCL2 protein.[188,189] A re-analysis of a cardiac scRNA-Seq dataset of sham or I/R-operated mice that clustered cell types into the main cardiac cell populations cardiomyocytes, fibroblasts, endothelial cells and immune cells confirmed that *Ccl2* mRNA expression was strongest in immune cells and fibroblasts but revealed that each annotated cell type increased *Ccl2* transcript expression early after reperfusion. In addition, spatial transcriptomics revealed that almost every cell type increased *Ccl2* mRNA expression after myocardial infarction, primarily in the infarct and border zone. However, cell annotation from this dataset must be interpreted with care, as the dataset has only near single cell resolution and cell type annotation is derived from the expression profile of the most likely cell type of the assessed area and is therefore susceptible to transcript contamination from other cell types.[152] As monocytes are relatively small, some of those results could be derived from the contamination of certain areas defined as a different cell population with transcripts of monocytes that were closely localized to the allocated spatial area. As the frequency of monocytes increases in the infarct area and border zone, this could give the appearance of an increased *Ccl2* mRNA expression in every cell type of the infarct and border zone as

observed in this thesis. With recent improvements in spatial transcriptomics techniques the definitive localization of *Ccl2* transcript expression across individual cells of the border zone and infarct area will be determined after myocardial infarction.[15,190]

As cardiomyocytes are a highly abundant cardiac cell type and *Ccl2* mRNA expression appears to primarily occur in the infarct and border zone, they are likely to significantly contribute to overall cardiac CCL2 protein levels. Indeed, cardiomyocyte-specific overexpression of 4EBP1 reduced serum CCL2 protein levels 24 hours after reperfusion by approximately one third, highlighting the contribution of cardiomyocytes to cardiac CCL2 protein release after myocardial ischemia/reperfusion. However, this data does not allow to conclude any relation between Ccl2 transcript translation and secretion. The observation that cardiomyocyte-restricted 4EBP1 overexpression alters serum Ccl2 levels may also be related to other mechanisms that alter Ccl2 processing, secretion or cardiac cell death. Ccl2 is a protein that is subjected to post-translational modification that controls its activity.[164]

For the anti-inflammatory effects, however, additional systemic effects of mTOR inhibition and translational dependence must be considered. This thesis specifically investigated the effects of rapamycin or 4EGI-1 on circulating monocytes and revealed the importance of a direct effect of mTORC1-4EBP1-eIF4E pathway inhibitors on circulating monocytes that impair their infiltration to the injured heart. Using a CD45.1/2 system, I observed reduced numbers of *ex vivo* treated monocytes to the heart after I/R surgery. However, due to the low total number of CD45.1 cells detected in the hearts of CD45.2 recipient mice, these results should be interpreted with caution, indicating that the majority of transplanted cells did not survive to procedure, or did not infiltrate the injured heart at the selected timepoint. In addition, it must be considered that anti-inflammatory and cardioprotective effects after systemic mTORC1 inhibition

may not only be derived from cardiac cells or circulating immune cells but may also involve other cell types of other organs that were not investigated in this thesis.

In summary, this work describes translational control of an inflammatory network in the heart in response to ischemia and reperfusion that may be targeted to improve outcomes after myocardial infarction.

## 6.5 Limitations

This study conducted experiments in mice, isolated cardiomyocytes from rodents, and various other cell lines. Although rodents are closely related to humans on a phylogenetic level, findings from rodent experiments do not necessarily apply to humans. This discrepancy can arise from several factors, including differences in physiology between rodents and humans, effects specific to those species, presence of comorbidities in the clinical setting, and lack of efficacy in chronic disease conditions, among others. For example, rodent and human immune cells show significant differences in cell function and different dynamics of immune cell activation in response to myocardial infarction and reperfusion. In addition, pharmacological inhibitors were used in this study just prior to reperfusion, a strategy that is possible but more difficult to implement in a clinical trial to test efficacy in humans. This study used simulated ischemia and reperfusion, which is based on restricting nutrient and oxygen supply to cells, followed by simulated ‘reperfusion’ (changing media to high-nutrient culture conditions and restoring oxygen levels). This model does not adequately capture the complex and dynamic conditions present in the multicellular heart during ischemia and reperfusion. As a mouse model, myocardial infarction was surgically induced in healthy young adult mice. While the mentioned techniques are established and widely used

models to study cardiac ischemia and reperfusion, it is important to note that none of these models can capture the full complexity of human disease and does not represent the conditions present in multimorbid patients with advanced age, commonly affected in the clinical setting. Even though some existing data points to the general involvement of translational regulation of cardiac gene expression and the involvement of the mTORC1 pathway in the inflammatory response, this study does not allow any definite conclusions about the studied pathways or pharmacological efficacy in humans. These findings should be considered preliminary and if other researchers can replicate these results, potentially using different model systems, it may pave the way for human translational studies, provided that adequate safety measures are ensured.

## 6.6 Outlook

This thesis describes the activation of a translational network of the infarct and border zone, which regulates the cardiac inflammatory response after ischemia/reperfusion. In addition, this thesis identifies a translation-dependent intrinsic mechanism of circulating monocytes that regulates their infiltration to the injured myocardium after I/R surgery in mice. However, several important mechanistic details remain unknown. While I provided some insight into the spatiotemporal regulation of this translational activation by investigating different timepoints after reperfusion, by dissecting the heart into the infarct, border zone and remote area, as well as by using immunofluorescent imaging of translation of cardiac sections, where and when this response becomes activated remains unknown. In addition, it is not known whether the translational response is of transient nature or rather represent a longer lasting process that drives gene expression over several days and whether it remains limited

to certain areas of the myocardium or extends throughout the heart, for example to mediate cardiac remodeling. Future experiments should therefore try to describe the spatiotemporal dynamics of this translational response in more detail. The usage of genetic labeling of newly synthesized protein, e.g. by methods recently used by Liu et al.[172] may circumvent some of the limitations the arise from pharmacological labeling of newly synthesized polypeptides. As further described above, the translational activation may not only occur in response to reperfusion but could instead represent a general response of the heart to injury. Similar experiments as the ones described in this thesis should be performed in different cardiac injury model, for example permanent LAD ligation, electric- or cryoinjury.

In this thesis I focused specifically on cardiomyocytes, however many other cell types such as immune cells, fibroblasts and endothelial cells will contribute to the translational activation after cardiac ischemia/reperfusion. The Ribo-tag model used in this thesis can be crossed to other cell-type specific Cre-reporter lines to specifically investigate the translational response of those cell-types to cardiac injury.[83] In addition, mouse models that genetically label newly synthesized proteins could be engineered to specifically examine translation of a selected cell population. While those different cardiac cell types may share certain translational gene programs, many aspects of translation will be mediated in a cell-type-specific manner, which were missed in this thesis. With the recent progressions made in spatial omics techniques, as well as single-cell ribosome profiling, a spatial single cell atlas of cardiac translation in health and disease may be feasible in the near future.[190–192]

Here, I demonstrated that a treatment protocol of either of the two pharmacological compounds, rapamycin and 4EGI-1, shows cardioprotective effects

in an ischemia/reperfusion model in mice. However, neither of the two drugs may represent ideal candidate drugs for clinical use. 4EGI-1, a eIF4E/eIF4G interaction inhibitor, that blocks cap-dependent translation by disrupting the eIF4F complex, has imperfect solubility and only a small range of efficacy without being toxic *in vivo*. Therefore, in its current state 4EGI-1 should be seen as a proof-of-principle compound that has serious safety concerns for clinical applications. Whether the toxicity of 4EGI-1 is due to its general inhibition of cap-dependent translation, a concept that itself may not be translatable to the clinic, or target specific, as observed for other eIF4E-binding compounds,[180,181] is unknown. Rapamycin, on the other hand, is a partially selective mTORC1 inhibitor with limited efficacy against certain downstream targets of mTORC1, including 4EBP1. Rapamycin has a relatively weak direct effect on the total amount of cellular protein synthesis and influences many functions other than translation. Whether this broader effect, that is mediated by the inhibition of mTORC1, is a good or bad thing in the context of ischemia/reperfusion is not known, based on previous literature I would argue that those properties may actually be beneficial compared to a general and strong inhibition of protein synthesis. Rapamycin, for example, leads to an activation of autophagy which, despite some controversy, is generally considered beneficial.[193] While generally considered as a relatively safe drug, the broader effect of rapamycin may, however, be associated with certain undesired side-effect, such as stomatitis, hypercholesterolemia, hypertriglyceridemia, hyperglycemia, insulin resistance and immunosuppression.[194] Several mTORC1 inhibitors that have better mTORC1-selectivity over mTORC2 were recently identified.[195–199] Their usage may results in better efficacy and less side effects, however whether they are safe alternatives to conventional mTORC1 inhibitors such as rapamycin should be tested in future studies, including in the context of cardiac ischemia/reperfusion. In addition, interesting pharmacological targets may be

endogenous mTORC1-selective elements such as PRAS40, RHEB or the TSC complex, target other elements of the eIF4F complex such as eIF4G or eIF4A, or act more specifically on selected transcripts such as by targeting RNA-binding proteins or by using antisense oligonucleotides.

Targeting the mTORC1 pathway and translation are promising strategies to treat various cardiovascular disease. Future studies need to further explore the mechanisms that determine gene expression, protein synthesis and the inflammatory response in the heart. While this thesis uncovered novel mechanisms that determine cardiac function, many more remain unexplored, the study of which will improve our understanding of cardiovascular pathophysiology and guide the development of new treatments for cardiovascular disease.

# 7 References


1. Muthiah V, A. MG, Varieur TJ, Valentin F, A. RG. The Global Burden of Cardiovascular Diseases and Risk. *J Am Coll Cardiol* [Internet]. 2022;80:2361–2371. Available from: https://doi.org/10.1016/j.jacc.2022.11.005
2. Nowbar AN, Gitto M, Howard JP, Francis DP, Al-Lamee R. Mortality From Ischemic Heart Disease. *Circ Cardiovasc Qual Outcomes* [Internet]. 2019;12:e005375. Available from: https://doi.org/10.1161/CIRCOUTCOMES.118.005375
3. Khera A V, Kathiresan S. Genetics of coronary artery disease: discovery, biology and clinical translation. *Nat Rev Genet* [Internet]. 2017;18:331–344. Available from: https://doi.org/10.1038/nrg.2016.160
4. Thygesen K, Alpert JS, Jaffe AS, Chaitman BR, Bax JJ, Morrow DA, White HD, Corbett S, Chettibi M, Hayrapetyan H, Roithinger FX, Aliyev F, Sujayeva V, Claeys MJ, Smajić E, Kala P, Iversen KK, Hefny E El, Marandi T, Porela P, Antov S, Gilard M, Blankenberg S, Davlouros P, Gudnason T, Alcalai R, Colivicchi F, Elezi S, Baitova G, Zakke I, Gustiene O, Beissel J, Dingli P, Grosu A, Damman P, Juliebo V, Legutko J, Morais J, Tatu-Chitoiu G, Yakovlev A, Zavatta M, Nedeljkovic M, Radsel P, Sionis A, Jemberg T, Müller C, Abid L, Abaci A, Parkhomenko A. Fourth Universal Definition of Myocardial Infarction (2018). *Circulation* [Internet]. 2018 [cited 2024 Apr 11];138:e618–e651. Available from: https://www.ahajournals.org/doi/abs/10.1161/CIR.0000000000000617
5. Dai H, Much AA, Maor E, Asher E, Younis A, Xu Y, Lu Y, Liu X, Shu J, Bragazzi NL. Global, regional, and national burden of ischaemic heart disease and its attributable risk factors, 1990–2017: results from the Global Burden of Disease Study 2017. *Eur Hear J - Qual Care Clin Outcomes* [Internet]. 2022;8:50–60. Available from: https://doi.org/10.1093/ehjqcco/qcaa076
6. Khan MAB, Hashim MJ, Mustafa H, Baniyas MY, Al Suwaidi SKBM, AlKatheeri R, Alblooshi FMK, Almatrooshi MEAH, Alzaabi MEH, Al Darmaki RS, Lootah SNAH. Global Epidemiology of Ischemic Heart Disease: Results from the Global Burden of Disease Study. *Cureus* [Internet]. 2020;12:e9349. Available from: http://dx.doi.org/10.7759/cureus.9349
7. Martin SS, Aday AW, Almarzooq ZI, Anderson CAM, Arora P, Avery CL, Baker-Smith CM, Barone Gibbs B, Beaton AZ, Boehme AK, Commodore-Mensah Y, Currie ME, Elkind MS V, Evenson KR, Generoso G, Heard DG, Hiremath S, Johansen MC, Kalani R, Kazi DS, Ko D, Liu J, Magnani JW, Michos ED, Mussolino ME, Navaneethan SD, Parikh NI, Perman SM, Poudel R, Rezk-Hanna M, Roth GA, Shah NS, St-Onge M-P, Thacker EL, Tsao CW, Urbut SM, Van Spall HGC, Voeks JH, Wang N-Y, Wong ND, Wong SS, Yaffe K, Palaniappan LP, null null. 2024 Heart Disease and Stroke Statistics: A Report of US and Global Data From the American Heart Association. *Circulation* [Internet]. 2024;149:e347–e913. Available from: https://doi.org/10.1161/CIR.0000000000001209
8. Reed GW, Rossi JE, Cannon CP. Acute myocardial infarction. *Lancet* [Internet]. 2017;389:197–210. Available from: https://doi.org/10.1016/S0140-6736(16)30677-8
9. Anderson JL, Morrow DA. Acute Myocardial Infarction. *N Engl J Med* [Internet]. 2017 [cited 2024 Apr 11];376:2053–2064. Available from: https://www.nejm.org/doi/full/10.1056/NEJMra1606915
10. Damluji AA, Van Diepen S, Katz JN, Menon V, Tamis-Holland JE, Bakitas M,

Cohen MG, Balsam LB, Chikwe J. Mechanical Complications of Acute Myocardial Infarction: A Scientific Statement From the American Heart Association. *Circulation* [Internet]. 2021 [cited 2024 Apr 11];144:E16–E35. Available from: https://www.ahajournals.org/doi/abs/10.1161/CIR.0000000000000985
11. Lamas GA, Mitchell GF, Flaker GC, Smith SC, Gersh BJ, Basta L, Moyé L, Braunwald E, Pfeffer MA. Clinical Significance of Mitral Regurgitation After Acute Myocardial Infarction. *Circulation* [Internet]. 1997 [cited 2024 Apr 11];96:827–833. Available from: https://www.ahajournals.org/doi/abs/10.1161/01.CIR.96.3.827
12. Imazio M, Hoit BD. Post-cardiac injury syndromes. An emerging cause of pericardial diseases. *Int J Cardiol* [Internet]. 2013 [cited 2024 Apr 11];168:648–652. Available from: http://www.internationaljournalofcardiology.com/article/S0167527312011588/fulltext
13. Crossman DC. The pathophysiology of myocardial ischaemia. *Heart* [Internet]. 2004;90:576 LP – 580. Available from: http://heart.bmj.com/content/90/5/576.abstract
14. Goodwill AG, Dick GM, Kiel AM, Tune JD. Regulation of Coronary Blood Flow [Internet]. In: Comprehensive Physiology. 2017. p. 321–382.Available from: https://doi.org/10.1002/cphy.c160016
15. Kuppe C, Ramirez Flores RO, Li Z, Hayat S, Levinson RT, Liao X, Hannani MT, Tanevski J, Wünnemann F, Nagai JS, Halder M, Schumacher D, Menzel S, Schäfer G, Hoeft K, Cheng M, Ziegler S, Zhang X, Peisker F, Kaesler N, Saritas T, Xu Y, Kassner A, Gummert J, Morshuis M, Amrute J, Veltrop RJA, Boor P, Klingel K, Van Laake LW, Vink A, Hoogenboezem RM, Bindels EMJ, Schurgers L, Sattler S, Schapiro D, Schneider RK, Lavine K, Milting H, Costa IG, Saez-Rodriguez J, Kramann R. Spatial multi-omic map of human myocardial infarction. *Nature* [Internet]. 2022;608:766–777. Available from: https://doi.org/10.1038/s41586-022-05060-x
16. Hayat S, Kramann R. Mapping the border zone in myocardial infarction. *Nat Cardiovasc Res* [Internet]. 2022;1:978–979. Available from: https://doi.org/10.1038/s44161-022-00161-2
17. Byrne RA, Rossello X, Coughlan JJ, Barbato E, Berry C, Chieffo A, Claeys MJ, Dan G-A, Dweck MR, Galbraith M, Gilard M, Hinterbuchner L, Jankowska EA, Jüni P, Kimura T, Kunadian V, Leosdottir M, Lorusso R, Pedretti RFE, Rigopoulos AG, Rubini Gimenez M, Thiele H, Vranckx P, Wassmann S, Wenger NK, Ibanez B. 2023 ESC Guidelines for the management of acute coronary syndromes: Developed by the task force on the management of acute coronary syndromes of the European Society of Cardiology (ESC). *Eur Heart J* [Internet]. 2023;44:3720–3826. Available from: https://doi.org/10.1093/eurheartj/ehad191
18. Heusch G. Myocardial ischaemia–reperfusion injury and cardioprotection in perspective. *Nat Rev Cardiol* [Internet]. 2020;17:773–789. Available from: https://doi.org/10.1038/s41569-020-0403-y
19. McNamara RL, Wang Y, Herrin J, Curtis JP, Bradley EH, Magid DJ, Peterson ED, Blaney M, Frederick PD, Krumholz HM. Effect of Door-to-Balloon Time on Mortality in Patients With ST-Segment Elevation Myocardial Infarction. *J Am Coll Cardiol* [Internet]. 2006;47:2180–2186. Available from: https://www.sciencedirect.com/science/article/pii/S0735109706006139
20. Fröhlich GM, Meier P, White SK, Yellon DM, Hausenloy DJ. Myocardial

reperfusion injury: looking beyond primary PCI. *Eur Heart J* [Internet]. 2013;34:1714–1722. Available from: https://doi.org/10.1093/eurheartj/eht090
21. Kloner RA. Does reperfusion injury exist in humans? *J Am Coll Cardiol* [Internet]. 1993;21:537–545. Available from: https://www.sciencedirect.com/science/article/pii/073510979390700B
22. Frangogiannis NG, Smith CW, Entman ML. The inflammatory response in myocardial infarction. *Cardiovasc Res* [Internet]. 2002;53:31–47. Available from: https://doi.org/10.1016/S0008-6363(01)00434-5
23. Matter MA, Paneni F, Libby P, Frantz S, Stähli BE, Templin C, Mengozzi A, Wang Y-J, Kündig TM, Räber L, Ruschitzka F, Matter CM. Inflammation in acute myocardial infarction: the good, the bad and the ugly. *Eur Heart J* [Internet]. 2024;45:89–103. Available from: https://doi.org/10.1093/eurheartj/ehad486
24. Algoet M, Janssens S, Himmelreich U, Gsell W, Pusovnik M, Van den Eynde J, Oosterlinck W. Myocardial ischemia-reperfusion injury and the influence of inflammation. *Trends Cardiovasc Med* [Internet]. 2023;33:357–366. Available from: https://www.sciencedirect.com/science/article/pii/S1050173822000299
25. Mitsis A, Kyriakou M, Sokratous S, Karmioti G, Drakomathioulakis M, Myrianthefs M, Ziakas A, Tzikas S, Kassimis G. Exploring the Landscape of Anti-Inflammatory Trials: A Comprehensive Review of Strategies for Targeting Inflammation in Acute Myocardial Infraction. Biomedicines. 2024;12.
26. Ridker PM, Bhatt DL, Pradhan AD, Glynn RJ, MacFadyen JG, Nissen SE. Inflammation and cholesterol as predictors of cardiovascular events among patients receiving statin therapy: a collaborative analysis of three randomised trials. *Lancet* [Internet]. 2023;401:1293–1301. Available from: https://doi.org/10.1016/S0140-6736(23)00215-5
27. Libby P, Maroko PR, Bloor CM, Sobel BE, Braunwald E. Reduction of Experimental Myocardial Infarct Size by Corticosteroid Administration. *J Clin Invest* [Internet]. 1973;52:599–607. Available from: https://doi.org/10.1172/JCI107221
28. Roberts R, DeMello V, Sobel BE. Deleterious effects of methylprednisolone in patients with myocardial infarction. *Circulation* [Internet]. 1976;53:I204-6. Available from: http://europepmc.org/abstract/MED/1253361
29. Kloner RA, Fishbein MC, Lew H, Maroko PR, Braunwald E. Mummification of the infarcted myocardium by high dose corticosteroids. *Circulation* [Internet]. 1978;57:56–63. Available from: https://doi.org/10.1161/01.CIR.57.1.56
30. Zhang RYK, Cochran BJ, Thomas SR, Rye K. Impact of Reperfusion on Temporal Immune Cell Dynamics After Myocardial Infarction. *J Am Heart Assoc* [Internet]. 2023;12:e027600. Available from: https://doi.org/10.1161/JAHA.122.027600
31. Prabhu SD, Frangogiannis NG. The Biological Basis for Cardiac Repair After Myocardial Infarction. *Circ Res* [Internet]. 2016;119:91–112. Available from: https://doi.org/10.1161/CIRCRESAHA.116.303577
32. Rusinkevich V, Huang Y, Chen Z, Qiang W, Wang Y, Shi Y, Yang H. Temporal dynamics of immune response following prolonged myocardial ischemia/reperfusion with and without cyclosporine A. *Acta Pharmacol Sin* [Internet]. 2019;40:1168–1183. Available from: https://doi.org/10.1038/s41401-018-0197-1
33. Yan X, Anzai A, Katsumata Y, Matsuhashi T, Ito K, Endo J, Yamamoto T, Takeshima A, Shinmura K, Shen W, Fukuda K, Sano M. Temporal dynamics of cardiac immune cell accumulation following acute myocardial infarction. *J Mol*

*Cell Cardiol* [Internet]. 2013;62:24–35. Available from: https://doi.org/10.1016/j.yjmcc.2013.04.023
34. Maugeri N, Rovere-Querini P, Evangelista V, Godino C, Demetrio M, Baldini M, Figini F, Coppi G, Slavich M, Camera M, Bartorelli A, Marenzi G, Campana L, Baldissera E, Sabbadini MG, Cianflone D, Tremoli E, D'Angelo A, Manfredi AA, Maseri A. An Intense and Short-Lasting Burst of Neutrophil Activation Differentiates Early Acute Myocardial Infarction from Systemic Inflammatory Syndromes. *PLoS One* [Internet]. 2012;7:e39484. Available from: https://doi.org/10.1371/journal.pone.0039484
35. Li Y, Chen B, Yang X, Zhang C, Jiao Y, Li P, Liu Y, Li Z, Qiao B, Bond Lau W, Ma X, Du J. S100a8/a9 Signaling Causes Mitochondrial Dysfunction and Cardiomyocyte Death in Response to Ischemic/Reperfusion Injury. *Circulation* [Internet]. 2019;140:751–764. Available from: https://doi.org/10.1161/CIRCULATIONAHA.118.039262
36. Sreejit G, Abdel-Latif A, Athmanathan B, Annabathula R, Dhyani A, Noothi SK, Quaife-Ryan GA, Al-Sharea A, Pernes G, Dragoljevic D, Lal H, Schroder K, Hanaoka BY, Raman C, Grant MB, Hudson JE, Smyth SS, Porrello ER, Murphy AJ, Nagareddy PR. Neutrophil-Derived S100A8/A9 Amplify Granulopoiesis After Myocardial Infarction. *Circulation* [Internet]. 2020;141:1080–1094. Available from: https://doi.org/10.1161/CIRCULATIONAHA.119.043833
37. Marinković G, Grauen Larsen H, Yndigegn T, Szabo IA, Mares RG, de Camp L, Weiland M, Tomas L, Goncalves I, Nilsson J, Jovinge S, Schiopu A. Inhibition of pro-inflammatory myeloid cell responses by short-term S100A9 blockade improves cardiac function after myocardial infarction. *Eur Heart J* [Internet]. 2019;40:2713–2723. Available from: https://doi.org/10.1093/eurheartj/ehz461
38. Dentali F, Nigro O, Squizzato A, Gianni M, Zuretti F, Grandi AM, Guasti L. Impact of neutrophils to lymphocytes ratio on major clinical outcomes in patients with acute coronary syndromes: A systematic review and meta-analysis of the literature. *Int J Cardiol* [Internet]. 2018;266:31–37. Available from: https://doi.org/10.1016/j.ijcard.2018.02.116
39. Puhl S-L, Steffens S. Neutrophils in Post-myocardial Infarction Inflammation: Damage vs. Resolution? [Internet]. Front. Cardiovasc. Med. . 2019;6. Available from: https://www.frontiersin.org/articles/10.3389/fcvm.2019.00025
40. Daseke MJ, Chalise U, Becirovic-Agic M, Salomon JD, Cook LM, Case AJ, Lindsey ML. Neutrophil signaling during myocardial infarction wound repair. *Cell Signal* [Internet]. 2021;77:109816. Available from: https://www.sciencedirect.com/science/article/pii/S089865682030293X
41. Bajpai G, Bredemeyer A, Li W, Zaitsev K, Koenig AL, Lokshina I, Mohan J, Ivey B, Hsiao H-M, Weinheimer C, Kovacs A, Epelman S, Artyomov M, Kreisel D, Lavine KJ. Tissue Resident CCR2− and CCR2+ Cardiac Macrophages Differentially Orchestrate Monocyte Recruitment and Fate Specification Following Myocardial Injury. *Circ Res* [Internet]. 2019;124:263–278. Available from: https://doi.org/10.1161/CIRCRESAHA.118.314028
42. Dick SA, Macklin JA, Nejat S, Momen A, Clemente-Casares X, Althagafi MG, Chen J, Kantores C, Hosseinzadeh S, Aronoff L, Wong A, Zaman R, Barbu I, Besla R, Lavine KJ, Razani B, Ginhoux F, Husain M, Cybulsky MI, Robbins CS, Epelman S. Self-renewing resident cardiac macrophages limit adverse remodeling following myocardial infarction. *Nat Immunol* [Internet]. 2019;20:29–39. Available from: https://doi.org/10.1038/s41590-018-0272-2

43. Epelman S, Lavine KJ, Beaudin AE, Sojka DK, Carrero JA, Calderon B, Brija T, Gautier EL, Ivanov S, Satpathy AT, Schilling JD, Schwendener R, Sergin I, Razani B, Forsberg EC, Yokoyama WM, Unanue ER, Colonna M, Randolph GJ, Mann DL. Embryonic and Adult-Derived Resident Cardiac Macrophages Are Maintained through Distinct Mechanisms at Steady State and during Inflammation. *Immunity* [Internet]. 2014;40:91–104. Available from: https://doi.org/10.1016/j.immuni.2013.11.019
44. Heidt T, Courties G, Dutta P, Sager HB, Sebas M, Iwamoto Y, Sun Y, Da Silva N, Panizzi P, van der Laan AM, Swirski FK, Weissleder R, Nahrendorf M. Differential Contribution of Monocytes to Heart Macrophages in Steady-State and After Myocardial Infarction. *Circ Res* [Internet]. 2014;115:284–295. Available from: https://doi.org/10.1161/CIRCRESAHA.115.303567
45. Nahrendorf M, Swirski FK. Monocyte and Macrophage Heterogeneity in the Heart. *Circ Res* [Internet]. 2013;112:1624–1633. Available from: https://doi.org/10.1161/CIRCRESAHA.113.300890
46. Nahrendorf M. Myeloid cell contributions to cardiovascular health and disease. *Nat Med* [Internet]. 2018;24:711–720. Available from: https://doi.org/10.1038/s41591-018-0064-0
47. Leuschner F, Rauch PJ, Ueno T, Gorbatov R, Marinelli B, Lee WW, Dutta P, Wei Y, Robbins C, Iwamoto Y, Sena B, Chudnovskiy A, Panizzi P, Keliher E, Higgins JM, Libby P, Moskowitz MA, Pittet MJ, Swirski FK, Weissleder R, Nahrendorf M. Rapid monocyte kinetics in acute myocardial infarction are sustained by extramedullary monocytopoiesis. *J Exp Med* [Internet]. 2012;209:123–137. Available from: https://doi.org/10.1084/jem.20111009
48. Swirski FK, Nahrendorf M, Etzrodt M, Wildgruber M, Cortez-Retamozo V, Panizzi P, Figueiredo JL, Kohler RH, Chudnovskiy A, Waterman P, Aikawa E, Mempel TR, Libby P, Weissleder R, Pittet MJ. Identification of splenic reservoir monocytes and their deployment to inflammatory sites. *Science (80- )* [Internet]. 2009 [cited 2024 Apr 17];325:612–616. Available from: https://www.science.org/doi/10.1126/science.1175202
49. van der Laan AM, ter Horst EN, Delewi R, Begieneman MP V, Krijnen PAJ, Hirsch A, Lavaei M, Nahrendorf M, Horrevoets AJ, Niessen HWM, Piek JJ. Monocyte subset accumulation in the human heart following acute myocardial infarction and the role of the spleen as monocyte reservoir. *Eur Heart J* [Internet]. 2014;35:376–385. Available from: https://doi.org/10.1093/eurheartj/eht331
50. Majmudar MD, Keliher EJ, Heidt T, Leuschner F, Truelove J, Sena BF, Gorbatov R, Iwamoto Y, Dutta P, Wojtkiewicz G, Courties G, Sebas M, Borodovsky A, Fitzgerald K, Nolte MW, Dickneite G, Chen JW, Anderson DG, Swirski FK, Weissleder R, Nahrendorf M. Monocyte-Directed RNAi Targeting CCR2 Improves Infarct Healing in Atherosclerosis-Prone Mice. *Circulation* [Internet]. 2013;127:2038–2046. Available from: https://doi.org/10.1161/CIRCULATIONAHA.112.000116
51. Leuschner F, Dutta P, Gorbatov R, Novobrantseva TI, Donahoe JS, Courties G, Lee KM, Kim JI, Markmann JF, Marinelli B, Panizzi P, Lee WW, Iwamoto Y, Milstein S, Epstein-Barash H, Cantley W, Wong J, Cortez-Retamozo V, Newton A, Love K, Libby P, Pittet MJ, Swirski FK, Koteliansky V, Langer R, Weissleder R, Anderson DG, Nahrendorf M. Therapeutic siRNA silencing in inflammatory monocytes in mice. *Nat Biotechnol* [Internet]. 2011;29:1005–1010. Available from: https://doi.org/10.1038/nbt.1989
52. DeBerge M, Yeap XY, Dehn S, Zhang S, Grigoryeva L, Misener S, Procissi D,

Zhou X, Lee DC, Muller WA, Luo X, Rothlin C, Tabas I, Thorp EB. MerTK Cleavage on Resident Cardiac Macrophages Compromises Repair After Myocardial Ischemia Reperfusion Injury. *Circ Res* [Internet]. 2017;121:930–940. Available from: https://doi.org/10.1161/CIRCRESAHA.117.311327

53. Frantz S, Hofmann U, Fraccarollo D, Schäfer A, Kranepuhl S, Hagedorn I, Nieswandt B, Nahrendorf M, Wagner H, Bayer B, Pachel C, Schön MP, Kneitz S, Bobinger T, Weidemann F, Ertl G, Bauersachs J. Monocytes/macrophages prevent healing defects and left ventricular thrombus formation after myocardial infarction. *FASEB J* [Internet]. 2013;27:871–881. Available from: https://doi.org/10.1096/fj.12-214049
54. Haider N, Boscá L, Zandbergen HR, Kovacic JC, Narula N, González-Ramos S, Fernandez-Velasco M, Agrawal S, Paz-García M, Gupta S, DeLeon-Pennell K, Fuster V, Ibañez B, Narula J. Transition of Macrophages to Fibroblast-Like Cells in Healing Myocardial Infarction. *J Am Coll Cardiol* [Internet]. 2019;74:3124–3135. Available from: https://www.sciencedirect.com/science/article/pii/S0735109719382622
55. Bajpai G, Schneider C, Wong N, Bredemeyer A, Hulsmans M, Nahrendorf M, Epelman S, Kreisel D, Liu Y, Itoh A, Shankar TS, Selzman CH, Drakos SG, Lavine KJ. The human heart contains distinct macrophage subsets with divergent origins and functions. *Nat Med* [Internet]. 2018;24:1234–1245. Available from: https://doi.org/10.1038/s41591-018-0059-x
56. Sager HB, Hulsmans M, Lavine KJ, Moreira MB, Heidt T, Courties G, Sun Y, Iwamoto Y, Tricot B, Khan OF, Dahlman JE, Borodovsky A, Fitzgerald K, Anderson DG, Weissleder R, Libby P, Swirski FK, Nahrendorf M. Proliferation and Recruitment Contribute to Myocardial Macrophage Expansion in Chronic Heart Failure. *Circ Res* [Internet]. 2016;119:853–864. Available from: https://doi.org/10.1161/CIRCRESAHA.116.309001
57. Boag SE, Das R, Shmeleva E V, Bagnall A, Egred M, Howard N, Bennaceur K, Zaman A, Keavney B, Spyridopoulos I. T lymphocytes and fractalkine contribute to myocardial ischemia/reperfusion injury in patients. *J Clin Invest* [Internet]. 2015;125:3063–3076. Available from: https://doi.org/10.1172/JCI80055
58. Karahan Z, Uçaman B, Uluğ AV, Aydınalp Ö, Uğurlu M, Çevik K, Kaya İ, Öztürk Ö. Effect of Hematologic Parameters on Microvascular Reperfusion in Patients With ST-Segment Elevation Myocardial Infarction Treated With Primary Percutaneous Coronary Intervention. *Angiology* [Internet]. 2015;67:151–156. Available from: https://doi.org/10.1177/0003319715583204
59. Zhang L, Wang Z, Wang D, Zhu J, Wang Y. CD8+CD28+ T cells might mediate injury of cardiomyocytes in acute myocardial infarction. *Mol Immunol* [Internet]. 2018;101:74–79. Available from: https://www.sciencedirect.com/science/article/pii/S0161589018301627
60. Hofmann U, Frantz S. Role of Lymphocytes in Myocardial Injury, Healing, and Remodeling After Myocardial Infarction. *Circ Res* [Internet]. 2015;116:354–367. Available from: https://doi.org/10.1161/CIRCRESAHA.116.304072
61. Medzhitov R. The spectrum of inflammatory responses. *Science (80- )* [Internet]. 2021 [cited 2024 Apr 26];374:1070–1075. Available from: https://www.science.org/doi/10.1126/science.abi5200
62. Weirather J, Hofmann UDW, Beyersdorf N, Ramos GC, Vogel B, Frey A, Ertl G, Kerkau T, Frantz S. Foxp3+ CD4+ T Cells Improve Healing After Myocardial Infarction by Modulating Monocyte/Macrophage Differentiation. *Circ Res* [Internet]. 2014;115:55–67. Available from:

https://doi.org/10.1161/CIRCRESAHA.115.303895
63. Rieckmann M, Delgobo M, Gaal C, Büchner L, Steinau P, Reshef D, Gil-Cruz C, Horst EN ter, Kircher M, Reiter T, Heinze KG, Niessen HWM, Krijnen PAJ, van der Laan AM, Piek JJ, Koch C, Wester H-J, Lapa C, Bauer WR, Ludewig B, Friedman N, Frantz S, Hofmann U, Ramos GC. Myocardial infarction triggers cardioprotective antigen-specific T helper cell responses. *J Clin Invest* [Internet]. 2019;129:4922–4936. Available from: https://doi.org/10.1172/JCI123859
64. Ilatovskaya D V, Pitts C, Clayton J, Domondon M, Troncoso M, Pippin S, DeLeon-Pennell KY. CD8+ T-cells negatively regulate inflammation post-myocardial infarction. *Am J Physiol Circ Physiol* [Internet]. 2019;317:H581–H596. Available from: https://doi.org/10.1152/ajpheart.00112.2019
65. Huang S, Frangogiannis NG. Anti-inflammatory therapies in myocardial infarction: failures, hopes and challenges. *Br J Pharmacol* [Internet]. 2018;175:1377–1400. Available from: https://doi.org/10.1111/bph.14155
66. Vascular and upper gastrointestinal effects of non-steroidal anti-inflammatory drugs: meta-analyses of individual participant data from randomised trials. *Lancet* [Internet]. 2013;382:769–779. Available from: https://www.sciencedirect.com/science/article/pii/S0140673613609009
67. Dumont FJ, Su Q. Mechanism of action of the immunosuppressant rapamycin. *Life Sci* [Internet]. 1995;58:373–395. Available from: https://www.sciencedirect.com/science/article/pii/0024320595022333
68. Maier W, Altwegg LA, Corti R, Gay S, Hersberger M, Maly FE, Sütsch G, Roffi M, Neidhart M, Eberli FR, Tanner FC, Gobbi S, von Eckardstein A, Lüscher TF. Inflammatory Markers at the Site of Ruptured Plaque in Acute Myocardial Infarction. *Circulation* [Internet]. 2005;111:1355–1361. Available from: https://doi.org/10.1161/01.CIR.0000158479.58589.0A
69. Neumann F-J, Ott I, Gawaz M, Richardt G, Holzapfel H, Jochum M, Schömig A. Cardiac Release of Cytokines and Inflammatory Responses in Acute Myocardial Infarction. *Circulation* [Internet]. 1995;92:748–755. Available from: https://doi.org/10.1161/01.CIR.92.4.748
70. Kleveland O, Kunszt G, Bratlie M, Ueland T, Broch K, Holte E, Michelsen AE, Bendz B, Amundsen BH, Espevik T, Aakhus S, Damås JK, Aukrust P, Wiseth R, Gullestad L. Effect of a single dose of the interleukin-6 receptor antagonist tocilizumab on inflammation and troponin T release in patients with non-ST-elevation myocardial infarction: a double-blind, randomized, placebo-controlled phase 2 trial†. *Eur Heart J* [Internet]. 2016;37:2406–2413. Available from: https://doi.org/10.1093/eurheartj/ehw171
71. Kaspar B, Kristine AA, Sindre W, Kapil S, Maria TI, Bjørn B, Svend A, Thor U, Høyem AB, Kristian DJ, Sturle BE, Elisabeth B, Christina B, Einar H, Ola K, Haakon SK, Anders O, Nils-Einar K, Ingebjørg S, Øystein AG, Rune W, Pål A, Lars G. Randomized Trial of Interleukin-6 Receptor Inhibition in Patients With Acute ST-Segment Elevation Myocardial Infarction. *J Am Coll Cardiol* [Internet]. 2021;77:1845–1855. Available from: https://doi.org/10.1016/j.jacc.2021.02.049
72. Morton AC, Rothman AMK, Greenwood JP, Gunn J, Chase A, Clarke B, Hall AS, Fox K, Foley C, Banya W, Wang D, Flather MD, Crossman DC. The effect of interleukin-1 receptor antagonist therapy on markers of inflammation in non-ST elevation acute coronary syndromes: the MRC-ILA Heart Study. *Eur Heart J* [Internet]. 2015;36:377–384. Available from: https://doi.org/10.1093/eurheartj/ehu272

73. Abbate A, Wohlford GF, Del Buono MG, Chiabrando JG, Markley R, Turlington J, Kadariya D, Trankle CR, Biondi-Zoccai G, Lipinski MJ, Van Tassell BW. Interleukin-1 blockade with anakinra and heart failure following ST-segment elevation myocardial infarction: results from a pooled analysis of the VCUART clinical trials. *Eur Hear J - Cardiovasc Pharmacother* [Internet]. 2022;8:503–510. Available from: https://doi.org/10.1093/ehjcvp/pvab075
74. Klingenberg R, Stähli BE, Heg D, Denegri A, Manka R, Kapos I, von Eckardstein A, Carballo D, Hamm CW, Vietheer J, Rolf A, Landmesser U, Mach F, Moccetti T, Jung C, Kelm M, Münzel T, Pedrazzini G, Räber L, Windecker S, Matter CM, Ruschitzka F, Lüscher TF. Controlled-Level EVERolimus in Acute Coronary Syndrome (CLEVER-ACS) - A phase II, randomized, double-blind, multi-center, placebo-controlled trial. *Am Heart J* [Internet]. 2022;247:33–41. Available from: https://www.sciencedirect.com/science/article/pii/S0002870322000102
75. Ottani F, Latini R, Staszewsky L, La Vecchia L, Locuratolo N, Sicuro M, Masson S, Barlera S, Milani V, Lombardi M, Costalunga A, Mollichelli N, Santarelli A, De Cesare N, Sganzerla P, Boi A, Maggioni A Pietro, Limbruno U. Cyclosporine A in Reperfused Myocardial Infarction: The Multicenter, Controlled, Open-Label CYCLE Trial. *J Am Coll Cardiol* [Internet]. 2016;67:365–374. Available from: https://www.sciencedirect.com/science/article/pii/S0735109715074343
76. Cung T-T, Morel O, Cayla G, Rioufol G, Garcia-Dorado D, Angoulvant D, Bonnefoy-Cudraz E, Guérin P, Elbaz M, Delarche N, Coste P, Vanzetto G, Metge M, Aupetit J-F, Jouve B, Motreff P, Tron C, Labeque J-N, Steg PG, Cottin Y, Range G, Clerc J, Claeys MJ, Coussement P, Prunier F, Moulin F, Roth O, Belle L, Dubois P, Barragan P, Gilard M, Piot C, Colin P, De Poli F, Morice M-C, Ider O, Dubois-Randé J-L, Unterseeh T, Le Breton H, Béard T, Blanchard D, Grollier G, Malquarti V, Staat P, Sudre A, Elmer E, Hansson MJ, Bergerot C, Boussaha I, Jossan C, Derumeaux G, Mewton N, Ovize M. Cyclosporine before PCI in Patients with Acute Myocardial Infarction. *N Engl J Med* [Internet]. 2015 [cited 2024 Apr 26];373:1021–1031. Available from: https://www.nejm.org/doi/full/10.1056/NEJMoa1505489
77. Investigators TAAMI. Pexelizumab for Acute ST-Elevation Myocardial Infarction in Patients Undergoing Primary Percutaneous Coronary InterventionA Randomized Controlled Trial. *JAMA* [Internet]. 2007;297:43–51. Available from: https://doi.org/10.1001/jama.297.1.43
78. Granger CB, Mahaffey KW, Weaver WD, Theroux P, Hochman JS, Filloon TG, Rollins S, Todaro TG, Nicolau JC, Ruzyllo W, Armstrong PW. Pexelizumab, an Anti-C5 Complement Antibody, as Adjunctive Therapy to Primary Percutaneous Coronary Intervention in Acute Myocardial Infarction. *Circulation* [Internet]. 2003;108:1184–1190. Available from: https://doi.org/10.1161/01.CIR.0000087447.12918.85
79. Dutta P, Courties G, Wei Y, Leuschner F, Gorbatov R, Robbins CS, Iwamoto Y, Thompson B, Carlson AL, Heidt T, Majmudar MD, Lasitschka F, Etzrodt M, Waterman P, Waring MT, Chicoine AT, van der Laan AM, Niessen HWM, Piek JJ, Rubin BB, Butany J, Stone JR, Katus HA, Murphy SA, Morrow DA, Sabatine MS, Vinegoni C, Moskowitz MA, Pittet MJ, Libby P, Lin CP, Swirski FK, Weissleder R, Nahrendorf M. Myocardial infarction accelerates atherosclerosis. *Nature* [Internet]. 2012;487:325–329. Available from: https://doi.org/10.1038/nature11260
80. Ridker PM, Everett BM, Thuren T, MacFadyen JG, Chang WH, Ballantyne C,

Fonseca F, Nicolau J, Koenig W, Anker SD, Kastelein JJP, Cornel JH, Pais P, Pella D, Genest J, Cifkova R, Lorenzatti A, Forster T, Kobalava Z, Vida-Simiti L, Flather M, Shimokawa H, Ogawa H, Dellborg M, Rossi PRF, Troquay RPT, Libby P, Glynn RJ. Antiinflammatory Therapy with Canakinumab for Atherosclerotic Disease. *N Engl J Med* [Internet]. 2017 [cited 2024 Apr 26];377:1119–1131. Available from: https://www.nejm.org/doi/full/10.1056/NEJMoa1707914

81. Tardif J-C, Kouz S, Waters DD, Bertrand OF, Diaz R, Maggioni AP, Pinto FJ, Ibrahim R, Gamra H, Kiwan GS, Berry C, López-Sendón J, Ostadal P, Koenig W, Angoulvant D, Grégoire JC, Lavoie M-A, Dubé M-P, Rhainds D, Provencher M, Blondeau L, Orfanos A, L'Allier PL, Guertin M-C, Roubille F. Efficacy and Safety of Low-Dose Colchicine after Myocardial Infarction. *N Engl J Med* [Internet]. 2019 [cited 2024 Apr 26];381:2497–2505. Available from: https://www.nejm.org/doi/full/10.1056/NEJMoa1912388
82. Buccitelli C, Selbach M. mRNAs, proteins and the emerging principles of gene expression control. *Nat Rev Genet* [Internet]. 2020;21:630–644. Available from: https://doi.org/10.1038/s41576-020-0258-4
83. Doroudgar S, Hofmann C, Boileau E, Malone B, Riechert E, Gorska AA, Jakobi T, Sandmann C, Jürgensen L, Kmietczyk V, Malovrh E, Burghaus J, Rettel M, Stein F, Younesi F, Friedrich UA, Mauz V, Backs J, Kramer G, Katus HA, Dieterich C, Völkers M. Monitoring Cell-Type-Specific Gene Expression Using Ribosome Profiling In Vivo During Cardiac Hemodynamic Stress. *Circ Res* [Internet]. 2019;125:431–448. Available from: https://pubmed.ncbi.nlm.nih.gov/31284834
84. Schafer S, Adami E, Heinig M, Rodrigues KEC, Kreuchwig F, Silhavy J, van Heesch S, Simaite D, Rajewsky N, Cuppen E, Pravenec M, Vingron M, Cook SA, Hubner N. Translational regulation shapes the molecular landscape of complex disease phenotypes. *Nat Commun* [Internet]. 2015;6:7200. Available from: https://doi.org/10.1038/ncomms8200
85. van Heesch S, Witte F, Schneider-Lunitz V, Schulz JF, Adami E, Faber AB, Kirchner M, Maatz H, Blachut S, Sandmann C-L, Kanda M, Worth CL, Schafer S, Calviello L, Merriott R, Patone G, Hummel O, Wyler E, Obermayer B, Mücke MB, Lindberg EL, Trnka F, Memczak S, Schilling M, Felkin LE, Barton PJR, Quaife NM, Vanezis K, Diecke S, Mukai M, Mah N, Oh S-J, Kurtz A, Schramm C, Schwinge D, Sebode M, Harakalova M, Asselbergs FW, Vink A, de Weger RA, Viswanathan S, Widjaja AA, Gärtner-Rommel A, Milting H, dos Remedios C, Knosalla C, Mertins P, Landthaler M, Vingron M, Linke WA, Seidman JG, Seidman CE, Rajewsky N, Ohler U, Cook SA, Hubner N. The Translational Landscape of the Human Heart. *Cell* [Internet]. 2019;178:242-260.e29. Available from: https://www.sciencedirect.com/science/article/pii/S0092867419305082
86. Gebauer F, Hentze MW. Molecular mechanisms of translational control. *Nat Rev Mol Cell Biol* [Internet]. 2004;5:827–835. Available from: https://doi.org/10.1038/nrm1488
87. Dever TE, Dinman JD, Green R. Translation Elongation and Recoding in Eukaryotes. *Cold Spring Harb Perspect Biol* [Internet]. 2018;10:a032649. Available from: http://cshperspectives.cshlp.org/content/10/8/a032649.abstract
88. Hellen CUT. Translation Termination and Ribosome Recycling in Eukaryotes. *Cold Spring Harb Perspect Biol* [Internet]. 2018;10:a032656. Available from: http://cshperspectives.cshlp.org/content/10/10/a032656.abstract
89. Brito Querido J, Díaz-López I, Ramakrishnan V. The molecular basis of

translation initiation and its regulation in eukaryotes. *Nat Rev Mol Cell Biol* [Internet]. 2024;25:168–186. Available from: https://doi.org/10.1038/s41580-023-00624-9
90. Jackson RJ, Hellen CUT, Pestova T V. The mechanism of eukaryotic translation initiation and principles of its regulation. *Nat Rev Mol Cell Biol* [Internet]. 2010;11:113–127. Available from: https://doi.org/10.1038/nrm2838
91. Wolf DA, Lin Y, Duan H, Cheng Y. eIF-Three to Tango: emerging functions of translation initiation factor eIF3 in protein synthesis and disease. *J Mol Cell Biol* [Internet]. 2020;12:403–409. Available from: https://doi.org/10.1093/jmcb/mjaa018
92. Tauber D, Tauber G, Khong A, Van Treeck B, Pelletier J, Parker R. Modulation of RNA Condensation by the DEAD-Box Protein eIF4A. *Cell* [Internet]. 2020;180:411-426.e16. Available from: https://www.sciencedirect.com/science/article/pii/S0092867419313935
93. Wang J, Shin B-S, Alvarado C, Kim J-R, Bohlen J, Dever TE, Puglisi JD. Rapid 40S scanning and its regulation by mRNA structure during eukaryotic translation initiation. *Cell* [Internet]. 2022;185:4474-4487.e17. Available from: https://www.sciencedirect.com/science/article/pii/S0092867422013204
94. Brito Querido J, Sokabe M, Díaz-López I, Gordiyenko Y, Fraser CS, Ramakrishnan V. The structure of a human translation initiation complex reveals two independent roles for the helicase eIF4A. *Nat Struct Mol Biol* [Internet]. 2024;31:455–464. Available from: https://doi.org/10.1038/s41594-023-01196-0
95. Vaysse C, Philippe C, Martineau Y, Quelen C, Hieblot C, Renaud C, Nicaise Y, Desquesnes A, Pannese M, Filleron T, Escourrou G, Lawson M, Rintoul RC, Delisle MB, Pyronnet S, Brousset P, Prats H, Touriol C, Vaysse C, Philippe C, Martineau Y, Quelen C, Hieblot C, Renaud C, Nicaise Y, Desquesnes A, Pannese M, Filleron T, Escourrou G, Lawson M, Rintoul RC, Bernadette Delisle M, Pyronnet S, Brousset P, Prats H, Touriol C. Key contribution of eIF4H-mediated translational control in tumor promotion. *Oncotarget* [Internet]. 2015 [cited 2024 May 1];6:39924–39940. Available from: https://www.oncotarget.com/article/5442/text/
96. Sonenberg N, Hinnebusch AG. Regulation of translation initiation in eukaryotes: mechanisms and biological targets. *Cell* [Internet]. 2009;136:731–745. Available from: https://pubmed.ncbi.nlm.nih.gov/19239892
97. Saxton RA, Sabatini DM. mTOR Signaling in Growth, Metabolism, and Disease. *Cell* [Internet]. 2017;169:361–371. Available from: https://doi.org/10.1016/j.cell.2017.03.035
98. Liu GY, Sabatini DM. mTOR at the nexus of nutrition, growth, ageing and disease. *Nat Rev Mol Cell Biol* [Internet]. 2020;21:183–203. Available from: https://doi.org/10.1038/s41580-019-0199-y
99. Ragupathi A, Kim C, Jacinto E. The mTORC2 signaling network: targets and cross-talks. *Biochem J* [Internet]. 2024;481:45–91. Available from: https://doi.org/10.1042/BCJ20220325
100. Thoreen CC, Chantranupong L, Keys HR, Wang T, Gray NS, Sabatini DM. A unifying model for mTORC1-mediated regulation of mRNA translation. *Nature* [Internet]. 2012;485:109–113. Available from: https://doi.org/10.1038/nature11083
101. Holz MK, Ballif BA, Gygi SP, Blenis J. mTOR and S6K1 Mediate Assembly of the Translation Preinitiation Complex through Dynamic Protein Interchange and Ordered Phosphorylation Events. *Cell* [Internet]. 2005;123:569–580.

Available from: https://doi.org/10.1016/j.cell.2005.10.024
102. Magnuson B, Ekim B, Fingar DC. Regulation and function of ribosomal protein S6 kinase (S6K) within mTOR signalling networks. *Biochem J* [Internet]. 2011;441:1–21. Available from: https://doi.org/10.1042/BJ20110892
103. Raught B, Gingras A-C, Gygi SP, Imataka H, Morino S, Gradi A, Aebersold R, Sonenberg N. Serum-stimulated, rapamycin-sensitive phosphorylation sites in the eukaryotic translation initiation factor 4GI. *EMBO J* [Internet]. 2000;19:434–444. Available from: https://doi.org/10.1093/emboj/19.3.434
104. Meyuhas O. Chapter Two - Ribosomal Protein S6 Phosphorylation: Four Decades of Research [Internet]. In: Jeon KWBT-IR of C and MB, editor. . Academic Press; 2015. p. 41–73.Available from: https://www.sciencedirect.com/science/article/pii/S1937644815000647
105. Lucas P, G. van den EAM, J. WM, C. TC. Global analysis of LARP1 translation targets reveals tunable and dynamic features of 5′ TOP motifs. *Proc Natl Acad Sci* [Internet]. 2020;117:5319–5328. Available from: https://doi.org/10.1073/pnas.1912864117
106. Jia J-J, Lahr RM, Solgaard MT, Moraes BJ, Pointet R, Yang A-D, Celucci G, Graber TE, Hoang H-D, Niklaus MR, Pena IA, Hollensen AK, Smith EM, Chaker-Margot M, Anton L, Dajadian C, Livingstone M, Hearnden J, Wang X-D, Yu Y, Maier T, Damgaard CK, Berman AJ, Alain T, Fonseca BD. mTORC1 promotes TOP mRNA translation through site-specific phosphorylation of LARP1. *Nucleic Acids Res* [Internet]. 2021;49:3461–3489. Available from: https://doi.org/10.1093/nar/gkaa1239
107. Sciarretta S, Forte M, Frati G, Sadoshima J. New Insights Into the Role of mTOR Signaling in the Cardiovascular System. *Circ Res* [Internet]. 2018;122:489–505. Available from: https://doi.org/10.1161/CIRCRESAHA.117.311147
108. Górska AA, Sandmann C, Riechert E, Hofmann C, Malovrh E, Varma E, Kmietczyk V, Ölschläger J, Jürgensen L, Kamuf-Schenk V, Stroh C, Furkel J, Konstandin MH, Sticht C, Boileau E, Dieterich C, Frey N, Katus HA, Doroudgar S, Völkers M. Muscle-specific Cand2 is translationally upregulated by mTORC1 and promotes adverse cardiac remodeling. *EMBO Rep* [Internet]. 2021;22:e52170–e52170. Available from: https://pubmed.ncbi.nlm.nih.gov/34605609
109. Zhang D, Contu R, Latronico MVG, Zhang J, Rizzi R, Catalucci D, Miyamoto S, Huang K, Ceci M, Gu Y, Dalton ND, Peterson KL, Guan K-L, Brown JH, Chen J, Sonenberg N, Condorelli G. MTORC1 regulates cardiac function and myocyte survival through 4E-BP1 inhibition in mice. *J Clin Invest* [Internet]. 2010;120:2805–2816. Available from: https://doi.org/10.1172/JCI43008
110. Yano T, Shimoshige S, Miki T, Tanno M, Mochizuki A, Fujito T, Yuda S, Muranaka A, Ogasawara M, Hashimoto A, Tsuchihashi K, Miura T. Clinical impact of myocardial mTORC1 activation in nonischemic dilated cardiomyopathy. *J Mol Cell Cardiol* [Internet]. 2016;91:6–9. Available from: https://doi.org/10.1016/j.yjmcc.2015.12.022
111. Lassaletta AD, Elmadhun NY, Zanetti AVD, Feng J, Anduaga J, Gohh RY, Sellke FW, Bianchi C. Rapamycin treatment of healthy pigs subjected to acute myocardial ischemia-reperfusion injury attenuates cardiac functions and increases myocardial necrosis. *Ann Thorac Surg* [Internet]. 2014;97:901–907. Available from: https://pubmed.ncbi.nlm.nih.gov/24266948
112. Ranek MJ, Kokkonen-Simon KM, Chen A, Dunkerly-Eyring BL, Vera MP, Oeing CU, Patel CH, Nakamura T, Zhu G, Bedja D, Sasaki M, Holewinski RJ,

Van Eyk JE, Powell JD, Lee DI, Kass DA. PKG1-modified TSC2 regulates mTORC1 activity to counter adverse cardiac stress. *Nature* [Internet]. 2019 [cited 2021 Mar 16];566:264–269. Available from: https://doi.org/10.1038/s41586-019-0895-y
113. Marin TM, Keith K, Davies B, Conner DA, Guha P, Kalaitzidis D, Wu X, Lauriol J, Wang B, Bauer M, Bronson R, Franchini KG, Neel BG, Kontaridis MI. Rapamycin reverses hypertrophic cardiomyopathy in a mouse model of LEOPARD syndrome-associated PTPN11 mutation. *J Clin Invest* [Internet]. 2011 [cited 2021 Mar 16];121:1026–1043. Available from: http://www.jci.org
114. Buss SJ, Muenz S, Riffel JH, Malekar P, Hagenmueller M, Weiss CS, Bea F, Bekeredjian R, Schinke-Braun M, Izumo S, Katus HA, Hardt SE. Beneficial Effects of Mammalian Target of Rapamycin Inhibition on Left Ventricular Remodeling After Myocardial Infarction. *J Am Coll Cardiol* [Internet]. 2009;54:2435–2446. Available from: https://www.sciencedirect.com/science/article/pii/S0735109709031982
115. Völkers M, Konstandin MH, Doroudgar S, Toko H, Quijada P, Din S, Joyo A, Ornelas L, Samse K, Thuerauf DJ, Gude N, Glembotski CC, Sussman MA. Mechanistic target of rapamycin complex 2 protects the heart from ischemic damage. *Circulation* [Internet]. 2013;128:2132–2144. Available from: https://pubmed.ncbi.nlm.nih.gov/24008870
116. Mazelin L, Panthu B, Nicot AS, Belotti E, Tintignac L, Teixeira G, Zhang Q, Risson V, Baas D, Delaune E, Derumeaux G, Taillandier D, Ohlmann T, Ovize M, Gangloff YG, Schaeffer L. mTOR inactivation in myocardium from infant mice rapidly leads to dilated cardiomyopathy due to translation defects and p53/JNK-mediated apoptosis. *J Mol Cell Cardiol* [Internet]. 2016 [cited 2021 Mar 17];97:213–225. Available from: http://www.jmcc-online.com/article/S0022282816300773/fulltext
117. Zhu Y, Pires KMP, Whitehead KJ, Olsen CD, Wayment B, Zhang YC, Bugger H, Ilkun O, Litwin SE, Thomas G, Kozma SC, Abel ED. Mechanistic Target of Rapamycin (Mtor) Is Essential for Murine Embryonic Heart Development and Growth. *PLoS One* [Internet]. 2013 [cited 2021 Mar 17];8:e54221. Available from: https://dx.plos.org/10.1371/journal.pone.0054221
118. Hahn A, Lauriol J, Thul J, Behnke-Hall K, Logeswaran T, Schänzer A, Böğürcü N, Garvalov BK, Zenker M, Gelb BD, von Gerlach S, Kandolf R, Kontaridis MI, Schranz D. Rapidly progressive hypertrophic cardiomyopathy in an infant with Noonan syndrome with multiple lentigines: palliative treatment with a rapamycin analog. *Am J Med Genet A* [Internet]. 2015;167A:744–751. Available from: https://pubmed.ncbi.nlm.nih.gov/25708222
119. Koyama M, Yano T, Kikuchi K, Miura T. Everolimus-responsive dilated cardiomyopathy in tuberous sclerosis. *Eur Heart J* [Internet]. 2015;36:2338. Available from: https://doi.org/10.1093/eurheartj/ehu526
120. Pallet N, Legendre C. Adverse events associated with mTOR inhibitors. *Expert Opin Drug Saf* [Internet]. 2013;12:177–186. Available from: https://doi.org/10.1517/14740338.2013.752814
121. Sciarretta S, Forte M, Frati G, Sadoshima J. The complex network of mTOR signalling in the heart. *Cardiovasc Res* [Internet]. 2022;118:424–439. Available from: https://doi.org/10.1093/cvr/cvab033
122. Das A, Salloum FN, Durrant D, Ockaili R, Kukreja RC. Rapamycin protects against myocardial ischemia–reperfusion injury through JAK2–STAT3 signaling pathway. *J Mol Cell Cardiol* [Internet]. 2012;53:858–869. Available from: https://www.sciencedirect.com/science/article/pii/S0022282812003409

123. Filippone SM, Samidurai A, Roh SK, Cain CK, He J, Salloum FN, Kukreja RC, Das A. Reperfusion Therapy with Rapamycin Attenuates Myocardial Infarction through Activation of AKT and ERK. *Oxid Med Cell Longev* [Internet]. 2017;2017:4619720. Available from: https://pubmed.ncbi.nlm.nih.gov/28373901
124. Ma MKM, Yung S, Chan TM. mTOR Inhibition and Kidney Diseases. *Transplantation* [Internet]. 2018;102. Available from: https://journals.lww.com/transplantjournal/fulltext/2018/02001/mtor_inhibition_and_kidney_diseases.7.aspx
125. Powell JD, Pollizzi KN, Heikamp EB, Horton MR. Regulation of Immune Responses by mTOR. *Annu Rev Immunol* [Internet]. 2012;30:39–68. Available from: https://www.annualreviews.org/content/journals/10.1146/annurev-immunol-020711-075024
126. Weichhart T, Hengstschläger M, Linke M. Regulation of innate immune cell function by mTOR. *Nat Rev Immunol* [Internet]. 2015;15:599–614. Available from: https://pubmed.ncbi.nlm.nih.gov/26403194
127. Cheng SC, Quintin J, Cramer RA, Shepardson KM, Saeed S, Kumar V, Giamarellos-Bourboulis EJ, Martens JHA, Rao NA, Aghajanirefah A, Manjeri GR, Li Y, Ifrim DC, Arts RJW, Van Der Meer BMJW, Deen PMT, Logie C, O'Neill LA, Willems P, Van De Veerdonk FL, Van Der Meer JWM, Ng A, Joosten LAB, Wijmenga C, Stunnenberg HG, Xavier RJ, Netea MG. MTOR- and HIF-1α-mediated aerobic glycolysis as metabolic basis for trained immunity. *Science (80- )* [Internet]. 2014 [cited 2024 May 3];345. Available from: https://www.science.org/doi/10.1126/science.1250684
128. Zhu L, Yang T, Li L, Sun L, Hou Y, Hu X, Zhang L, Tian H, Zhao Q, Peng J, Zhang H, Wang R, Yang Z, Zhang L, Zhao Y. TSC1 controls macrophage polarization to prevent inflammatory disease. *Nat Commun* [Internet]. 2014;5:4696. Available from: https://doi.org/10.1038/ncomms5696
129. Ivanov SS, Roy CR. Pathogen signatures activate a ubiquitination pathway that modulates the function of the metabolic checkpoint kinase mTOR. *Nat Immunol* [Internet]. 2013;14:1219–1228. Available from: https://doi.org/10.1038/ni.2740
130. Cao DJ. Macrophages in Cardiovascular Homeostasis and Disease. *Circulation* [Internet]. 2018;138:2452–2455. Available from: https://doi.org/10.1161/CIRCULATIONAHA.118.035736
131. Chen G, Phan V, Luo X, Cao DJ. The mechanistic target of rapamycin complex 1 critically regulates the function of mononuclear phagocytes and promotes cardiac remodeling in acute ischemia. *J Mol Cell Cardiol* [Internet]. 2021;159:62–79. Available from: https://doi.org/10.1016/j.yjmcc.2021.06.004
132. Mangione MC, Wen J, Cao DJ. Mechanistic target of rapamycin in regulating macrophage function in inflammatory cardiovascular diseases. *J Mol Cell Cardiol* [Internet]. 2024;186:111–124. Available from: https://doi.org/10.1016/j.yjmcc.2023.10.011
133. Hofmann C, Serafin A, Schwerdt OM, Fischer J, Sicklinger F, Younesi FS, Byrne NJ, Meyer IS, Malovrh E, Sandmann C, Jürgensen L, Kamuf-Schenk V, Stroh C, Löwenthal Z, Finke D, Boileau E, Beisaw A, Bugger H, Rettel M, Stein F, Katus HA, Jakobi T, Frey N, Leuschner F, Völkers M. Transient inhibition of translation improves cardiac function after ischemia/reperfusion by attenuating the inflammatory response. *Circulation*. 2024;
134. Siede D, Rapti K, Gorska AA, Katus HA, Altmüller J, Boeckel JN, Meder B, Maack C, Völkers M, Müller OJ, Backs J, Dieterich C. Identification of circular RNAs with host gene-independent expression in human model systems for

cardiac differentiation and disease. *J Mol Cell Cardiol* [Internet]. 2017;109:48–56. Available from: https://www.sciencedirect.com/science/article/pii/S0022282817301268
135. Byrne NJ, Matsumura N, Maayah ZH, Ferdaoussi M, Takahara S, Darwesh AM, Levasseur JL, Jahng JWS, Vos D, Parajuli N, El-Kadi AOS, Braam B, Young ME, Verma S, Light PE, Sweeney G, Seubert JM, Dyck JRB. Empagliflozin Blunts Worsening Cardiac Dysfunction Associated With Reduced NLRP3 (Nucleotide-Binding Domain-Like Receptor Protein 3) Inflammasome Activation in Heart Failure. *Circ Hear Fail* [Internet]. 2020;13:e006277. Available from: https://doi.org/10.1161/CIRCHEARTFAILURE.119.006277
136. Zhang G, Wang X, Li C, Li Q, An YA, Luo X, Deng Y, Gillette TG, Scherer PE, Wang Z V. Integrated Stress Response Couples Mitochondrial Protein Translation With Oxidative Stress Control. *Circulation* [Internet]. 2021;144:1500–1515. Available from: https://doi.org/10.1161/CIRCULATIONAHA.120.053125
137. Sicklinger F, Meyer IS, Li X, Radtke D, Dicks S, Kornadt MP, Mertens C, Meier JK, Lavine KJ, Zhang Y, Kuhn TC, Terzer T, Patel J, Boerries M, Schramm G, Frey N, Katus HA, Voehringer D, Leuschner F. Basophils balance healing after myocardial infarction via IL-4/IL-13. *J Clin Invest* [Internet]. 2021;131:e136778. Available from: https://pubmed.ncbi.nlm.nih.gov/34196299
138. Malone B, Atanassov I, Aeschimann F, Li X, Großhans H, Dieterich C. Bayesian prediction of RNA translation from ribosome profiling. *Nucleic Acids Res* [Internet]. 2017;45:2960–2972. Available from: https://pubmed.ncbi.nlm.nih.gov/28126919
139. Anders S, Pyl PT, Huber W. HTSeq--a Python framework to work with high-throughput sequencing data. *Bioinformatics* [Internet]. 2015;31:166–169. Available from: https://pubmed.ncbi.nlm.nih.gov/25260700
140. Huang DW, Sherman BT, Lempicki RA. Systematic and integrative analysis of large gene lists using DAVID bioinformatics resources. *Nat Protoc*. 2009;4:44–57.
141. Sherman BT, Hao M, Qiu J, Jiao X, Baseler MW, Lane HC, Imamichi T, Chang W. DAVID: a web server for functional enrichment analysis and functional annotation of gene lists (2021 update). *Nucleic Acids Res* [Internet]. 2022;50:W216–W221. Available from: https://doi.org/10.1093/nar/gkac194
142. Hughes CS, Moggridge S, Müller T, Sorensen PH, Morin GB, Krijgsveld J. Single-pot, solid-phase-enhanced sample preparation for proteomics experiments. *Nat Protoc* [Internet]. 2019;14:68–85. Available from: https://doi.org/10.1038/s41596-018-0082-x
143. Werner T, Sweetman G, Savitski MF, Mathieson T, Bantscheff M, Savitski MM. Ion Coalescence of Neutron Encoded TMT 10-Plex Reporter Ions. *Anal Chem* [Internet]. 2014;86:3594–3601. Available from: https://doi.org/10.1021/ac500140s
144. Reichel M, Liao Y, Rettel M, Ragan C, Evers M, Alleaume A-M, Horos R, Hentze MW, Preiss T, Millar AA. In Planta Determination of the mRNA-Binding Proteome of Arabidopsis Etiolated Seedlings. *Plant Cell* [Internet]. 2016;28:2435–2452. Available from: https://doi.org/10.1105/tpc.16.00562
145. Franken H, Mathieson T, Childs D, Sweetman GMA, Werner T, Tögel I, Doce C, Gade S, Bantscheff M, Drewes G, Reinhard FBM, Huber W, Savitski MM. Thermal proteome profiling for unbiased identification of direct and indirect drug targets using multiplexed quantitative mass spectrometry. *Nat Protoc* [Internet]. 2015;10:1567–1593. Available from:

https://doi.org/10.1038/nprot.2015.101
146. Ritchie ME, Phipson B, Wu D, Hu Y, Law CW, Shi W, Smyth GK. limma powers differential expression analyses for RNA-sequencing and microarray studies. *Nucleic Acids Res* [Internet]. 2015;43:e47–e47. Available from: https://doi.org/10.1093/nar/gkv007
147. Huber W, von Heydebreck A, Sültmann H, Poustka A, Vingron M. Variance stabilization applied to microarray data calibration and to the quantification of differential expression. *Bioinformatics* [Internet]. 2002;18:S96–S104. Available from: https://doi.org/10.1093/bioinformatics/18.suppl_1.S96
148. Molenaar B, Timmer LT, Droog M, Perini I, Versteeg D, Kooijman L, Monshouwer-Kloots J, de Ruiter H, Gladka MM, van Rooij E. Single-cell transcriptomics following ischemic injury identifies a role for B2M in cardiac repair. *Commun Biol* [Internet]. 2021;4:146. Available from: https://doi.org/10.1038/s42003-020-01636-3
149. Hao Y, Hao S, Andersen-Nissen E, Mauck WM, Zheng S, Butler A, Lee MJ, Wilk AJ, Darby C, Zager M, Hoffman P, Stoeckius M, Papalexi E, Mimitou EP, Jain J, Srivastava A, Stuart T, Fleming LM, Yeung B, Rogers AJ, McElrath JM, Blish CA, Gottardo R, Smibert P, Satija R. Integrated analysis of multimodal single-cell data. *Cell* [Internet]. 2021;184:3573-3587.e29. Available from: https://www.sciencedirect.com/science/article/pii/S0092867421005833
150. Stuart T, Satija R. Integrative single-cell analysis. *Nat Rev Genet* [Internet]. 2019;20:257–272. Available from: https://doi.org/10.1038/s41576-019-0093-7
151. Ouyang JF, Kamaraj US, Cao EY, Rackham OJL. ShinyCell: simple and sharable visualization of single-cell gene expression data. *Bioinformatics* [Internet]. 2021;37:3374–3376. Available from: https://doi.org/10.1093/bioinformatics/btab209
152. Boileau E, Li X, Vries ISN, Becker C, Casper R, Altmüller J, Leuschner F, Dieterich C. Full-Length Spatial Transcriptomics Reveals the Unexplored Isoform Diversity of the Myocardium Post-MI. *Front Genet* [Internet]. 2022;13:912572. Available from: https://app.readcube.com/library/undefined/item/3f4c1a7d-07ee-4831-9038-88935547541b
153. Beisaw A, Kuenne C, Guenther S, Dallmann J, Wu C-C, Bentsen M, Looso M, Stainier DYR. AP-1 Contributes to Chromatin Accessibility to Promote Sarcomere Disassembly and Cardiomyocyte Protrusion During Zebrafish Heart Regeneration. *Circ Res* [Internet]. 2020;126:1760–1778. Available from: https://doi.org/10.1161/CIRCRESAHA.119.316167
154. Bolger AM, Lohse M, Usadel B. Trimmomatic: a flexible trimmer for Illumina sequence data. *Bioinformatics* [Internet]. 2014;30:2114–2120. Available from: https://doi.org/10.1093/bioinformatics/btu170
155. Zhang Y, Liu T, Meyer CA, Eeckhoute J, Johnson DS, Bernstein BE, Nusbaum C, Myers RM, Brown M, Li W, Liu XS. Model-based Analysis of ChIP-Seq (MACS). *Genome Biol* [Internet]. 2008;9:R137. Available from: https://doi.org/10.1186/gb-2008-9-9-r137
156. Ramírez F, Dündar F, Diehl S, Grüning BA, Manke T. deepTools: a flexible platform for exploring deep-sequencing data. *Nucleic Acids Res* [Internet]. 2014;42:W187–W191. Available from: https://doi.org/10.1093/nar/gku365
157. Hofmann C, Löwenthal Z, Aghajani M, Kaufman RJ, Katus HA, Frey N, Glembotski CC, Völkers M, Doroudgar S. mTORC1 inhibition impairs activation of the unfolded protein response and induces cell death during ER stress in cardiomyocytes. *Am J Physiol Circ Physiol* [Internet]. 2023;325:H311–H320.

Available from: https://doi.org/10.1152/ajpheart.00682.2022
158. Williams EH, Kao RL, Morgan HE. Protein degradation and synthesis during recovery from myocardial ischemia. *Am J Physiol Metab* [Internet]. 1981;240:E268–E273. Available from: https://doi.org/10.1152/ajpendo.1981.240.3.E268
159. Wollenberger A, Onnen K, Hinterberger U, Rabitzsch G, Kleitke B. Myocardial Protein Synthesis in Acute Myocardial Hypoxia and Ischemia. *Cardiology* [Internet]. 2008;56:48–64. Available from: https://doi.org/10.1159/000169341
160. Lakshminrusimha S, Saugstad OD. The fetal circulation, pathophysiology of hypoxemic respiratory failure and pulmonary hypertension in neonates, and the role of oxygen therapy. *J Perinatol* [Internet]. 2016;36:S3–S11. Available from: https://doi.org/10.1038/jp.2016.43
161. Liu J, Xu Y, Stoleru D, Salic A. Imaging protein synthesis in cells and tissues with an alkyne analog of puromycin. *Proc Natl Acad Sci U S A* [Internet]. 2012;109:413–418. Available from: https://pubmed.ncbi.nlm.nih.gov/22160674
162. Gingras A-C, Raught B, Gygi SP, Niedzwiecka A, Miron M, Burley SK, Polakiewicz RD, Wyslouch-Cieszynska A, Aebersold R, Sonenberg N. Hierarchical phosphorylation of the translation inhibitor 4E-BP1. *Genes Dev* [Internet]. 2001;15:2852–2864. Available from: http://genesdev.cshlp.org/content/15/21/2852.abstract
163. Dewald O, Zymek P, Winkelmann K, Koerting A, Ren G, Abou-Khamis T, Michael LH, Rollins BJ, Entman ML, Frangogiannis NG. CCL2/Monocyte Chemoattractant Protein-1 Regulates Inflammatory Responses Critical to Healing Myocardial Infarcts. *Circ Res* [Internet]. 2005;96:881–889. Available from: https://doi.org/10.1161/01.RES.0000163017.13772.3a
164. Deshmane SL, Kremlev S, Amini S, Sawaya BE. Monocyte chemoattractant protein-1 (MCP-1): an overview. *J Interferon Cytokine Res* [Internet]. 2009;29:313–326. Available from: https://pubmed.ncbi.nlm.nih.gov/19441883
165. Hohensinner PJ, Kaun C, Rychli K, Ben-Tal Cohen E, Kastl SP, Demyanets S, Pfaffenberger S, Speidl WS, Rega G, Ullrich R, Maurer G, Huber K, Wojta J. Monocyte chemoattractant protein (MCP-1) is expressed in human cardiac cells and is differentially regulated by inflammatory mediators and hypoxia. *FEBS Lett* [Internet]. 2006;580:3532–3538. Available from: https://doi.org/10.1016/j.febslet.2006.05.043
166. Weinreuter M, Kreusser MM, Beckendorf J, Schreiter FC, Leuschner F, Lehmann LH, Hofmann KP, Rostosky JS, Diemert N, Xu C, Volz HC, Jungmann A, Nickel A, Sticht C, Gretz N, Maack C, Schneider MD, Gröne H-J, Müller OJ, Katus HA, Backs J. CaM Kinase II mediates maladaptive post-infarct remodeling and pro-inflammatory chemoattractant signaling but not acute myocardial ischemia/reperfusion injury. *EMBO Mol Med* [Internet]. 2014;6:1231–1245. Available from: https://doi.org/10.15252/emmm.201403848
167. Zhang W, Zhu T, Chen L, Luo W, Chao J. MCP-1 mediates ischemia-reperfusion-induced cardiomyocyte apoptosis via MCPIP1 and CaSR. *Am J Physiol Circ Physiol* [Internet]. 2019;318:H59–H71. Available from: https://doi.org/10.1152/ajpheart.00308.2019
168. Yang X, Lin Y, Shi Y, Li B, Liu W, Yin W, Dang Y, Chu Y, Fan J, He R. FAP Promotes Immunosuppression by Cancer-Associated Fibroblasts in the Tumor Microenvironment via STAT3–CCL2 Signaling. *Cancer Res* [Internet]. 2016;76:4124–4135. Available from: https://doi.org/10.1158/0008-5472.CAN-15-2973
169. Kanno T, Kamba T, Yamasaki T, Shibasaki N, Saito R, Terada N, Toda Y,

Mikami Y, Inoue T, Kanematsu A, Nishiyama H, Ogawa O, Nakamura E. JunB promotes cell invasion and angiogenesis in VHL-defective renal cell carcinoma. *Oncogene* [Internet]. 2012;31:3098–3110. Available from: https://doi.org/10.1038/onc.2011.475
170. Shaulian E, Karin M. AP-1 as a regulator of cell life and death. *Nat Cell Biol* [Internet]. 2002;4:E131–E136. Available from: https://doi.org/10.1038/ncb0502-e131
171. van Duijvenboden K, de Bakker DEM, Man JCK, Janssen R, Günthel M, Hill MC, Hooijkaas IB, van der Made I, van der Kraak PH, Vink A, Creemers EE, Martin JF, Barnett P, Bakkers J, Christoffels VM. Conserved NPPB+ Border Zone Switches From MEF2- to AP-1–Driven Gene Program. *Circulation* [Internet]. 2019;140:864–879. Available from: https://doi.org/10.1161/CIRCULATIONAHA.118.038944
172. Shijie L, Vaibhav D, Fangfei W, Jie L, Jenna C, Xiao L, F. MJ. Myocardial Infarction Suppresses Protein Synthesis and Causes Decoupling of Transcription and Translation. *JACC Basic to Transl Sci* [Internet]. 2024;9:792–807. Available from: https://doi.org/10.1016/j.jacbts.2024.02.014
173. Schreiber SS, Evans CD, Oratz M, Rothschild MA. Protein synthesis and degradation in cardiac stress. *Circ Res* [Internet]. 1981;48:601–611. Available from: https://doi.org/10.1161/01.RES.48.5.601
174. Oeing CU, Jun S, Mishra S, Dunkerly-Eyring BL, Chen A, Grajeda MI, Tahir UA, Gerszten RE, Paolocci N, Ranek MJ, Kass DA. MTORC1-Regulated Metabolism Controlled by TSC2 Limits Cardiac Reperfusion Injury. *Circ Res* [Internet]. 2021;128:639–651. Available from: https://doi.org/10.1161/CIRCRESAHA.120.317710
175. Di R, Wu X, Chang Z, Zhao X, Feng Q, Lu S, Luan Q, Hemmings BA, Li X, Yang Z. S6K inhibition renders cardiac protection against myocardial infarction through PDK1 phosphorylation of Akt. *Biochem J* [Internet]. 2011;441:199–207. Available from: https://doi.org/10.1042/BJ20110033
176. Choo AY, Yoon SO, Sang GK, Roux PP, Blenis J. Rapamycin differentially inhibits S6Ks and 4E-BP1 to mediate cell-type-specific repression of mRNA translation. *Proc Natl Acad Sci U S A* [Internet]. 2008 [cited 2024 Jul 17];105:17414–17419. Available from: https://www.pnas.org/doi/abs/10.1073/pnas.0809136105
177. Beretta L, Gingras AC, Svitkin Y V, Hall MN, Sonenberg N. Rapamycin blocks the phosphorylation of 4E-BP1 and inhibits cap-dependent initiation of translation. *EMBO J* [Internet]. 1996;15:658–664. Available from: https://doi.org/10.1002/j.1460-2075.1996.tb00398.x
178. Sarbassov DD, Ali SM, Sengupta S, Sheen J-H, Hsu PP, Bagley AF, Markhard AL, Sabatini DM. Prolonged Rapamycin Treatment Inhibits mTORC2 Assembly and Akt/PKB. *Mol Cell* [Internet]. 2006;22:159–168. Available from: https://www.sciencedirect.com/science/article/pii/S1097276506002188
179. Lamming DW, Ye L, Katajisto P, Goncalves MD, Saitoh M, Stevens DM, Davis JG, Salmon AB, Richardson A, Ahima RS, Guertin DA, Sabatini DM, Baur JA. Rapamycin-Induced Insulin Resistance Is Mediated by mTORC2 Loss and Uncoupled from Longevity. *Science (80- )* [Internet]. 2012;335:1638–1643. Available from: https://doi.org/10.1126/science.1215135
180. Masse M, Glippa V, Saad H, Le Bloas R, Gauffeny I, Berthou C, Czjzek M, Cormier P, Cosson B. An eIF4E-interacting peptide induces cell death in cancer cell lines. *Cell Death Dis* [Internet]. 2014;5:e1500–e1500. Available from: https://doi.org/10.1038/cddis.2014.457

181. Moerke NJ, Aktas H, Chen H, Cantel S, Reibarkh MY, Fahmy A, Gross JD, Degterev A, Yuan J, Chorev M, Halperin JA, Wagner G. Small-Molecule Inhibition of the Interaction between the Translation Initiation Factors eIF4E and eIF4G. *Cell* [Internet]. 2007;128:257–267. Available from: https://doi.org/10.1016/j.cell.2006.11.046
182. Moses JW, Leon MB, Popma JJ, Fitzgerald PJ, Holmes DR, O'Shaughnessy C, Caputo RP, Kereiakes DJ, Williams DO, Teirstein PS, Jaeger JL, Kuntz RE. Sirolimus-Eluting Stents versus Standard Stents in Patients with Stenosis in a Native Coronary Artery. *N Engl J Med* [Internet]. 2003 [cited 2024 Aug 6];349:1315–1323. Available from: https://www.nejm.org/doi/full/10.1056/NEJMoa035071
183. Hausleiter J, Kastrati A, Mehilli J, Vogeser M, Zohlnhöfer D, Schühlen H, Goos C, Pache J, Dotzer F, Pogatsa-Murray G, Dirschinger J, Heemann U, Schömig A. Randomized, Double-Blind, Placebo-Controlled Trial of Oral Sirolimus for Restenosis Prevention in Patients With In-Stent Restenosis. *Circulation* [Internet]. 2004;110:790–795. Available from: https://doi.org/10.1161/01.CIR.0000138935.17503.35
184. Stähli BE, Klingenberg R, Heg D, Branca M, Manka R, Kapos I, Müggler O, Denegri A, Kesterke R, Berger F, Stehli J, Candreva A, von Eckardstein A, Carballo D, Hamm C, Landmesser U, Mach F, Moccetti T, Jung C, Kelm M, Münzel T, Pedrazzini G, Räber L, Windecker S, Templin C, Matter CM, Lüscher TF, Ruschitzka F. Mammalian Target of Rapamycin Inhibition in Patients With ST-Segment Elevation Myocardial Infarction. *J Am Coll Cardiol* [Internet]. 2022;80:1802–1814. Available from: https://www.jacc.org/doi/abs/10.1016/j.jacc.2022.08.747
185. MacKeigan JP, Krueger DA. Differentiating the mTOR inhibitors everolimus and sirolimus in the treatment of tuberous sclerosis complex. *Neuro Oncol* [Internet]. 2015;17:1550–1559. Available from: https://pubmed.ncbi.nlm.nih.gov/26289591
186. Bhat M, Charlton M. Preserving Flow in Liver Transplant Recipients: mTOR Inhibitors Everolimus and Sirolimus Are Not Peas From a Pod. *Am J Transplant* [Internet]. 2013;13:1633–1635. Available from: https://doi.org/10.1111/ajt.12290
187. Su K-H, Dai C. mTORC1 senses stresses: Coupling stress to proteostasis. *BioEssays* [Internet]. 2017;39:1600268. Available from: https://doi.org/10.1002/bies.201600268
188. Demicheva E, Hecker M, Korff T. Stretch-Induced Activation of the Transcription Factor Activator Protein-1 Controls Monocyte Chemoattractant Protein-1 Expression During Arteriogenesis. *Circ Res* [Internet]. 2008;103:477–484. Available from: https://doi.org/10.1161/CIRCRESAHA.108.177782
189. Braun J, Hoffmann SC, Feldner A, Ludwig T, Henning R, Hecker M, Korff T. Endothelial Cell EphrinB2-Dependent Activation of Monocytes in Arteriosclerosis. *Arterioscler Thromb Vasc Biol* [Internet]. 2011;31:297–305. Available from: https://doi.org/10.1161/ATVBAHA.110.217646
190. Jain S, Eadon MT. Spatial transcriptomics in health and disease. *Nat Rev Nephrol* [Internet]. 2024;Available from: https://doi.org/10.1038/s41581-024-00841-1
191. VanInsberghe M, van den Berg J, Andersson-Rolf A, Clevers H, van Oudenaarden A. Single-cell Ribo-seq reveals cell cycle-dependent translational pausing. *Nature* [Internet]. 2021;597:561–565. Available from: https://doi.org/10.1038/s41586-021-03887-4

192. Ozadam H, Tonn T, Han CM, Segura A, Hoskins I, Rao S, Ghatpande V, Tran D, Catoe D, Salit M, Cenik C. Single-cell quantification of ribosome occupancy in early mouse development. *Nature* [Internet]. 2023;618:1057–1064. Available from: https://doi.org/10.1038/s41586-023-06228-9
193. Xie M, Cho GW, Kong Y, Li DL, Altamirano F, Luo X, Morales CR, Jiang N, Schiattarella GG, May HI, Medina J, Shelton JM, Ferdous A, Gillette TG, Hill JA. Activation of Autophagic Flux Blunts Cardiac Ischemia/Reperfusion Injury. *Circ Res* [Internet]. 2021;129:435–450. Available from: https://doi.org/10.1161/CIRCRESAHA.120.318601
194. Nguyen LS, Vautier M, Allenbach Y, Zahr N, Benveniste O, Funck-Brentano C, Salem J-E. Sirolimus and mTOR Inhibitors: A Review of Side Effects and Specific Management in Solid Organ Transplantation. *Drug Saf* [Internet]. 2019;42:813–825. Available from: https://doi.org/10.1007/s40264-019-00810-9
195. Schreiber KH, Arriola Apelo SI, Yu D, Brinkman JA, Velarde MC, Syed FA, Liao C-Y, Baar EL, Carbajal KA, Sherman DS, Ortiz D, Brunauer R, Yang SE, Tzannis ST, Kennedy BK, Lamming DW. A novel rapamycin analog is highly selective for mTORC1 in vivo. *Nat Commun* [Internet]. 2019;10:3194. Available from: https://doi.org/10.1038/s41467-019-11174-0
196. Mahoney SJ, Narayan S, Molz L, Berstler LA, Kang SA, Vlasuk GP, Saiah E. A small molecule inhibitor of Rheb selectively targets mTORC1 signaling. *Nat Commun* [Internet]. 2018;9:548. Available from: https://doi.org/10.1038/s41467-018-03035-z
197. Kang SA, O'Neill DJ, Machl AW, Lumpkin CJ, Galda SN, Sengupta S, Mahoney SJ, Howell JJ, Molz L, Hahm S, Vlasuk GP, Saiah E. Discovery of Small-Molecule Selective mTORC1 Inhibitors via Direct Inhibition of Glucose Transporters. *Cell Chem Biol* [Internet]. 2019;26:1203-1213.e13. Available from: https://doi.org/10.1016/j.chembiol.2019.05.009
198. Lee BJ, Boyer JA, Burnett GL, Thottumkara AP, Tibrewal N, Wilson SL, Hsieh T, Marquez A, Lorenzana EG, Evans JW, Hulea L, Kiss G, Liu H, Lee D, Larsson O, McLaughlan S, Topisirovic I, Wang Z, Wang Z, Zhao Y, Wildes D, Aggen JB, Singh M, Gill AL, Smith JAM, Rosen N. Selective inhibitors of mTORC1 activate 4EBP1 and suppress tumor growth. *Nat Chem Biol* [Internet]. 2021;Available from: https://doi.org/10.1038/s41589-021-00813-7
199. Burnett GL, Yang YC, Aggen JB, Pitzen J, Gliedt MK, Semko CM, Marquez A, Evans JW, Wang G, Won WS, Tomlinson ACA, Kiss G, Tzitzilonis C, Thottumkara AP, Cregg J, Mellem KT, Choi JS, Lee JC, Zhao Y, Lee BJ, Meyerowitz JG, Knox JE, Jiang J, Wang Z, Wildes D, Wang Z, Singh M, Smith JAM, Gill AL. Discovery of RMC-5552, a Selective Bi-Steric Inhibitor of mTORC1, for the Treatment of mTORC1-Activated Tumors. *J Med Chem* [Internet]. 2023;66:149–169. Available from: https://doi.org/10.1021/acs.jmedchem.2c01658

## 8 Acknowledgements

I want to thank Prof. Mirko Völkers for being an outstanding mentor and his support, consistent guidance, and encouragement throughout the years.

I also want to thank Prof. Markus Hecker for his support and for serving as a supervisor for this thesis.

I am very thankful to all the members of the Völkers lab for being good friends and their continuous assistance.

I thank all collaborators for their technical help in conducting experiments that would not have been possible without them.

Most importantly, none of this could have happened without my family. I am forever grateful for your unconditional love and want to thank all of you for knowing that I can always count on you.